Design and Control of Resilient Interconnected Microgrids for Reliable Mass Transit Systems

by

Taylor J. G. Egan

A thesis submitted to the
School of Graduate and Postdoctoral Studies in partial
fulfillment of the requirements for the degree of

Master of Applied Science in Electrical and Computer Engineering

Faculty of Engineering and Applied Science
University of Ontario Institute of Technology
Oshawa, Ontario, Canada
March 2019

THESIS EXAMINATION INFORMATION

Submitted by: **Taylor J. G. Egan**

Master of Applied Science in **Electrical and Computer Engineering**

Thesis title:
Design and Control of Resilient Interconnected Microgrids for Reliable Mass Transit Systems

An oral defense of this thesis took place on September 13, 2018 in front of the following examining committee:

Examining Committee:

Chair of Examining Committee	Dr. Shahryar Rahnamayan
Research Supervisor	Dr. Hossam Gaber
Research Co-supervisor	Dr. Ruth Milman
Examining Committee Member	Dr. Mohammed Youssef
University Examiner	Dr. Ibrahim Dincer

The above committee determined that the thesis is acceptable in form and content and that a satisfactory knowledge of the field covered by the thesis was demonstrated by the candidate during an oral examination. A signed copy of the Certificate of Approval is available from the School of Graduate and Postdoctoral Studies.

Abstract

Mass transit systems are relied on a daily basis to transport millions of passengers and bring billions of dollars' worth of economic goods to market. While some forms of mass transit rely on a fuel, electrified railway systems are dependent on the electric grid. The electric grid is becoming more vulnerable to disruptions, due to extreme weather, changing supply and demand patterns, and cyber-terrorism. An interruption to the energy supply of a railway infrastructure can have cascading effects on the economy and social livelihood. Resilient interconnected microgrids are proposed to maintain reliable operation of electrified railway infrastructures. An engineering design framework, and supporting methods and techniques, is proposed for an electrified railway infrastructure to be upgraded from its existing form, to one with resilient interconnected microgrids. The sizing of the interconnected microgrids is performed using an iterative sizing analysis, considering multiple resiliency key performance indicators to inform the designer of the trade-offs in sizing options. Hierarchical control is proposed to monitor and control the interconnected microgrids. A multi-objective problem cast in the tertiary level of control is proposed to be solved using game theory. The proposed designs are modelled and simulated in Simulink. Four case studies of railway infrastructures in Canada and the United Kingdom are used to demonstrate the effectiveness of the proposed designs. While results for each case study vary, resilient interconnected microgrids for railway infrastructures demonstrates a reduced dependence on the electric grid. The examples here are all scalable and can perform within the framework of any available energy system. The results are both extremely impressive and promising towards a more resilient and stable energy future for our railway and other critical infrastructures.

Keywords: interconnected microgrids; resilience; hierarchical control; game theory; railway electrification; energy management

Acknowledgements

When I look back at my time at the University of Ontario Institute of Technology, there are two quotes that accurately describe the past two years:

"If somebody offers you an amazing opportunity but you are not sure you can do it, say yes – then learn how to do it later!" – Richard Branson

"I knew exactly what to do. But, in a much more real sense, I had no idea what to do." – Michael Scott

Attending UOIT has been an aspiration I have had since beginning my post-secondary career. A Queen Elizabeth II Diamond Jubilee scholar, a 2017 finalist in the Ignite Durham OPG category competition, a 2018 UOIT 3MT finalist, promoting UOIT as a student ambassador and teaching at the undergraduate level are just some of the many highlights of my time at UOIT. As such, I would like to thank the many people in my life who made this all possible.

First, I would like to express my appreciation to members of the UOIT community. I would not have been able to complete my research without the guidance of my supervisor, Dr. Hossam A. Gabbar. The opportunities he has provided to me have far exceeded my expectations and have allowed my UOIT experience to be better than what I had imagined. I would also like to extend appreciation to my co-supervisor Dr. Ruth Milman, for insightful discussions regarding my research, and helping me become a better writer. I've thoroughly enjoyed our conversations as I navigate through the process of this thesis and graduate studies. To Dr. Sheldon Williamson, I thank you for sparking my interest in topics related to transportation electrification and providing the familiarity I needed with mass transit systems to pursue my research.

I would like to offer my thanks to members of the Energy Safety and Control Lab, specifically Mohamed Ahmed, Yahya Koraz, Mohamed Aboughaly, and Dr. Ahmed Othman, for their technical guidance and discussions on our way frequent walks to Tim Hortons. And many thanks to the UOIT staff and the students, both graduate and undergraduate, who made my time at UOIT a great experience.

A special thanks to Dr. Hasimah Rahman, the staff at the Centre of Electrical Energy systems, and the friends I made while on international exchange to Malaysia at the Universiti Teknologi of Malaysia (yes, that is how it is spelled in Malaysia). My three-month exchange trip allowed me to live outside the boundaries of my comfort zone, gain a better perspective of the similarities and differences among various cul-

tures and religions, and cross a few items off my bucket list.

Outside of the UOIT community there are many people I need to thank who have never left my side throughout this endeavour, have patiently waited for me to complete this thesis and are still trying to decipher its contents.

While I would like to acknowledge everyone individually, there are some who deserve special mention:

— Garrett L. who gave me the push I needed to apply to UOIT, our road trip to Oshawa and tour of campus before I started, his frequent visits to Oshawa when I should have been working on this thesis, and for grudgingly reviewing parts of my thesis for spelling and grammar mistakes. You've read far more of this thesis than anyone else will.

— John C. for the one time I listened to your advice and decided to pursue a thesis-based masters. While I may think twice before I take your advice next time, don't let the negative aspects of my experience deter you from pursuing graduate studies.

— Kenny C.-E. for thinking my research is about protecting us from the white walkers. Was the operation a success?

— Megan W. and Jenny L. for always having (sometimes colourful) words of encouragement throughout this endeavor and countless gossip hour(s).

— Steve D. and Cathrine L. for providing me a place to stay and their patience as I completed this thesis, and always having a good snack on the table. What's for dinner?

My friends I've made in the Durham region (except the Tupperware thief), my brodas and sistas back in Ottawa, and my family: I am so glad that I will never again have to hear any of you say, "You're not done your thesis yet!". Throughout this process you have always provided me with a place to go when I needed to escape the graduate student life.

Finally, to my parents, for the support they have provided throughout my educational career... even if my father didn't know the name of the school I was attending until I gave him a sweater for Christmas.

Taylor Egan, EIT
March 2019

Author's Declaration

I hereby declare that this thesis consists of original work of which I have authored. This is a true copy of the thesis, including any required final revisions, as accepted by my examiners.

I authorize the University of Ontario Institute of Technology to lend this thesis to other institutions or individuals for the purpose of scholarly research. I further authorize University of Ontario Institute of Technology to reproduce this thesis by photocopying or by other means, in total or in part, at the request of other institutions or individuals for the purpose of scholarly research. I understand that my thesis will be made electronically available to the public.

Taylor J. G. Egan

Statement of Contributions

I hereby certify that I am the sole author of this thesis. I have used standard referencing practices to acknowledge ideas, research techniques, or other materials that belong to others. Furthermore, I hereby certify that I am the sole source of the creative works and/or inventive knowledge described in this thesis.

Part of the work described in Chapter 5 and 6 has been published as:

T. Egan, H. A. Gabbar, A. M. Othman and R. Milman, "Design and control of resilient interconnected microgrid for sustained railway", *2017 IEEE International Conference on Smart Energy Grid Engineering (SEGE)*, Oshawa, ON, 2017, pp. 131-136. doi: 10.1109/SEGE.2017.8052788

I performed the majority of the simulation testing and writing of the manuscript.

Part of the work described in this thesis (Chapter 3, Chapter 5, and Chapter 6) is under consideration for publication:

H. A. Gabbar, T. Egan, A. M. Othman and R. Milman, "Enhanced Resilience of Mass Transit Systems through Hierarchical Control of Interconnected Microgrids"

H. A. Gabbar, T. Egan, A. M. Othman and R. Milman, "Framework for Enhanced Resilience of Mass Transit Systems with Interconnected Microgrids"

I performed the majority of the design, simulation testing, and writing for each manuscript.

Contents

List of Figures

List of Tables

Nomenclature

Constants & Variables

$a_{\mathrm{ij}}, b_{\mathrm{ij}}$	Payoff for player 1 and 2, respectively	$[unitless]$
a	Diode ideality factor	$1\,[unitless]$
A	Rolling friction Davis coefficient	$[N]$
A_{WT}	Cross-section area of the WT blades	$[m^2]$
B	Flange friction Davis coefficient	$[N\ s\ m^{-1}]$
c_{p}	WT power coefficient	$[unitless]$
C	Aerodynamic resistance Davis coefficient	$[N\ s^2\ m^{-2}]$
D	Duty cycle	$[unitless]$
D_{s}	Damping coefficient	$[N\ m\ s\ rad^{-1}]$
E_{gap}	Energy of the band gap for silicon	$1.1\,[eV]$
E_{RES}	Sum of energy from RESs within an IMG	$[Wh]$
E_{sys}	Sum of energy within an IMG	$[Wh]$
f	Frequency	$[Hz]$
f	Objective function	$[W]$
F_{curve}	Resistance force due to curve in railway track	$[N]$
F_{grad}	Resistance force due to a gradient	$[N]$
F_{res}	Resistance force due to rolling stock movement	$[N]$
F_{trac}	Tractive effort of rolling stock	$[N]$
FF	Fill factor	$[unitless]$
g	Acceleration due to gravity	$9.81\,[m\ s^{-2}]$
G	Solar irradiance	$[W\ m^{-2}]$
G_{ref}	Reference solar irradiance	$1,000\,[W\ m^{-2}]$
H_{g}	Moment of inertia constant for the DFIG	$[kg\ m^{-2}]$
H_{t}	Moment of inertia constant for the WT	$[kg\ m^{-2}]$
I_{a}	Input current to solar PV average model boost converter	$[A]$
I_{batt}	Battery current	$[A]$
I_{d}	Shockley diode equation	$[A]$
I_{dc}	Output current of solar PV average model boost converter	$[A]$
$\bar{I}^{\mathrm{dq}}{}_{\mathrm{grid}}$	Electric grid current in DQ-frame	$[A]$
I_{mpp}	Current of PV cell at maximum power point	$[A]$

I_{ph}	Light generated current of a PV cell	$[A]$
I_{PV}	Current of a PV array	$[A]$
I_{rr}	Reverse saturation current of a PV cell at $\mathrm{T_{ref}}$	$[A]$
I_{sat}	Diode saturation current	$[A]$
I_{SC}	Short circuit current of PV cell	$[A]$
I_{SCS}	Short circuit current of PV cell at STC	$[A]$
$\bar{I}^{\mathrm{dq}}{}_{\mathrm{r}}$	DFIG rotor current in DQ-frame	$[A]$
$\bar{I}^{\mathrm{dq}}{}_{\mathrm{ref}}$	Reference current in DQ-frame	$[A]$
$\bar{I}^{\mathrm{dq}}{}_{\mathrm{s}}$	DFIG stator current in DQ-frame	$[A]$
I^*	Battery current passed through a low-pass filter	$[A]$
k	Boltzman constant	$1.3806e-23\,[J\ K^{-1}]$
K	Polarization factor	$[m\Omega\ Ah^{-1}]$
K_{A}	Exponential voltage factor	$[V]$
K_{B}	Exponential capacity factor	$[Ah]$
K_{i}	Integral gain in a PID controller	$[unitless]$
$K_{\mathrm{I_{SC}}}$	Short circuit current temperature coefficient	$[\%\ ^{\circ}C^{-1}]$
K_{p}	Proportional gain in a PID controller	$[unitless]$
K_{s}	Shaft stiffness	$[N\ m\ rad^{-1}]$
KPI_{DoS}	Diversity of supply KPI	$[unitless]$
KPI_{DS}	IMG demand served KPI	$[unitless]$
KPI_{GD}	IMG electric grid dependency KPI	$[\%]$
KPI_{IMGD}	IMG demand KPI	$[W]$
KPI_{IMGR}	IMG reliance KPI	$[\%]$
KPI_{IMGS}	IMG supply KPI	$[W]$
KPI_{RG}	IMG renewable generation KPI	$[\%]$
L_{r}	DFIG rotor inductance	$[H]$
L_{m}	DFIG mutual inductance	$[H]$
L_{s}	DFIG stator inductance	$[H$
L_{tot}	Total transformer leakage and choke impedance	$[H]$
m_{pass}	Mass of the passengers on the rolling stock	$[kg]$
m_{rs}	Mass of an unloaded rolling stock	$[kg]$
m_{eff}	Effective mass of the rolling stock	$[kg]$
N_{DER}	Number of DER in an IMG	$[unitless]$
N_{ESS}	Number of ESS in an IMG	$[unitless]$
N_{IMG}	Number of IMGs	$[unitless]$
N_{load}	Number of loads	$[unitless]$
N_{p}	Number of pole pairs in DFIG	$[unitless]$
N_{PV}	Number of PV arrays in an IMG	$[unitless]$
$N_{\mathrm{PV_p}}$	Number of PV modules connected in parallel	$[unitless]$
$N_{\mathrm{PV_s}}$	Number of PV modules connected in series	$[unitless]$
N_{WT}	Number of WTs in an IMG	$[unitless]$
p	Proportion of DER of overall IMG rated capacity	$[unitless]$

P	Player in a bimatrix game	$[unitless]$
P_{aux}	Auxiliary power of the rolling stock	$[W]$
P_{chg}	Charing power of the battery	$[W]$
$P_{\text{chg,max}}$	Upper limit for charging the battery	$[W]$
P_{DER}	Power generated from a DER	$[W]$
$P_{\text{DER,lim}}$	Sum of the export limit for a DER	$[W]$
$P_{\text{DER,max}}$	Upper limit for DER generation	$[W]$
$P_{\text{DER,min}}$	Lower limit for DER generation	$[W]$
$P_{\text{DER}\rightarrow\text{grid}}$	Power from DER exported to the electric grid	$[W]$
$P_{\text{DER}\rightarrow\text{grid,max}}$	Upper limit to export power from DER to electric grid	$[W]$
$P_{\text{DER}\rightarrow\text{grid,min}}$	Lower limit to export power from DER to electric grid	$[W]$
P_{dis}	Discharging power of the battery	$[W]$
$P_{\text{dis,max}}$	Upper limit for discharging from the battery	$[W]$
P_{ESS}	Total power discharged from or absorbed by an ESS	$[W]$
P_{grid}	Power imported from or exported to the electric grid	$[W]$
$P_{\text{grid,max}}$	Upper limit the electric grid can absorb/supply	$[W]$
P_{IMG}	Sum of power from DER(s) and ESS(s) for an IMG	$[W]$
$P_{\text{IMG}\rightarrow\text{IMG,lim}}$	Exchange limit between two IMGs, determined by IMGSC	$[W]$
P_{load}	Demand of railway infrastructure	$[W]$
P_{mpp}	Maximum power point of PV cell	$[W]$
P_{nom}	Nominal capacity of the DER	$[W]$
P_{PV}	Total power generated by the solar PV array(s)	$[W]$
P_{regen}	Power recovered by the rolling stock during braking	$[W]$
P_{t}	Power generated by a wind turbine	$[W]$
P_{trac}	Traction power of the rolling stock	$[W]$
P_{WT}	Total power generated by the wind turbine(s)	$[W]$
P_{δ}	Power supplied by an IMG to another IMG	$[W]$
q	Electron charge	$1.6022e-19\,[C]$
Q	Current capacity of the battery	$[Ah]$
Q_{nom}	Nominal capacity of the battery	$[Ah]$
R_{batt}	Internal resistance of the battery	$[\Omega]$
R_{r}	DFIG rotor resistance	$[\Omega]$
R_{s}	DFIG stator resistance	$[\Omega]$
R_{ser}	Series resistance in a PV cell equivalent circuit	$[\Omega]$
R_{sh}	Shunt resistance in a PV cell equivalent circuit	$[\Omega]$
R_{tot}	Total transformer leakage and choke impedance	$[\Omega]$
s	Player 1 strategy in a bimatrix game	$[unitless]$
S	Finite strategy set of a player in a bimatrix game	$[unitless]$
SP_{DER}	DER set-point from the MG regulation system	$[unitless]$
SP_{ESS}	ESS set-point from the MG regulation system	$[unitless]$
SOC	State of Charge	$[unitless]$
SOC_{max}	Upper limit on battery state of charge	$[unitless]$

$SOC_{\min}$	Lower limit on battery state of charge	$[unitless]$
t	Player 2 strategy in a bimatrix game	$[unitless]$
t_{IMGR}	Time the IMG is reliant on any other IMG	$[s]$
t_{GD}	Time the IMG is dependent on the electric grid	$[s]$
t_{sim}	Simulation time	$[s]$
$t_{\text{sim,control}}$	DC bus inverter control system sample time	$[s]$
$t_{\text{sim,power}}$	Simulation sample time of power systems	$[s]$
T	Time period	$[s]$
T_{cell}	Temperature of the PV cell	$[K]$
T_{ref}	Reference temperature of PV cell	$298\,[K]$
u_1, u_2	Payoff functions in a bimatrix game	$[unitless]$
U	Utility function of the players in a bimatrix game	$[unitless]$
v_{ci}	Cut-in wind speed of the WT	$[m\ s^{-1}]$
v_{co}	Cut-out wind speed of the WT	$[m\ s^{-1}]$
v_{rated}	Rated wind speed of the WT	$[m\ s^{-1}]$
v_{rs}	Speed of the rolling stock	$[m\ s^{-1}]$
v_{w}	Wind speed	$[m\ s^{-1}]$
V_{a}	Input voltage to solar PV average model boost converter	$[V]$
V_{chg}	Battery's external voltage during charging	$[V]$
V_{dc}	Output voltage of solar PV average model boost converter	$[V]$
$V_{\text{DC,meas}}$	Measured voltage on DC link of DC bus inverter	$[V]$
$V_{\text{DC,nom}}$	Nominal voltage of DC bus inverter DC link	$[V]$
$V_{\text{DC,ref}}$	Reference voltage of DC bus inverter DC link	$[V]$
V_{dis}	Battery's external voltage during discharging	$[V]$
$\bar{V}^{\text{dq}}{}_{\text{grid}}$	Electric grid voltage in DQ-frame	$[V]$
V_{mpp}	Voltage of PV cell at maximum power point	$[V]$
V_{nom}	Nominal voltage of battery	$[V]$
V_{oc}	Open circuit voltage of PV cell	$[V]$
V_{PV}	Voltage of a PV array	$[V]$
$\bar{V}^{\text{dq}}{}_{\text{r}}$	DFIG rotor voltage in DQ-frame	$[V]$
$\bar{V}^{\text{dq}}{}_{\text{ref}}$	Reference voltage in DQ-frame	$[V]$
$\bar{V}^{\text{dq}}{}_{\text{s}}$	DFIG stator voltage in DQ-frame	$[V]$
V_{ref}	PV MPPT reference voltage	$[V]$
V_{T}	Thermal voltage of series connected PV modules	$[V]$

Greek Letters

α	Solar PV converter duty cycle increment value	$[unitless]$
β	Blade pitch angle	$[^\circ]$
ϵ_1	Output signal of battery power loop regulator	$[unitless]$
ϵ_2	Output signal of battery current loop regulator	$[unitless]$
η_{PV}	PV module peak efficiency	$[unitless]$

η_{regen}	Regenerative braking efficiency of the rolling stock	$[unitless]$
η_{trac}	Drive-train efficiency of the rolling stock	$[unitless]$
θ_{grad}	Angle of gradient	$[^{\circ}]$
θ_{s}	Angle of shaft in WT drive train	$[rad]$
λ	Tip speed ratio of the rotor blade to wind speed	$[unitless]$
$\bar{\lambda}^{\text{dq}}{}_{\text{r}}$	DFIG rotor flux linkage in DQ-frame	$[kg\ m^2\ s^{-2}\ A^{-1}]$
$\bar{\lambda}^{\text{dq}}{}_{\text{s}}$	DFIG stator flux linkage in DQ-frame	$[kg\ m^2\ s^{-2}\ A^{-1}]$
λ_{w}	Rotary allowance of the rolling stock	$[unitless]$
ρ_{a}	Density of air	$1.2\,[kg\ m^{-3}]$
τ_{elec}	Electrical torque of DFIG	$[N\ m]$
τ_{mech}	Mechanical torque of WT	$[N\ m]$
ω_{g}	Angular speed of the DFIG	$[rad\ sec^{-1}]$
ω_{r}	DFIG rotor angular speed	$[rad\ sec^{-1}]$
ω_{s}	DFIG stator angular speed	$[rad\ sec^{-1}]$
ω_{s}	DFIG rotor slip frequency	$[rad\ sec^{-1}]$
ω_{ref}	DFIG reference frame angular speed	$[rad\ sec^{-1}]$
ω_{t}	Angular speed of the WT	$[rad\ sec^{-1}]$

Abbreviations

AC	Alternating Current
AREMA	American Railway Engineering and Maintenance-of-Way Association
Birm	Birmingham, UK
DC	Direct Current
DER	Distributed Energy Resource
DFIG	Double Fed Induction Generator
EM	Energy Management
ESS	Energy Storage System
GHG	Greenhouse Gas Emissions
HVAC	Heating, Ventilation and Air Conditioning
IEEE	Institute of Electrical and Electronic Engineers
IESO	Independent Electric System Operator
IMG	Interconnected Microgrid
IMGSC	Interconnected Microgrid Supervisory Controller
KPI	Key Performance Indicator
Ldn	London, UK
MG	Microgrid
MO	Multi-Objective
MPPT	Maximum Power Point Tracking
PCC	Point of Common Coupling
PI	Proportional-integral

PID	Proportional-integral-derivative
PLL	Phase Lock Loop
PSE&G	Public Service Electric & Gas Company
PV	Photovoltaic
PWM	Pulse Width Modulation
RES	Renewable Energy Source
RIMG	Resilient Interconnected Microgrid
SOC	State of Charge
STC	Standard Test Conditions
Strat	Stratford-upon-Avon, UK
THD	Total Harmonic Distortion
TPS	Traction Power Substation
WT	Wind Turbine

Chapter 1

Introduction

In recent years, the world has made major advances in technology and experienced exponential population growth. As the world population and economies scale upwards, the transportation sector continues to expand to support the growing demand. However, to support this growing demand, the transportation sector requires a large amount of energy. In 2017, the International Energy Agency reported that the transportation sector amounted to nearly 30% of worldwide secondary energy use, as seen in Figure 1.1 [1].

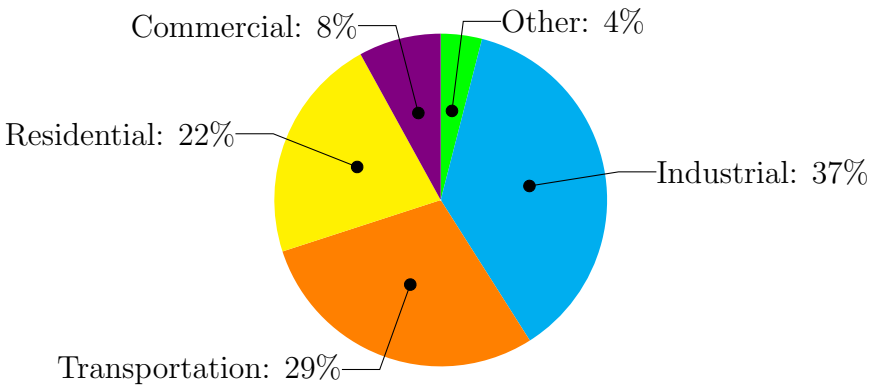

Figure 1.1: Global secondary energy use by sector, 2017 [1]

Figure 1.2 further breaks down global secondary energy use of the transportation sector by type of travel [1]. The transportation sector consists of both passenger and freight vehicles, travelled either by road, rail, marine or aviation systems. Considering all types of travel, many variations of mass transit systems exist:

— By road, there are busses

— By rail, there is underground subways, monorails, intercity, and high-speed trains

— By marine, there are ferries

— By air, there is gondolas and airplanes

This type of transportation typically follows a fixed schedule and route within a city, province, or country and is available to the public. This thesis will further explore mass transit by rail.

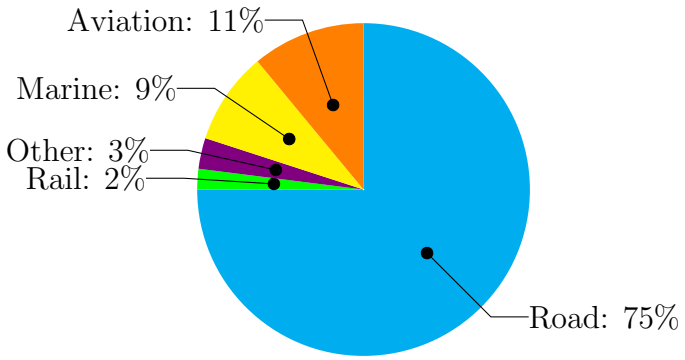

Figure 1.2: Global secondary energy use in the transportation sector, 2017 [1]

1.1 Mass Transit by Rail: Why It Matters

Railway infrastructures have been a primary transportation system since the 19th century. Comparable to other countries across the world, Canada's use of transportation by rail is a major player in the success of its economy and movement of its citizens. For example, in Canada, the railway sector annually contributes $10 billion to its economy, by transporting 82 million passengers and $210 billion worth of goods [2, 3]. Currently, transportation by rail accounts for 2% of worldwide secondary energy use in the transportation sector [1].

Railway infrastructures can be classified under two types of transport: passenger and freight [4]. While freight transport is crucial to the well-being of a local, national, and international economy, priority is usually deferred to passenger comfort and requirements. Most people are unconcerned when a freight train must be left sitting on the railway tracks during an electric grid outage, whereas a passenger railway infrastructure that experiences even a brief interruption in service may cause frustration and panic amongst the riders, and long-term mistrust in the reliability of the railway infrastructure. Therefore, this thesis will focus on passenger railway infrastructures.

Passenger railway infrastructures consist of smaller sets of rolling stock, compared to freight systems, and are used to transport people for work and/or leisure purposes.

Passenger transportation by rail is an important segment of the transportation sector to consider, as the comfort and safety of the passengers is important. Passenger railway infrastructures are classified as one of three types: urban (commuter), high speed, and intercity. The characteristics of the railway infrastructure play an important role in the design, implementation, and control of the railway infrastructure [5]. The energy requirements will significantly vary between each type of railway infrastructure, due to the difference in route characteristics and rolling stock parameters.

The continued use of fossil fuels remains a constant hot topic as governments, non-government organizations, utilities, businesses and people attempt to move away from the reliance on fossil fuels in favor of renewable, clean energy technologies. As evidence continues to collect, the continuing consumption of fossil fuels at current rates has caused higher amounts of GHG emissions to be released to the atmosphere. This is causing a change in climate and increasing the frequency of natural disasters, disrupting the reliability of critical infrastructures many rely on every second of the day [6, 7]. While diesel is the primary fuel source for the rolling stock, other alternatives are being studied.

Liquified natural gas is showing promise in trials around the world. It has been a prime study for applications in railway infrastructures due to its lower costs and GHG emissions compared to diesel fuel [4]. However, the mass adoption of liquified natural gas still faces many limitations. Dincer et al. [4] highlight that the current North American infrastructure is built for diesel fuel and would require costly infrastructure changes. In addition, Engerer et al. [8] highlight that natural gas in Europe plays a small role due to the lack of infrastructure and dependence on fossil fuel imports.

Hydrogen as an alternate fuel has been a long-held promose and has undergone extensive research for applications in railwaty infrastructures. While still in the piloting stage, the exuberant costs associated with the generation of hydrogen and the absent distribution infrastructure and regulations make this fuel still impractical for a large-scale railway infrastructure [4, 9, 10]. Compressed natural gas, ammonia, biodiesel, and methanol have also been explored as possible fuel sources for rolling stocks. Most fuels are either still under research and development or are currently being piloted [4, 9].

A common alternative to using a dedicated fuel source is electricity. An electrified railway system supplies electric power to the rolling stock without a local fuel supply. Electrified railways date back to the 19^{th} century, and has seen mass adop-

tion in various parts of the world since.

1.2 Railway Electrification

Today, about 31.5% of railway tracks are electrified, with Japan (64%), Russia (62%), India (62%), European Union (61%), and China (46%) being leaders in the shift towards railway electrification [1]. While an electric railway infrastructure may have its own generation, transmission and distribution network, most rely on the existing public electric grid [11–13]. Figure 1.3 provides a general layout of a power supply system for an AC electric railway infrastructure[1] [11]. This thesis will focus on passenger railway infrastructures using an AC electrification system.

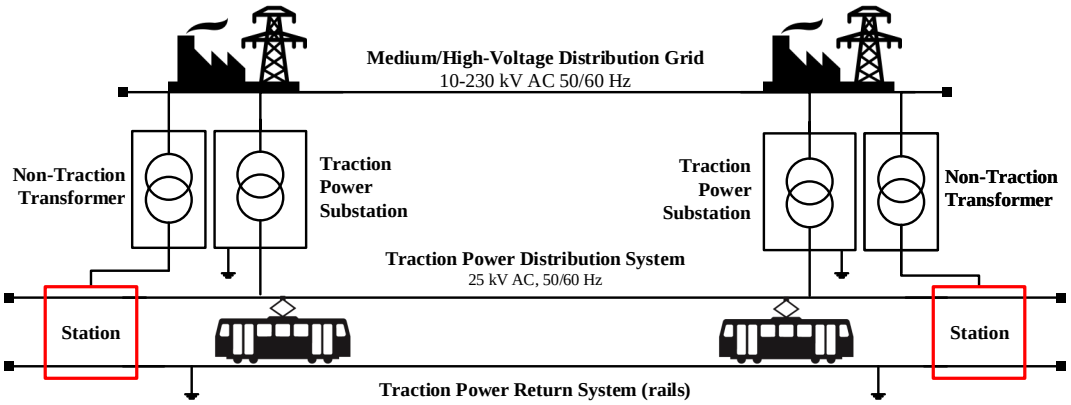

Figure 1.3: Generic layout of an AC electrified railway infrastructure

1.2.1 Emerging Challenges for Energy Infrastructures

Today the world is becoming more familiar with blackouts, as existing energy infrastructures fall to a higher number of threats. In addition to an aging infrastructure and lack of government willingness to invest in newer, larger, centralized energy infrastructures, there are many more frequent disruptions to the world's energy infrastructures. The most common reason for disruptions to any energy system is primarily due to natural disasters, such as hurricanes, floods, ice storms, etc. [14]. However, other challengers are emerging, such as terrorism, cyber-attacks, geopolitical conflicts, and dwindling fossil fuel reserves.

Examples on the growing list of major disruptions to mass transit systems caused by various disturbances in the electric grid include:

[1] DC electric railway systems also exist. In addition to a transformer, an AC/DC diode rectifier is also installed in the TPS [11].

— **Hurricane Irene, September 20, 2017**: years of electric grid infrastructure decay and massive debt obligations, combined with the forces of the hurricane, crippled critical infrastructures in Puerto Rico and left many without power for months [15].

— **Turkey, March 31, 2015**: approximately ten hours, three quarters of Turkey experienced its worst blackout in 15 years, as homes, offices and mass transit systems were cut-off from the electric grid, with some people trapped in underground tunnels [16].

— **Hurricane Sandy, October 2012**: at the height of the storm, New York City (largest city in the USA) underground subway system shutdown for four days [17].

— **Ontario & Northeastern US, August 14th, 2003**: ambient temperature rose above 31 °C and 50 million people were plunged into darkness, and caused millions of passengers who relied on streetcars, subways, railways and airports to be stranded [18]. Depending on location, the blackout ranged from a couple of hours to a few days.

— **Great Ice Storm of 1998**: eastern regions of Canada and the USA were hit with an ice storm, leaving millions in the dark in the middle of the winter, and forcing mass transit systems to halt operations at the height of the storm [19].

The annual number of electric grid disruptions in the United States of America has grown significantly since 2000 [20]. US Department of Energy reports that approximately $26 billion is spent annually on electric grid outages [21], while weather-related power outage incidents have cost the American economy approximately $300 billion US between 2003 and 2012 [16]. In Canada, the annual economic costs related to electric grid outages induced by the weather are estimated to increase from $5 billion to $43 billion by 2050 [6].

Panteli et al. [22] state that a shift from reliability-oriented to resilience-oriented design is required to augment the resilience of critical infrastructures (e.g. transportation, power systems, water, communication) against critical threats. On February 12, 2013, *U.S. Presidential Policy Directive 21: Critical Infrastructure Security and Resilience* was released [23]. The policy defines resilience as the "the ability to prepare for and adapt to changing conditions and withstand and recover rapidly from disruptions". For many critical infrastructures across the world, the need to improve resiliency is not a dream but a grim reality. In order to provide a reliable mass transit system, railway infrastructures are no exception.

1.2.2 Resiliency Options for Energy Infrastructures

Any interruption to an energy infrastructure that supplies a railway infrastructure can have a cascading effect on the economy and social livelihoods. As such, many options to improve the reliability of railway infrastructures, each met with their own disadvantages, have been suggested, studied and/or implemented. These include:

— Infrastructure hardening

— Dedicated fuel source, with emergency reserve, for the rolling stock

— Hydrogen fueled railways

— On-board energy storage for the rolling stock

— Wayside energy storage for the rolling stock

— Microgrids

Hardening of the electric grid infrastructure involves adding redundancy and reliability to an existing infrastructure [24]. However, this requires a large investment and maintenance costs, and regardless of how resistant and redundant the electric grid is designed for, there is always still the possibility for a component or system to fail due to its complexity and numerous dependencies [25].

Emergency fuel supply is riddled with environmental emissions and supply and demand issues due to natural disasters, geopolitical conflict, and diminishing reserves [9, 10, 26–28]. Alternate (e.g. liquid natural gas, hydrogen) or duel fuel systems (e.g. diesel and liquid natural gas) offer a promising alternative to diesel with lower GHG emissions, however most options are either still in the research and development or piloting stages [4,8,9,27]. In addition, the absence of a distribution infrastructure and regulations, and similar issues of continuity of supply during a natural disaster make this concept impractical to consider as a solution for improving the resilience of the railway infrastructure [10, 29].

The implementation of on-board and wayside energy storage systems (ESS), a device which can store energy in some form, to be converted to electrical energy when required, has been a study for decades. Commonly used ESS studied for railway infrastructures include: 1) the battery, 2) supercapacitor, and 3) the flywheel. On-board storage imposes a burden of additional weight on the rolling stock and reduced passenger seating [30–33]. The sizing and siting of wayside ESSs can be optimized based on characteristics of the railway route, however the losses associated with this option cannot be neglected and could attribute to higher energy usage [31–33].

Furthermore, in the long-term ESSs on their own are unsustainable [6]. If an electric grid outage occurs so too does the supply source to the ESSs. In addition, the high capital investment and low life cycle precludes on-board and wayside ESSs as a viable option [34, 35].

As such, to promote the reliability of the railway infrastructure, the study of the MG for railway infrastructures is identified as an ideal solution. Resilient IMGs will allow the railway infrastructure to realize a higher level of reliability to sustain its operation.

1.2.3 Interconnected Microgrids

To help mitigate the consequences of these threats, extensive research, development and commercialization has been performed to introduce microgrids as an option to augment energy infrastructure resilience [16, 36–39]. The MG is a small-scale grid, which includes distributed energy resources, energy storage systems, and loads capable of operating in parallel to or independently from the electric grid [21, 40]. When two or more MGs are mutually joined to share resources, they are referred to as interconnected microgrids.

The MG concept is not new, having first been introduced in the late 1800's by the late Thomas Edison [41]. The Manhattan Pearl Street Station was constructed in 1882, years before a central electric grid was established, and served a small set of loads for industrial purposes. While a centralized electric grid expanded and dominated in the 20th century, growth in MGs is becoming more mainstream in the 21st century to compliment the development and implementation of the smart grid.

Due to the increasing frequency of extreme weather events, the MG has experienced mass adoption from communities, institutions and industry in an attempt to remain operational when the electric grid goes dark. While the USA and Asia are considered the frontrunners, the deployed capacity of the of the MG is growing worldwide. It is predicted that MG capacity will grow from 1.4 GW, in 2015, to either a modest 5.7 GW or an aggressive 8.6 GW by 2024 [42]. MGs are becoming common place for most essential institutions, such as transportation systems, university campuses, military operations, health networks, and residential and commercial sectors [16, 42–50]. In response to Hurricane Maria, MGs are being promoted as a key pillar to the modernization of Puerto Rico's electric grid, offering a viable solution to improve the resilience of the system against future threats [24, 51].

Considering the emergence of frequent power outages, New Jersey (NJ) Transit is responding to the protection of its critical infrastructures. NJ Transit currently relies on the Public Service Electric and Gas Company (PSE&G), a public electric grid, to provide power to its railway infrastructure. However, in the face of a growing number of electric grid outages caused by weather events, NJ Transit has explored options to allow the transit operator to maintain operation during emergencies.

NJ Transitgrid is a public transportation resilience project, which is being implemented in response to three major events: Hurricane Irene in 2011, an early snowfall in 2011, and Hurricane Sandy in 2012 [52]. These events resulted in stranded travellers and a threat to regional security and economy. For situations where the electric grid is compromised, the MG will be relied upon to provide resilient energy to NJ Transit and Amtrak railway infrastructures. The project consists of two phases [52]:

— **NJ Transitgrid Traction Power System** will result in a limited electrified portion of NJ Transit and Amtrak corridors to remain operational during natural disasters. A 104 MW natural gas power plant will be relied on to power the designated railway corridors.

— **NJ Transitgrid Distributed Generation Solutions** will implement distributed and renewable energy systems to provide resilient energy to key NJ Transit facilities (e.g. stations, maintenance facilities, bus garages and other buildings).

This is the first large-scale implementation of a resilient focussed MG in the world. This project is expected to bring improved mobility during natural disasters and minimize pollutants from out-dated technologies.

1.3 Motivation

Currently, electrified railway infrastructures are dependent on the electric grid. Historically, the electric grid has not been resilient to emerging challenges (e.g. natural disasters, terrorism, cyber-attacks, geopolitical conflicts), which has resulted in disturbances to the reliability of railway infrastructures around the world [14–21]. These types of incidents are expected to continue with increasing frequency and severity, resulting in significant economic losses and diminishing confidence in reliability of our critical infrastructures. The need to shift from reliability-oriented to resiliency-oriented design is receiving more attention from railway operators [6, 52]. Many solutions to improve the resiliency of the energy supply system for railway infrastructures have been studied, such as infrastructure hardening, emergency fuel

reserves, and energy storage systems. However, each of these solutions is met with similar disadvantages of being dependent on the fragile electric grid. While NJ Transit is taking the lead on an alternative solution (the microgrid), the resilience of the NJ Transit railway energy supply is still poor. A single microgrid, consisting of one fossil-fueled distributed energy source, serving a portion of the railway infrastructure is as susceptible to the same emerging challenges as the electric grid. Of the proposed solutions, resilient interconnected microgrids are identified as showing a higher degree of reliability for railway infrastructures. However, the resilience and interconnection of microgrids still requires further research. This thesis focuses on the design of resilient interconnected microgrids to provide reliability to mass transit systems, in particular electrified passenger railways.

1.4 Problem Definition

There is a lack of understanding on how to transform an existing electrified railway infrastructure to one that includes resilient interconnected microgrids. A 'systems thinking' approach, where the whole system is required to solve real-world problems, compared to looking at individual parts. From this issue, spurns many others. This includes a gap in how to apply and measure resiliency for interconnected microgrids and railway infrastructures. Resiliency objectives are seldom considered for microgrid sizing problems and control strategies. Agility, a principle of resiliency, is required to be incorporated in the techniques researched for an interconnected microgrid control architecture, in order to make quick, effective decisions.

1.5 Thesis Objectives

The scope of this thesis is to design resilient interconnected microgrids, with an appropriate control architecture, for reliable mass transit systems. The objective of this thesis are as follows:

1. Propose a novel engineering design framework to replace an existing railway infrastructure with RIMGs for sustained operations of railway infrastructure. The engineering design framework is supported by:
    - Defining a list of proposed key performance indicators that can be used to assess the resiliency of the proposed designs.
    - Performing a requirement analysis, using quality function deployment methods, with an emphasis on resiliency, for the design and implementation of RIMGs to supply reliable energy to railway infrastructures.

— A proposed iterative sizing analysis method for the IMG components with appropriate resilience targets considered.

2. Develop an integrated, deterministic mathematical model of a hybrid AC-DC RIMG. The RIMG model is supported by:
   — Modelling the system in Simulink using electrical component wise models of DERs, ESSs, power converters, the electric grid, and AC electrified railway infrastructure.
   — Conducting a resiliency performance analysis using the defined list of resiliency KPIs.
   — Performing a weather disturbance analysis to observe the effects of varying climate on the performance of the RIMG model.
3. Design a supervisory control architecture to coordinate a sustained operation of the IMGs and railway infrastructure. The control architecture is supported by:
   — Synthesizing a resilient control strategy for each IMG.
   — Modelling the control systems for the DERs and ESSs in Simulink.
4. Implement a multi-objective decision making tool, using game theory techniques, to coordinate the exchange of energy between IMGs.
   — Define the objective functions and appropriate decision variable for the systems.
   — Define the constraints for the system.
   — Integrate the decision making tool in the supervisory control architecture and map the tool to the RIMG model.

1.6 Contributions of this Thesis

The main contributions of this thesis are as follows:

1. A novel engineering design framework to integrate resilient interconnected microgrids within an existing AC electrified passenger railway infrastructure.
2. Modelling and evaluating resiliency key performance indicators, consisting of commonly used KPIs from familiar domains (e.g. socio-cultural, economic, technical), that can be used to provide an understanding of the resiliency of IMGs.

3. An iterative sizing analysis method that uses multiple resiliency KPIs to size the IMG components.

4. A RIMG model to provide resilient energy to a railway infrastructure. The flexible model includes RESs and ESSs, the ability for integration of other energy systems, and can be applied to various railway infrastructures around the world. The model features an interconnection between MGs, which is demonstrated to increase the resilience of the energy supply for the railway infrastructure.

5. A hierarchical control scheme to handle coordination of IMGs. Within the control scheme, the implementation of an algorithm, using game theory techniques and the IMG demand served KPI, in the tertiary control layer to handle the energy exchange interaction between IMGs.

Further details on the contributions are provided in Chapter 9.

1.7 Organization of this Thesis

This thesis consists of nine chapters:

Chapter 1 contains the necessary information regarding the background, motivation, problem definition, research objectives, contributions and organization of this thesis.

Chapter 2 provides a detailed, technical literature review in light of the existing challenges for energy infrastructures that support railway infrastructures. This chapter includes the following topics: microgrids, energy systems used in microgrids, sizing the microgrid, control architectures for microgrids, game theory and how it can be used in a hierarchical control architecture, and how to evaluate the resiliency of a microgrid.

Chapter 3 presents the methods and techniques proposed for the study of the design and control of resilient interconnected microgrids. The methods and techniques proposed are to support the developed engineering design framework to transform an existing electrified railway infrastructure to one with resilient interconnected microgrids.

Chapter 4 presents the requirements of the resilient interconnected microgrids to sustain the railway infrastructure. In this chapter requirements imposed by and/or

on the passenger, rail operator, regulator, utility and technology provider are presented. The requirements are then used to create a house of quality to map the stakeholder's requirements to design requirements. The control requirements for the proposed hierarchical control architecture are also presented.

Chapter 5 presents the proposed design of resilient interconnected microgrids to sustain railway operations. The chapter then provides the control strategies and architecture for the proposed resilient interconnected microgrid design. Strategies for the three levels of control architecture are synthesized to manage the interconnected microgrids. The multi-objective problem is introduced with the applicable system constraints. The application of game theory is presented to solve the multi-objective problem and implemented in the interconnected microgrid supervisory control level.

Chapter 6 includes the component modeling for the proposed resilient interconnected microgrid design, which includes the distributed energy resources, energy storage system, rolling stock, and miscellaneous components. Commonly available technologies in the market are used for the resilient interconnected microgrid model. Each of the component models are integrated together, with the control architecture, to form a resilient interconnected microgrid model in Simulink for analysis.

Chapter 7 presents the four case studies that are used to validate the proposed methods and designs. The case studies selected consist of four railway infrastructures, either currently in operation or proposed, that are proposed to be electrified, and that serve a large population.

Chapter 8 presents the results of the sizing analysis (applied to the simulation models), simulation and resiliency key performance indicator results, and weather disturbance analysis for each case study. Various aspects of the proposed methods and designs are compared to existing literature for validation. The chapter concludes with a discussion of the results.

Chapter 9 provides a summary of this thesis, the major contributions of this thesis in reflection of the research objectives, and suggestions for future research based on the findings of this thesis.

Appendices A to F present additional information that support this thesis.

Chapter 2

Literature Review

The previous chapter identified that railway infrastructures are an important service, but are heavily dependent on the centralized electric grid. The current electric grid is unfortunately becoming more prone to outages due to various threats (e.g. natural disasters, cyber-terrorism, geopolitical conflicts). Given the existing challenges in augmenting the resilience of the energy infrastructure for railways, a technical literature review is provided to more deeply understand the various topics and aspects related to the microgrid (MG). The literature review is composed of six major topics:

— Microgrids

— Microgrid energy systems

— Sizing of the microgrid energy systems

— Microgrid control architectures

— Game theory

— Resiliency analysis of microgrids

2.1 Existing Challenges for Mass Transit Energy Infrastructures

Challenges exist to augment the resilience of the energy supply for electrified railway systems. Hardening the electric grid infrastructure can only do so much before a component or system fails, and requires a large sum of capital and maintenance investment [24, 25]. Other options face a supply and demand issue, where if the supply is cut-off for whatever reason, the railway infrastructure ceases to operate.

Emergency fuel supply (e.g. diesel) supply and demand issues are related to natural disasters, geopolitical conflict, and diminishing reserves [9,26,27]. Alternative fuels, in addition to supply and demand concerns, are still in the research and development or piloting stages and lack a supporting distribution infrastructure [4, 9, 27]. Hydrogen, or fuel cells, are a long-held promise still in research and development, lack adequate regulations and a distribution infrastructure, and remains a costly initiative [9, 10, 27]. On-board and wayside energy storage systems are unsustainable in the long-term [6]. If an electric grid outage occurs so too does the supply source for the ESSs. The microgrid (MG) is an emerging technology concept and shows much promise in improving the resiliency of the energy supply for electrified railway infrastructures [16].

2.2 Microgrids

The MG is a small-scale grid, which includes distributed energy resources, energy storage systems, and loads capable of operating in parallel to or independently from the electric grid [21,40]. A DER is a system that converts energy from one form to useable electrical energy. A DER is classified as: 1) a renewable energy source (e.g. solar PV, wind turbines); or 2) a small-scale fossil fueled source (e.g. microturbine, combined heat and power plant, diesel generator) [53]. An ESS is a device (e.g. battery, compressed air energy storage, pumped-storage hydroelectricity, flywheel, supercapacitor) that stores energy in some form (e.g. electrochemical, mechanical, thermal), to be converted to electrical energy when required. MGs arranged in an arbitrary DC, AC, or hybrid AC-DC configuration [40,54]. Of these options, the hybrid configuration offers lower cost and higher efficiency but requires more complex control. A hybrid AC-DC MG consists of both an AC and DC bus, and a power converter to interface the busses together with the electric grid. The general concept of the MG is demonstrated in Figure 2.1 [55].

The MG can operate in either one of two modes: (1) grid-connected or (2) islanded [40]. When grid-connected, the MG will be able to exchange energy through a single PCC with the electric grid. The connection to the electric grid will be maintained and relied upon most of the time. However, during maintenance, failures, or while experiencing power quality issues, the MG may disconnect from the electric grid for protection and to ensure the continuity of supply to its respective load(s). This mode is commonly referred to as islanded mode. When islanded, the loads will have their demand satisfied by the MG or curtailed until a connection to the electric grid can be restored.

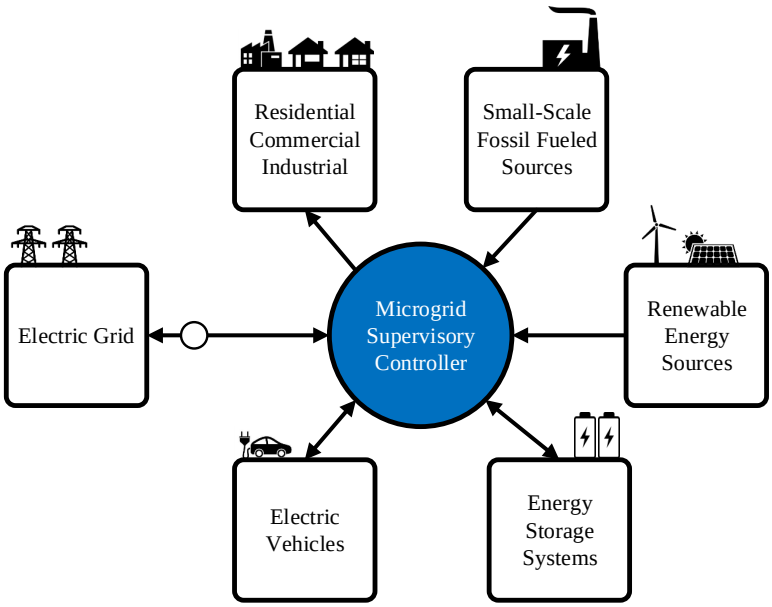

Figure 2.1: The microgrid concept with distributed energy generation and energy storage systems

Extensive research has been carried out on the MG. The MG offers many benefits and features that can be realized by the consumer, operator, electric grid operators and the environment. Common themes found in research of the MG include:

— Integration of RESs to facilitate a reduction in GHGs [56–58]

— Continuous supply to load during maintenance and energy system threats, even in the absence of a connection to the electric grid (e.g. rural electrification) [57–60]

— Reduced capital, operating, and maintenance costs [50, 61, 62]

— Closer proximity to system load, herein improving power quality, and reducing stress and losses on the transmission system [24, 38, 53, 63]

— Allow for higher degree of resilience in the event of an energy system threat (e.g. weather disasters, terrorism) [24, 38, 53, 64–66]

— Interconnected microgrids, also referred to as multi-microgrids and clustered microgrids [21, 63, 67–71]

Interconnected microgrids are of particular interest, as they can improve the security of supply and improve the utilization of assets [21, 72]. In addition, due to the intermittency of RESs and the diversity of the load profile, IMGs allow for potentially smaller sizing of individual MGs (i.e. reduced capital costs). They also feature

greater efficiency of the overall system, a higher level of redundancy, and a more robust operation under emergency events (e.g. natural disasters, terrorism).

2.3 Microgrid Energy Systems

The MG will consist of various energy systems, classified as either a DER or ESS. A DER is a system that converts energy from one form to useable electrical energy, while an ESS is a device that stores energy in some form, to be converted to electrical energy when required. This thesis will identify the appropriate RESs and ESSs suitable for the MG to supply resilient energy to a railway infrastructure.

2.3.1 Distributed Energy Resources

A DER is classified as either a local RES or a small-scale fossil fueled source. The integration of RESs offers cleaner generation than a small-scale fossil fueled source. RESs do not emit GHG emissions and do not depend on a finite source of energy, unlike small-scaled fossil fuel sources. Table 2.1 provides a comparative analysis of various RES options, which may be considered for integration in the MG [73].

Considering the characteristics of each of the RESs listed, wind and solar PV are the most practical energy systems to be deployed in the MG for railway infrastructures. These two technologies are more mature, practical, and commonly used in MG research compared to some of the other options considered:

— Global Wind Energy Council reported the installed global wind capacity was approximately 486 GW (2017) [74]

— GE Energy offers on-shore WTs with rated capacity ranging from 1.7 to 4.8 MW [75]

— Calgary's C-Train is the first railway infrastructure in North America to run entirely on energy produced from WTs (2009) [76]

— Largest solar PV systems have capacities which exceed 250 MW (2016) [77]

— Total installed global solar PV capacity estimated to be greater than 300 GW (2017) [78]

Table 2.1: Comparison of strengths and weaknesses of renewable energy sources for the MG

Renewable Energy Source	Advantages	Disadvatages
Wind	— Proximity to load — No variable fuel cost — Minimal GHG emissions	— Visual and noise pollution — High capital costs — Intermittent output
Solar PV	— Proximity to load — No variable fuel cost — Minimal GHG emissions — Low operating costs	— Intermittent output — Requires large real estate footprint — High capital costs
Hydro	— No variable fuel cost — Reliable generation output — Minimal GHG emissions	— High capital costs — Disruption to marine ecosystem — Fixed generation site
Fuel Cell	— Hydrogen is abundant — High energy content — High electrical eficiency — Minimal GHG emissions	— High operating costs — Limited infrastructure
Geothermal	— Efficient operation — Low operating costs — Minimal GHG emissions	— High capital costs — Requires large real estate footprint — Limited geothermal stores
Tidal	— Reliable generation output — Efficient generation at low tides — Minimal GHG emissions	— Disruption to marine ecosystem — Fixed generation site — Large-scale plants uncommon

2.3.2 Energy Storage Systems

Energy storage systems are an ideal component of the MG, especially when considering the integration of a RES which may experience intermittent generation [79]. ESS technology can offer many benefits, such as short term power supply (to counter RES intermittency), peak shaving, power quality improvements and ancillary services [80]. The energy storage unit will convert energy between two forms, one of which is electric, and store the energy until it is required to meet the electric demand.

The selection of which ESS to install in the MG depends on the characteristics of the railway infrastructure and whether it is appropriate for the load. Common characteristics used to evaluate an ESS are its specific energy (energy per unit mass, or volume) and power (power per unit mass, or volume). The battery, supercapacitor and flywheel are the most mature and commonly considered ESSs for railway infrastructures [11, 31, 81–83].

Table 2.2 provides a comparison of the characteristics of these energy storage technologies [84], with other literature reporting similar results [79, 85, 86]. Each of the ESS technologies listed have a trade-off amongst its respective characteristics. Based on those trade-offs, the ideal ESS technology to meet the energy use of a railway and improve the resilience must be chosen.

The **supercapacitor** is ideal for applications in urban rail systems since it can handle the sudden transients in the railway traction demand. However, the low energy density makes the technology ill-suited for improving the resiliency of the railway infrastructure in the long-term.

The **flywheel** has ideal specific energy and power densities, which make it an interesting technology for application in railway infrastructures. However, due to the high self-discharge rate and the continued need for safety considerations, the flywheel is still in the research and development stage.

The **battery** is ideal for use in the MG, as it is a mature technology. It can absorb any surplus energy generated from a DER, and be used to store energy recovered from the rolling stock during braking.

With any ESS an appropriate charging/discharging strategy is required, in order to maximize the life of the ESS. Zhang et al. [87] provide details on three charging strategies for a lithium-ion battery: 1) constant current, 2) constant voltage, and 3) two-stage (containing both constant current and constant voltage). The two-stage strategy will counter the deficiencies of each charging strategy. The authors use piecewise linear functions to determine the charging/discharging power limitations. This is used in contrast to hard limits on the charging/discharging limits of the battery, which improves the life cycle of the battery. Banguero et al. [88] suggest that fuzzy logic and model predictive control are better suited than the two-stage approach, due to improved handling of the ESS resulting in a longer life.

Issues with RESs include intermittency and fast power generation ramps (both positive and negative). The battery is an ideal technology to allow the RES to be an ideal dispatchable DER. Teleke et al. [89] develop a control strategy to mitigate the intermittency of the RES, while respecting the operating conditions of the battery technology. It is important to respect the charging and discharging limits of the battery to prolong its operating life. Salas-Puente et al. [90] propose a strategy that respects the grid tariffs, while also maximizing the lifetime of the battery. Using predicted PV generation, load profile, and electricity rates, the power management strategy will set the charging rates for the ESS for the day while respecting the two objectives.

Liu et al. [91] contend that strategies either focus on reducing peaks and valleys in the demand or to take advantage of lower electricity rates to charge the ESS, and

Table 2.2: Comparison of energy storage technology characteristics suitable for railway infrastructures [84]

Energy Storage System	Specific Power (W kg^{-1})	Specific Energy (Wh kg^{-1})	Cycle Life (cycles)	Self-Discharge (daily % of rated capacity)	Efficiency (%)	Cost ($ kWh^{-1})
Flywheel	1,000-5,000	5-100	10^5-10^7	100	90-95	1,000-5,000
Super-capacitor	500-5,000	2.5-15	10^5-10^6	20-40	90-100	300-2,000
Lead-acid Battery	25-300	20-50	200-2,000	0.05-0.3	70-90	50-400
NiMH Battery	200-250	60-80	1,500-3,000	1-2	65-70	400-2,400
Ni-Cd Battery	50-300	30-75	1,500-3,000	0.2-0.6	60-80	400-2,400
Li-ion Battery	100-350	75-200	10^3-10^4	0.1-0.3	90-100	500-2,500

discharge the ESS when rates are higher. The authors propose a strategy which combines the two strategies, in an attempt to improve the utilization of the ESS. The strategy first looks at the load fluctuations, before observing the electric grid rates, all at the same time as maintaining the energy storage system within its operating limits (i.e. min/max SOC).

Traditionally research on charging and discharging strategies for a battery revolve around economic (i.e. capital cost, life cycle, replacement cost) and technical objectives (i.e. SOC limits, depth of discharge limitations) [87,89–91]. Recently, research has become more active in focusing on strategies to improve resiliency [92,93].

Hussain et al. [92] highlight the unpredictability of determining when an emergency event may occur. In light of the unpredictability, the authors propose a fuzzy logic controller. The controller consists of two common inputs: 1) SOC and 2) rate of electricity from the electric grid. The authors include a third input, which is the probability of an emergency event occurring. The controller will then decide the battery ESS mode of operation: 1) subservient, where the charging/discharging is controlled by the energy management system, or 2) resilient, where the battery ESS controller issues scheduling commands to the energy management system.

2.4 Microgrid Sizing

The generation mix and nominal capacity of each DER and ESS within the MG is a complex decision-making process. Nominal capacity, otherwise known as nameplate

capacity or rated capacity, is the intended full-load sustained output of an energy system. The sizing problem involves determining the optimal generation mix and storage systems for a MG in order to satisfy the design requirements. The sizing problem requires models for the DERs and ESSs, historical weather information, and a load profile (historical or modelled). Traditionally, the MG sizing problem will attempt to solve an economic, environmental and/or reliability objectives and applicable constraints (e.g. power balance, ESS charging/discharging limits) [80, 94, 95].

Numerous tools can be used to solve the sizing problem of the MG [94]:

— Artificial intelligence, otherwise referred to as meta-heuristics

— Multi-objective (MO) design approach

— Analytical methods

— Iterative methods

— Probabilistic approach

— Graphical construction method

— Computer tools

Unlike classic optimization techniques, which may be difficult to solve, CPU/time intensive, and often resolve to a local optimum point, heuristic and meta-heuristics techniques have been researched to reduce computational time and include a larger set of feasible solutions [95]. **Artificial intelligence** is a powerful and commonly used meta-heuristic optimization technique in decision-making scenarios, such as the sizing of the MG [97]. Using a defined objective function (e.g. minimize capital investment, minimize GHG emissions), an iterative procedure is applied to solve the optimization problem and to converge to a global solution, thus avoiding getting into the specifics of a problem, unlike heuristic techniques. Commonly used meta-heuristic techniques inspired from real-world interactions in nature include genetic algorithms, particle swarm optimization, the firefly algorithm, and ant colony algorithms [80, 94–96].

The **multi-objective** design approach considers multiple conflicting objectives and an optimal solution point is determined. The approach can either be solved by combining the objective functions into a single or weighted objective or be finding the Pareto optimal solution. Pareto optimal approach will determine the optimal solution for considering all objectives and is referred to as the dominant solution since increasing the benefit of one objective will deteriorate the benefit of another.

Iterative, analytical, probabilistic, and graphical construction methods are available to solve the MG sizing problem. They are less commonly used techniques in comparison to artificial intelligence and the MO design approaches.

— **Iterative** techniques require a recursive algorithm to solve the MG sizing problem, and can easily be implemented. However, this may require more computational effort and may not lead to an optimal solution.

— **Analytica**l methods are used to determine the feasibility of the MG size given a specified configuration.

— **Probabilistic** methods allow for the consideration of changing weather patterns, and avoid pre-determined data, but do not consider the performance of the MG.

— **Graphical construction** has only been used to consider two decision variables, while eliminating other design aspects from consideration.

Various **computer simulation tools** are available for MG sizing, including HOMER, HYBRID2, HOGA, HYBRIDS, TRNSYS and RETScreen [94]. HOMER (Hybrid Optimization Model for Electric Renewables) is the most popular tool used. It models the behaviour of a power system and allows the user to compare different configurations, based on economic and technical merits.

Many authors have researched techniques to solve the MG sizing problem. Of the research sampled, traditionally an economic, environmental, and/or reliability objective for a single MG is considered:

— Cavanini et al. [97] propose to size the MG, with solar PV arrays, WTs and battery ESSs, for profit maximization, using genetic algorithm, particle swarm optimization, artificial bee colony algorithm, and gravitational search algorithm. Particle swarm optimization and artificial bee colony optimizations demonstrated the best results.

— Laws et al. [98] explore the need to include resilience in the assessment of a solar PV and battery ESS. The authors point out that optimization of multi-objective typically does not include resiliency considerations, but primarily economic and environmental objectives. Using traditional objectives, the authors include the Value of Lost Load in their design of a solar PV and battery ESS.

— Li et al. [99] propose a simple sizing algorithm for a WT/solar PV/battery

MG, using an iterative procedure to determine the number of WTs and solar PVs for the MG. The authors propose to minimize the life cycle cost of the MG, without any load curtailment. The authors understand the difficulty of sizing the MG when considering the ESS. Their work proposes a invariance criteria of the ESS SOC, which removes consideration of the ESS SOC at each time step.

— A parametric sizing algorithm is proposed by Bartolucci et al. [100], where economic, resiliency, renewable penetration and environmental indicies are considered. The research suggests that the ideal sizing of the solar PV in a MG will facilitate a more efficient operation of the battery and a reduced dependence on the electric grid.

— Ramli et al. [101] adopt a multi-objective approach to reduce computational time and treat the economic and reliability objectives simultaneously. The results presented from the algorithm provide a set of ideal options for the designer to consider, instead of one optimal solution. For the case studies selected, the solar PV, WT and battery ESS dominate the contribution of energy supplied to the load, with very low dependence on the diesel generator (<6%). This result demonstrates that a MG with RESs and an ESS can operate with a high probability of success without a dependence on the electric grid.

— Akram et al. [102] consider two sizing methods for the MG. The RESs in the MG are sized, with the ESS sized afterwards. This ensures no over- or under-sizing of the MG. Economic and reliability objectives are considered for the sizing problem.

Of the literature sampled, literature considering resiliency objectives and interconnected microgrids in the sizing problem are scarce.

2.5 Microgrid Control Architectures

A control system is an integral component of the MG, with multiple DERs and ESSs, intermittent renewable generation and varying load profiles. When interconnecting multiple MGs together, the control system becomes even more critical to the successful operation of the system. A suitable design of the IMG control system will allow each MG to be properly utilized, while maintaining the reliability, security and economic operation of the entire system [21, 40, 71, 81, 94, 95, 103].

Olivares et al. [40] highlight the two common methodologies to implementing a

control scheme for the MG. The first scheme involves a centralized system, where a central controller collects all data and determines all control actions. This scheme is heavily dependent on communication systems. The second scheme consists of implementing a decentralized system, where all systems are controlled individually with no awareness of the control actions imposed on the other systems. To counter the deficiencies of both methodologies, a hierarchical control system is proposed, consisting of multiple layers of control.

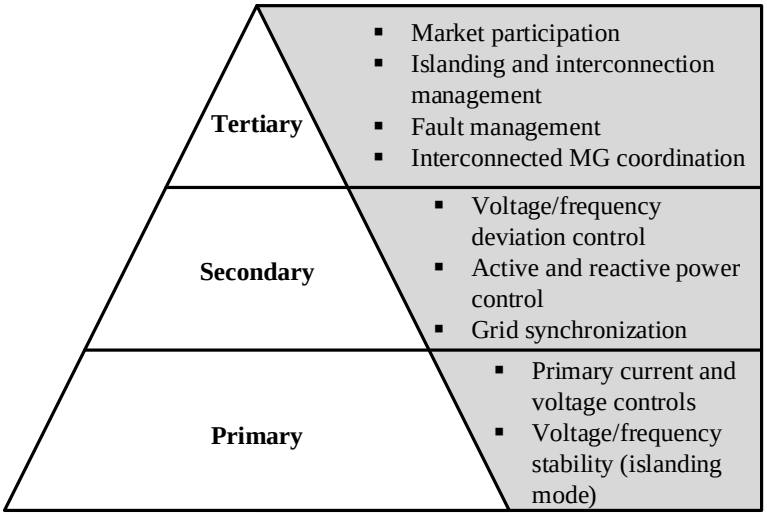

Figure 2.2: Three-level hierarchical control architecture for microgrids, and typical functions associated to each control level

A hierarchical control system features many levels of control, typically at least three. The primary control level is used by local controllers to regulate each individual system (i.e. DER(s) and/or ESS(s)). At this level, local measurements are primarily used to speed up the response time of the controller. The secondary level will ensure the ideal operation of the MG, regardless of operation mode. The tertiary level focusses on the long-term operation of the overall system. As the level of control is increased, the computation time increases for the control level tasks. Thus, the primary level will typically respond faster than the secondary level, and so on. Figure 2.2 lists some activities that are performed at each level of a hierarchical control architecture for the MG [54, 104].

Unamuno et al. [54] provide insight into the different approaches imposed on each level of MG control for hybrid AC-DC MGs. The authors highlight the control tasks for each level of control, while also listing the many characteristics of a MG control strategy. Reviewing the schemes available for the levels of control, the authors identify that centralized control in a hierarchical control scheme is preferrable for

single-user MGs.

Feng et al. [105] study the advantages and disadvantages of hierarchical and distributed control systems. While more complex in terms of design, a hierarchical approach features a lower communication bandwidth and more optimal performance compared to a distributed approach. The authors also highlight the superiority of the hierarchical control approach for large-scale MGs, with multiple types of DERs and ESSs.

Birdam et al. [106] further discuss the different approaches used for various layers of a hierarchical control system are discussed, focusing mostly on control techniques for the primary level. The disadvantages of a centralized MG are also highlighted, due to the reduced reliability of a dedicated communication system.

Dou et al. [107] propose a hierarchical control system for the MG, employing a multi-agent based system to solve the economic optimization problem. The complexity of an intelligent hierarchical control architecture is exposed. Multi-agent based system allows for multiple intelligent techniques to be embedded in the control architecture. This approach is further explored and improved on an experimental test-bed [108].

Sahoo et al. [109] perform a literature survey on control techniques for the three MG configurations (i.e. AC, DC, AC-DC). Compared to the AC configuration, control systems for DC and AC-DC MGs are gaining popularity in research. The authors also highlight some of the intelligent techniques that can be used for a centralized secondary control level, that can similarily be adopted for the tertiary. The authors identify IMG control and game theory control techniques as future trends in research of MG control, which need further exploration.

Considering the complexity of hierarchical control design, Mahmoud et al. [110] consider a unique approach by applying system of systems. This approach considers the entire system and not just the individual components. The authors present a framework for treating the microgrid DERs as sub-systems, to ensure the overall system (i.e. microgrid) functions properly. The authors discuss the application of serveral strategies, in light of the framework presented.

2.6 Game Theory

Systems are becoming more complex with every passing day, due to the integration of multiple domains. Multi-objective decision making is an important tool to handle these complex systems. A resilient infrastructure requires quick and effective decision making [16].

A common approach for MG energy management is to use meta-heuristic methods. Meta-heuristic methods include evolutionary algorithms, such as genetic algorithm, particle-swarm optimization, ant colony optimization, and artificial bee colony algorithm. Meta-heuristic methods can be used in a hierarchical control architecture, however due to their centralized implementation they face major disadvantages [105, 111–113]:

— The method is not always going to be able to consider every possible scenario

— The method may converge to a suboptimal control measure

— The method is typically used for offline optimization and require significant computational time

— The computational burden increases when considering multiple objectives, and is typically translated to a single objective problem with fixed, biased weighted coefficients

— The method is typically constrained to a centralized controller, which could encounter communication issues and destabilize the system

— The method becomes more difficult to manage and solve as the MG is scaled, due to increasing number of constraints and decision variables

Fuzzy logic is a commonly used alternative control method for MG coordination [111, 114]. However, Karavas et al. [115] demonstrate that a game theory approach for an energy management system is more efficient in operation compared to a fuzzy logic approach.

Game theory, first introduced in 1944, is the study of multiple players in a game scenario, where each player makes decisions for themselves, while also considering the reactions of other players [116]. Beginning as an economic tool, game theory has since been adopted by a wide range of disciplines in social sciences, science, and engineering. The conceptual framework includes a set of mathematical tools and allows for the study of complex interactions among independent rational players [117]. Unlike meta-heuristic methods and fuzzy controllers, game theory is a distributed

control method.

Two of the major branches of game theory are cooperative and non-cooperative. In a cooperative game, the players form an alliance to find the best solution for the alliance, while non-cooperative games involve selfish players who only consider finding the best outcome for themselves. An emerging research direction is the exchange of energy between DERs, MGs and electric grids, using cooperative and non-cooperative game theory techniques [109, 112, 116, 117].

While game theory has been studied for the purpose of energy trading between IMGs, research has been limited to economic considerations [64, 70, 118–124]. Examples of research related to energy trading between IMGs for economic considerations include:

— Wang et al. [70] use game theory for energy trading between IMGs. Using the diverse supply and load profiles of each MG, game theory is used to achieve a reduction in energy costs. A Nash bargaining mechanism is employed to reach a fair deal for each MG to participate in energy trading.

— Lee et al. [118] develop a trading mechanism to handle the economic considerations of energy trading between IMGs in a competitive market. Game theory is used to maximize the payoff among players.

— In Park et al. [119], energy trading is considered using a trading mechanism, and an allocation policy allocates to consumers the surplus of energy collected by the MGs. This problem is cast as a non-cooperative game in a competitive market.

— Yaagoubi et al. [120] use game theory to study how IMGs can reduce costs from the electric grid and reduce GHG emissions through energy trading. Initially, a centralized optimization problem is cast to provide an optimal configuration of buyers and sellers. This is followed by a non-cooperative game between the buyers, in a decentralized format, to solve the energy trading problem.

— Ni et al. [122] use cooperative game theory techniques to reduce electric grid costs for IMGs. A three-stage algorithm is used to form coalitions between IMGs to exchange energy and incur a transmission fee, which is lower than electric grid fees.

Based on existing literature, it is commonly found that MO decision-making revolves around traditional objectives found in MG research (i.e. economic and environmen-

tal). While there is previous research where game theory is explored in the operation of IMGs, there is little evidence that research has been conducted to apply game theory for resiliency considerations. In addition, there is also scant research available related to the application of game theory in IMGs for railway infrastructures.

Game theory is an ideal tool for IMG coordination, as it can handle multiple conflicting strategies and make effective decisions for each IMG [116]. A multi-objective problem can be translated to a game, where each objective is considered a player. The players are subjected to limited resources as they strive to optimize their standing.

2.7 Microgrid Resiliency

Resiliency is the "the ability to prepare for and adapt to changing conditions and withstand and recover rapidly from disruptions", as defined by 2013 *U.S. Presidential Policy Directive 21* [23]. While many authors provide a varying definition for resilience [16, 22, 125–127], the main themes are captured in *U.S. Presidential Policy Directive 21*. According to authors in [14, 24, 128], resiliency is still a developing research field as it is applied to critical infrastructures (e.g. electric grid, transportation systems). It is a complex attribute, and encompases many considerations and trade offs.

Using the definition provided by the United Kingdom Cabinet Office, resilience encompasses four features: fault tolerance, recovery, fast response and reliability [16]. The directive indicates the embodiment of these features, not just in the design and operation of the electric grid, but in the critical infrastructures the electric grid is requires for support (e.g. telecommunications). A resilient energy infrastructure must be able to handle effectively and quickly handle multiple critical conditions, potentially at the same time.

Sharifi et al. [14] describe four abilities of a resilient energy infrastructure: preparation, absorption, recovery, adaptation. The abilities are further mapped to 17 underlying, non-mutually exclusive, overlapping principles for resilient energy infrastructures: robustness, stability, flexibility, resourcefulness, coordination capacity, redundancy, diversity, foresight capacity, independence, interconnectedness, collaboration, agility, adaptability, self-organization, creativity, equity and efficiency. These principles are not exclusive to energy infrastructures, but all critical infrastructures (e.g. transportation, water, communication).

Francis et al. [125] focus on a framework consiting of system identification, resilience objective setting, vulnerability analysis, and stakeholder engagement. They use the same four abilities as Sharifi et al. [14] to describe infrastructure resilience, and identify 14 classes of resiliency, which must all be considered. With some overlap of the principles identified by Sharifi et al. [14], the classes include maintainability, reliability, flexibility, robustness, secutiy, metrics, natural disasters, sustainability, resourcefullness, knowledge, cross-function, efficiency, proactive measures, and system complexity networks. The authors consider some of these classes to be interconnected, while some are independent considerations.

Matzenberger et al. [129] further defines resilience as a relationship between adaptability and vulnerability. By increasing the adaptability or decreasing vulnerabilities the resilience of the energy system is augmented. Vulnerability is a common theme found in the literature when discussing resiliency.

Many authors indicate in MG research that resilience has been improved, but do not provide any significant metrics to back up their statements, suggesting a need for defined indicators that can be used for resiliency evaluation [22, 23, 125, 130, 131]. It is also commonly stated that resilience is not measured simply through quantitative methods, but is also measured qualitatively [24, 130]. These authors further mention that resiliency analysis must be closely performed with life cycle and reliability assessments. A. Kwasinski [132] further elaborates that the number of dependencies within the MG will affect its resilience, and cautions on the number of metrics used to describe resiliency, since using a set of unique metrics may lead to generalizations, and could omit certain aspects or be insufficient to fully assess the resiliency of the MG and its load(s).

Some authors provide metrics analogous to commonly used reliability metrics. For example, Kwon et al. [23] propose to evaluate the resilience of the MG using a metric analogous to availability, a common reliability metric. Xu et al. [133] propose a vulnerability index, analogous to the reliability metric, to measure the effects of an outage caused by various scenarios, which is introduced in the planning problem of the MG. A descriptive resiliency metric, which defines the amount of electricity not supplied to the customer(s) within a specified period, is proposed by Cano-Andrade et al. [134]. The metric is used in a MO formulation with other reliability, economic, and environmental metrics related to the design of the MG. The authors use fuzzy logic and weighting factors to compute the resiliency index.

Bakke [41] performs a study of the North American electric grid, and the strengths and weaknesses it will face in the 21st century. Without providing specific metrics, her research provides five characteristics of a resilient energy infrastructure considering the surge in electric grid outages due to weather events. They include a diverse supply of energy, inclusion of RESs, adequate flexibility and sizing, and ideal quality to meet the end-user's requirements. Sharifi et al. [14] also mention resource diversification and low-carbon intensity as critical features in a resilient energy infrastructure.

The complexity of MGs and railway infrastructure requires the use of KPIs to assess the resilience of the overall system. A KPI is a measurement of the performance of a system. It is important to derive KPIs that provide the maximum possible of information related to the resilience of the IMGs and railway infrastructure. Therefore, a KPI should meet the following requirements [135]:

— Valid for all configurations and types of railway infrastructures

— Provide a holistic overview of the entire system, any dependencies on subsystems, and cover any specific issues related to the assessment of the system

— Easily quantifiable and justified using scientifically, valid information

— Sufficiently easy to be interpreted by multiple stakeholders with varying backgrounds

— Effective in comparing multiple options to determine an ideal scenario, strategy, or purchase

It is common for resiliency KPIs in research to revolve around the reliability and vulnerabilities of the MG. Many authors consider resilience to be measured using a sub-set of KPIs available in other domains (i.e. economic, environmental, technical, quality) and applying a weighting factor to each sub-category. There are also mixed reviews on using simple KPIs, which can be easily be adopted by industry, and instead, some authors opt for complex strategies to measure the resilience. It is also expressed that resilience is not just a quantitative measurement, but can also be expressed without KPIs through qualitative analysis.

Chapter 3

Proposed Methods and Techniques

It was identified in Chapter 1 that electrified railway infrastructures are an important service but are heavily dependent on the centralized electric grid. Unfortunately, the electric grid is becoming more prone to outages due to various threats and disrupting the reliability of railway infrastructures around the world. An extensive, technical literature review on topics related to the design and control of the MG was presented in Chapter 2. Using this information, this chapter presents the proposed methods and techniques, which will be used to satisfy the objectives of this thesis.

The following is a summary of the proposed methods and techniques:

— An engineering design framework is proposed to improve the resiliency of the energy supply for a mass transit system.

— A proposed set of KPIs, which can be used collectively to evaluate the resilience of the proposed RIMG design and railway infrastructure.

— A methodology is proposed to summarize the requirements of the design of RIMG for a railway infrastructure and translate them to design requirements.

— A new iterative sizing analysis method for the design of the RIMGs is proposed. This method uses multiple resiliency KPIs to understand the trade-offs between the design requirements and expected performance.

— A hierarchical control architecture is proposed, using three levels of control, to manage the operation of the proposed RIMG design.

— Multi-objective decision-making and game theory techniques are proposed, to be implemented in the tertiary level of the proposed control architecture to coordinate the exchange of energy between IMGs.

3.1 Engineering Design Framework

An engineering design framework is proposed in Figure 3.1, to transform an existing mass transit system from its current form to one with a more resilient energy infrastructure to protect itself from various energy threats. This methodology applies a 'systems thinking' approach, where the whole system is considered to solve real-world problems, compared to looking at individual parts [136]. Electrified passenger railway infrastructures will be used to demonstrate the framework in this thesis. Various aspects of the framework are explored in this thesis.

The mass transit system studied in this thesis is passenger electrified railway infrastructures. Case studies are defined and carried out to assess the resilience of the proposed RIMG design and control system. Various types of railway infrastructures which exist in Canada and the United Kingdom, are studied. Using rolling stock data and speed-distance profiles for the railway infrastructures, collected from literature and case study reports, the energy requirements of the rolling stock are determined. Details related to the case studies are presented in Chapter 7.

The resiliency plan for the selected mass transit system is to use RIMGs. These RIMGs will provide a resilient energy supply to the railway infrastructure, which will allow the railway infrastructure to maintain a reliable operation. As part of the resiliency plan, resiliency KPIs are defined in Section 3.2, and, where applicable, assigned targets as part of the requirement analysis in Chapter 4. The risk impact assessment is outside the scope of this thesis.

For a system to meet the customer expectations, it is important to note the customer requirements for the system. The method proposed for the requirement analysis is outlined in Section 3.3, and the results presented in Chapter 4. This involves the review of current railway infrastructures and the requirements of various stakeholders who operate, use, and/or regulate the railway infrastructure and RIMGs. These requirements are then used to derive the design requirements and KPI targets for the proposed target system.

The system design consists of preparing the design of RIMGs, sizing of the system components, and system modelling. The design of RIMGs is presented in Chapter 5. The economic cost analysis is outside the scope of this thesis. The method for the proposed sizing analysis is presented in Section 3.4, and the results for each case study presented in Chapter 8. The piece-wise component modelling of the proposed designs is done using MATLAB, Simulink, and SimPowerSystems software pack-

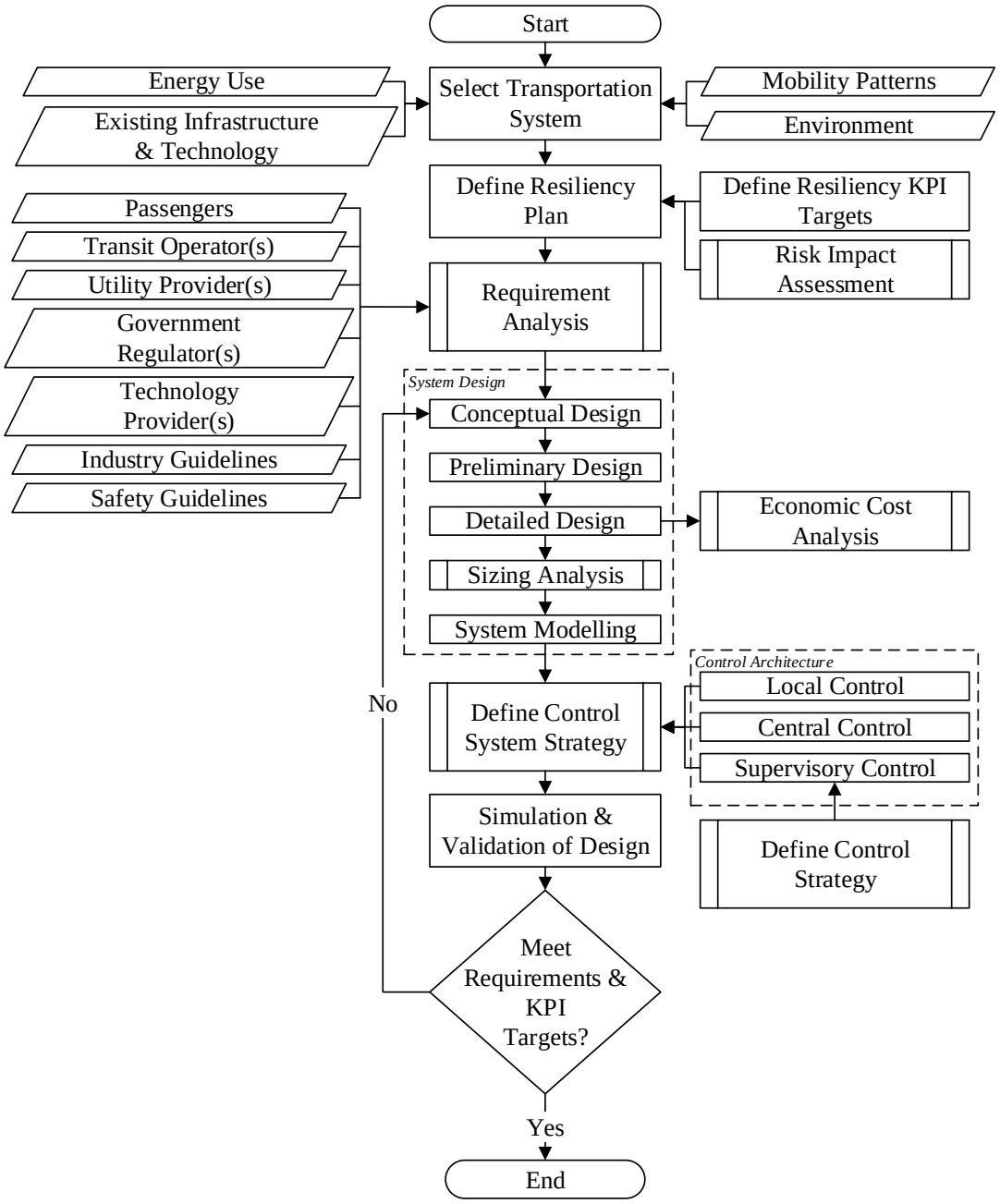

Figure 3.1: Proposed engineering design framework to augment the resilience of a mass transit system

ages [137], and presented in Chapter 6.

Due to the complexity of the proposed RIMG design, an appropriate control architecture is required, as proposed in Section 3.5. A quick, effective decision making tool is required and implemented in the tertiary level of the proposed control architecture. The tool has been proposed to solve the multi-objective problem of minimizing the dependence of the electric grid for each IMG using game theory.

The techniques proposed for the tertiary level are presented in Section 3.6.1 and Section 3.6.2. Further details and implementation of the proposed control strategies and architecture are presented in Chapter 5.

Using the proposed methods and designs, the RIMG model is simulated and verified using the case study information. For each case study, the results are presented in Chapter 8.

After the design phase is complete and validated, the project would proceed to the following phases: (1) implementation, integration and testing, and (2) operation and maintenance. These phases are outside the scope of this thesis.

3.2 Resiliency Key Performance Indicators

The complexity of RIMGs requires the use of KPIs to assess the resilience of the overall system. A KPI is a measurement of the performance of a system. It is important to derive KPIs that provide the maximum possible of information, related to the resilience of the IMGs and railway infrastructure.

Figure 3.2 shows the relationship between resiliency and commonly used KPIs. With an understanding of resiliency, previously outlined in Chapter 1, a set of resiliency KPIs can be derived from the principles of resiliency. Socio-cultural, economic, environmental, reliability, or technical KPIs are ideal to assess the resilience of a system, in addition to newly formed indicators, which are applicable to IMGs and railway infrastructure. These KPIs must meet the requirements of an effective KPI, outlined in Figure 3.2.

The configuration of each IMG will dictate the set of KPIs that are applied to measure resilience. For example, if no DER in the IMG depends on a fossil fuel source, then environmental KPIs are negligible. A static KPI is based on the design, configuration or a snapshot of the IMG performance, whereas a dynamic KPI varies with operation time.

In this thesis, in addition to any qualitative analysis, a specific set of KPIs are adopted. The set can be used to analyze the static and dynamic performance of the IMG and railway infrastructure, as well as assess the resilience of the proposed design. The set is applied to each IMG individually.

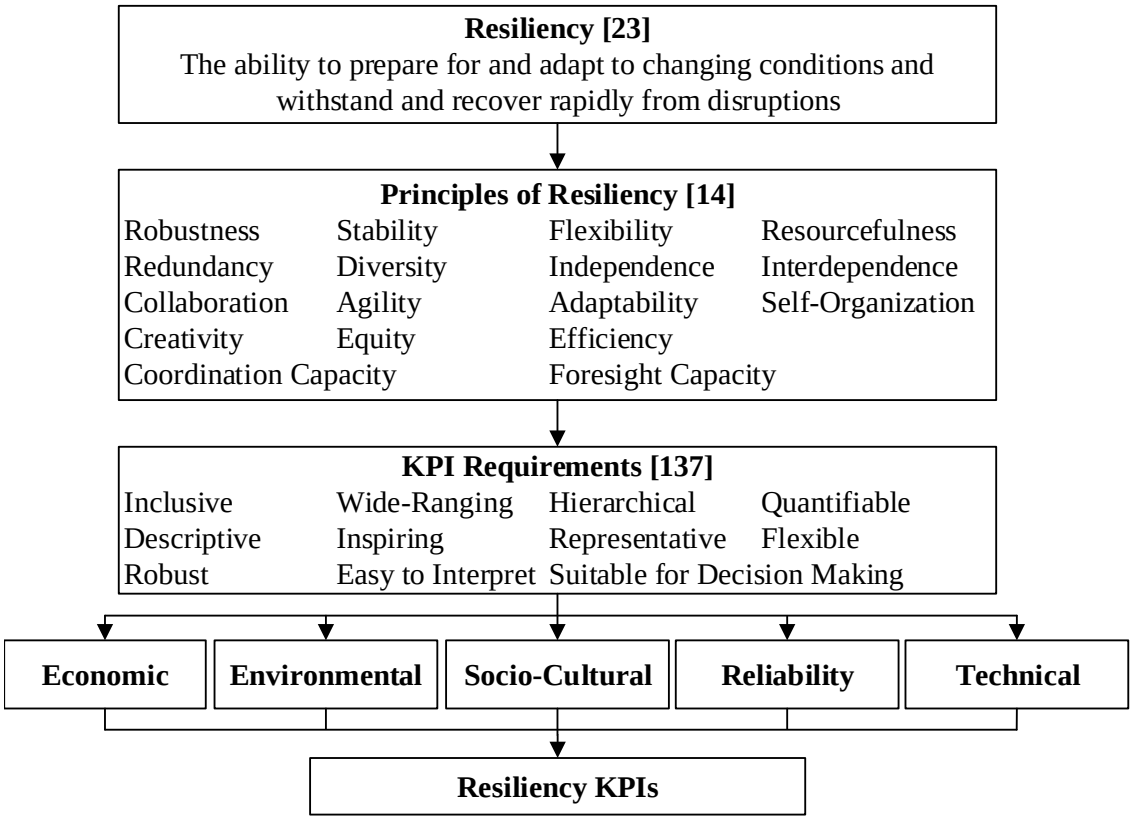

Figure 3.2: Relationship between resiliency and commonly used KPIs to evaluate the resilience of IMGs

IMG Diversity of Supply: is defined as the diversity of the energy supply to meet the demand. It is measured using the Shannon-Wiener index [138]. The higher the value, the more diverse the IMG is and less vulnerable to shortage in fuel supply or other applicable threats. Diversity of supply is a static KPI, which is used in the design stage of the IMG. Diversity of supply does not consider the nominal capacity of an ESS, since the ESS does not augment the diversity of supply of the IMG. The ESS allows the IMG to store excess energy, which can be used in times of an IMG generation shortage or when the IMG operates in island mode. This KPI is measured for each IMG individually.

$$KPI_{DoS} = -\sum_{i=1}^{N_{DER}} p_i \ln p_i \tag{3.1}$$

IMG Renewable Generation: provides a percentage of renewable energy generation within each IMG [135]. The inclusion of renewable generation results in less GHG emissions and less dependency on a fuel source, which may have its supply chain compromised during an energy threat. This KPI is measured for each IMG individually.

$$KPI_{RG}(t) = \frac{E_{RES}}{E_{sys}}, \forall t \epsilon T \tag{3.2}$$

IMG Supply: is defined as the sum of generation for the IMG to satisfy the demand. It includes the generation of each DER, energy discharged by each ESS, and energy imported by each IMG over time. This KPI improves on the KPI suggested by Honarmand [139], by translating the KPI from a static indicator to a dynamic indicator. This KPI is measured for each IMG individually.

$$KPI_{IMGS}(t) = \sum_{i=1}^{N_{DER}} P_{DER_i}(t) + \sum_{j=1}^{N_{ESS}} P_{ESS_j}(t) + \sum_{k=1}^{N_{IMG}} P_{\delta_k}(t), \forall t \epsilon T \tag{3.3}$$

IMG Demand: is defined as the sum of the demand of the IMG and any exports from the IMG to another IMG over time. This KPI improves on the KPI suggested by Honarmand [139], by translating the KPI from a static indicator to a dynamic indicator. This KPI is measured for each IMG individually.

$$KPI_{IMGD}(t) = \sum_{i=1}^{N_{load}} P_{load_i}(t) + \sum_{j=1}^{N_{IMG}} P_{IMG_j}(t), \forall t \epsilon T \tag{3.4}$$

IMG Demand Served: is defined as the ratio of IMG supply (Equation 3.3) to IMG demand (Equation 3.4), and whether the IMG can support itself over time. A result of one or higher is desired, since a performance of less than one indicates the IMG requires support from the electric grid. This KPI improves on the KPI suggested by Honarmand [139], by translating the KPI from a static indicator to a dynamic indicator. This KPI is measured for each IMG individually.

$$KPI_{DS}(t) = \left| \frac{KPI_{IMGS}(t)}{KPI_{IMGD}(t)} \right|, \forall t \epsilon T \tag{3.5}$$

IMG Reliance: is analogous to the level of autonomy metric suggested by Chauhan et al. [94]. This dynamic KPI is used to inform the operator by how reliant any IMG is on other IMGs to supply a deficit between the supply and demand, over time. This metric is important to understand how dependent certain IMGs may be on others, indicating improper sizing of the IMG, or a consistent dependence due to component or system failures. This KPI is measured for each IMG individually.

$$KPI_{IMGR}(t) = \frac{\sum t_{IMGR}}{T}, \forall t \epsilon T \tag{3.6}$$

IMG Electric Grid Dependence: is analogous to the level of autonomy metric suggested by Chauhan et al. [94]. This dynamic KPI measures the amount of time the IMG relies on the electric grid to supply the deficit between supply and demand, or when the railway infrastructure has excess, recovered energy from braking that cannot be stored in an ESS or exported to another IMG. The dependency ratio of

the IMG on the electric grid is crucial to understanding how likely it is that the demand will not be served if the IMG must island itself. The higher the KPI, the less effective the IMG is to serve the demand in times of emergency operations. This KPI is measured for each IMG individually.

$$KPI_{GD}(t) = \frac{\sum t_{GD}}{T}, \forall t \epsilon T \tag{3.7}$$

3.3 Requirement Analysis Methodology

Quality function deployment is an ideal, systematic tool to map qualitative, customer requirements to technical, quantifiable and measurable requirements. The three main objectives of quality function deployment are to (1) prioritize customer needs (2) translate customer needs into technical specifications and (3) design a system, which focusses on customer satisfaction. Putting together a house of quality is an important phase in the quality function deployment process. The process adoptd in this thesis is a modified version of the one offered by AUT University, as outlined in Table 3.1 [140].

3.4 Interconnected Microgrid Sizing Analysis

As previously indicated by Bakke [41], proper sizing of the MG is required to augment its resilience, as well as a diverse supply of energy, including renewable energy sources (RES). Proper sizing of the IMG to meet the demand of the railway infrastructure will allow for improved resilience, reduced cost, better efficiency and a prolonged life cycle of the overall system. Extensive research has taken place with respect to sizing of the MG and individual components, as discussed in Section 2.4. However, little research has been performed for ideal sizing methods of the IMG under resiliency and interconnection considerations.

Figure 3.3 depicts a proposed iterative sizing analysis to size the IMGs. In this analysis, a trade-off is made between maximizing the diversity of supply, minimizing the electric grid dependence, and minimizing the IMG reliance of each IMG. Diversity of supply, electric grid dependence, and IMG reliance KPIs are used to assess the resilience of the energy supply for railway infrastructures. IMGs are sized simultaneously to understand how the sizing of one IMG may affect the performance of another.

The key inputs for the sizing analysis include:

Table 3.1: Quality function deployment process to perform a requirements analysis and form a house of quality

Step 1	**Customer Requirements** Identify who the customers are, gather information from the customers on the requirements they have for the system.
Step 2	**Regulatory Requirements** Determine requirements that may be imposed by regulatory bodies, which are unknown to the customer.
Step 3	**Customer Importance Ratings** On a scale from 1 (low) to 5 (high), rate the importance of each requirement.
Step 4	**Technical Descriptors** Attributes about the product which can be measured and benchmarked. Descriptors can be predefined metrics or newly formed metrics which can be used to ensure the system meets the customer requirements.
Step 5	**Relationship Matrix** Relationship is made between the customer requirements and technical descriptors. Relationships can be strong negative, weak negative, weak positive or strong positive.
Step 6	**Target Values for Technical Descriptors** Target values represent "how much" for the technical descriptors and can then act as a base-line to compare against when the design is complete. The technical descriptors will be translated into the design requirements.
Step 7	**Correlation Matrix** Examine how each technical descriptor impacts each other. Relationships can be strong negative, weak negative, weak positive or strong positive.

— Weather resource data (solar irradiance, wind speed, and temperature)

— Route profile data for the rolling stock (speed-distance profile, gradient)

— Technical parameters of the rolling stock (i.e. rolling stock and passenger masses, rotary allowance, Davis coefficients, drive-train and regenerative braking efficiencies, and auxiliary power)

— Technical parameters of solar PV, wind turbine, and the ESS (e.g. nominal capacity, efficiency)

The key outputs of the sizing analysis include:

— Various resiliency metrics (i.e. IMG diversity of supply, IMG reliance, and IMG electric grid dependence) that represent the system for the selected nominal capacities of the DER technology (i.e. solar PV and wind turbine)

The scope of this thesis involves the sizing of the DERs. An ESS is sized to demon-

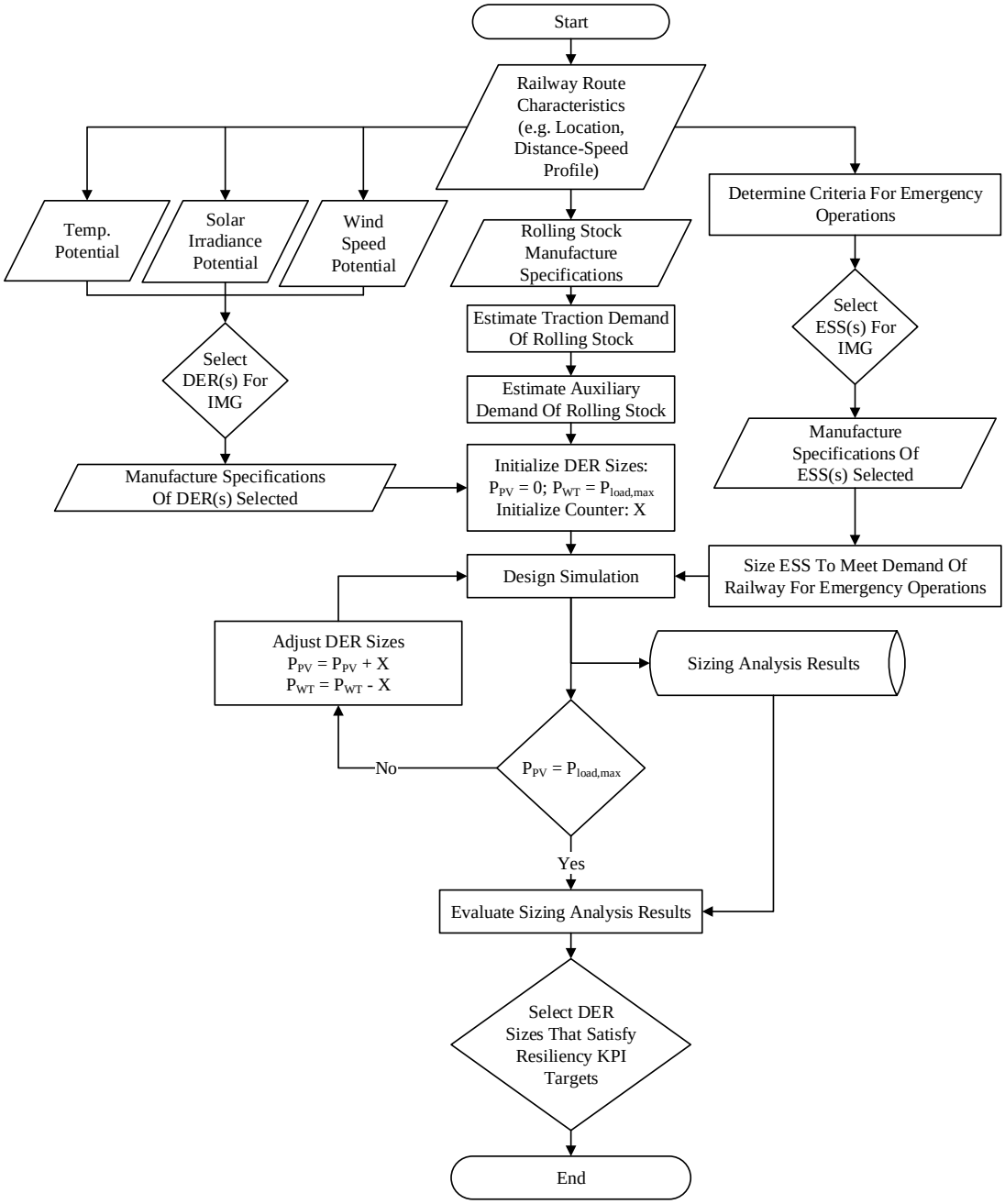

Figure 3.3: Proposed IMG sizing analysis using resiliency KPIs

strate its importance within the IMG to store recovered energy when the rolling stock is braking, as well as when a DER generates a surplus of energy. The ESS reduces the dependence of the electric grid to export recovered energy and avoid dissipating the energy on resistor banks. Sizing of an ESS to satisfy resiliency objectives is considered for future work. The implementation of the sizing analysis in MATLAB is available in Appendix B. The results for each case study using the proposed sizing analysis are presented in Chapter 8.

3.5 Interconnected Microgrid Control Architecture

A control system is an integral component of the proposed RIMG design, due to integration of multiple DERs and ESSs, intermittent renewable generation, and varying load profiles. When interconnecting multiple MGs together, the control system becomes even more critical to the operation of the railway infrastructure. The control system improves the resilience of the IMGs, since it can react quickly to sudden, unexpected disturbances.

Figure 3.4 illustrates the proposed control architecture for the proposed design of RIMGs. Each IMG operates separately from one another, and do not communicate with each other. The secondary level makes most decisions for each IMG. These decisions are executed at the primary level. The tertiary control level monitors the resiliency KPI(s) and can adjust the IMGs performance as required. Details related to the implementation of each level of the control architecture are further discussed in Chapter 5.

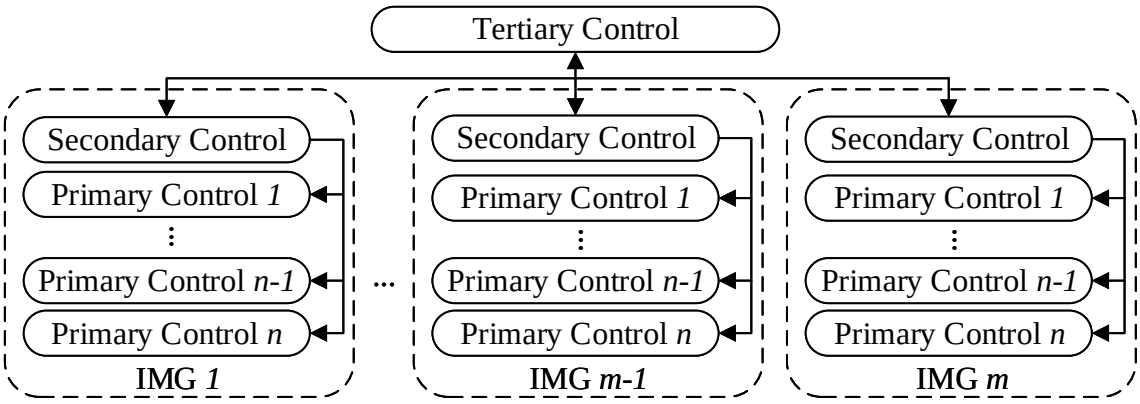

Figure 3.4: Proposed control architecture for IMGs, where the tertiary control layer will monitor all m IMGs, and each IMG has a secondary control layer regulating its own n primary control layers

3.6 Interconnected Microgrid Supervisory Control Algorithm

The tertiary control layer of the proposed control architecture will monitor all the IMGs in the system. As such, the tertiary control layer will need to be able to quickly resolve multiple objectives at the same time. Multi-objective design and game theory are proposed techniques for a decision-making tool to be implemented. A multi-objective problem can be translated to a game, where each objective is considered

a player. The tool will coordinate the exchange of energy between IMGs to ensure a resilient energy supply for the railway infrastructure. Implementation of multi-objective design and game theory in the tertiary control level of the hierarchical control system is presented and discussed further in Chapter 5.

3.6.1 Multi-Objective Design

A multi-objective problem exists when there are conflicting objectives that must be solved simultaneously [141]. Each IMG has its own set of objectives, leading to a multi-objective situation. The objective function of a multi-objective problem is formulated as:

$$min[f_1(P), ..., f_k(P)], k \geq 2 \tag{3.8}$$

subject to the following constraints:

$$h_i = 0, i = 1, 2, ..., q \tag{3.9}$$

$$g_j \leq 0, j = 1, 2, ..., p \tag{3.10}$$

$$p_i^{min} \leq P_i \leq p_i^m ax, \forall i = 1, ..., N \tag{3.11}$$

The conflicting objective functions, f_k: $\mathbb{R}^n \rightarrow \mathbb{R}$, must be solved simultaneously. A decision vector, $P=(P_1,P_2,\ldots,P_N)$, is optimal if nothing can be improved without deterioration of any other aspect. The solution of the multi-objective problem, solved with game theory, is used to determine a power output vector, P, which will provide the WT export set-point for each IMG, such that the overall demand of the railway infrastructure is served.

3.6.2 Bimatrix Games

A cooperative game is one where the players, i.e. individual MGs, can coordinate their strategies to achieve the best outcome for the group. A coalition is formed when two or more players can agree to coordinate their strategy. A bimatrix game is a two-player cooperative game, using a finite set of pure strategies [142]. A bimatrix game has the following structure: $\Gamma = \langle P,S,U \rangle$, where:

— The number of players is determined by $P = \{1,2\}$

— Each player has its own finite strategy set $S = \{s_1,s_2,\ldots,s_m\}$

— Each player selects a strategy, and the payoff for each player is determined using the payoff functions $U=\{u_1(s_i,t_j),u_2\ (s_i,t_j)\} = \{a_{ij},b_{ij}\}$

The values of the payoff functions form a bimatrix, illustrated in Table 3.2 [142].

The strategy set that has the higher probability of selection is used to determine whether the tertiary level of control adjusts the performance of one IMG to assist the other IMG. The scope of this thesis will demonstrate the effectiveness of the proposed algorithm considering only two players. The work is scalable to include multiple players, without any significant burden on computation time.

Table 3.2: Sample payoff matrix for a two-player bimatrix game

		Player 2			
	Strategy	t_1	t_2	...	t_n
Player 1	s_1	(a_{11},b_{11})	(a_{12},b_{12})	...	(a_{1n},b_{1n})
	s_2	(a_{21},b_{21})	(a_{22},b_{22})	...	(a_{2n},b_{2n})
	$\vdots$	$\vdots$	$\vdots$	$\vdots$	$\vdots$
	s_m	(a_{m1},b_{m1})	(a_{m2},b_{m2})	...	(a_{mn},b_{mn})

Chapter 4

Requirement Analysis for Proposed Design

The requirement analysis is the collection of requirements, marketing and engineering, for the design of RIMGs. Requirements are abstract, verifiable, unambiguous, traceable, and realistic. In this chapter, the target system is described, followed by an analysis of the requirements for the stakeholders. Varying requirements must be met for passengers, railway operator, regulators, utilities and technology providers. The list of requirements is then transformed into a house of quality to determine design requirements. The requirement analysis will follow the method proposed in Section 3.3.

The scope of this thesis involves the design of a RIMGs for reliable railway operations and includes a limited number of stakeholders. The requirements listed below are limited to this thesis and revolve around what is necessary to provide resilient energy to the railway infrastructure. In the future, the scope of the analysis can be expanded to a larger set of stakeholders and a complete set of requirements related to the railway electrification system, signalling and communication systems, rolling stock monitoring systems, and rolling stock maintenance facilities.

4.1 Target System Design

The target system design includes a proposed design of RIMGs for an AC railway electrification system. Electric traction power is supplied to each rolling stock from wayside TPSs through an overhead contact system. A pantograph collector on each rolling stock maintains contact with the overhead system. The TPS will receive energy from multiple DERs and ESSs, which constitutes a MG, and also import or

export energy from/to the electric grid. Each individual MG is arranged in a hybrid AC-DC configuration. Each MG is interconnected through the existing traction power distribution system, so that each IMG can supply energy to another IMG to reduce the railway infrastructures dependence on the electric grid. A hierarchical control system will monitor the performance of each IMG and make quick, effective decisions to maintain the reliability of the railway infrastructure.

When dealing with railway electrification systems, the system must be maintained with a reliable energy source. During normal operation, where a stable connection to the electric grid is maintained, the IMGs can operate in parallel and accrue some benefits. Each IMG can store energy in the ESS(s), provide energy to an IMG, or sell the excess energy to the electric grid at competitive rates. The ESS can be used for situations where buying electricity from the electric grid may be prohibitive, reducing the demand charge of the electric grid, or it can be relied on during emergency situations. During emergency situations, energy is required for more than just the rolling stock, but to also support the critical, non-traction loads such as a railway stations, signaling and communication systems. This thesis will focus on providing energy to the traction power substations to allow the rolling stock during normal operation.

The requirement analysis emphasizes the incorporation of resilience within the design of interconnected microgrids. Figure 4.1 depicts the proposed target system design for sustained railways. The traction electrification system must supply sufficient power to each rolling stock to provide safe, efficient, and continuous operation of the entire railway infrastructure. Design of the target system is coordinated amongst the appropriate stakeholders in the project.

4.2 Stakeholder Information

The stakeholders must first be identified to understand what is required in the design of the target system. The stakeholders are those who are directly involved in the lifecycle of the target system. In the scope of this thesis, the stakeholders include the passengers, railway operators, regulators, electric utility providers and technology providers. The stakeholders can provide their requirements through many forums, including discussion, research, and technical analysis [143].

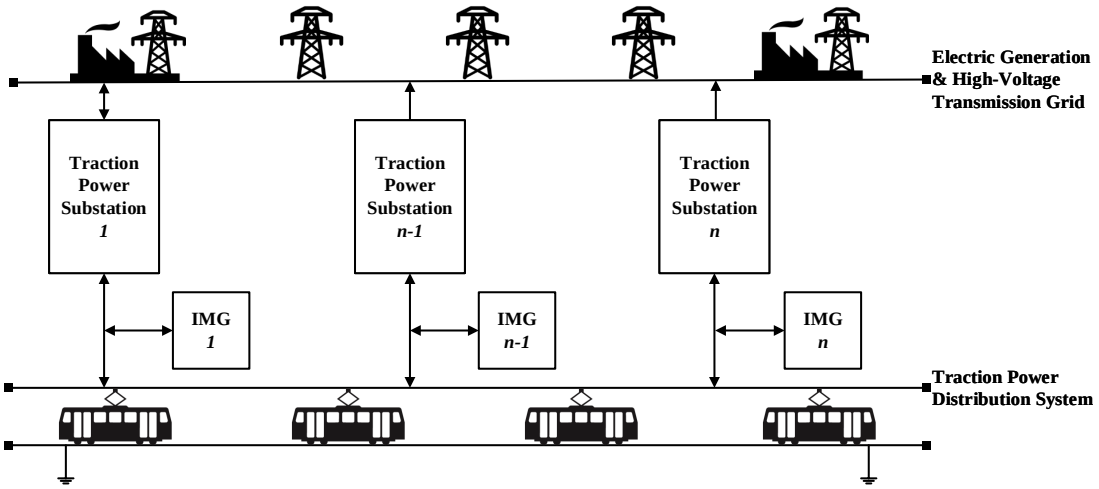

Figure 4.1: Target system consisting of n RIMGs integrated at each TPS along the railway corridor

4.3 Passenger Requirements

A passenger is anyone who uses the railway infrastructure for travel, either for personal or business purposes. Passenger requirements, listed in Table 4.1, are simply features to make the mass transit system attractive to people on an individual level.

4.4 Railway Operator Requirements

The railway operator is the entity that owns and operates the railway infrastructure within the specified region. The railway operator will have a list of requirements to maintain operation of the infrastructure during normal and emergency situations. The requirements of the railway operator are listed in Table 4.2.

4.5 Regulator Requirements

Regulation requirements are rules, regulations, and laws that an organization, system or user must follow in order to comply with local, state, and federal governments. The railway operator will also need to comply with standards, regulations and laws administered by both domestic and international agencies. Regulations and standards imposed on railway infrastructures vary from country to country.

Using Canada as an example, railway operators must consider regulations imposed by Transport Canada, the Canadian Transportation Agency, the Railway Safety Act, and the Railway Association of Canada. The main purpose of these standards,

Table 4.1: Summary list of passenger requirements for the proposed target system of RIMGs for reliable mass transit systems

Number	Requirement
Req. 4-1	Passengers strongly desire the shortest travel time. Passenger demand needs to be met with an appropriate combination of headway between rolling stock, rolling stock speed, passenger seating and rolling stock lengths.
Req. 4-2	Transit routes and services responsive to passenger travel patterns. Variation in stopping patterns should be minimized to avoid passenger confusion.
Req. 4-3	The rolling stock must operate at speeds that maintain passenger comfort and security.
Req. 4-4	Service should be configured for routes designed to provide a one-seat ride for the greatest number of passengers.
Req. 4-5	Passengers desire the rolling stock to be properly heated, cooled, and ventilated, adequate combination of natural and artificial lighting, and external sound and vibration minimized.
Req. 4-6	Regenerative braking effect should not be noticeable by the passenger.
Req. 4-7	Passengers desire the railway infrastructure to be operational, accessible, and experience minimal downtime during normal and emergency situations.

regulations and laws is to make the railway infrastructure safe, secure, accessible, and environmentally responsible. CSA3 C22.3 No. 8-M91 Railway Electrification Guidelines provide a set of standards, which can be applied to the design, maintenance and quality of an electrified railway infrastructure. It is also important to note that many standards and regulations for railway electrified systems are developed by international organizations. The American Railway Engineering and Maintenance-of-Way Association (AREMA), located in the United States, is the primary association which recommends design and maintenance standards for railway infrastructures in North America. In Canada, AREMA standards are enforced by Transport Canada. It is important to note that the standards, regulations and laws enforced by one country, many not be enforced in another country. When applying the proposed engineering design framework to an existing railway infrastructure, it is important to consider the specific expectations for relevant countries.

In Canada, all materials, apparatus and equipment, installation methods, and testing must conform to the requirements of the applicable portions of the latest edition of IEC, ANSI, NEMA, CEC, NFPA, NESC, IEEE, UL, ICEA, ASTM and CSA. Other standards may be enforced depending on the location of the railway infrastructure, creating more requirements to be considered for the design and operation of the IMGs and railway infrastructure.

Table 4.2: Summary list of railway operator requirements for the proposed target system of RIMGs for reliable mass transit systems

Number	Requirement
Req. 4-8	Provide a safe, secure, reliable, and convenient service within the operating region.
Req. 4-9	Meet the demand of population growth and work travel times within the operating region.
Req. 4-10	Minimize the operating costs associated with the delivery of transit services, so that rider fees can be minimized to attract riders.
Req. 4-11	Maintain a geographic information system (GIS) to maintain the functionality of all equipment required to operate the railway infrastructure.
Req. 4-12	Maintain reasonable speeds to minimize passenger travel time and ensure safety considerations. The speed limitations imposed on the rolling stock will depend on local, state and/or federal laws and regulations.
Req. 4-13	The perimeter of the railway infrastructure must be secured from passenger traffic to avoid trespassing and protection of infrastructure.
Req. 4-14	Operations should be planned to assume on-time performance of at least 95% during peak service periods, and 97% during off-peak service periods [144].
Req. 4-15	Response time to an emergency should occur within less than 15 minutes [144].
Req. 4-16	For satisfying operational-related reliability criteria, each TPS must be designed with sufficient capacity, redundancy, and reliability to support peak period operations under normal and emergency operating conditions.
Req. 4-17	The number of TPSs, and IMGs should be minimized to reduce capital investment. The location of said systems should be optimized with respect to system safety, performance, and efficiency targets. Right-of-way availability, substation site availability, stray current control, life cycle cost, and interconnection to the electric grid should also be considered when determining the number of systems required.
Req. 4-18	If a TPS, or its applicable IMG, is out-of-service for any reason, nearby TPSs and IMGs should be able to provide adequate energy to maintain railway operations.
Req. 4-19	A centralized control system is required to monitor, display, control and report all information related to the rolling stock demand, DER generation of energy in each IMG, state of charge of each ESS, connection to the electric grid, and any other pertinent information related to energy use in the railway infrastructure.

One important consideration that must be made worldwide in the 21st century is the reduction of GHG emissions. Any design should strive to minimize the emission of GHG emissions and air pollutants, such as, carbon dioxide, carbon monoxide, nitrogen dioxide, sulfur dioxide, and particulate matter. The reduction of these pollutants allows for a better quality of air and will reduce the likelihood of acute and chronic health effects for those who use, operate, and/or live in proximity to the railway infrastructure.

When an IMG has a surplus of energy, which cannot be stored in an ESS or shared with another IMG, the energy may be sold back to the electric grid. For example, in Ontario, Canada net metering is available for any project size, and the energy exported will be credited at the same rate it was purchased from the electric grid [145]. Ontario's Independent Electric System Operator (IESO) sets the export limits for each DER type, which the MG control system must regulate using a set-point for the local control of the DER.

If the rolling stock has regenerative braking technology, energy recovered by the railway can also be exported to the electric grid. Typically, this is a secondary use of recovered energy. The first priority is to use it locally by either storing it in the ESS or sharing it with an IMG. Any energy recovered that cannot be used within the IMG and overall railway infrastructure would be exported to the electric grid, and also fall under the net metering concept.

4.6 Utility Requirements

Utilities include the electric grid generation, transmission and distribution operators, water utilities, gas companies, and telecommunication providers. Utility requirements are those that the utility must meet in order for the proposed design of RIMGs and railway infrastructure to be implemented and operate successfully. Table 4.3 provides a list of requirements that the electric grid operators must meet for the design and operation of the railway electrification system, and RIMGs.

The electric utility operator must provide a reliable connection between the electric high-voltage grid and the railway traction electrification system. Many existing electrified networks connect to the electric grid using a 115 kV or 230 kV three-phase connection (the choice of frequency depends on country standards). The electric utility operator must impose limitations on the minimum and maximum voltage

Table 4.3: Summary list of utility requirements for the proposed target system of RIMGs for reliable mass transit systems

Number	Requirement
Req. 4-20	The electric utility company must provide each TPS 3-phase, 230 kV, 60 Hz power [147].
Req. 4-21	Each TPS will be integrated with an IMG to ensure a resilient source of energy to the rolling stock.
Req. 4-22	The railway load will be served by single-phase, 25 kV, 60 Hz power [147].
Req. 4-23	Total harmonic distortion (THD) will be minimized and kept within reasonable limits as mandated by IEEE 519-1992 [148].
Req. 4-24	The nominal capacity of an IMG cannot be greater than 10 MVA, as mandated by IEEE 1547 [128].
Req. 4-25	Losses in transmission must be minimized so as not to increase operating costs and effect power quality [12].
Req. 4-26	The proposed design will consider options that reduce the need for the electric utility to make infrastructure improvements.
Req. 4-27	Each IMG must be able to handle a disconnect from the electric grid as required either by the electric grid or IMG operator using a static switch.
Req. 4-28	Each TPS must be equipped with revenue metering to provide information on AC line current, AC bus voltage, active and reactive power measurements, and power factor [149].
Req. 4-29	Provide a favorable rate schedule and tariffs to the railway operator. The electric grid will impose a demand charge on the railway operator.
Req. 4-30	The electric grid distribution system should be designed to be flexible, capable of accommodating future additional loads, and easily and economically maintained [41].
Req. 4-31	The electric grid distribution system design must take advantage of the intermittent operation and any applicable load diversity factors in rating feeders and equipment [41].

Table 4.4: AREMA 25 kV railway traction electrification system voltage limits

System Requirement	Voltage (kV)
Traction power substation input voltage	230
Traction power substation normal upper output voltage limit	27.5
Traction power substation no-load output voltage	26.25
Traction power substation nominal output voltage	25.0
Traction power disribution system normal lower voltage limit for all systems in service	20.0
Traction power disribution system emergency minimum operating voltage for outage conditions	17.5

levels of the load to ensure a safe and efficient operation of the railway infrastructure. AREMA specifies the system voltage limitations for an electrified rail network

using a 230 kV input voltage from the electric grid, listed in Table 4.4 [146].

4.7 Technology Provider Requirements

Technology providers include DER, ESS, power electronics, rolling stock, and energy management control system manufacturers. Table 4.5 provides a list of requirements that technology providers will need to meet for the design and operation of RIMGs to sustain the railway infrastructure.

4.8 House of Quality

A house of quality is used to convert the qualitative function requirements expressed in Table 4.1 - Table 4.5, into quantitative requirements that can drive the design of the RIMGs, as well as any modifications to the electric railway infrastructure. Figure 4.2 depicts the house of quality, the direct result of the requirements analysis. The result of the house of quality leads to ten design requirements for the proposed design of RIMGs. The design requirements are summarized in Table 4.6.

4.9 Control System Requirements

In the requirement analysis for the proposed RIMG design, design requirement 4-10 indicated a hierarchy control system is implemented to control the IMGs. A hierarchical control system is desirable for IMGs since the control system can be divided into individual layers to manage the DERs and ESSs properly. Before a control architecture can be implemented, the requirements of the control architecture must first be established. The requirements will list what is required of each level of control, and any constraints and assumptions that must be followed. The list of control requirements has been summarized in Table 4.7.

Table 4.5: Summary list of technology provider requirements for the proposed target system of RIMGs for reliable mass transit systems

Number	Requirement
Req. 4-32	Low propagation delay between DER and ESS measurement systems, and their respective controllers [150].
Req. 4-33	Efficient operation of all components, with reduced losses, minimal THD, and high reliability [149].
Req. 4-34	The rolling stock must use an optimized combination of acceleration, deceleration, and maximum operating speed sufficient to provide passengers with a high degree of ride comfort and the fastest possible travel time.
Req. 4-35	The rolling stock must be equipped with regenerative braking capability.
Req. 4-36	The rolling stock must be equipped with appropriate HVAC equipment to meet heating, cooling and ventilation demands (season and location dependent). ASHRAE Standard 37 or equivalent should be used as a benchmark [149].
Req. 4-37	The design service life of all components and systems should be maximized to reduce replacement costs.
Req. 4-38	To handle the large demand of the railway infrastructure, all transformers and power substations need to be capable of handling a load of 15 MVA or higher, depending on spacing between each TPS. The size of the equipment can be reduced when placed within closer proximity to the electrified railway, but this could result in higher acquisition and operating costs.
Req. 4-39	One issue with railway electrification is the consistently transient nature of the demand. At any point in time a rolling stock may be accelerating, cruising or braking. When multiple rolling stock are in operation this creates a variation in demand throughout the network. The traction equipment (i.e. IMGs, TPSs, traction distribution systems) need to be sized to handle the large peaks in demand of the rolling stock. This may result in equipment being oversized, which will lead to higher costs. It may also result in equipment only being fully utilized for a small percentage of its operating time.

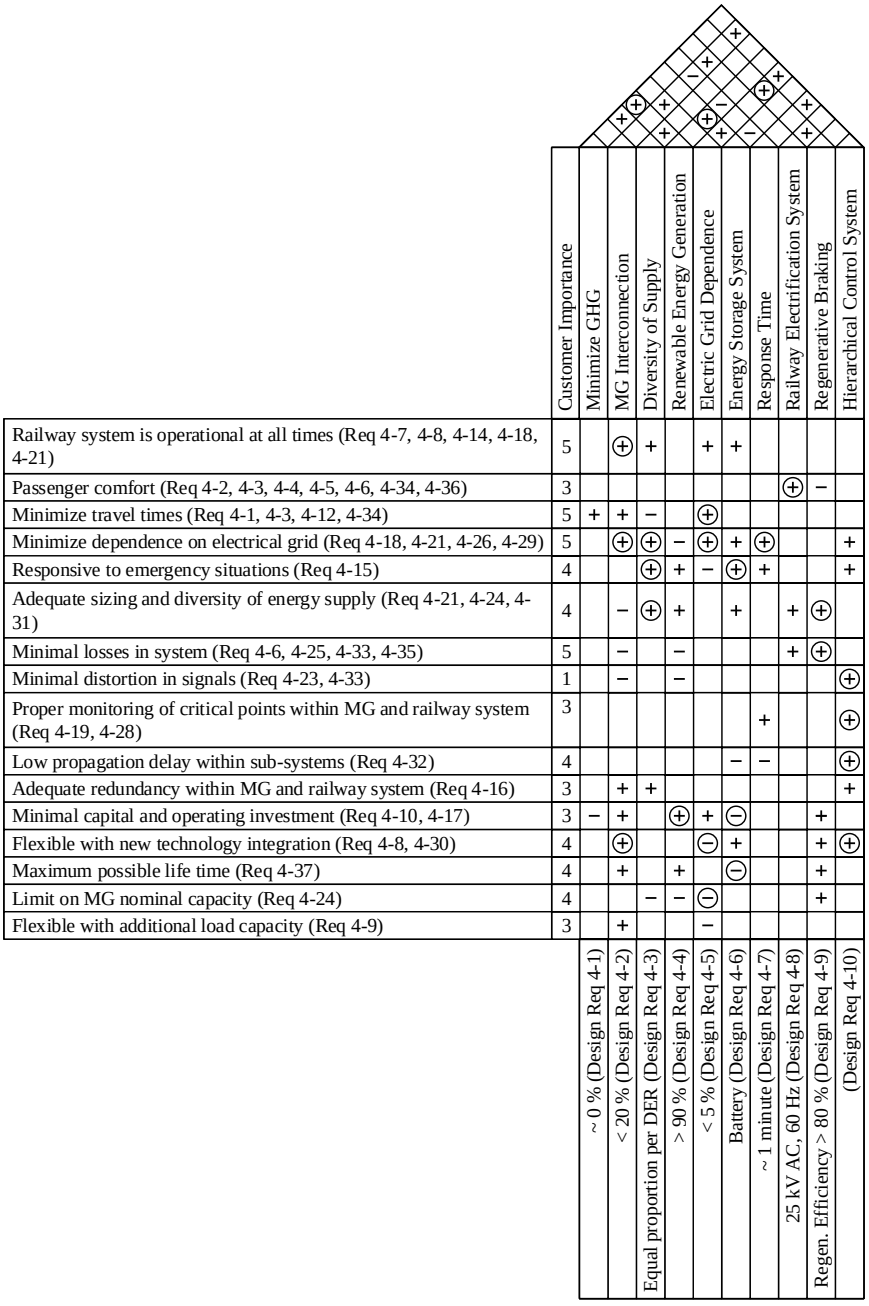

Figure 4.2: House of quality to translate the requirements of the stakeholders to design requirements for the proposed target system of RIMGs for reliable mass transit systems

Table 4.6: Summary of design requirements for the proposed target system of RIMGs for reliable mass transit systems

Number	Requirement
Design Req. 4-1	GHG emissions generated from DERs are approximately 0% [6].
Design Req. 4-2	IMG reliance (KPI_{IMGR}) is less than 20% per IMG [130].
Design Req. 4-3	Diversity of supply (KPI_{DoS}) is maximized for each IMG, with equal proportion per DER [41].
Design Req. 4-4	RES generation (KPI_{RG}) within each IMG is greater than 90% [41].
Design Req. 4-5	Electric grid dependence (KPI_{GD}) for each IMG is less than 5% [144].
Design Req. 4-6	A battery is used as the energy storage system.
Design Req. 4-7	Response time of the system must be less than 1 minute to changes [150].
Design Req. 4-8	The electric utility company must provide each TPS 3-phase, 230 kV, 60 Hz power. The railway load will be single-phase, 25 kV, 60 Hz power [149].
Design Req. 4-9	Regenerative braking efficiency, η_{regen}, is greater than 80% [151].
Design Req. 4-10	A hierarchical control system is used to manage the flow of energy between IMGs.

Table 4.7: Summary list of control system requirements for the proposed target system of RIMGs for reliable mass transit systems

Number	Requirement
Req. 4-40	A three-level control architecture: — Primary level: accommodate the local power converters for each DER and ESS — Secondary level: regulate the DER and ESS set-points (using information measured within the IMG, and requests from the tertiary level) and determine the flow of energy within the IMG — Tertiary level: monitor the state of all IMGs and facilitate the exchange of energy between IMGs
Req. 4-41	The secondary level will need to receive measurements regarding the generation of each DER, the SOC of each ESS, and the demand of the railway infrastructure.
Req. 4-42	The secondary level will need to formulate a set-point for each DER and ESS, based on a control strategy and methodology.
Req. 4-43	The secondary level will determine the flow of energy within the IMG. Switches will be used to direct energy from a bus to either the railway load, the electric grid, or both [54].
Req. 4-44	The energy used to meet the demand from each bus (AC, DC, electric grid) must be measured to account for economic costs, and to verify the demand is being served.
Req. 4-45	Each DER and ESS controller must track their given set-point value and ensure any oscillations are properly damped [152].
Req. 4-46	DERs must be able to accommodate sudden active power imbalances, either excess or shortage, keeping frequency and voltage deviations within acceptable ranges [54].
Req. 4-47	Changes in demand may occur quickly. At the primary level, each local controller must be capable of responding to a set-point change within milliseconds. The secondary and tertiary levels must be able to respond to changes within seconds [153].
Req. 4-48	The secondary and tertiary levels of the control system will monitor the IMG demand served KPI (KPI_{DS}), outlined in Section 3.2 [54].
Req. 4-49	Stability of the IMGs and railway infrastructure is the ultimate priority of the control system. The control system must maintain the stability of each IMG by not allowing the IMG to generate or export more energy than is feasible [54].
Req. 4-50	The tertiary level, which monitors the IMGs, will make decisions as to whether IMGs should engage in energy exchange with each other. The secondary level for each IMG will handle requests dictated by the tertiary level.

Chapter 5

Proposed System Design

In this chapter the design of RIMGs for reliable railway infrastructure is proposed and detailed. Currently, railway infrastructures rely on the centralized electric grid for a reliable stream of energy. The proposed system of RIMGs is designed with the intent of providing a resilient energy supply to the railway infrastructure. The chapter consists of the proposed system design of RIMGs, and the design of the supervisory IMG control system.

5.1 Proposed System Design of Interconnected Microgrids

The proposed design of RIMGs is carried out in layers, with each layer adding more detail and consideration than the previous one.

5.1.1 Conceptual Design of Interconnected Microgrids

Using the target system design and information acquired from the requirements analysis in Chapter 4, a conceptual design of RIMGs for railway infrastructures is proposed in Figure 5.1. Based on the traditional system design of an AC electrified railway infrastructure presented in Figure 1.3, this system has been modified to include an IMG at each TPS. Each individual IMG is interconnected via the traction power distribution system.

In practice, a TPS provides energy to a section of the railway infrastructure, with rolling stock moving in either direction within the section. To prove the concept of IMGs and the proposed control architecture and strategies, each IMG will provide energy to the rolling stock moving from one terminal station to the other terminal

station. For the purposes of this thesis only two IMGs will be considered. This does not limit the scalability of the proposed system and designs to two IMGs, but is to prove the concept without any degradation of the data extracted from the literature.

5.1.2 Preliminary Design of Interconnected Microgrids

Figure 5.2 presents a preliminary design of a single IMG connected at the TPS. The preliminary design constitutes a hybrid AC-DC IMG, which relegates the DC and AC DERs and ESSs to their respective bus and reduces the number of converters required in the IMG. The inverter on the DC bus is required to convert the DC signal of the solar PV and battery ESS to the same AC signal of the AC bus, electric grid, and railway load. This design would be applied to each IMG along the railway corridor as it is connected to each TPS.

5.1.3 Detailed Design of Interconnected Microgrids

The design of the RIMG consists of several components integrated together in a hybrid AC-DC configuration. Each IMG consists of two DERs (solar PV and WT), and an ESS (battery). A central control system (i.e. MG regulation system), are used to mange the flow of energy within the IMG, and the set-points for each DER and ESS. Power converters for each DER and ESS are contolled through local controllers. The detailed design in Figure 5.3 illustrates the integration of the DERs and ESS to form the IMG with a connection to the electric grid, which then operates in parallel with the electric grid to supply resilient energy to the railway infrastructure. MGs are interconnected together through a 25 km feeder, along the railway corridor. The individual MGs are interconnected through a 25 km feeder via the traction power distribution system. The IMGs are controlled using all three levels of the proposed control architecture (outlined in Section 5.2.2).

5.2 Proposed Interconnected Microgrid Control System

The control system is an essential component to the proposed RIMG design. The description of the proposed control system is organized as follows:

— A control system strategy and a hierarchical control architecture are proposed, based on the requirements of the control system, for the RIMGs.

— The proposed strategy of the MG regulation system to control the exchange of energy within the IMG and determine the DER and ESS set-points.

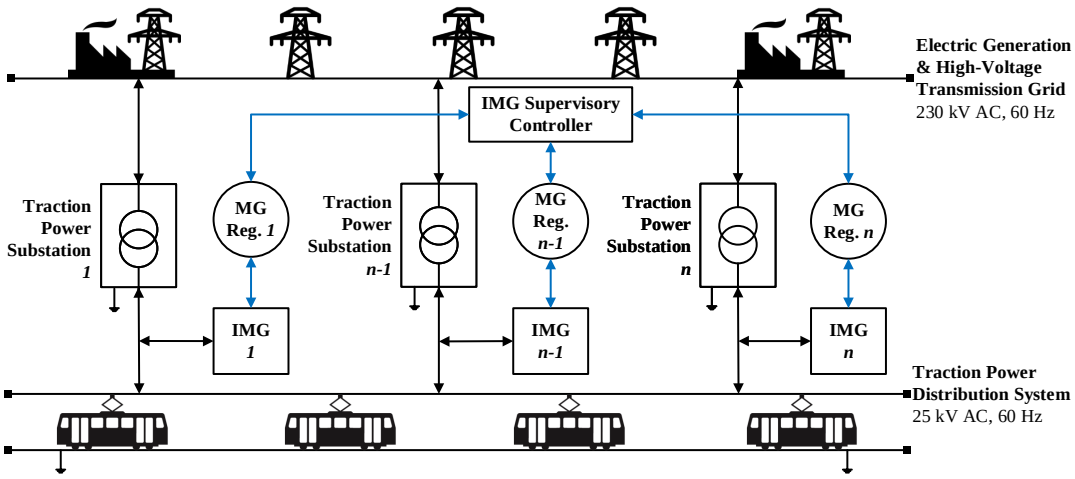

Figure 5.1: Proposed conceptual design consisting of n RIMGs integrated at each TPS along the railway corridor, where the IMGs are controlled using a hierarchical control architecture

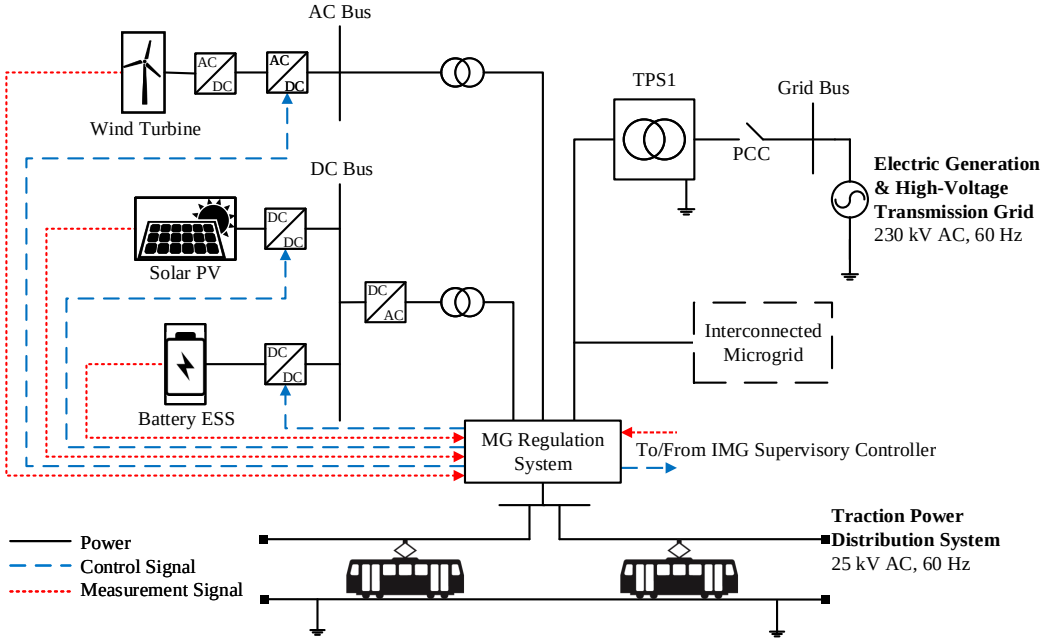

Figure 5.2: Proposed preliminary system diagram of a hybrid AC-DC RIMG, with solar PV, wind turbine, and battery ESSs

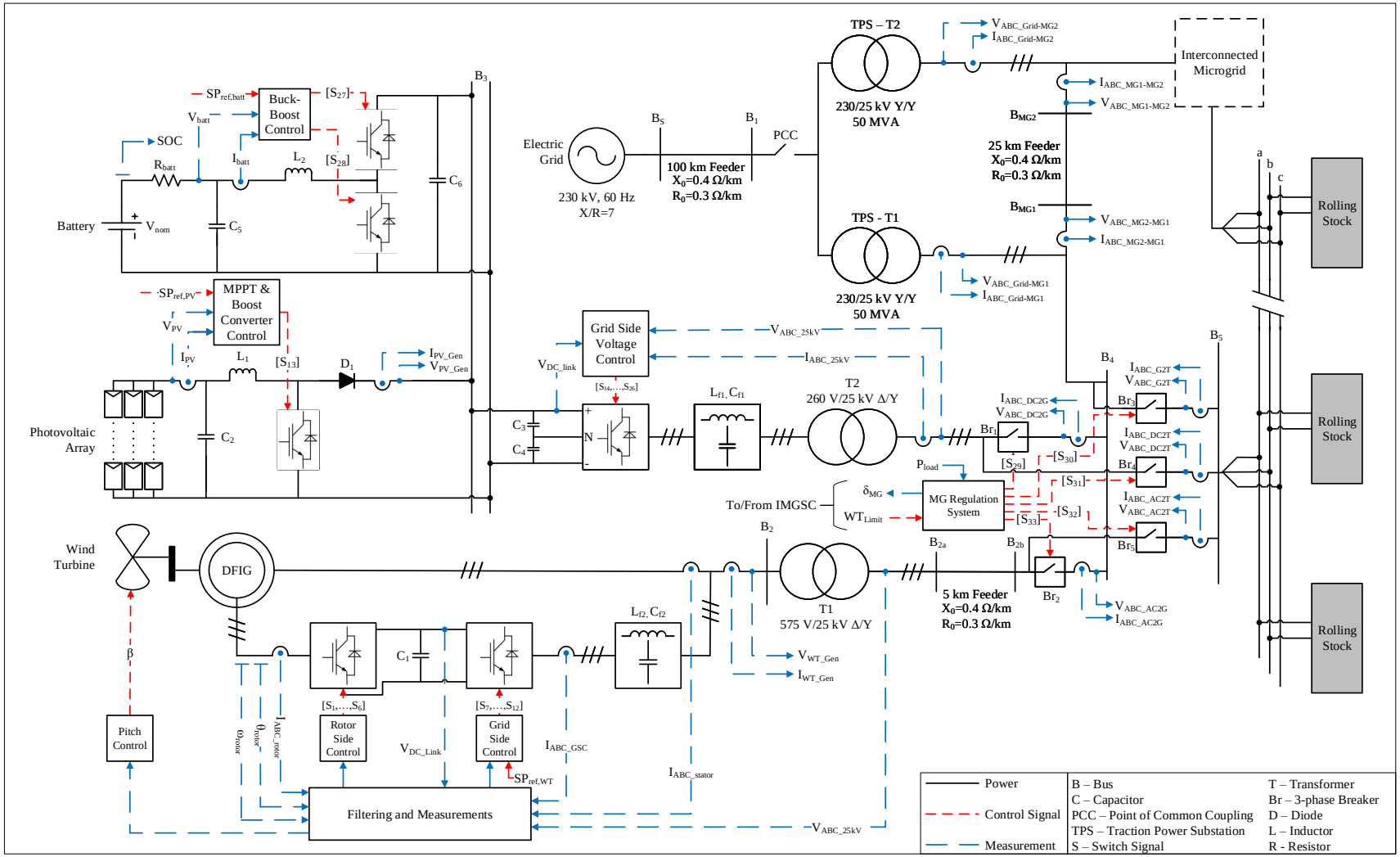

Figure 5.3: Detailed system diagram of a RIMG, with solar PVs, wind turbine, and battery ESSs

— The proposed tool for the tertiary level solves the multi-objective problem using game theory techniques and the IMG demand served KPI, to determine whether two IMGs should participate in exchange of energy.

5.2.1 Control System Strategy

Using the requirements of the control system listed in Table 4.7, a control system strategy is required. A regulator for each IMG provides the autonomous operation with the required measurements, decisions and controls by collecting data through sensors installed in the IMG and producing the set-points for the DER and ESS power converters. When considering the IMG demand served KPI, the following operating stategy is proposed:

— The power generated by the solar PV and WT systems have priority in satisfying the demand of the rolling stock.

— If the total power generated by the solar PV and WT systems is higher than the demand, the additional power will be used to charge the battery ESS (see Section 5.2.4).

— After charging the battery ESS, the remaining power can be exported to any other IMG (see Section 5.2.5).

— After charging the battery ESS and exporting to another IMG (if required), any remaining power can be exported to the electric grid. The limit to export to the electric grid is determined using the DER set-point (see Section 5.2.4).

— If the total electric power generated by the solar PV and WT systems is less than the demand, the battery ESS wil be discharged (see Section 5.2.4).

— If the demand of the rolling stock exceeds the power generated by the WT, solar PV, and ESS, the difference is supplied by an IMG, if allowable (see Section 5.2.5).

— As a last resort, the electric grid will supply the difference.

— If the demand of the rolling stock is negative (i.e. regenerative braking), the same process will be followed as if the total power generated by the solar PV and WT systems is higher than the demand.

The control strategy is illustrated in Figure 5.4. This strategy can be used for each IMG during normal and emergency situations, however is only applicable for grid-connected IMGs. Islanded IMGs are not part of the scope of this thesis, and is recommended for future considerations. To implement the strategy, control systems

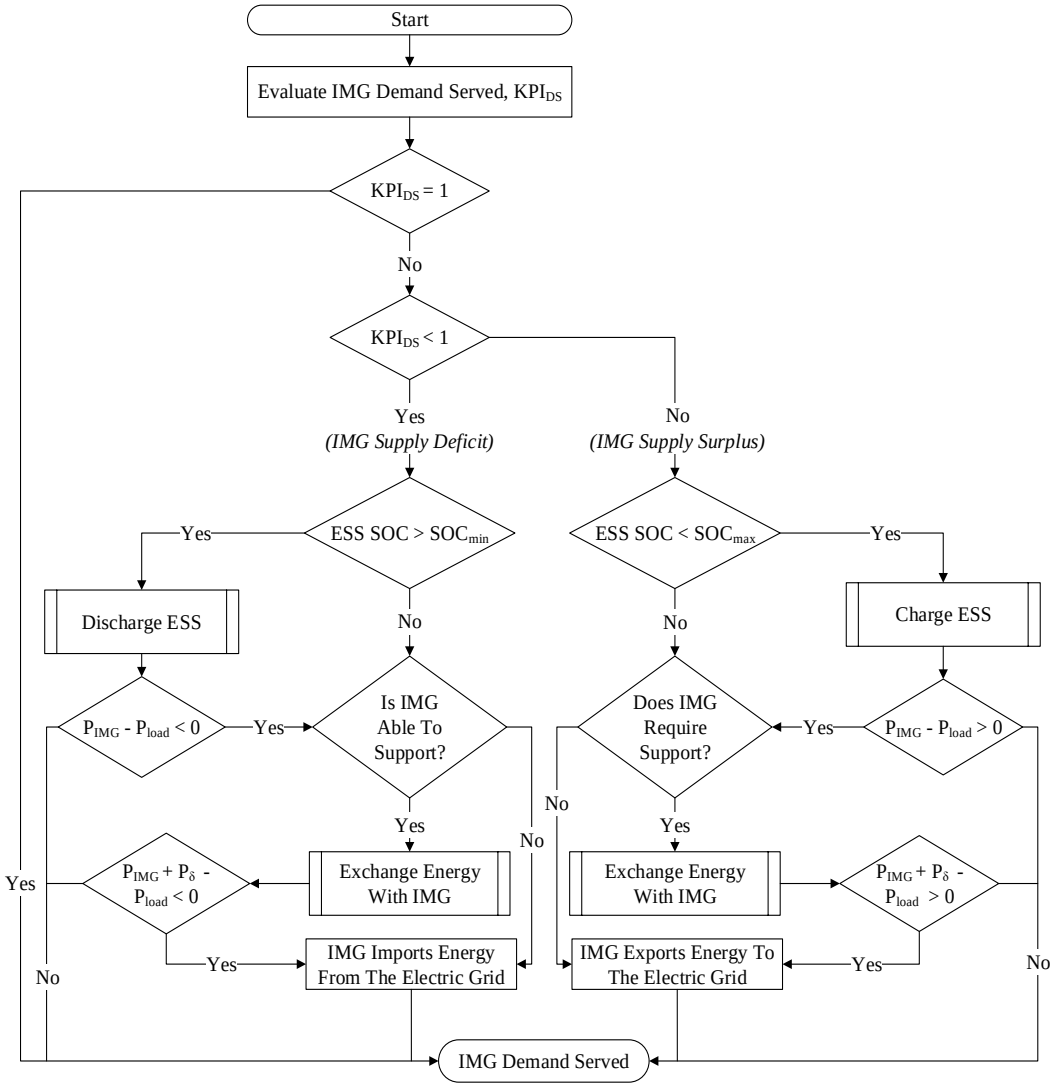

Figure 5.4: Proposed control strategy for each IMG, using the IMG demand served KPI, to provide resilient energy to the railway infrastructure

are required at relevant points in the IMG.

5.2.2 Control System Architecture

To implement the proposed control strategy, depicted in Figure 5.4, a hierarchical control scheme is required for the IMGs. As proposed in Section 3.5, in this scheme there are three levels of control, each with their own responsibilities. The levels work together to improve the resilience of the IMGs. Figure 5.5 provides a depiction of the proposed control architecture, for m IMGs, and n local controllers in each IMG. Each level will perform the following task:

— **Primary**: also known as local controller, is the control of each DER and ESS within an individual IMG

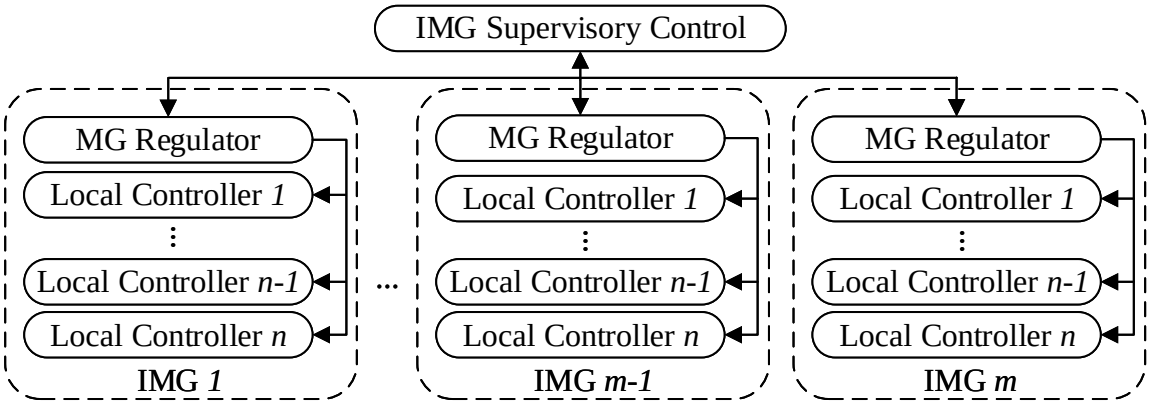

Figure 5.5: Hierarchical control architecture for proposed RIMG design: (1) tertiary level monitors all m IMGs, (2) secondary level computes the reference set-points for respective IMG DERs and ESSs, and (3) primary level follows its respective reference set-point

— **Secondary**: also known as the MG regulation system, regulates the set-points for each DER and ESS of its respective IMG and the flow of energy within the IMG

— **Tertiary**: also known as the IMG supervisory control, which monitors the IMGs, the connection to the electric grid, and, if required, will arrange the exchange of energy between two IMGs

The levels of contol are further detailed in the following sections.

5.2.3 Primary Control - Local DER and ESS Control

A local controller is used for each DER and ESS to control the amount of active and reactive power injected into the IMG. The local controller receives a set-point from the MG regulation system and attempts to follow the set-point using proportional-integral (PI) control systems. While a RES is considered a non-dispatchable source, when exporting energy to an IMG or to the electric grid, there may be limitations imposed on the amount of active power exported. To account for those limitations, all applicable converters for each DER and ESS are provided a set-point from its respective MG regulation system (secondary control).

5.2.4 Secondary Control - Microgrid Regulation

The secondary control layer of the hierarchical control system consists of the MG regulation system. The MG regulation system monitors information related to the demand, DERs and ESS within its own IMG. This includes the energy generated by each DER, SOC of the ESS, and the demand of the railway load, and if applicable,

any other local loads (e.g. railway station, maintenance station, signalling and communication system). Using the real-time measurements, the MG regulation system will determine the appropriate set-points for each DER and ESS and determine how to supply the demand.

The MG regulation system receives the following information from within the IMG:

— DER generation

— ESS SOC

— Railway demand

— Set-point override from IMGSC

— Total active power measurements from AC and DC bus

— Active power measurement for each possible flow of energy within the IMG (e.g. AC bus to electric grid bus)

Using the information provided and the strategies and algorithms previously mentioned, the following is determined by the MG regulation system:

— DER and ESS set-point

— Switch state for each possible flow of energy within the IMG (e.g. AC bus to electric grid bus)

The MG regulation system can decide to supply the demand using the energy generated by each DER, energy stored in an ESS, or the electric grid. As seen in Figure 5.3, there are two paths for the energy generated by each DER to flow. Energy from each bus can either be directed to supply the railway demand or be exported to the electric grid. Three-phase breakers are used to manage the flow of energy for each IMG bus (AC and DC). Another three-phase breaker is used to manage the flow of energy between the IMGs, electric grid and the railway load, which is used when the railway load cannot be entirely satisfied by the IMG, or the energy recovered from braking is greater than what can be stored in the ESS. If energy is being provided to an IMG, the transfer of energy occurs on the railway electric distribution system, through the electric grid bus. The switching strategy the MG regulation system follows is set out in Figure 5.6.

The MG regulation system will determine whether to regulate the DER set-point or allow MPPT to extract the maximum possible amount of energy, as seen in Figure 5.7. If the MG regulation system determines to regulate the DER, the regulator will compute the set-point for each DER in the IMG using Equation 5.1:

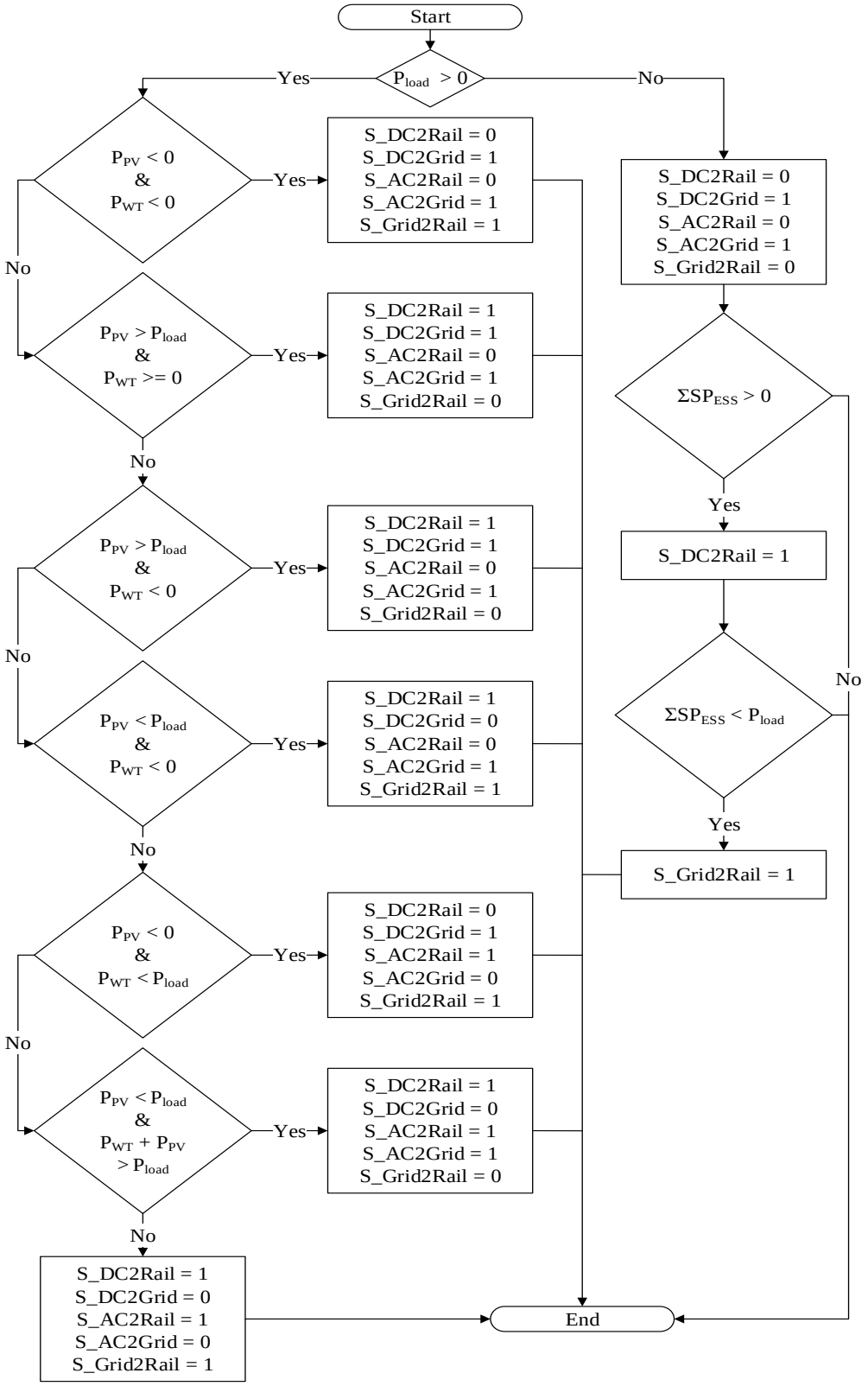

Figure 5.6: Proposed MG regulation system switching strategy to facilitate the exchange of energy between the DC bus, AC bus, railway load, and electric grid

$$SP_{DER_i} = \frac{P_{DER_i}(t) - P_{DER_i \to grid}(t) + P_{DER,lim_i}(t)}{P_{nom}}, 0 \leq SP_{DER_i} \leq 1 \tag{5.1}$$

where $P_{DER,lim}$ is the sum of the export limit imposed by the electric grid operator, $P_{DER \to grid,max}$, and the allowable limit of exchange between two IMGs, as decided by the IMGSC for the DER, $P_{IMG \to IMG,lim}$.

The ESS set-point will dictate whether the system is charging or discharging and by how much. The set-point for the ESS is determined based on various conditions since it can either be charging or discharging. The mode of operation depends on the SOC of the battery, RES generation, and demand conditions in the IMG. Figure 5.8 depicts the strategy used to determine the battery set-point by the MG regulation system, while respecting the constraints of the battery technology.

5.2.5 Tertiary Control - IMG Supervisory Control

The IMGSC monitors the IMGs and maintains the resilient energy supply for the railway infrastructure. The objective of the IMGSC is to minimize the dependence of each IMG on the electric grid, a KPI used to measured resilience. The tertiary level uses the multi-objective and bimatrix game theory techniques proposed in Section 3.6.

5.2.5.1 Control Objective

The multi-objective problem discussed in this thesis emphasizes the minimization of the dependence of each IMG on the electric grid, which will improve the resilience of the energy supply for the railway infrastructure. The objective of the problem is to determine the optimal set-point combination for each IMG to minimize each other's dependence on the electric grid. The set-point will be communicated to each MG regulation system and used in the calculation of the DER set-point computation. As described in Section 3.6.1, the MO problem is formulated as:

$$Minimize[f_1, f_2] \tag{5.2}$$

where,

$$f_1 = P_{load_1}(t) - \big(P_{IMG_1}(t) + P_\delta(t)\big), \forall t \epsilon T \tag{5.3}$$

$$f_2 = P_{load_2}(t) - \big(P_{IMG_2}(t) + P_\delta(t)\big), \forall t \epsilon T \tag{5.4}$$

The first objective function, *(f_1)*, is to minimize the imbalance of power between the railway load within IMG1 and the sum of the power generated by the DERs

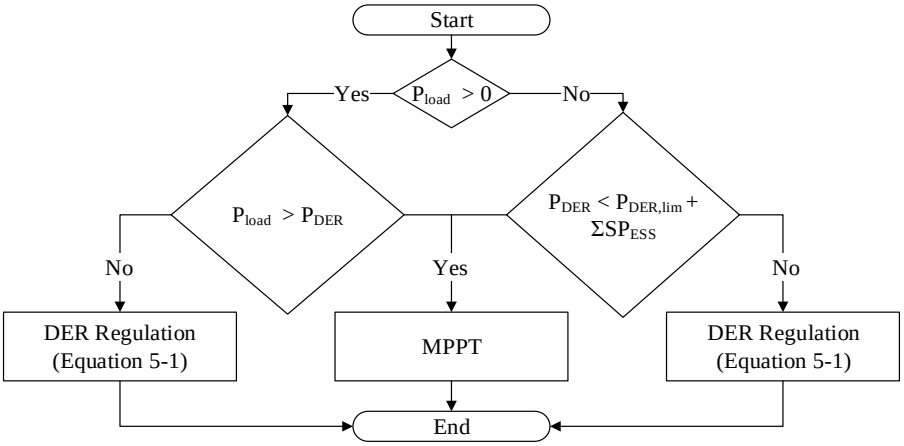

Figure 5.7: Proposed MG regulation strategy to determine DER set-point for local controller

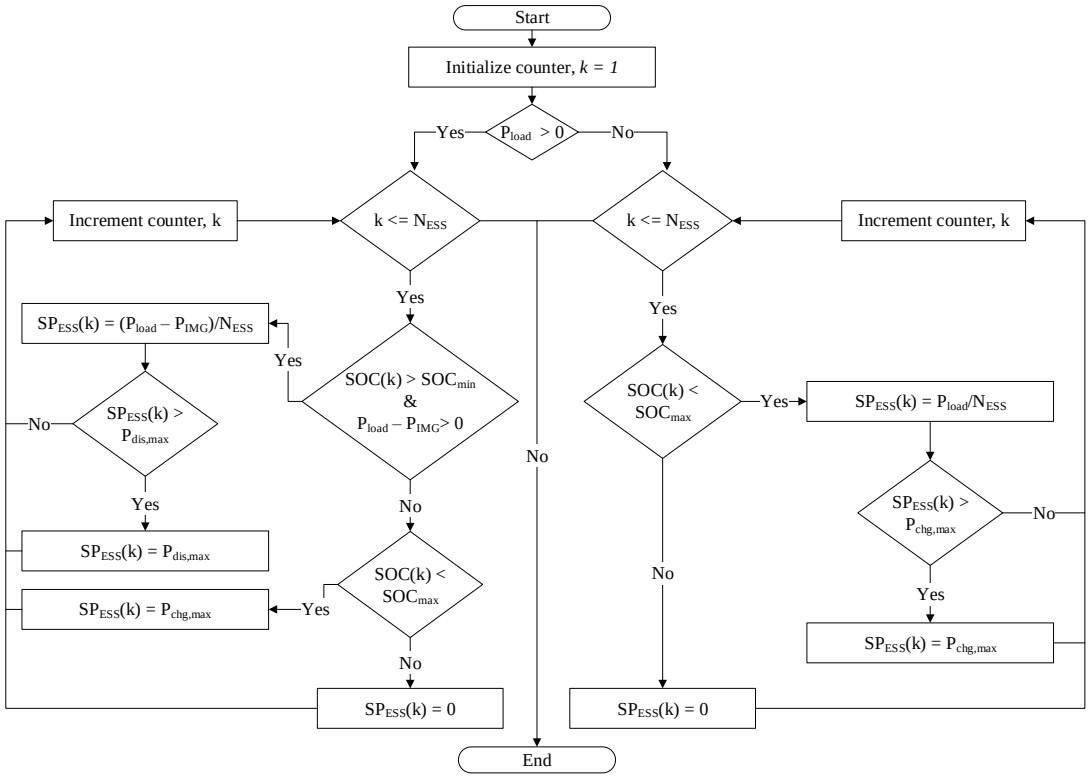

Figure 5.8: Proposed MG regulation strategy to determine ESS set-point for local controller, considering the technical limitations of the technology

and available from the ESS. A reduced dependence on the electric grid allows for increased resilience during normal and emergency situations where access to the electric grid may be hindered due to a failure within the centralized network, and the railway infrastructure to remain functional.

The second objective function, *(f_2)*, is to minimize the imbalance of power between the railway load within IMG2 and the sum of the power generated by the DERs and available from the ESS. A reduced dependence on the electric grid allows for increased resilience during normal and emergency situations where access to the electric grid may be hindered due to a failure within the centralized network, and the railway infrastructure to remain operational.

5.2.5.2 System Constraints

System constraints are an important consideration in the multi-objective decision making, as they play a significant role on the formulation of the set-points for each IMG. Equalities, inequalities and upper and lower bounds defining system constraints are listed below.

The system constraint shown in Equation 5.5 depicts that the system must maintain the following load balance amongst the DERs, ESS, railway load, IMGs, and electric grid:

$$P_{load}(t) = \sum_{i=1}^{N_{PV}} P_{PV_i}(t) + \sum_{j=1}^{N_{WT}} P_{WT_j}(t) + \sum_{k=1}^{N_{ESS}} P_{ESS_k}(t) + P_{\delta} + P_{grid}(t), \forall t \epsilon T \quad (5.5)$$

In addition, each DER has a constraint on the amount of active power it can generate. Equation 5.6 is used to ensure that the set-point signal is not higher or lower than what is possible for the DER:

$$P_{DER,min_i}(t) \leq P_{DER_i}(t) \leq P_{DER,max_i}, \forall i = 1, ..., N_{DER}, \forall t \epsilon T \quad (5.6)$$

A DER can sell energy to the electric grid, but may have a limit imposed by a regulator (e.g. IESO). When the IMG exports to the electric grid, the MG regulation system will set the set-point for each DER considering the limit of energy exchanged does not exceed the amount limited by the electric grid, where

$$P_{DER_i \rightarrow grid,min} \leq P_{DER_i \rightarrow grid} \leq P_{DER_i \rightarrow grid,max}, \forall i = 1, ..., N_{DER}, \forall t \epsilon T \quad (5.7)$$

Another consideration is that the electric grid must have a higher nominal capacity than the IMG, where

$$|P_{grid}(t)| \leq P_{grid,max}, \forall t \epsilon T \tag{5.8}$$

This is so that the electric grid can supply or absorb energy to/from any IMG, as required.

To prolong the lifetime of the battery there are constraints on how much charge the battery may store. In addition, due to limits on the battery technology and composition, each battery can only be charged, or discharged, at certain rates.

$$SOC_{min} \leq SOC_i(t) \leq SOC_{max}, \forall i = 1, ..., N_{ESS}, \forall t \epsilon T \tag{5.9}$$

$$P_{chg_i}(t) \leq P_{chg,max}, \forall i = 1, ..., N_{ESS}, \forall t \epsilon T \tag{5.10}$$

$$P_{dis_i}(t) \leq P_{dis,max}, \forall i = 1, ..., N_{ESS}, \forall t \epsilon T \tag{5.11}$$

5.2.6 Using Game Theory for the IMG Supervisory Control

The multi-objective problem defined in Section 5.2.5 can be translated to a game, where each objective is considered a player. The players are subjected to limited resources (i.e. system constraints) as they strive to determine the ideal decision. Game theory is the study of multiple players who make decisions for themselves, while also considering the reactions of other players [116]. A cooperative game is one where the players (i.e. individual IMGs) can coordinate their strategies to achieve the best outcome for the group. A coalition is formed when two or more players can agree to coordinate their strategy. As each player has their own set of strategies, this is considered a bimatrix game, previously defined in Section 3.6.2.

To achieve this objective, each MG regulation system will communicate to the IMGSC the generation on the DC and AC bus and the demand of the railway load. If the IMGSC detects the IMGs demand served KPI to be less than one, it will determine whether any IMGs are able to supply the deficit. If so, the IMGSC will compare the current demand served KPIs for each IMG, and the updated KPI if the deficit were to be covered. Based on which strategy has the higher probability of selection, the IMGSC will either allow a transfer of energy between IMGs, or the IMG will depend on the electric grid. Communication between IMGs only occurs through the IMGSC.

The steps involved to solve the bimatrix game, which controls the exchange of energy between IMGs, is outlined in Table 5.1 and Figure 5.9.

Table 5.1: Steps to solve the bimatrix game between two IMGs under consideration

Step 1	**Read the following input data from each IMG:** — Interconnected microgrid supply, P_{IMG} — Railway demand, P_{load}
Step 2	**Calculate the IMG demand served KPI for each IMG:** $$KPI_{DS_{IMGi}} = \left\lvert \frac{P_{IMG_i}}{P_{load_i}} \right\rvert, \forall i = 1, ..., N_{IMG}$$
Step 3	**Evaluate the IMG demand served KPIs:** — If both KPIs are greater than or equal to one, the WT's in each IMG can export at the base limit set by the electric grid, then go to step 9 — If both KPIs are less than one, WT's in each IMG are not allowed to exchange energy with an IMG or export to the electric grid, then go to step 9 — Otherwise one IMG has a KPI less than one (requires exchange of energy with an IMG), and the other IMG has a KPI greater or equal to one (can support exchange of energy with an IMG)
Step 4	**Calculate IMG deficit, P_δ:** — Calculate the deficit required by the IMG to cover the demand — Adjust the deficit value to ensure its within the limits of the IMG
Step 5	**Evaluate the IMG demand served KPI with P_δ:** — The IMG that is suppling energy to the IMG will add P_δ to its load $$KPI_{DS_{IMG1}} = \left\lvert \frac{P_{IMG_1}}{P_{load_1} + P_\delta} \right\rvert$$ — The IMG that is receiving energy from another IMG will add P_δ to its supply $$KPI_{DS_{IMG2}} = \left\lvert \frac{P_{IMG_2} + P_\delta}{P_{load_2}} \right\rvert$$
Step 6	**Form payoff matrix:** $$PayoffMatrix =$$ $$log_{10} \begin{bmatrix} (KPI_{DS_{IMG_1}}, KPI_{DS_{IMG_2}}) & (0,0) \\ (0,0) & (KPI^*_{DS_{IMG_1}}, KPI_{DS^*_{IMG_2}}) \end{bmatrix}$$
Step 7	**Solve the game:** — Determine the probabilities for each player to select a strategy
Step 8	**Assess the results of the game:** — If both IMGs expect a higher probability of selection with IMG exchange, than the IMG with the surplus will increase its WT export set-point to accommodate the IMG exchange — Otherwise, WT's in each IMG export set-point remains at the base limit set by the electric grid regulator
Step 9	**Output set-points to MG regulation systems**

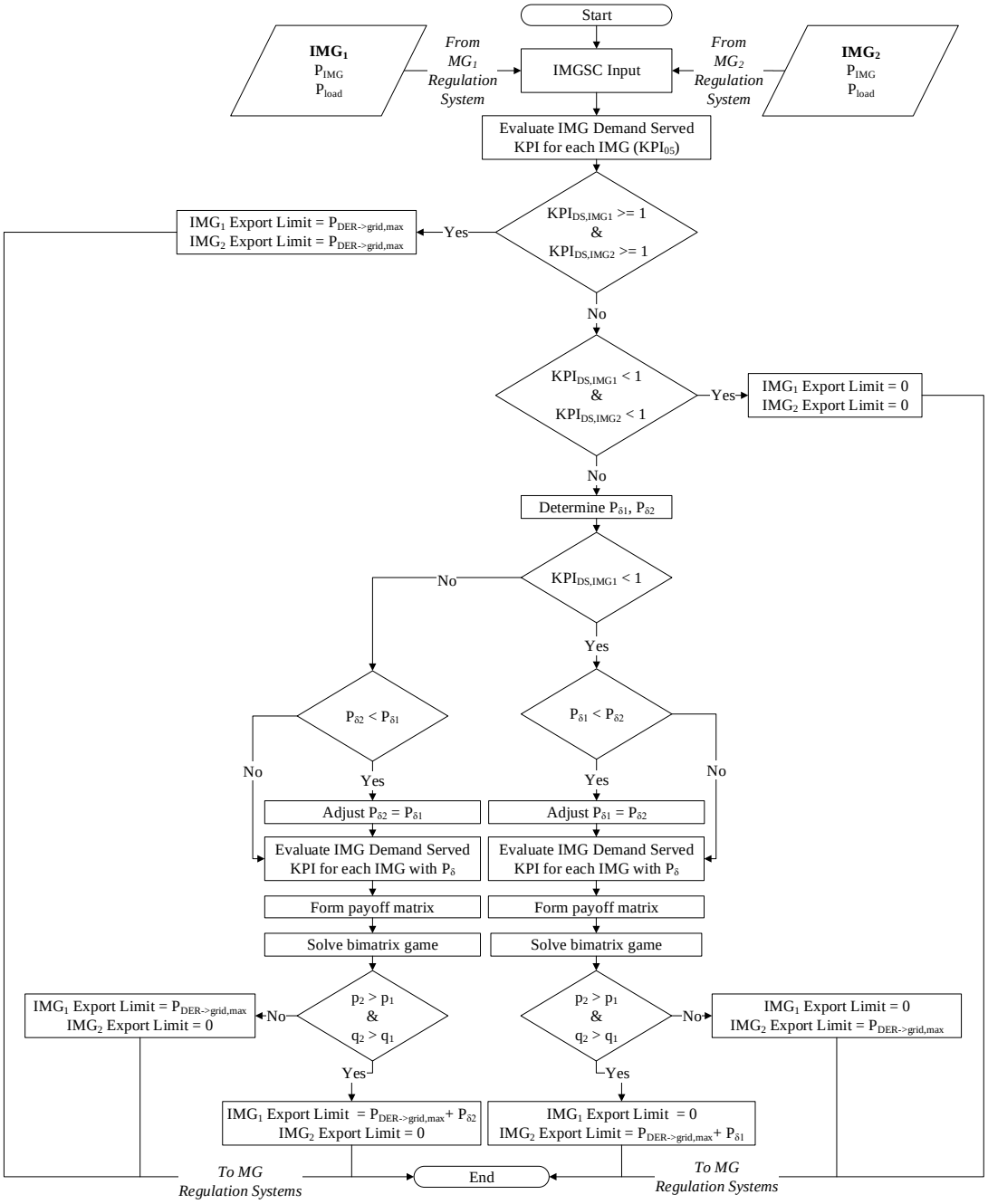

Figure 5.9: Proposed IMGSC strategy, using the IMG demand served KPI ($\mathrm{KPI_{DS}}$) and game theory techniques, to determine if two IMGs should exchange energy

Chapter 6

System Modelling

The designs proposed in Chapter 5 are modelled and simulated in MATLAB, Simulink, and SimPowerSystems software packages [137]. This thesis adopts piece-wise component modelling of the individual components of the proposed design [154]. The components include the distributed energy resources (wind turbine and solar PV systems), energy storage system (battery), electric grid, traction power substation, MG interconnection, and railway infrastructure. The strategies of the MG regulation system and IMGSC are mapped and implemented to Simulink (see Appendix C for sample code). Real world technologies that are available on the open market are used for this thesis.

6.1 System Modelling Assumptions

The major assumptions considered for the system modelling of resilient interconnected microgrids for reliable mass transit systems are as follows:

— Steady state operation is considered

— The system frequency is 60 Hz

— Measures to account for energy losses are neglected

— The effects of THD are ignored

— The demand of a single rolling stock is considered as the load [9, 151]

— Interconnected MGs operate in grid-connected mode [155]

— Only active power is considered, while reactive power is held constant at zero [155]

— Each TPS is able to handle bidirectional power flow [13, 156]

— A weather profile for the sizing and simulation analysis is assumed for each case study (see Section 6.4) [137], and similar to existing data available in literature [157, 158].

— Unless explicitly stated in this chapter, the default values are used to model a Simulink component (e.g. phase lock loop, DC bus inverter, DFIG) [137]

6.2 Interconnected Microgrid Modelling

The modelling of the proposed RIMG design consists of the DERs, ESSs, the electric grid, and any necessary control systems and miscellaneous components (e.g. DC bus inverter).

6.2.1 Wind Turbine

The WT is the only AC DER used in the IMG, and therefore the only DER on the AC bus. The power generated by the WT is dependent on the wind speed for the installed location, and the characteristics of the WT. The WT requires machines to convert the energy from the kinetic energy of the wind to electrical energy. For this thesis, the WT electrical power conversion system consists of a DFIG, a machine-side converter (AC-DC) and a grid-side converter (DC-AC). The models for the WT system are outlined below.

The energy captured by the WT rotors is modelled using Equation 6.1 [159]:

$$P_t = \begin{cases} 0 & v_w \leq v_{ci}, v_w \geq v_{co} \\ \frac{1}{2} c_p(\lambda, \beta) \rho_a A_{WT} v_w^3 v_{rated} \left(\frac{v_w^3 - v_{ci}^3}{v_{rated}^3 - v_{ci}^3} \right) & v_{ci} \leq v_w \leq v_{rated} \\ \frac{1}{2} c_p(\lambda, \beta) \rho_a A_{WT} v_w^3 & v_{rated} \leq v_w \leq v_{co} \end{cases} \tag{6.1}$$

The power coefficient is computed based on two variables: the tip speed ratio of the rotor blade to wind speed and the blade pitch angle. The blade pitch angle is fixed at 0°, thus the power coefficient can be determined using the WT specific c_p-λ characteristics. The power coefficient is calculated using Equation 6.2 and Equation 6.3 [160]:

$$c_p(\lambda, \beta) = 0.5176 \left(\frac{116}{\lambda_i} - 0.4\beta - 5 \right) e^{\frac{21}{\lambda_i}} + 0.05508 \tag{6.2}$$

$$\frac{1}{\lambda_i} = \frac{1}{8.1 + 0.08\beta} - \frac{0.035}{\beta^3 + 1} \tag{6.3}$$

Table 6.1: Characteristics of GE 1.5sle MW used to model a wind turbine in Simulink

Parameter	**Value**
Nominal power of the WT DER, P_{nom} (MW)	1.5
Cross-section area of the WT blades, A_{WT} (m^2)	4,657
Rated wind speed of the WT, v_r (m s^{-1})	14
Cut-in wind speed of the WT, v_{ci} (m s^{-1})	3.5
Cut-out wind speed of the WT, v_{co} (m s^{-1})	25

The mechanical torque produced by the WT rotor is determined using Equation 6.4 [159]:

$$\tau_{mech} = \frac{P_t}{\omega_t} \tag{6.4}$$

The drive train is the mechanical system which translates the mechanical torque, τ_{mech}, into the generator torque, τ_{elec}. Equation 6.5 - Equation 6.7 represent the commonly used two-mass drive train model [159]:

$$2H_g\dot{\omega}_g = \tau_{elec} - K_s\theta_s - D_s(\omega_g - \omega_t) \tag{6.5}$$

$$2H_t\dot{\omega}_t = K_s\theta_s - \tau_{mech} + D_s(\omega_g - \omega_t) \tag{6.6}$$

$$\dot{\theta}_s = \omega_g - \omega_t \tag{6.7}$$

The DFIG, a commonly used generator in WT systems, consists of a stator and rotor, where the rotor operates at a lower level than the stator allowing for variable speed in the generator and reduced cost for power converters [159]. A major advantage of the DFIG is the fact that a high amount of kinetic energy is stored in the rotors, which reduces the impact of the power output to fluctuating wind speeds. The DFIG is modelled using equations Equation 6.8 - Equation 6.12 [159]:

$$\overline{V}_s^{dq} = R_s\overline{I}_s^{dq} + \omega_s \begin{bmatrix} 0 & -1 \\ 1 & 0 \end{bmatrix} \overline{\lambda}_r^{dq} + \frac{d\overline{\lambda}_s^{dq}}{dt} \tag{6.8}$$

$$\overline{V}_r^{dq} = R_r\overline{I}_r^{dq} + (\omega_{ref} - \omega_r) \begin{bmatrix} 0 & -1 \\ 1 & 0 \end{bmatrix} \overline{\lambda}_r^{dq} + \frac{d\overline{\lambda}_r^{dq}}{dt} \tag{6.9}$$

$$\overline{\lambda}_s^{dq} = L_s\overline{I}_s^{dq} + L_m\overline{I}_r^{dq} \tag{6.10}$$

$$\overline{\lambda}_r^{dq} = L_r\overline{I}_r^{dq} + L_m\overline{I}_s^{dq} \tag{6.11}$$

$$\tau_{elec} = \frac{3}{2}\frac{N_p}{2}L_m(\overline{I}_s^q\overline{I}_r^d - \overline{I}_s^d\overline{I}_r^q) \tag{6.12}$$

There are three local controllers for the WT, which must be modeled:

— Speed regulator and pitch control system

— Rotor-side controller

— Grid-side controller

The speed regulator and pitch controller are used to control various aspects of the WT [159]. The speed regulator is used for comparing the WT speed to its reference value, and the output, which is used by the rotor-side controller. The pitch control is used to maintain the blade pitch angle of the WT to its reference value. The blade pitch angle is desired to be maintained at 0°. Figure 6.1 depicts the pitch control and speed regulator systems modelled in Simulink. The MG regulation system does not regulate either of these systems.

The second WT control system consists of the rotor-side controller, depicted in Figure 6.2 [159]. The controller consists of an electromagnetic torque controller, current regulator, and a PWM generator. The MG regulation system does not regulate the rotor-side controller. The electromagnetic torque controller generates the reference rotor current in d-frame. A volt and vars regulator are used to compute the reference rotor current for the q-frame.

The current regulator generates the reference rotor voltage in dq-frame, using Equation 6.13 and Equation 6.14:

$$V_{ref}^{d} = R_r I_{ref}^{d} - \omega_{slip}(L_r + L_m) I_{ref}^{q} + \left(K_p + \frac{K_i}{s}\right)(I_{ref}^{d} - I_r^{d}) \tag{6.13}$$

$$V_{ref}^{q} = R_r I_{ref}^{q} + \omega_{slip}(L_r + L_m) I_{ref}^{d} + \left(K_p + \frac{K_i}{s}\right)(I_{ref}^{q} - I_r^{q}) \tag{6.14}$$

The reference voltages, in dq-frame, are used to generate the pulses for the switches in the rotor-side controller. The reference values are converted back to abc-frame using the phase information [159]. The voltage waveforms are then compared to a carrier waveform to generate the pulses.

The third controller for the WT consists of the grid-side controller, depicted in Figure 6.3 [159]. This controller consists a power regulator, current regulator, and PWM generator. The grid-side controller uses the PQ control strategy. This method is used so that the WT will inject the active and reactive power determined by the set-point provided by the MG regulation system. For this thesis, the reactive power injected by the WT is set to zero.

The active power output of the WT will be compared to the set-point supplied by the MG regulation system. A PI controller is used to compute the reference current in d-frame, while the reference current in q-frame is held constant at 0.

$$I_{ref}^{d} = \left(K_p + \frac{K_i}{s}\right)\left(\frac{P_t}{P_{nom}} - SP_{WT}\right) \tag{6.15}$$

$$I_{ref}^{q} = 0 \tag{6.16}$$

These reference values are compared to the actual electric grid converter current (in dq-frame), to compute the reference voltage in dq-frame, via PI control.

$$V_{ref}^{d} = V_s^d - R_r I_{ref}^{d} + \omega L_r I_{ref}^{q} - \left(K_p + \frac{K_i}{s}\right)(I_{ref}^{d} - I_{grid}^{d}) \tag{6.17}$$

$$V_{ref}^{q} = V_s^q - R_r I_{ref}^{q} - \omega L_r I_{ref}^{d} - \left(K_p + \frac{K_i}{s}\right)(I_{ref}^{q} - I_{grid}^{q}) \tag{6.18}$$

The reference voltages, in dq-frame, are used to generate the pulses for the switches in the grid-side controller. The reference values are converted back to abc-frame using the phase information [159]. The voltage waveforms are then compared to a carrier waveform to generate the pulses.

The WT energy system is modelled in Simulink using:

— The equations to model a WT, drivetrain, and DFIG (Equation 6.1 - Equation 6.12)

— The characteristics of the GE 1.5sle MW WT listed in Table 6.1

— The three WT control systems (Figure 6.1 - Figure 6.3) and accompanying equations

The WT energy system Simulink model is depicted in Figure 6.4. Table 6.2 lists the technical parameters of the WT Simulink model (e.g. drivetrain, converter control parameters, DFIG), in addition to the parameters listed in Table 6.1.

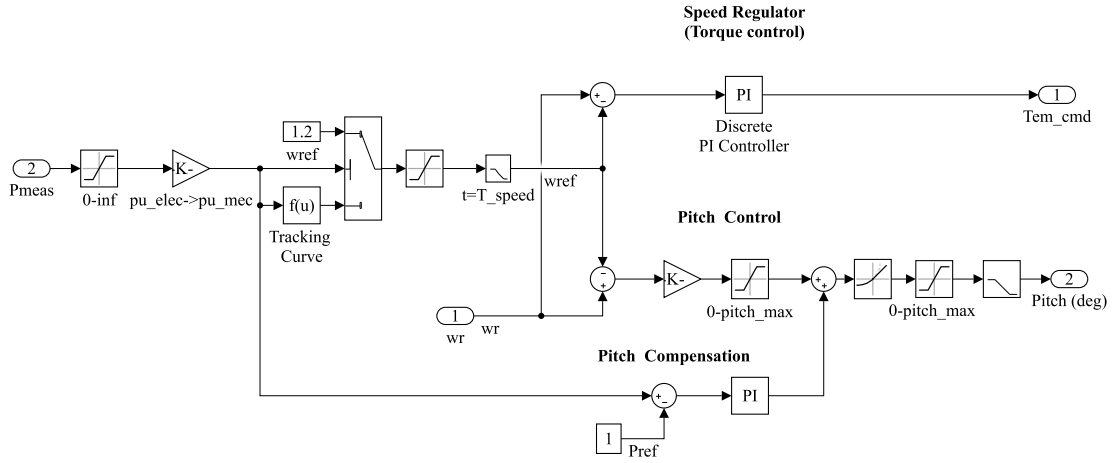

Figure 6.1: Wind turbine pitch and speed controller modelled in Simulink

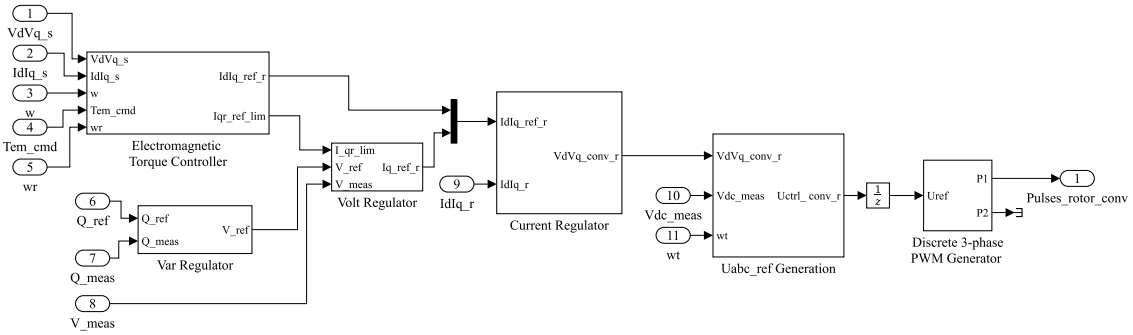

Figure 6.2: Wind turbine rotor-side controller modelled in Simulink

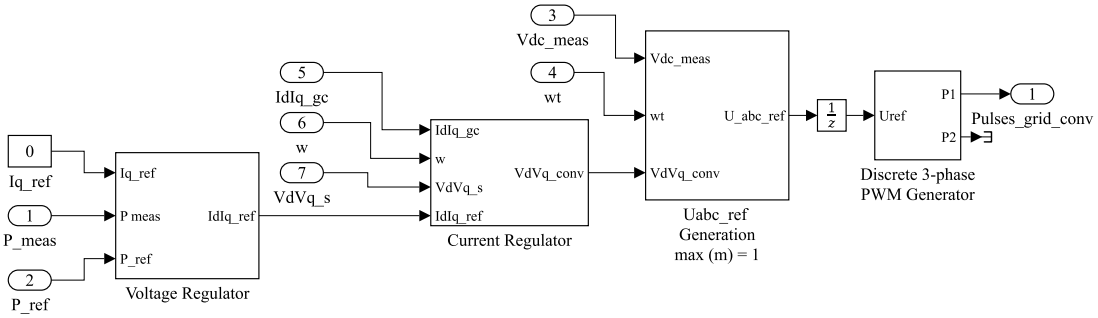

Figure 6.3: Wind turbine grid-side controller modelled in Simulink

Table 6.2: Technical parameters used to model a wind turbine energy system in Simulink

Parameter	**Value**
Nominal power of the WT DER, P_{nom} (MW)	1.5
Nominal primary line-to-line voltage (kV)	25
Nominal secondary (stator) line-to-line voltage (V)	575
Nominal rotor line-to-line voltage (V)	1,975
Nominal system frequency, f (Hz)	60
DFIG stator resistance, R_s (Ω)	0.023
DFIG stator inductance, L_s (H)	0.18
DFIG rotor resistance, R_r (Ω)	0.016
DFIG rotor inductance, L_r (H)	0.16
DFIG mutual inductance, L_m (H)	2.9
Moment of inertia constant for the DFIG, H_g (kg m^{-2})	0.685
Number of pair poles, N_p	3
Nominal DC bus voltage (V)	1,150
DC bus capacitor (μF)	0.01
Moment of inertia constant for the WT, H_t (kg m^{-2})	4.32
Damping coefficient, D_s (Nms rad^{-1})	1.5
Shaft stiffness, K_s (Nm rad^{-1})	1.11
Speed regulator gains, [K_p K_i]	[3, 0.6]
Pitch compensation gains, [K_p K_i]	[3, 30]
Pitch controller gain, [K_p]	[150]
Rotor-side converter Var regulator gain, [K_i]	[0.05]
Rotor-side converter Volt regulator gain, [K_i]	[20]
Rotor-side converter current regulator gains, [K_p K_i]	[0.6, 8]
Carrier frequency of rotor-side PWM (Hz)	1,620
Grid-side converter power regulator gains, [K_p K_i]	[-2.4305, -0.6371]
Grid-side converter current regulator gains, [K_p K_i]	[0.83, 5]
Carrier frequency of grid-side PWM (Hz)	2,700

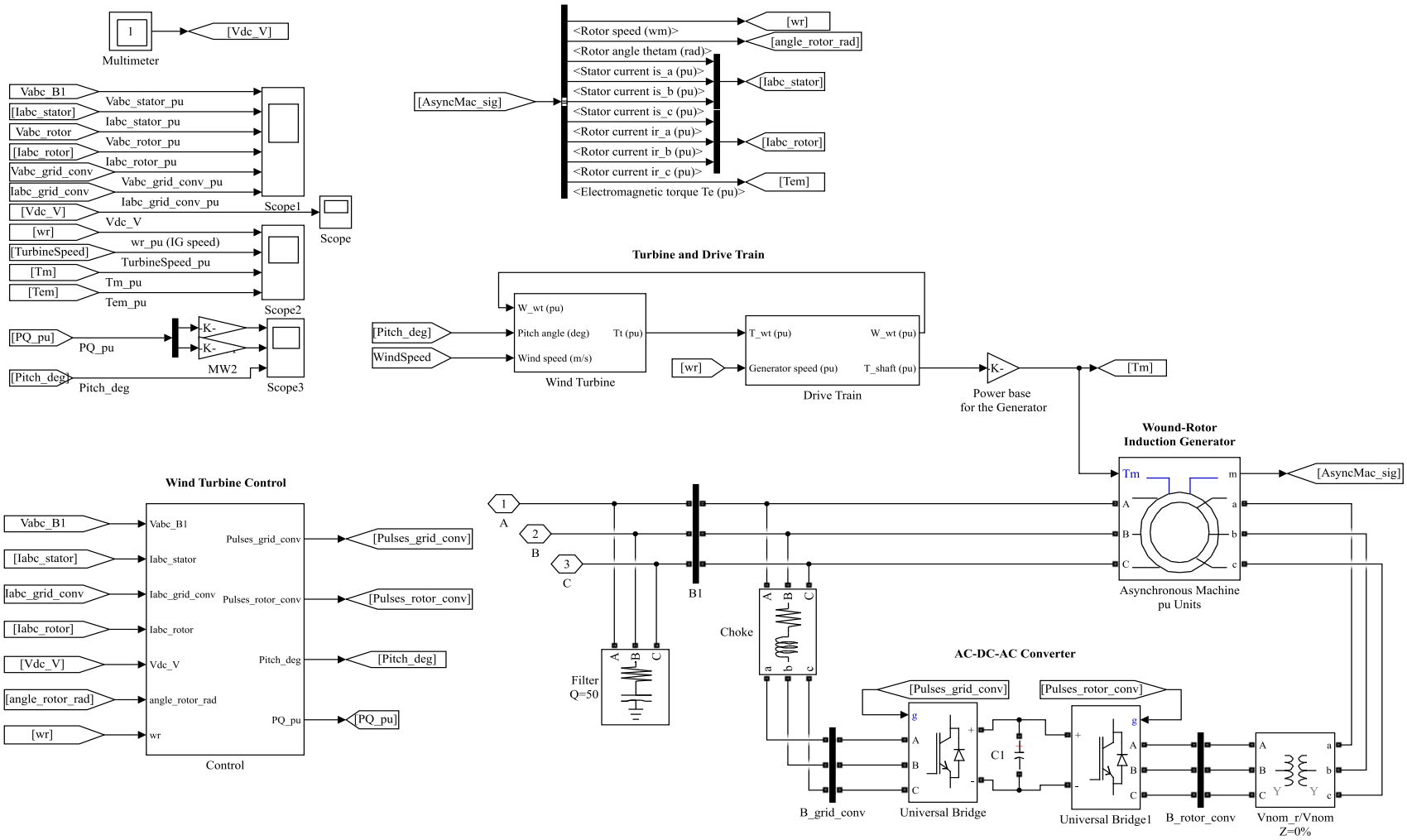

Figure 6.4: Wind turbine and AC-DC-AC converters modelled in Simulink

6.2.2 Solar Photovoltaic System

The solar PV model consists of a solar PV array (modules connected in a series and parallel combination) and a DC-DC boost converter using MPPT. The standard single-diode equivalent circuit is used to model a single solar PV cell, as shown in Figure 6.5 [157]. The circuit consists of four components: a photo current source, a diode, shunt resistor (R_{sh}) (each parallel to the source), and a series resistor (R_{ser}).

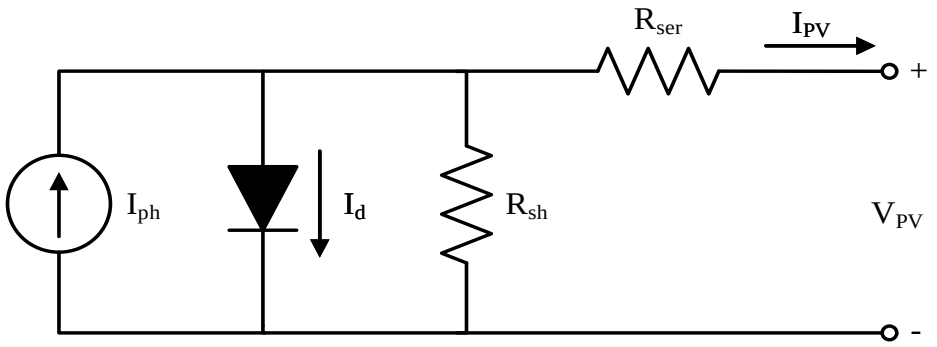

Figure 6.5: Standard single-diode equivalent circuit of a solar PV cell used to model a solar PV module in Simulink

The solar PV module when combined with multiple modules in series, N_{PV_s}, and parallel strings, N_{PV_p}, forms an array, and is modelled using Equation 6.19 - Equation 6.22 [157]:

$$I_{PV} = I_{ph} - I_d = I_{ph} - I_{sat}\left[exp\left(\frac{(V_{PV} + R_{ser}I_{PV}}{aV_T}\right) - 1\right] - \frac{V_{PV} + R_{ser}I_{PV}}{R_{sh}} \quad (6.19)$$

$$I_{ph} = \frac{G}{G_{ref}}(I_{SCS} + K_{I_{SC}}(T_{cell} - T_{ref}))N_{PV_P} \quad (6.20)$$

$$I_{sat} = I_{rr}\left(\frac{T_{cell}}{T_{ref}}\right)^3 exp\left(\frac{qE_{gap}}{ak}\right)\left(\frac{1}{T_{ref}} - \frac{1}{T_{cell}}\right) \quad (6.21)$$

$$V_T = \left(\frac{kT_{cell}}{q}\right)N_{PV_s} \quad (6.22)$$

The SPR-305E-WHT-D is selected for the simulation model, due to its higher efficiency compared to other conventional PV modules and thin film technology. The SunPower SPR-305E-WHT-D PV module characteristics are listed in Table 6.3[2] [161].

[2]Fill factor is a dimensionless measure of the deviation of the real I-V characteristics of a solar PV cell from the ideal characteristics, due to the series and shunt resistances [157]. The fill factor can be calculated as: $FF{=}V_{mpp}I_{mpp}/V_{oc}I_{sc}$

Table 6.3: Characteristics of the SunPower SPR-305E-WHT-D used to model a solar PV module in Simulink

Parameter	**Value**
Semiconductor material	Si
Temperature range (°C)	-40 - 85
Number of cells per module	96
Modules dimensions (m)	1.59 x 1.046
Peak efficiency, η_{PV} (%)	18.7
Maximum power per module, P_{mpp} (W)	305.226
Voltage at maximum power point per module, V_{mpp} (V)	54.7
Current at maximum power point per module, I_{mpp} (A)	5.58
Open circuit voltage per module, V_{oc} (V)	64.2
Short circuit current per module, I_{sc} (A)	5.96
Fill factor, FF	0.798

The solar PV module uses MPPT to extract the maximum possible amount of energy. There are numerous techniques available for MPPT, which include incremental conductance, Perturb and Observe, current sweep and constant voltage [157]. The Perturb and Observe technique, commonly used, is highlighted in Figure 6.6 and adopted for this thesis [157]. The sample code for the implementation of the Perturb and Observe algorithm is provided in Appendix C.

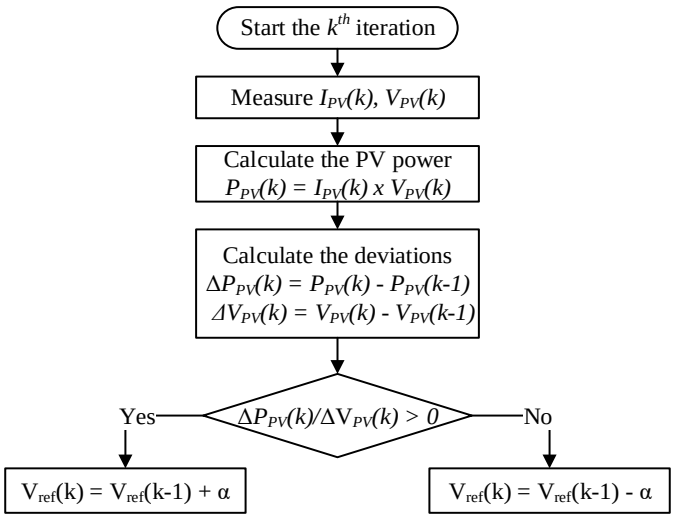

Figure 6.6: Perturb and observe MPPT methodology used to model a solar PV MPPT algorithm in Simulink

A DC-DC boost converter is used to regulate the voltage of the solar PV system to a higher voltage on the DC bus. The controller for the DC-DC boost converter requires one duty signal to be generated. The duty signal is determined from the MPPT algorithm. The MPPT algorithm will receive the current and voltage of the

solar PV module to determine the duty ratio for the boost controller. The output of the DC-DC boost converter is connected to the DC bus.

For this thesis, an average model with a controlled voltage source as the input (denoted as V_a and I_a) and controlled current source as the output (denoted as V_{dc} and I_{dc}) is used for the boost converter. The model uses equations Equation 6.23 and Equation 6.24 [162]:

$$V_a(k) = (1 - D)V_{dc}(k - 1) \tag{6.23}$$

$$I_{dc}(k) = \left(\frac{(1 - D)V_{dc}(k - 2)I_a(k - 1)}{2V_{dc}(k - 2) - V_{dc}(k - 3)} \right) SP_{PV} \tag{6.24}$$

The solar PV energy system is modelled in Simulink using:

— The equations to model a standard single-diode equivalent circuit (Equation 6.19 - Equation 6.22)

— The MPPT algorithm outlined in Figure 6.6

— The characteristics of a solar PV module listed in Table 6.3

— The solar PV average boost converter model (Equation 6.23 - Equation 6.24)

The solar PV energy system Simulink model is depicted in Figure 6.7. Table 6.4 lists the technical parameters of the solar PV Simulink model, in addition to the parameters listed in Table 6.3. At standard test conditions (solar irradiance 1,000 W m^{-2}, cell temperature 25°C), the solar PV system can output 100 kW/array.

Table 6.4: Technical parameters used to model a solar PV array in Simulink

Parameter	**Value**
Number of paralle strings per solar PV array, N_{PV_p}	66
Number of series connected PV modules per string, N_{PV_s}	5
Nominal capacity of the solar PV DER, P_{nom} (kW/array)	100
Series resistance in a PV cell equivalent circuit, R_{ser} (Ω)	0.37
Shunt resistance in a PV cell equivalent circuit, R_{sh} (Ω)	269.59
Boost converter inductor, L_1 (mH)	5
Boost converter capacitor, C_1 (μF)	100
Boost converter switching frequency (Hz)	5,000
Nominal DC link voltage (V)	500

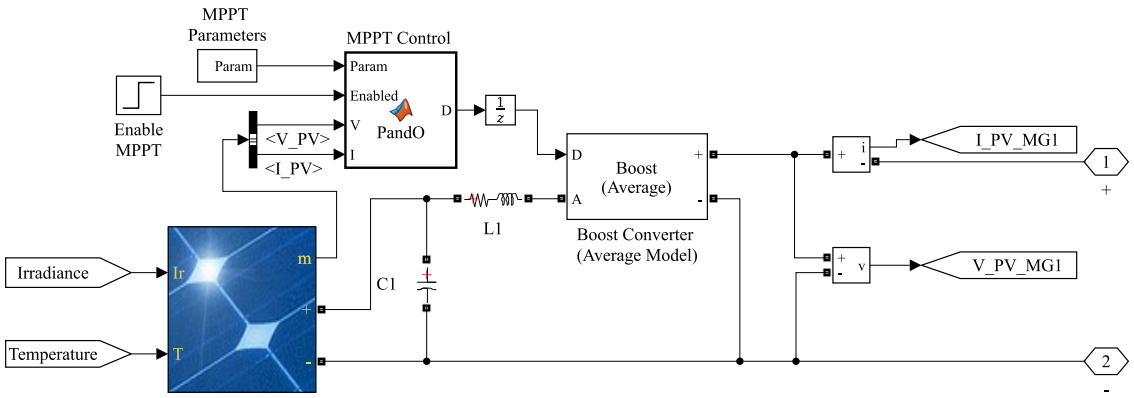

Figure 6.7: Solar PV array and DC-DC boost converter modelled in Simulink

6.2.3 Battery Energy Storage System

Many methods exist to model a battery, the most common being the equivalent circuit models, of which the most popular is the Thevenin model [163]. Equivalent circuit models will use basic electric elements to model the battery. However, the secondary battery equivalent circuit model, depicted in Figure 6.8, is more universal, and simpler to model [163]. This model is based on the battery discharge curve parameters. The magnitude, direction, duration time of the current, and the battery SOC influence the controlled voltage source at the same time.

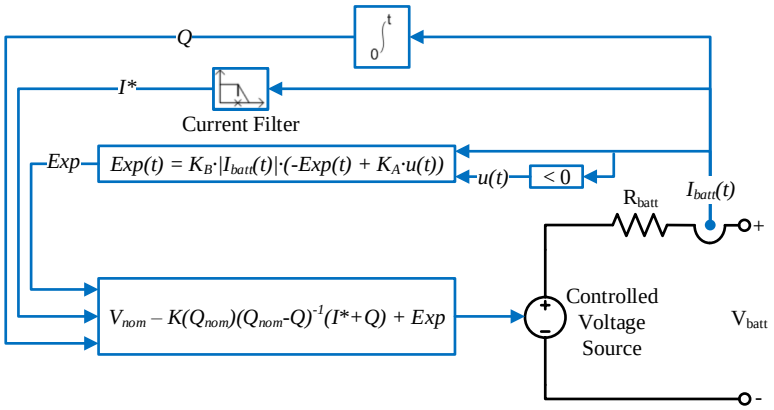

Figure 6.8: Secondary battery equivalent circuit model used to model a battery ESS in Simulink

The secondary battery equivalent circuit is modelled using equations Equation 6.25 - Equation 6.27 [163]:

$$V_{dis}(Q, I^*, I_{batt}) = V_{nom} - K\frac{Q_{nom}}{Q_{nom} - Q}(I^* - Q) + K_A exp(-K_B Q) - R_{batt} I_{batt} \quad (6.25)$$

$$V_{chg}(Q, I^*, I_{batt}) =$$
$$V_{nom} - K\left[\frac{Q_{nom}}{0.1Q_{nom}+Q}I^* - \frac{Q_{nom}}{Q_{nom}-Q}Q\right] + K_A exp(-K_B Q) - R_{batt}I_{batt} \quad (6.26)$$

$$SOC = 100\left(1 - \frac{1}{Q_{nom}}\int_0^t I_{batt}dt\right) \quad (6.27)$$

The lithium-ion battery will be used in this thesis due to the higher specific energy and power densities than other battery chemistries (see Table 2.2). The Tesla Powerpack battery is selected for the battery model, and the characteristics are listed in Table 6.5 [164]. The Tesla Powerpack is used for commercial and utility projects worldwide, most recently implemented in California and Australia.

Table 6.5: Characteristics of a Tesla Powerpack used to model a Lithium-ion battery ESS in Simulink

Parameter	**Value**
Type of battery	Lithium-ion
Power (kW/battery)	50
Rated capacity, Q_{nom} (Ah)	200
Nominal voltage, V_{nom} (V)	480
Internal battery resistance, R_{batt} (Ω)	0.02304

The battery requires a bidirectional DC-DC buck-boost converter in order to allow for the battery to charge and discharge. When the battery is discharging it acts in boost mode, and when being charged it acts in buck mode. The output of the DC-DC buck-boost converter is connected to the DC bus with the solar PV system.

The DC-DC controller uses current-mode control techniques to determine the duty cycle for the two switches [165]. The controller generates two signals: one for boost mode (discharging) and the other for buck mode (charging). Figure 6.9 shows the DC-DC bidirectional buck-boost controller was modelled in Simulink.

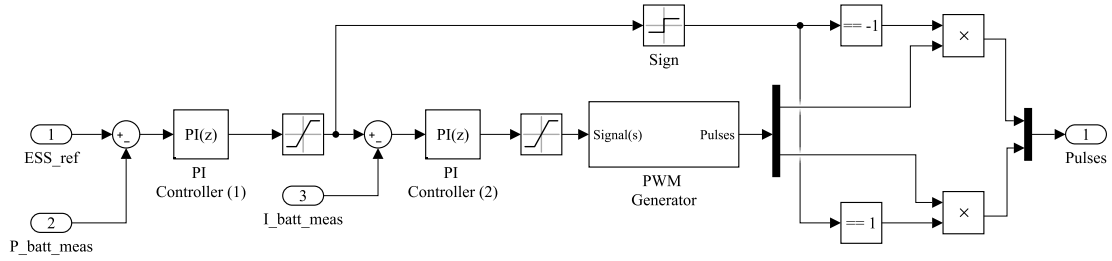

Figure 6.9: DC-DC bidirectional buck-boost controller for a battery ESS modelled in Simulink

The controller consists of two regulators: 1) power regulator (external loop) and

2) current regulator (internal loop). The power regulator will use a PI controller to regulate the difference between the set-point provided by the MG regulation system and the measured power (Equation 6.28). The current regulator, using a PI controller, will compare the reference current from the external loop, ϵ_1, to the actual inductor current measured (Equation 6.29). The output of the internal loop, ϵ_2, is used to generate the two PWM pulses for the DC-DC converter.

$$\epsilon_1 = \left(K_p + \frac{K_i}{s}\right)(SP_{ESS} - P_{ESS}) \tag{6.28}$$

$$\epsilon_2 = \left(K_p + \frac{K_i}{s}\right)(\epsilon_1 - I_{batt}) \tag{6.29}$$

The battery ESS is modelled in Simulink using:

— The equations to model a secondary battery equivalent circuit (Equation 6.25 - Equation 6.27)

— The characteristics of a battery ESS listed in Table 6.5

— The bidirectional buck-boost converter model (Figure 6.9) and accompanying equations (Equation 6.28 and Equation 6.29)

The battery ESS Simulink model is depicted in Figure 6.10. Table 6.6 lists the technical parameters of the battery ESS Simulink model, in addition to the parameters listed in Table 6.5.

Table 6.6: Technical parameters used to model a battery ESS in Simulink

Parameter	**Value**
Capacitor, C_1 (mF)	1
Inductor, L_1 (mH)	1
Capacitor, C_2 (mF)	1.2
Switching frequency, f (Hz)	10,000
External loop controller gains, [K_p, K_i]	[0.65, 150]
Internal loop controller gains, [K_p, K_i]	[1.5, 1]
SOC usage window (%)	20 - 90%

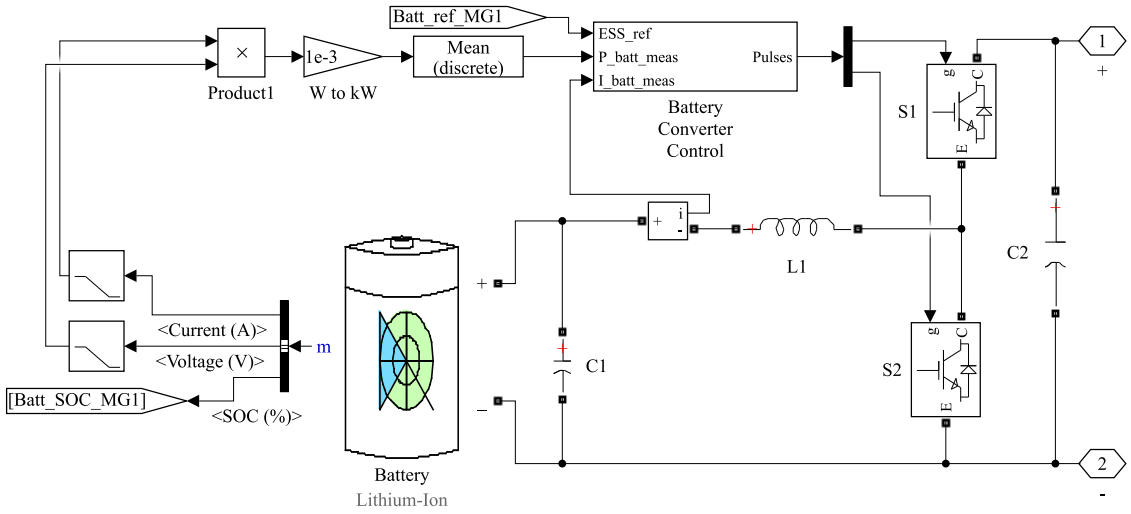

Figure 6.10: Battery ESS and bidirectional DC-DC buck-boost converter modelled in Simulink

6.2.4 DC Bus Inverter

A voltage-source inverter converter is required to convert the DC signals generated by the solar PV and battery systems, to the same AC signal of the IMG AC bus, railway load, and the electric grid. The inverter consists of a DC link, which reduces voltage ripples and maintains a constant voltage, and a grid-side converter, which converts the DC signal to AC using the switch information provided by the grid side voltage controller. An LC filter is used to filter out any harmonic distortion created by the inverter.

The voltage source converter consists of four components: Phase-Lock Loop, DC voltage regulator, current regulator, and a PWM generator. Figure 6.11 shows the modeling of the control system in Simulink. In the *PLL & Measurements* sub-

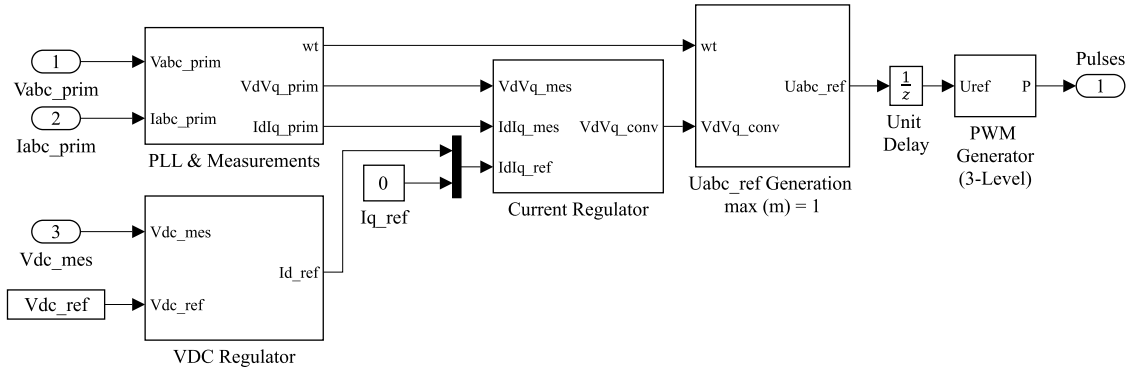

Figure 6.11: DC bus inverter voltage source converter controller modelled in Simulink

system, the electric grid phase information is measured. For further reading on the Phase-Lock Loop, see Appendix D. The measured three-phase voltage and current values from the electric grid are converted from abc-frame to dq-frame [166]. The control system consists of two loops:

1. External loop to regulate the DC link voltage
2. Internal loop to regulate the dq-frame currents

The purpose of the external loop is to maintain the DC link voltage to a set reference value. It will achieve this objective by adjusting the active power reference (i.e. d-frame current reference), as required. The input to the external loop is the measured voltage on the DC link. The output of the external loop is the d-frame current reference, while the q-frame current reference is set to zero for unity power factor to be achieved. Equation 6.30 and Equation 6.31 are used to model the external loop [166].

$$I^d_{ref} = \left(K_p + \frac{K_i}{s}\right)\left(\frac{V_{DC,meas} - V_{DC,ref}}{V_{DC,nom}}\right) \tag{6.30}$$

$$I^q_{ref} = 0 \tag{6.31}$$

The internal loop will be used to determine the dq-frame voltage references. The measured voltage and current of the electric grid, in dq-frame, are provided from the *PLL & Measurements* sub-system. Equation 6.32 and Equation 6.33 are used to model the internal loop [166].

$$V^d_{ref} = V^d_{grid} + R_{tot}I^d_{grid} - L_{tot}I^d_{grid} + \left(K_p + \frac{K_i}{s}\right)(I^d_{ref} - I^d_{grid}) \tag{6.32}$$

$$V^q_{ref} = V^q_{grid} + R_{tot}I^q_{grid} - L_{tot}I^q_{grid} + \left(K_p + \frac{K_i}{s}\right)(I^q_{ref} - I^q_{grid}) \tag{6.33}$$

The reference voltages, in dq-frame, are used to generate the pulses for the switches in the inverter. The reference values are converted back to abc-frame using the phase information from the *PLL & Measurements* sub-system [166]. The voltage waveforms are then compared to a carrier waveform to generate the pulses.

The technical parameters of the DC bus inverter are listed in Table 6.7 [166]. The inverter is modelled in Simulink, as depicted in Figure 6.12.

Table 6.7: Technical parameters used to model the DC bus inverter in Simulink

Parameter	Value
Nominal system frequency, f (Hz)	60
Nominal primary line-to-line voltage (kV)	25
Nominal secondary line-to-line voltage (kV)	260
DC link capacitor, (mF)	20
Modulation index	0.85
DC voltage regulator gains, [K_p K_i]	[7 800]
Current regulator gains, [K_p K_i]	[0.3 20]
Carrier frquency of PWM (Hz)	1,980

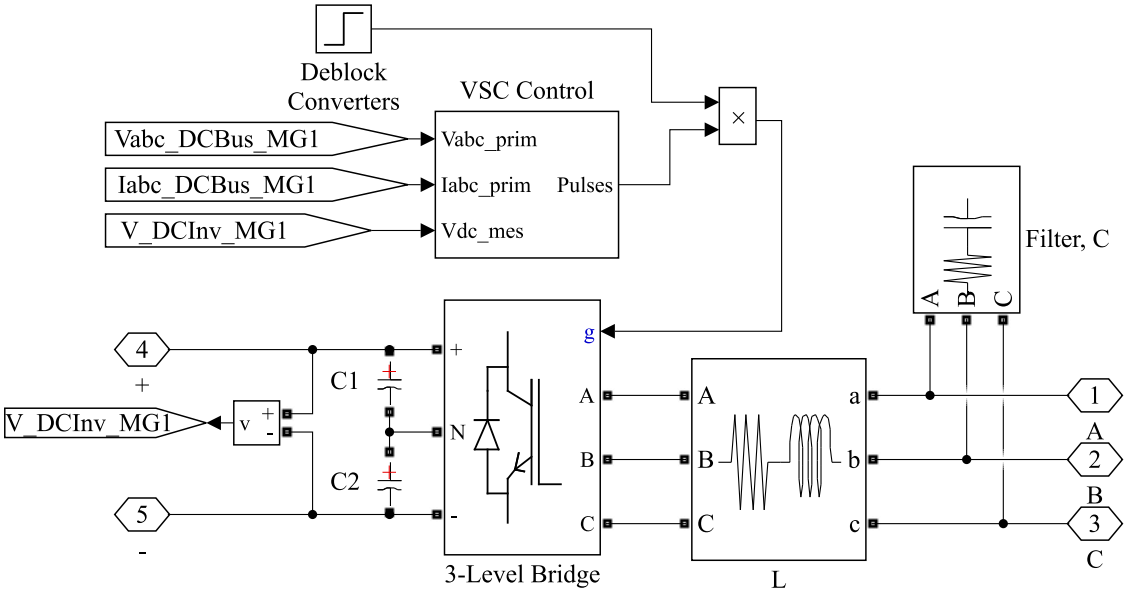

Figure 6.12: DC bus inverter, to convert the DC signal of the solar PV and battery ESS to an AC signal, modelled in Simulink

6.2.5 Electric Grid, Traction Power Substation, Microgrid Interconnection

The electric grid, traction power substation, and MG interconnection are modelled after Figure 1.3. When the demand of the railway infrastructure cannot be satisfied by the IMG and any other IMG, the electric grid can be relied on to supply the deficit. The nominal capacity of the electric grid is modelled to be much higher than that of the IMG. This allows for each IMG to import/export electricity to/from the electric grid, as required. MGs are interconnected together through a 25 km feeder, along the railway corridor.

Table 6.8 provides the technical parameters used to model the electric grid. Figure 6.13 shows the modeling of the electric grid and traction power substation in Simulink.

Table 6.8: Technical parameters used to model the electric grid and traction power substation in Simulink

Parameter	Value
Nominal system frequency, f (Hz)	60
Nominal primary line-to-line voltage (kV)	230
Nominal secondary line-to-line voltage (kV)	25

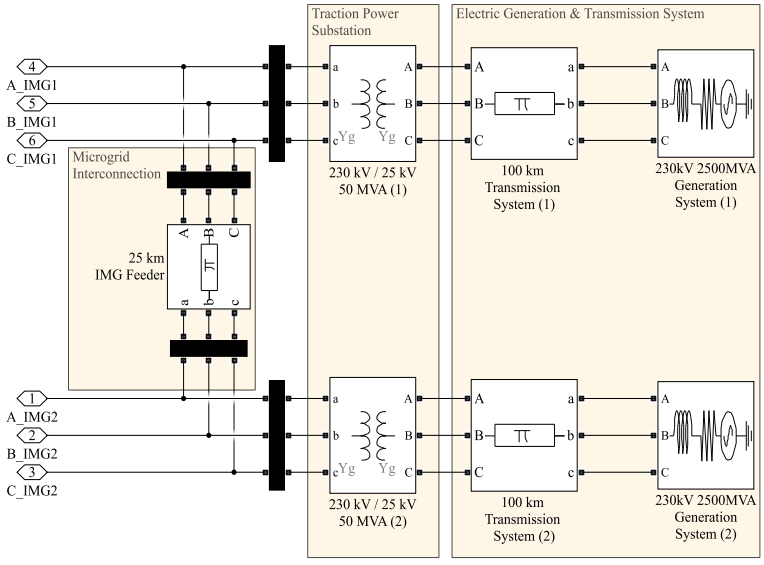

Figure 6.13: Electric grid and traction power substation, with an interconnection between two IMGs, modelled in Simulink

6.2.6 Microgrid Regulation System

The proposed strategy for the MG regulation system, described in Section 5.2.4, has been mapped to Simulink. Figure 6.14 depicts the Simulink model for the possible paths for energy to be exchanged within a single IMG. Figure 6.15 depicts the Simulink block that implements the MG regulation switch strategy and set-point calculation. The sample code for the MG regulation system is provided in Appendix C.

As described in Section 5.2.4, the limit of power a DER can export is the sum of the export limit imposed by the electric grid regulator and the amount required to support an IMG, as determined by the IMG supervisory controller (IMGSC). The DER export capacity imposed by the electric grid operator is decided by a regional electrical system operator (e.g. Ontario Independent Electric System Operator (IESO)). For this thesis, the DER export capacity set by the Ontario IESO Feed-In-Tarrif program is adopted (see Table 6.9) [145]. The criteria for exporting to the electric grid is outlined in the control strategy, Figure 5.4.

Table 6.9: IESO export capacity for a RES to the electric grid

RES	IESO Export Capacity	Simulation Export Capacity
Solar (PV) (Non-rooftop)	> 10 kW & ≤ 500 kW	20 kW/PV array
On-shore wind	≤ 500 kW	500 kW/WT

6.2.7 Interconnected Microgrid Supervisory Controller

The proposed strategy for the IMGSC, described in Section 5.2.5, has been mapped and implemented in Simulink, as shown in Figure 6.16. The applicable code for the IMGSC is available in Appendix C.

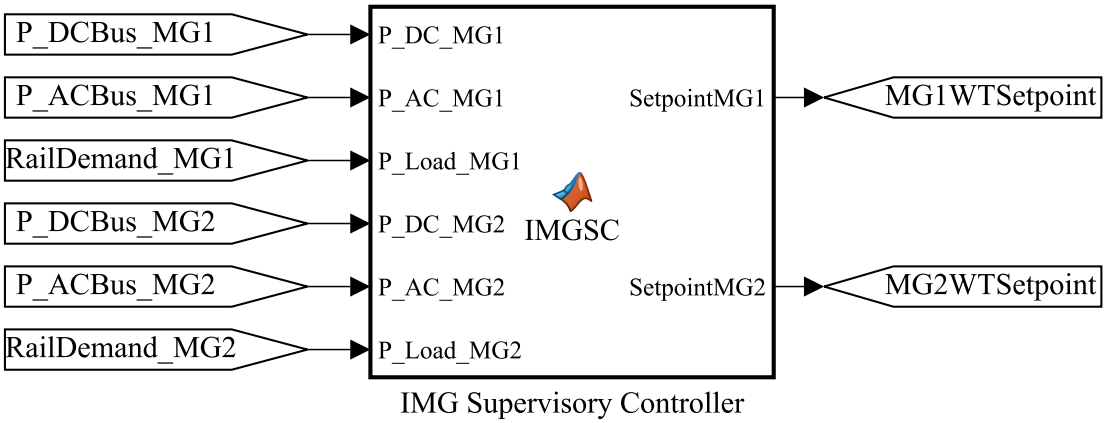

Figure 6.16: Interconnected microgrid supervisory controller strategy implemented in Simulink

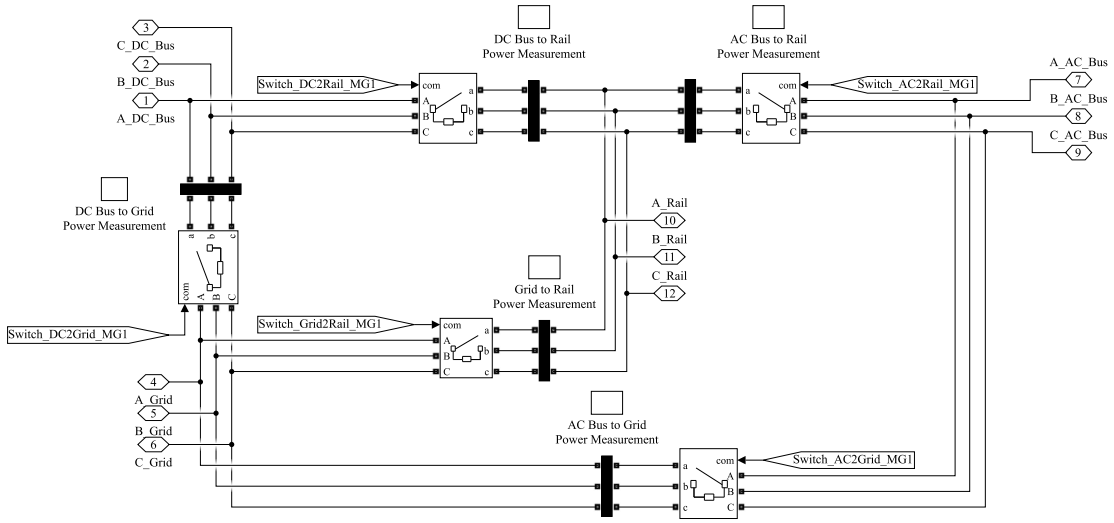

Figure 6.14: Microgrid regulation system to facilitate the exchange of energy between the MG busses, electric grid, and railway load modelled in Simulink

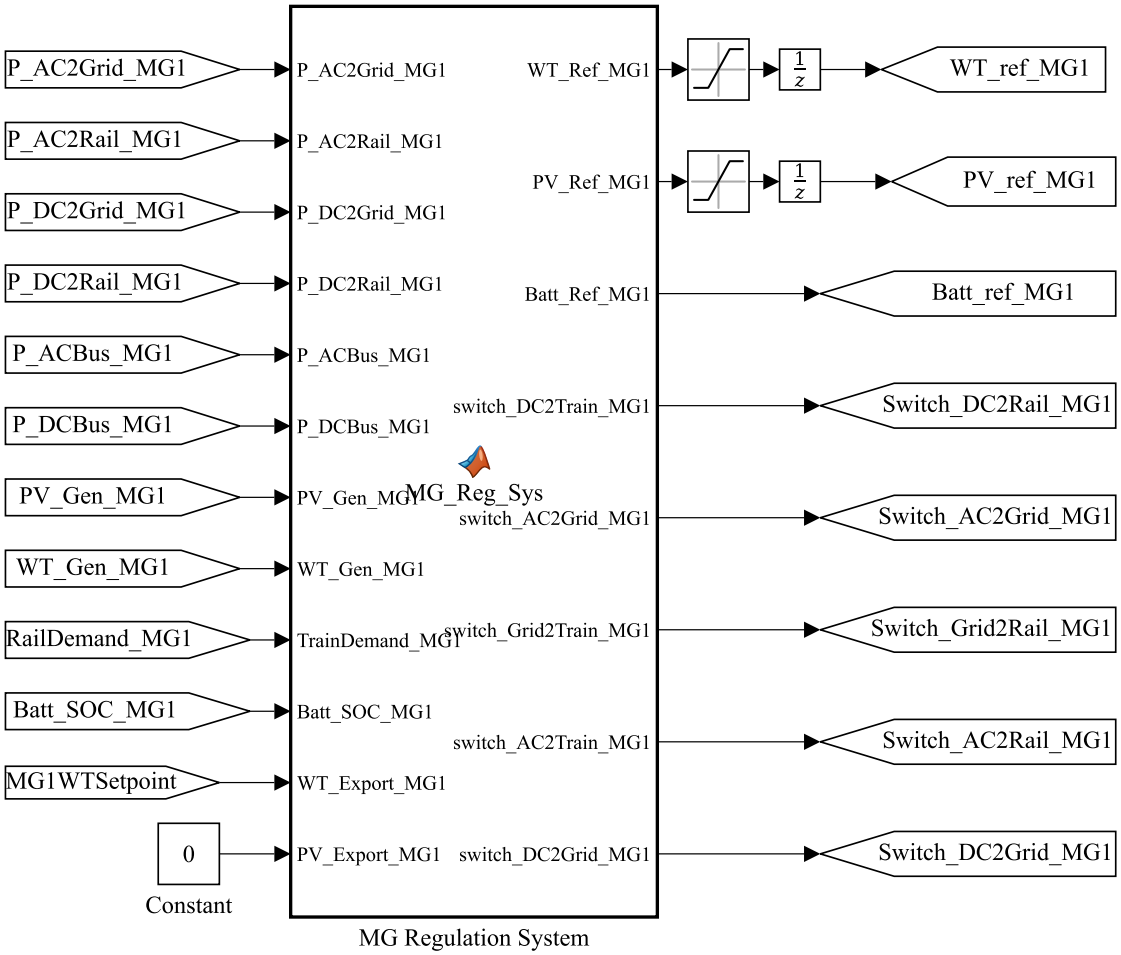

Figure 6.15: Microgrid regulation system switching strategy and set-point calculation strategies implemented in Simulink

6.3 Railway Infrastructure Modelling

While a railway infrastructure consists of many loads, for this thesis only the demand of a single rolling stock will be considered as the load. The rolling stock requires energy to accelerate and overcome mechanical resistances. Based on basic principles of physics and vehicle properties, the traction power required by the rolling stock can be determined using a net force diagram of a single rolling stock on an incline Figure 6.17 [167].

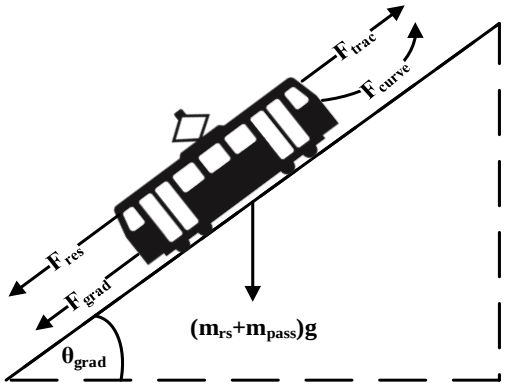

Figure 6.17: Net force diagram of a rolling stock on an incline used to model a single ride of a rolling stock in Simulink

The tractive effort required to move a rolling stock can be expressed using Newton's second law of motion [167]:

$$F_{trac} - F_{grad} - F_{res} - F_{curve} = m_{eff}\frac{dv_{rs}}{dt} \tag{6.34}$$

The effects of resistance due to curves is only necessary when considering a route that exhibits tight curves, and as such has been neglected for the scope of this thesis [167].

The effective mass of the rolling stock combines the mass of the rolling stock and the passenger load. A rotary allowance is incorporated in the mass of the rolling stock to account for the rotational inertia of the rotating components. Equation 6.35 shows the calculation of the effective mass [167]:

$$m_{eff} = m_{rs}(1 + \lambda_w) + m_{pass} \tag{6.35}$$

The gradient force is dependent on the grade of the railway track along the proposed route, and calculated using Equation 6.36 [167]:

$$F_{grad} = (m_{rs} + m_{pass})g \sin\theta_{grad} \tag{6.36}$$

The "Davis equation" provides a general formula for calculating the resistance forces experienced by a rolling stock [167]. The equation combines the rolling friction, flange friction, and aerodynamic resistances using the Davis coefficients. The Davis coefficients are determined based on the design and configuration of the rolling stock. The resistance force is calculated using Equation 6.37 [167]:

$$F_{res} = A + Bv_{rs} + Cv_{rs}^2 \tag{6.37}$$

The traction power of the rolling stock is calculated usingEquation 6.38 [167]:

$$P_{trac} = \frac{F_{trac}v_{rs}}{\eta_{trac}}, v_{rs} > 0 \tag{6.38}$$

Due to energy saving concerns and technology advancements, newer built rolling stock are taking advantage of regenerative braking technologies. When the rolling stock is braking, the energy that is typically lost is partially recovered and used for other purposes (see Appendix A for further reading). The power regenerated by the rolling stock during braking operations is calculated using Equation 6.39 [167]:

$$P_{regen} = F_{trac}v_{rs}\eta_{regen}, v_{rs} < 0 \tag{6.39}$$

Ignoring losses throughout the railway infrastructure (i.e. conversion efficiencies, transformer losses, current losses), this approach to modeling the energy consumption of the rolling stock can be simplified to a standard approach. The total active power required by the rolling stock is the sum of the traction, regenerative and auxiliary power (Equation 6.40) [167]:

$$\sum P_{load} = P_{trac} + P_{regen} + P_{aux} \tag{6.40}$$

Auxiliary power is used for opening the doors, communication, lighting, HVAC, and any other non-traction related features. While the traction power of the rolling stock is predictable given that railway infrastructures operate on fixed schedules and routes, the auxiliary power will vary based on the current rolling stock features and as seasons change throughout the year. Typically, auxiliary power is considered as a constant when modeling the expected rolling stock energy consumption [151].

The railway load (i.e. the rolling stock) is modelled in Simulink as a controlled single-phase current source. Equation 6.34 - Equation 6.40 are used to generate the traction power of the rolling stock. The auxiliary power is assumed constant throughout the movement of the rolling stock. The sum of the traction and auxiliary power of a single rolling stock is calculated using the speed-distance profile of the

railway route and technical parameters of the rolling stock, as seen in Figure 6.18.

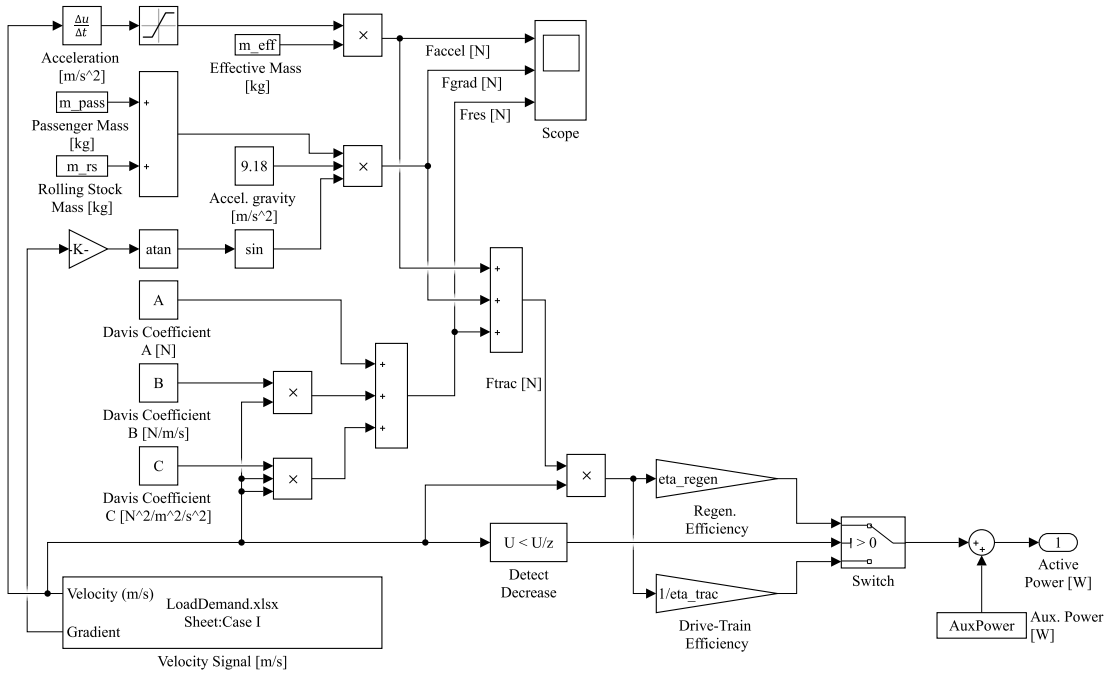

Figure 6.18: Active power of a single rolling stock computation modelled in Simulink

The output signal is then fed into a single-phase dynamic source, which acts as the railway load in the simulation, as seen in Figure 6.19. In this thesis, only active power is considered, while reactive power is held constant at 0 Vars.

The simulation model studies the behaviour of a single rolling stock moving in both directions. However, the model is scalable to consider a railway infrastructure with multiple rolling stock moving throughout the specified study period (i.e. hour, day, month, year). The input in the model in Figure 6.19, is capable of considering any load profile that is pre-determined by software typically used by railway operators for schedule optimization.

6.4 Resilient Interconnected Microgrid Model

Using the proposed detailed design in Figure 5.3, the overall RIMG design has been mapped to Simulink, using the individual simulation models of the DERs, ESS, electric grid, railway load, and all other necessary components described in this chapter. Figure 6.21 shows the implementation of the Simulink model, which consists of the two MGs interconnected together.

The key inputs to the model include:

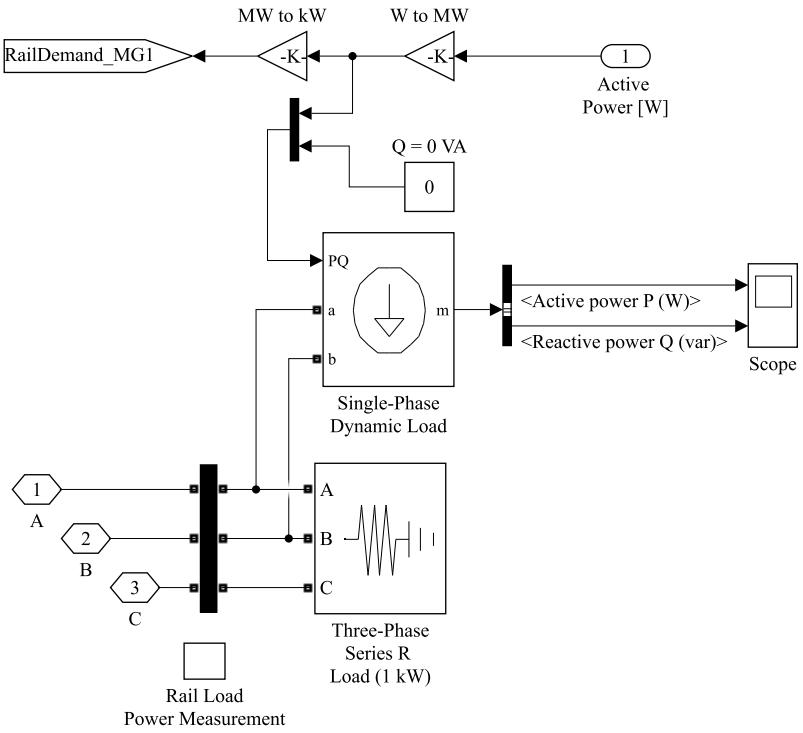

Figure 6.19: Single-phase load used to represent rolling stock demand modelled in Simulink

— Weather resource data (solar irradiance, wind speed, and temperature)

— Route profile data for the rolling stock (speed-time, gradient)

— Component technical parameters of the rolling stock (i.e. rolling stock and passenger masses, rotary allowance, Davis coefficients, drive-train and regenerative braking efficiencies, and auxiliary power)

— Component technical parameters of solar photovoltaic, wind turbine, ESS, power-electronic converters, and the electric grid

The key outputs of the model include:

— Energy analysis: The outputs include total energy production of each DER, energy charged/discharged in each ESS, energy imported from and exported to the electric grid, load consumption, and any other information that describes the system performance.

— Resiliency analysis: The outputs are various resiliency metrics that describe the system (i.e. renewable generation, IMG demand served, IMG reliance, and electric grid dependence).

The parameters listed in Table 6.10 are used to execute the simulation model in Simulink. The simulation run-time is set to five seconds, with all input and output

data being scaled appropriately. Figure 6.20 depicts input data for the weather resources (i.e. solar irradiance, outdoor temperature, and wind speed) provided by Simulink [137].

Table 6.10: Technical parameters used to simulate the proposed RIMG model in Simulink

Parameter	**Value**
Model	Discrete
Simulation run time, t_{sim} (s)	5
Simulation sample time, $t_{sim,power}$ (μs)	50
DC bus inverter control system sample time, $t_{sim,control}$ (μs)	100

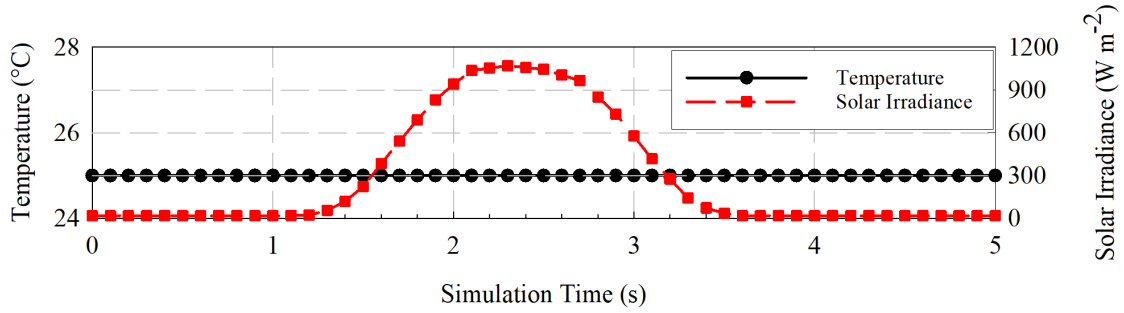

(a) Solar irradiance and ambient temperature

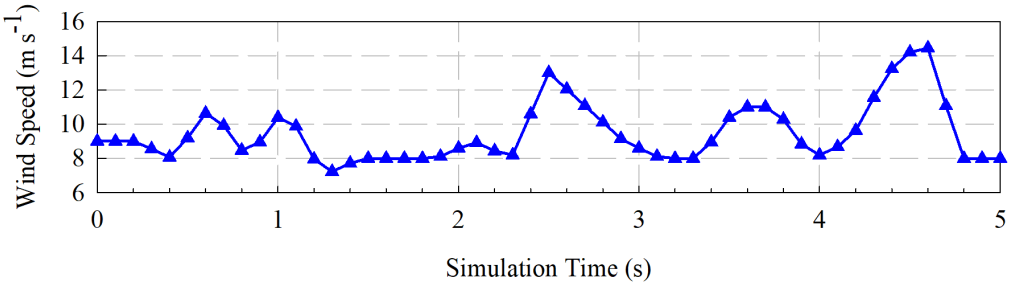

(b) Wind speed

Figure 6.20: Weather data assumed for sizing and simulation analysis

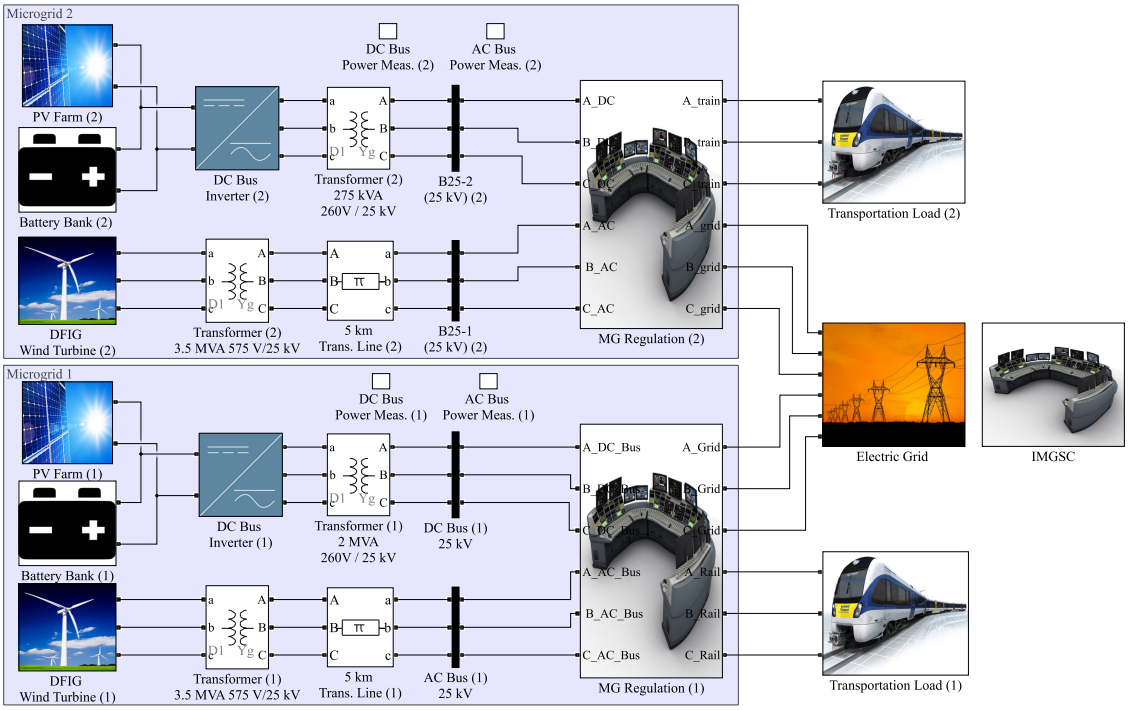

Figure 6.21: Simulink RIMG model, which consists of RESs (i.e. solar PV and wind turbine systems), an ESS (i.e. battery), and an interconnection between MGs where a supervisory controller monitors the resilience of the overall system

Chapter 7

Case Studies

Four case studies are considered to evaluate the impact of the proposed RIMG design. Different types of passenger railway infrastructures in the United Kingdom and Canada, which exhibit different speed-distance profiles and rolling stock characteristics, are studied. Railway infrastructures considered are assumed to be electrified, regardless of current state. This is to prove the concept of RIMGs for reliable mass transit systems. Results are adaptable to other existing electrified railway systems.

The following case studies are used to demonstrate the effectiveness of the proposed methods and designs:

— **High Speed 2**, a high-speed railway approved by the United Kingdom Government in 2017, which will transport passengers between London Euston and Birmingham Curzon Street

— **North Warwickshire Line**, an intercity railway, which transports passengers between Birmingham Moor St. and Stratford-upon-Avon, UK

— **GO Transit**, two of seven intercity lines in the Greater Toronto Area, each departing from Union Station in downtown Toronto, Ontario

— **UP Express**, the first dedicated link in North America between two major transportation hubs in the Greater Toronto Area: Union Station and Pearson Airport

7.1 Case Study Assumptions

While railway lines are typically divided into sections, to preserve the quality of the data, two IMGs will be simulated where: one IMG will simulate the movement

of the rolling stock from one terminal station to the other, and the other IMG will simulate the movement of the rolling stock moving in the opposite direction, simultaneously [83]. As such, the following assumptions are made for each case study:

— The active power profile of the rolling stock includes the traction and auxiliary power and is determined using Equation 6.34 - Equation 6.40 [167]

— The auxiliary power is assumed constant throughout the journey [151]

— A straight alignment is assumed, with no curves or gradient [167]

— A seated load (AW1) is considered, which consists of the mass of the rolling stock and a passenger in each seat [144]

— The mass of a passenger is assumed to be 70 kg [144]

— Unless provided by the original study, the drive-train efficiency, η_{trac}, is assumed to be 85% [168]

— The rolling stock can recover energy from braking operations and unless provided by the original study, the regenerative braking efficiency, η_{regen}, is assumed to be 80% [151]

7.2 Case Study I: High Speed 2 - London to Birmingham, UK

The first case study considered is a proposed high-speed route from London to Birmingham in the United Kingdom. In 2017, the United Kingdom Government approved of the implementation of a high-speed railway from London Euston to Birmingham Curzon Street, also referred to as High Speed 2. This project is the successor to the High Speed 1 high-speed railway between London and the Channel Tunnel, which began operation in 2003. High-speed railway infrastructures are becoming an important transportation mode in the UK to relieve capacity constraints on existing railway networks, reduce passenger travel time and push for an increase in electrified railways. Proposals for High Speed 3 were announced in 2014, linking more cities in the north of the UK to the high-speed railway infrastructure.

The rolling stock parameters in Table 7.1 are adopted from the AGV-11 rolling stock produced by Alstom [151]. The original study of the proposed route looked at energy consumption trends for various rolling stock speeds, while this thesis will consider the rolling stock operating at the maximum allowed speed (360 km h^{-1}),

where permissible. The 175 km route departs from London Euston, with two inter-station stops for two minutes, before arriving at Birmingham Curzon. The rolling stock has a one-minute dwell time before repeating the route in the reverse direction to London Euston. Figure 7.1 depicts the speed-distance profile for the proposed route, including a return trip.

The active power profile of the rolling stock depicted in Figure 7.2 is calculated using the technical parameters of the rolling stock Table 7.1, the speed-distance profile of the route Figure 7.1, and Equation 6.34 - Equation 6.40.

Figure 7.3 and Figure 7.4 are the input data for the weather disturbance analysis [169]. The weather data consists of historical data for each of the terminal stations of the route (i.e. London and Birmingham, UK). The data includes the solar irradiance, temperature, and wind speed.

Details of a parametric analysis of the drive-train efficiency and its effects on the performance of the proposed system design is provided in Appendix E.

Table 7.1: Alstom AVV-11 rolling stock technical parameters used in case study I

Parameter	**Value**
Rolling stock mass, m_{rs} (kg)	373,360
Passenger mass, m_{pass} (kg)	36,287.4
Rotary allowance, λ_w (%)	6
Davis equation parameters, [A (N), B (Ns m^{-1}), (C Ns^2 m^{-2})]	[6,540, 38, 6]
Auxiliary power, P_{aux} (W)	585,000
Regenerative braking efficiency, η_{regen} (%)	80
Drive-train efficiency, η_{trac} (%)	82.3
Number of seats	510

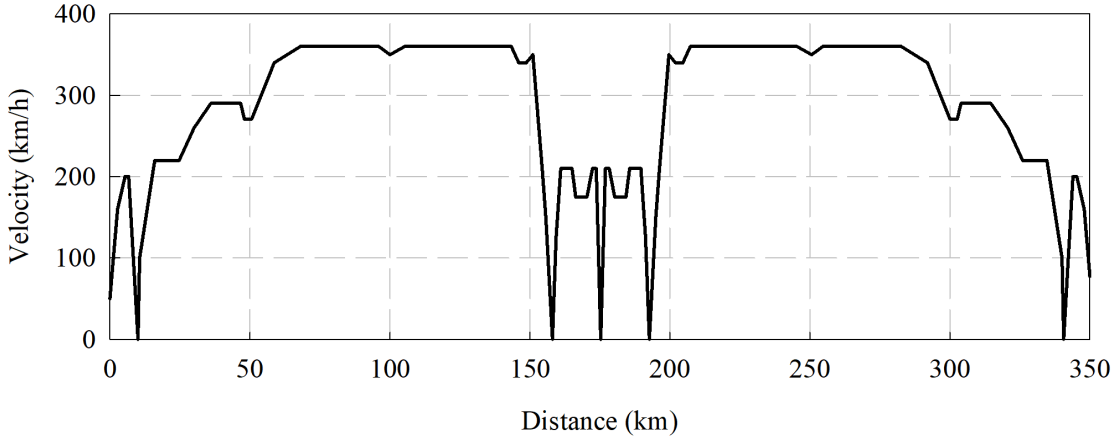

Figure 7.1: Speed-distance profile of the rolling stock moving from London Euston to Birmingham Curzon, including return trip

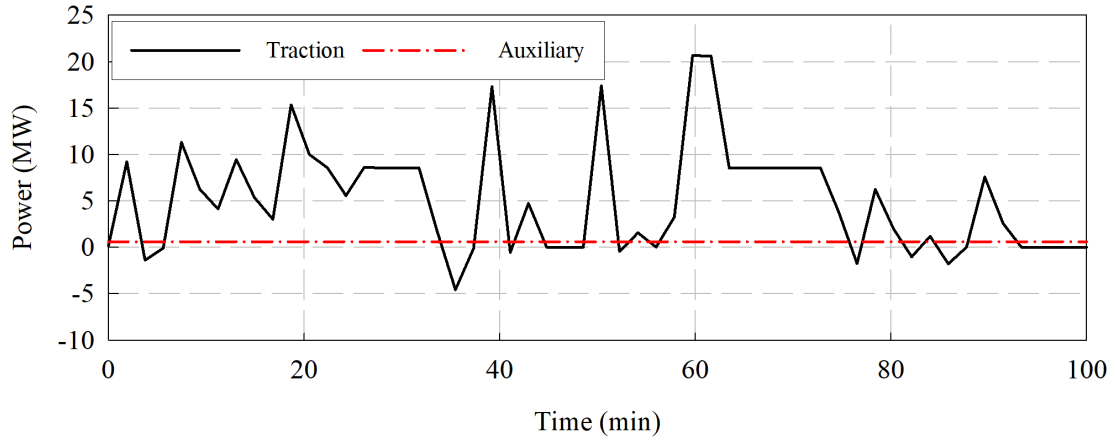

Figure 7.2: Active power of the rolling stock, calculated using rolling stock characteristics, speed-distance profile of the route moving from London Euston to Birmingham Curzon, including return trip, and system modelling equations

7.3 Case Study II: North Warwickshire Intercity Line - Birmingham Moor Street to Stratford-upon-Avon, UK

The second case study considers an existing intercity route from Birmingham Moor Street to Stratford-upon-Avon in the United Kingdom. The study authored by Hoffrichter et al. [9] aimed to benchmark the conceptual design of a hydrogen-powered rolling stock and to determine the energy savings by switching from diesel powered rolling stock to hydrogen-powered. However, as mentioned previously there is a lack

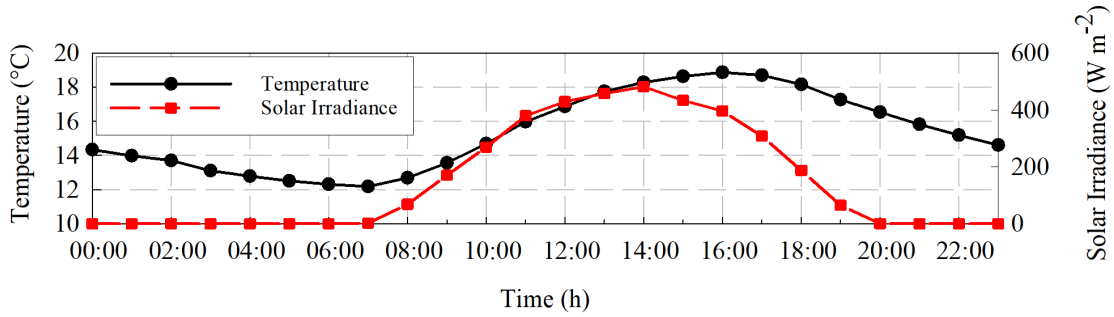

(a) Solar irradiance and ambient temperature

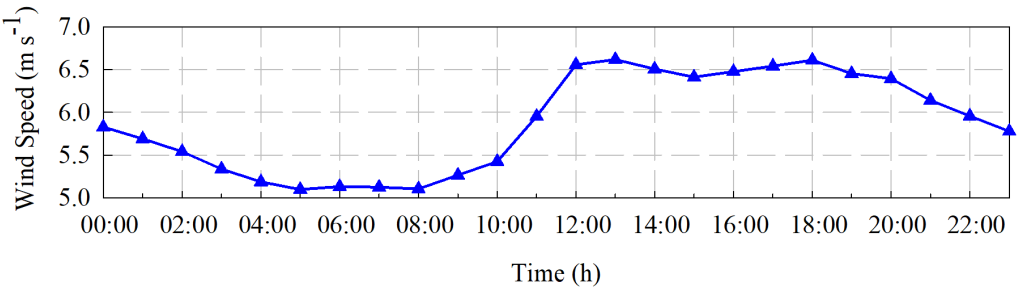

(b) Wind speed

Figure 7.3: Weather input data for London, UK

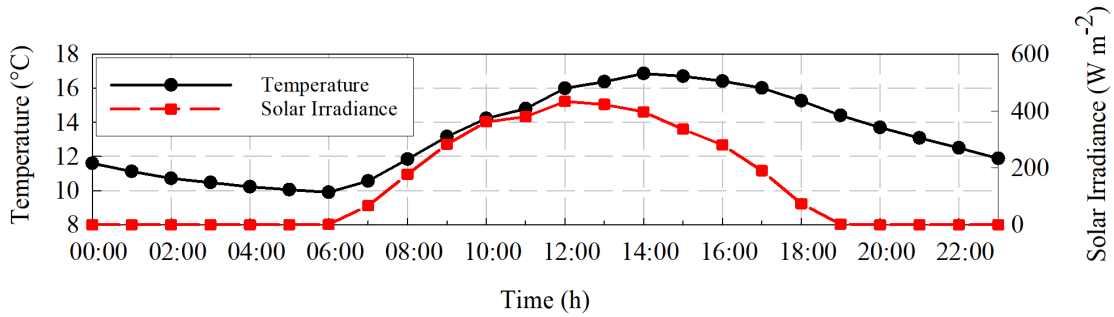

(a) Solar irradiance and ambient temperature

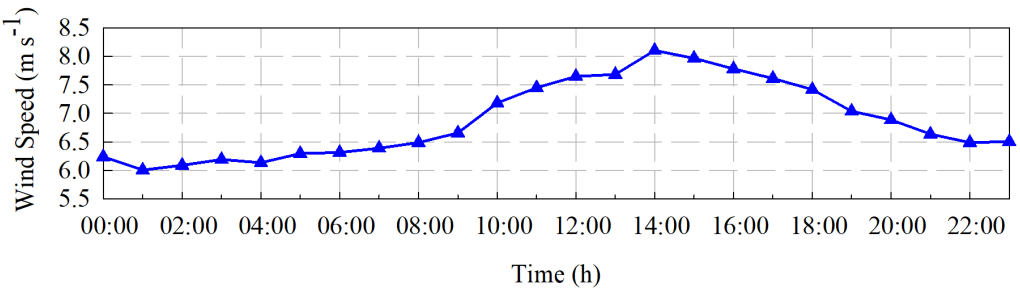

(b) Wind speed

Figure 7.4: Weather input data for Birmingham, UK

of full-service hydrogen-powered railways, a supporting infrastructure, and the UK is considering electrification of existing railway lines before considering other options. In addition, the Birmingham Moor Street station is proposed to be adjacent to the Birmingham terminus station of the High Speed 2 railway route (see Section 7.2), which will result in higher passenger demand in the future.

The rolling stock parameters listed in Table 7.2, are adopted from the Gelenktriebwagen 2/6 rolling stock produced by Stadler AG and is commonly used around the world, and have either been assumed (bold) or used from reference [9]. While this rolling stock has a diesel-electric drive-train, it is commonly used for intercity and regional railway routes and is a suitable benchmark for this case study. The speed-distance profile in Figure 7.5 is provided by Hoffrichter et al. [9]. In this route, the rolling stock travels 78.58 km, with sixteen 30 second stops at each station. Upon arrival in Stratford-upon-Avon, the rolling stock experiences a five-minute rest, before repeating the trip in the reverse direction to Birmingham Moor Street station.

Table 7.2: Stadler AG Gelenktriebwagen 2/6 rolling stock technical parameters used in case study II

Parameter	**Value**
Rolling stock mass, m_{rs} (kg)	65,317.3
Passenger mass, m_{pass} (kg)	18,143.7
Rotary allowance, λ_w (%)	**10**
Davis equation parameters, [A (N), B (Ns m^{-1}), (C Ns^2 m^{-2})]	[1,500, 6, 6.7]
Auxiliary power, P_{aux} (W)	65,000
Regenerative braking efficiency, η_{regen} (%)	**80**
Drive-train efficiency, η_{trac} (%)	88
Number of seats	138

The active power profile of the rolling stock depicted in Figure 7.6 is calculated using the technical parameters of the rolling stock Table 7.2, the speed-distance profile of the route Figure 7.5, and Equation 6.34 - Equation 6.40.

Figure 7.4 and Figure 7.7 are the input data for the weather disturbance analysis [169]. The weather data consists of historical data for each of the terminal stations of the route (i.e. Birmingham and Stratford-upon-Avon, UK). The data includes the solar irradiance, temperature, and wind speed.

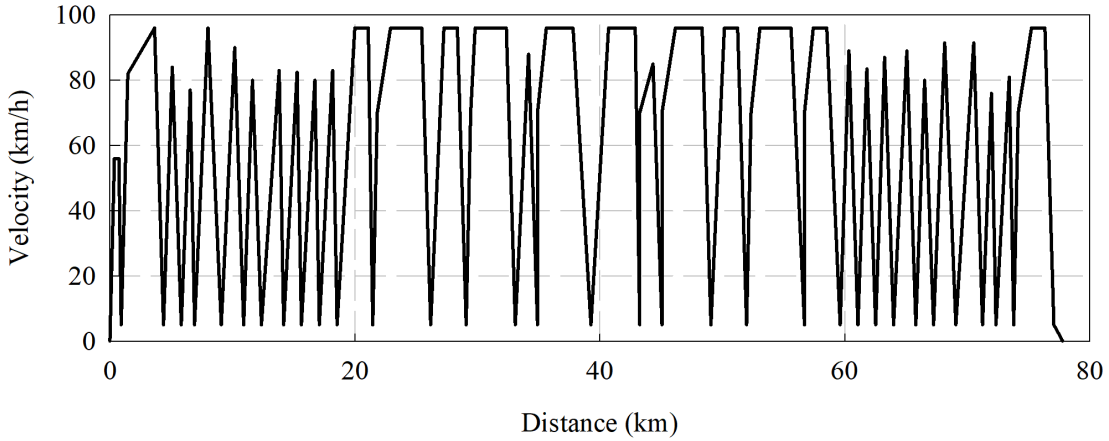

Figure 7.5: Speed-distance profile of the rolling stock moving from Birmingham Moor Street to Stratford-upon-Avon, including return trip

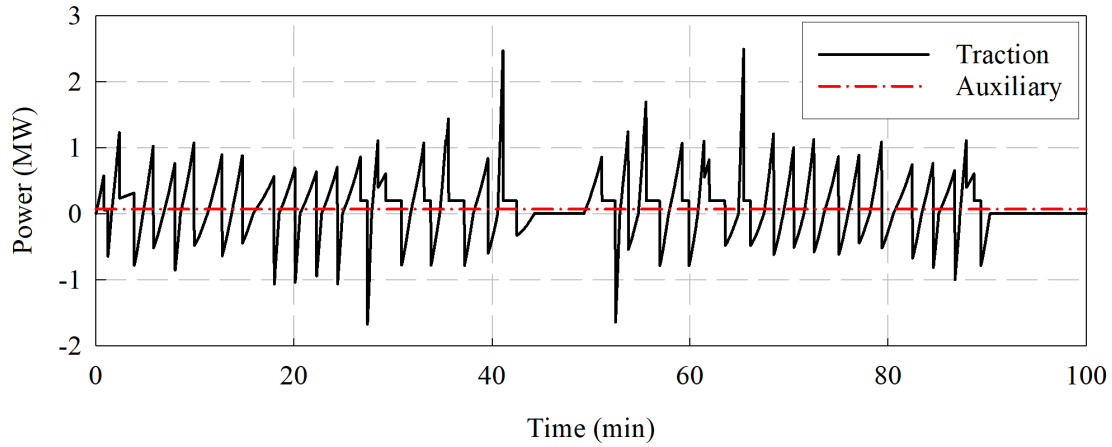

Figure 7.6: Active power of the rolling stock, calculated using rolling stock characteristics, speed-distance profile of the route moving from Birmingham Moor Street to Stratford-upon-Avon, including return trip, and system modelling equations

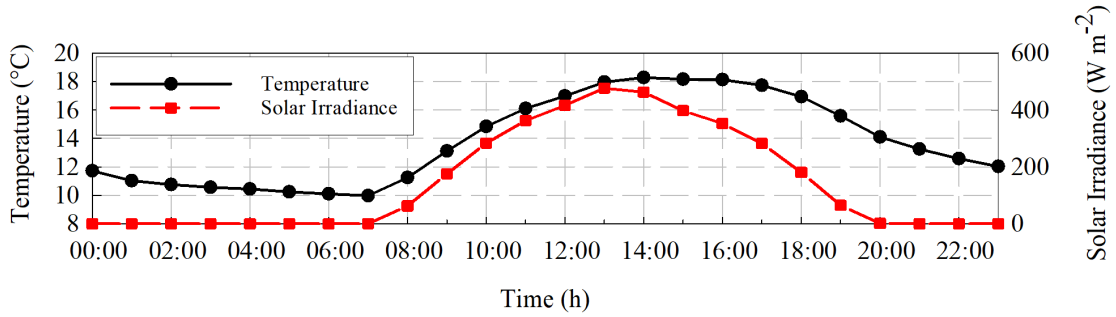

(a) Solar irradiance and ambient temperature

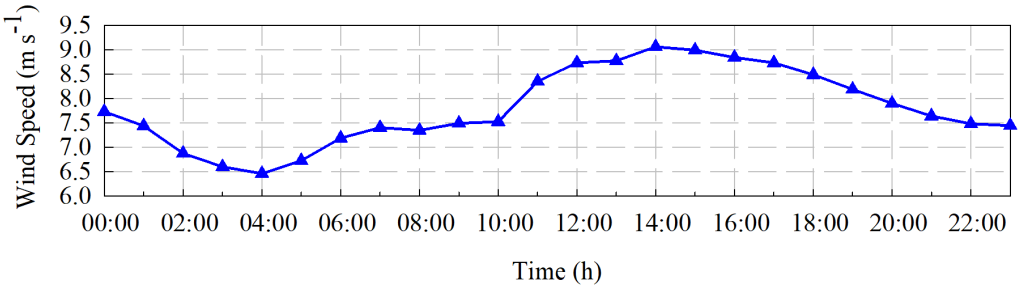

(b) Wind speed

Figure 7.7: Weather input data for Stratford-upon-Avon, UK

7.4 Case Study III: GO Transit Network - Lakeshore Corridors

The GO Transit network consists of a complex rail and bus network, which serves the population of the Greater Toronto Area. Currently, the network consists of seven commuter rail lines and boasts an annual ridership of approximately 55 million people [147]. The current GO rail infrastructure operates with diesel fuel, however numerous assessment studies have been undertaken in the last eight years for the electrification of the rail network [147]. Metrolinx (GO Transit operator) and the Ontario Government are currently targeting an increase in service from its current form to all-day, two-way, 15-minute electrified GO service by 2025 [6, 170].

The network consists of 65 stations, including Union Station which receives all inbound and outbound services [147]. The Lakeshore East and West lines are the most commonly travelled routes of the GO network, while the other four routes are currently used for peak service on weekdays. In an electrification assessment study for the GO network, a bi-level rolling stock was used for the evaluation of electrifying the Lakeshore corridor. Technical parameters of a bi-level rolling stock were gathered from rolling stock currently being used today (i.e. Siemens Desiro RABe 514 Double-Deck EMU and Alstom Coradia Duplex), and an average model was used, though the data closely resembles the Desiro RABe 514. The technical

Table 7.3: Bi-Level EMU rolling stock technical parameters, averaged using existing models, used in case study III

Parameter	Value
Rolling stock mass, m_{rs} (kg)	197,766
Passenger mass, m_{pass} (kg)	70,941.6
Rotary allowance, λ_w (%)	10
Davis equation parameters, [A (N), B (Ns m^{-1}), (C Ns^2 m^{-2})]	[623, 69, 7.7]
Auxiliary power, P_{aux} (W)	180,000
Regenerative braking efficiency, η_{regen} (%)	**80**
Drive-train efficiency, η_{trac} (%)	**85**
Number of seats	756

parameters of a bi-level rolling stock are listed in Table 7.3, and have either been assumed (bold) or used from reference [171].

A rolling stock operating on the Lakeshore East corridor will move between Union Station, and Oshawa, Ontario, making eight interstation stops along the way. It takes approximately 37 minutes for the rolling stock to travel the 55 km route with 45 second stops at each station. Using information from a previous electrification study, the speed-distance profile for the Lakeshore East corridor is depicted in Figure 7.8 [171].

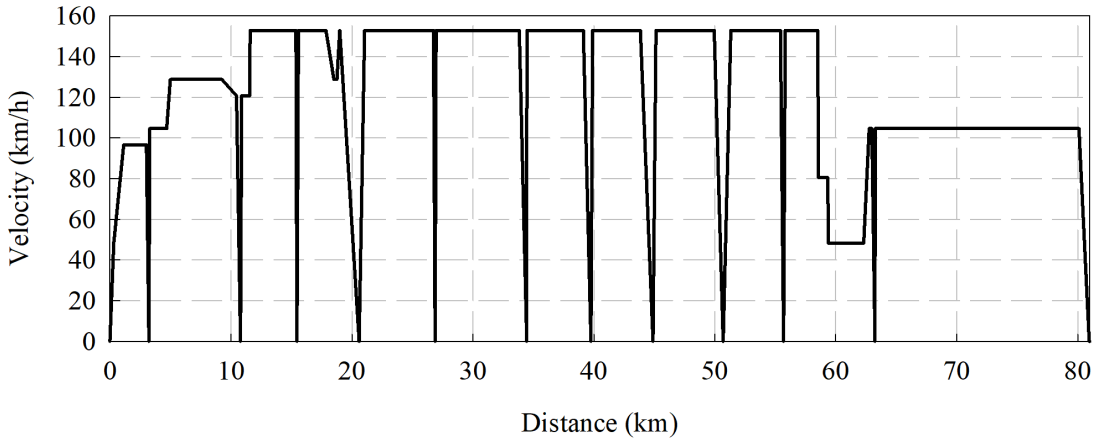

Figure 7.8: Speed-distance profile of the rolling stock moving on the Lakeshore East corridor (Union Station to Oshawa, ON)

A rolling stock operating on the Lakeshore West corridor will move between Union Station, and Hamilton, Ontario, making 11 interstation stops along the way. It takes approximately 44 minutes for the rolling stock to travel the 81 km route with 45 second stops at each station. Using information from a previous electrification study, the speed-distance profile for the Lakeshore West corridor is depicted in Figure 7.9 [171].

The active power profile of the rolling stock depicted in Figure 7.10 and Figure 7.11 is calculated using the technical parameters of the rolling stock Table 7.3, the speed-distance profile of the route Figure 7.8 and Figure 7.9, and Equation 6.34 - Equation 6.40, for the Lakeshore East and West corridors, respectively.

Figure 7.12 and Figure 7.13 are the input data for the weather disturbance analysis [169]. The weather data consists of historical data for each of the terminal stations of the route (i.e. Oshawa and Hamilton, ON). The data includes the solar irradiance, temperature, and wind speed.

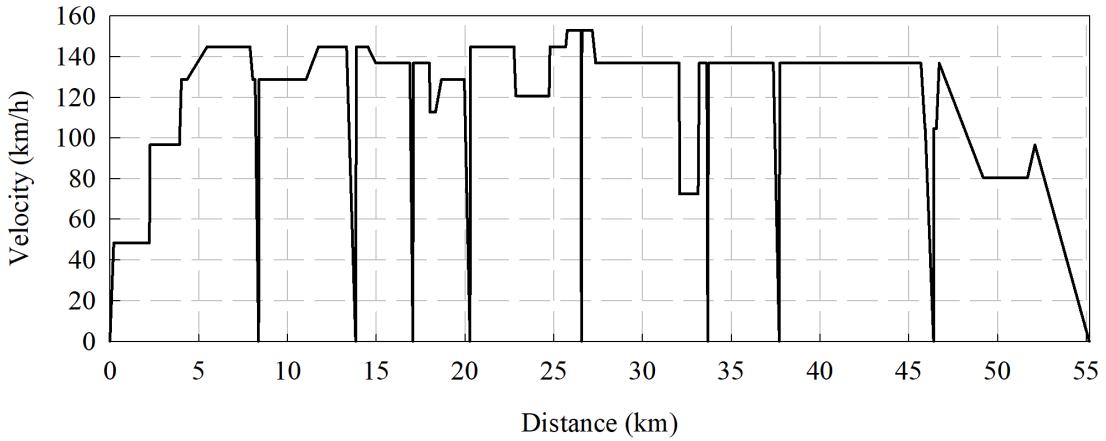

Figure 7.9: Speed-distance profile of the rolling stock moving on the Lakeshore West corridor (Union Station to Hamilton, ON)

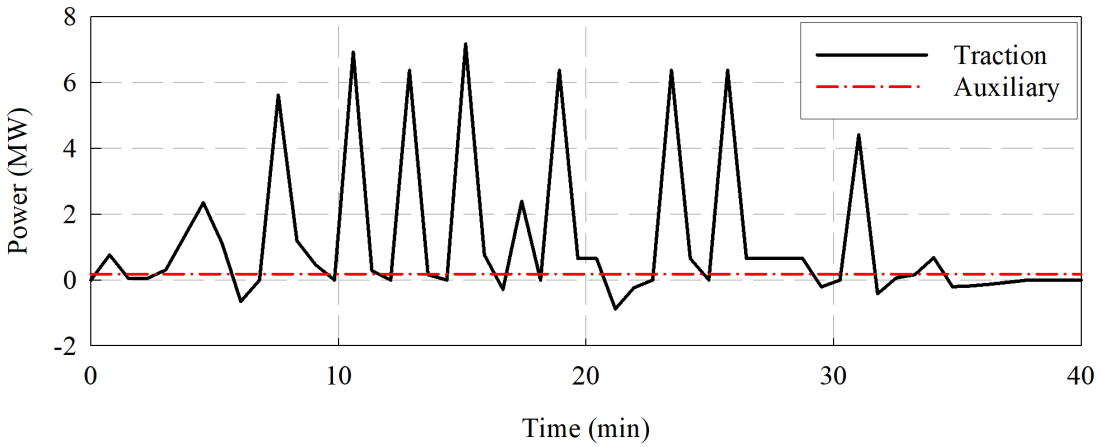

Figure 7.10: Active power of the rolling stock, calculated using rolling stock characteristics, speed-distance profile of the route moving on the Lakeshore East corridor (Union Station to Oshawa, ON), and system modelling equations

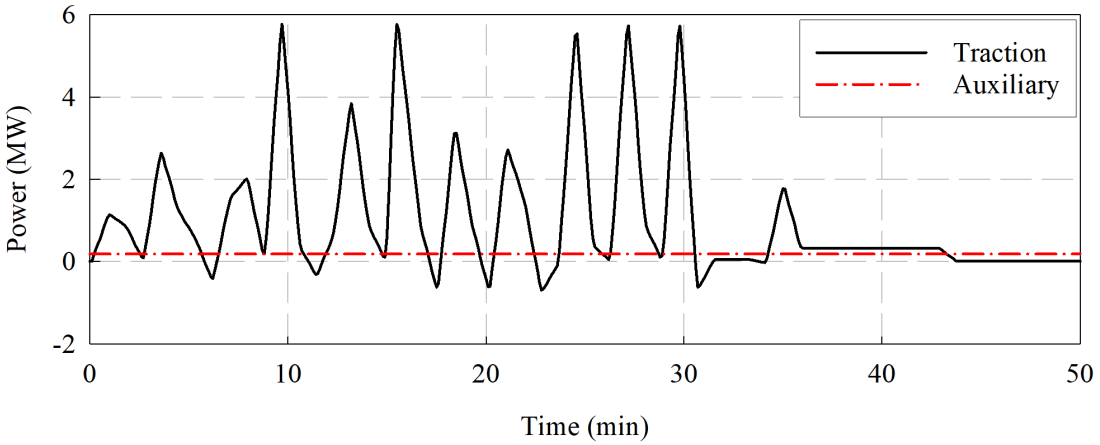

Figure 7.11: Active power of the rolling stock, calculated using rolling stock characteristics, speed-distance profile of the route moving on the Lakeshore West corridor (Union Station to Hamilton, ON), and system modelling equations

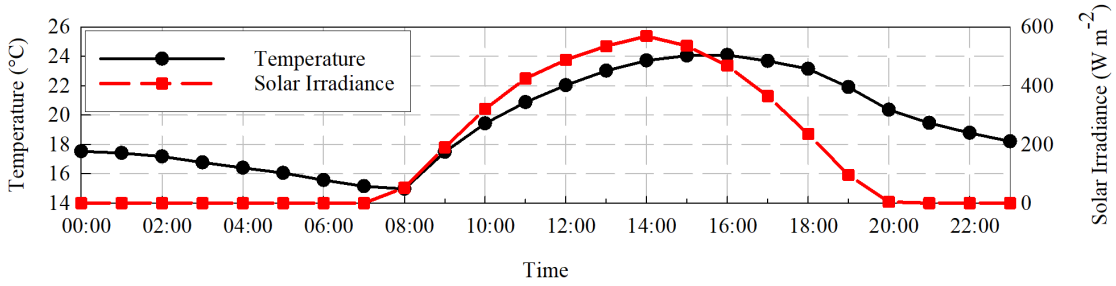

(a) Solar irradiance and ambient temperature

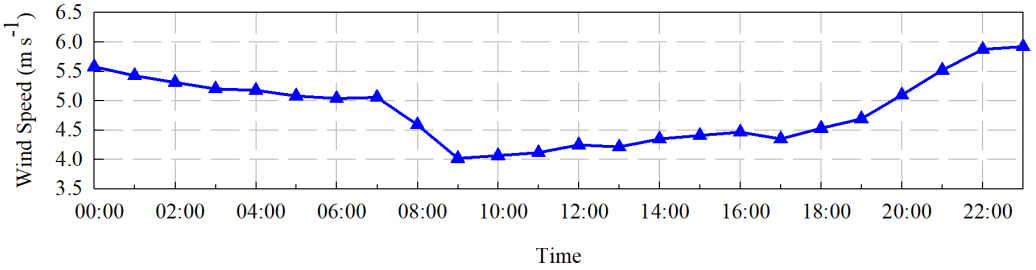

(b) Wind speed

Figure 7.12: Weather input data for Oshawa, ON

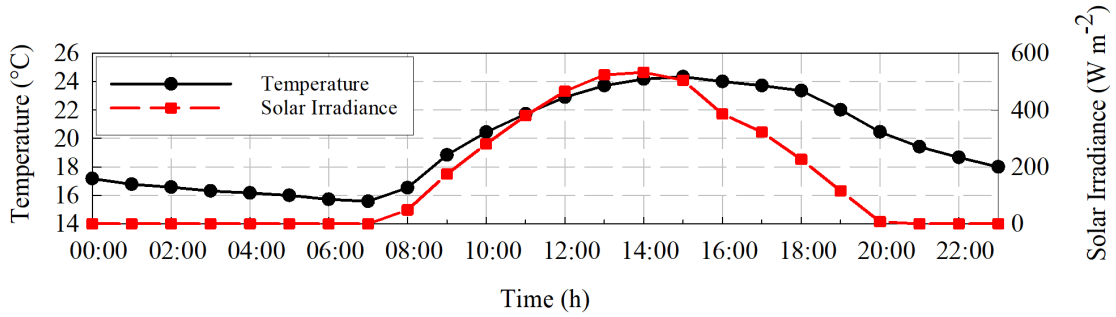

(a) Solar irradiance and ambient temperature

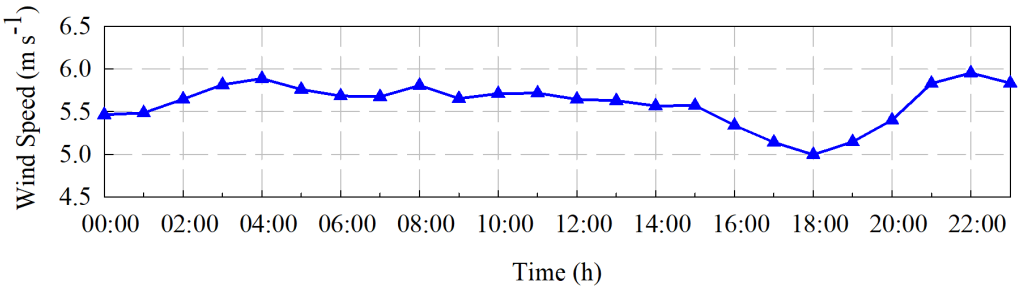

(b) Wind speed

Figure 7.13: Weather input data for Hamilton, ON

7.5 Case Study IV: Union Pearson Express Airport Rail Link

The Union Pearson Express airport rail link is the first dedicated link in North America between the two busiest transportation hubs in the Greater Toronto Area: Union Station and Pearson Airport. The 25 km route travels every 15 minutes with two station stops between the two hubs and boasts a weekly ridership of 200,000 passengers [147, 171]. As part of the assessment of electrifying the GO transit infrastructure, plans to electrify the UP Express are included due to the importance of this transportation link and the expected growth in ridership.

In an electrification assessment study for the GO network, a single-level rolling stock was used for the evaluation of electrifying the airport rail link. Technical parameters of a single-level electric multiple unit rolling stock were gathered from rolling stock currently being used today (i.e. Silverliner V, Denver EMU, M-8, and Arrow IV), and an average model was used, though the data closely resembles the Silverliner V. The parameters are listed in Table 7.4, and have either been assumed (bold) or used from reference [171].

Using information from an assessment study of an electrified network, Figure 7.14

depicts the speed-distance profile of the UP Express [171]. The rolling stock departs from Union Station and has two 45 second stops before arriving at Pearson Airport. After a 5-minute dwell time, the rolling stock returns to Union Station.

The active power profile of the rolling stock depicted in Figure 7.15 is calculated using the technical parameters of the rolling stock Table 7.4, the speed-distance profile of the route Figure 7.14, and Equation 6.34 - Equation 6.40.

Table 7.4: Single-Level EMU rolling stock technical parameters, averaged using existing models, used in case study IV

Parameter	**Value**
Rolling stock mass, m_{rs} (kg)	63,502.9
Passenger mass, m_{pass} (kg)	14,061.36
Rotary allowance, λ_w (%)	10
Davis equation parameters, [A (N), B (Ns m^{-1}), (C Ns^2 m^{-2})]	[410, 31, 7.7]
Auxiliary power, P_{aux} (W)	90,000
Regenerative braking efficiency, η_{regen} (%)	**80**
Drive-train efficiency, η_{trac} (%)	**85**
Number of seats	378

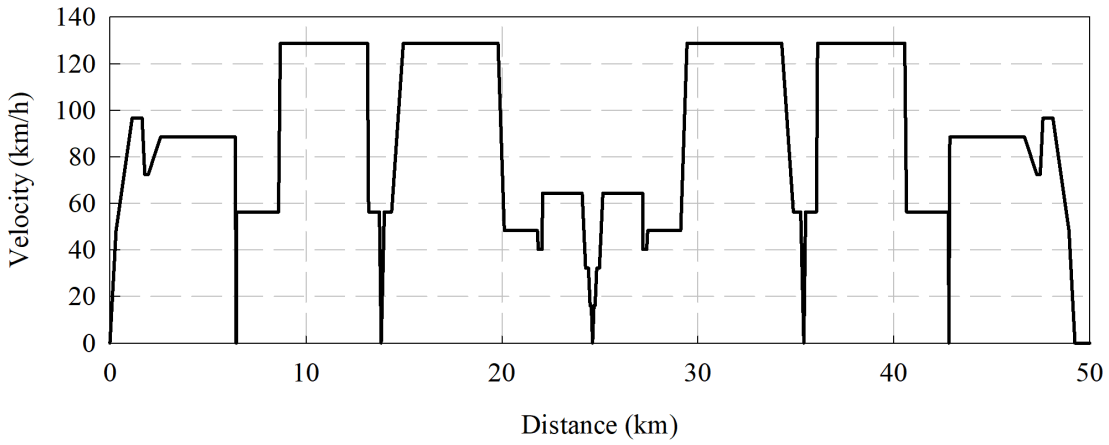

Figure 7.14: Speed-distance profile of the rolling stock moving from Union Station to Pearson Airport, including return trip

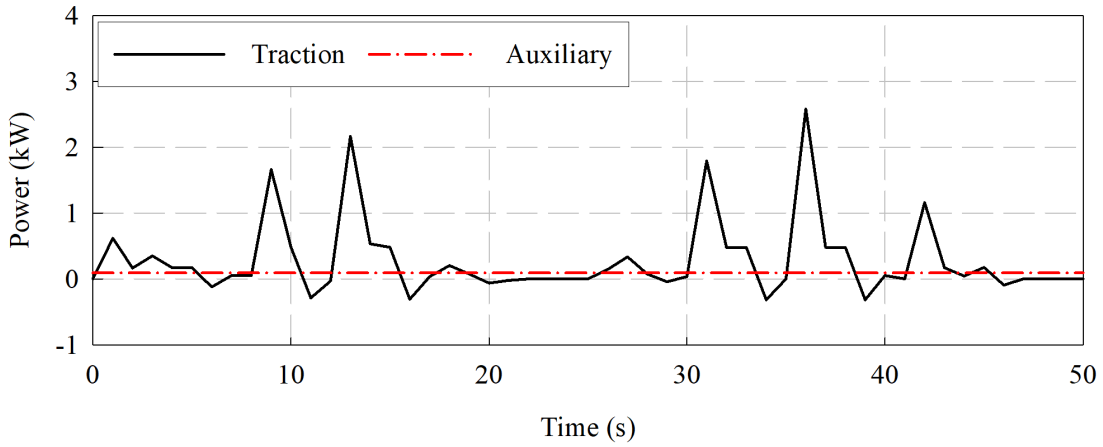

Figure 7.15: Active power of the rolling stock, calculated using rolling stock characteristics, speed-distance profile of the route moving from Union Station to Pearson Airport, including return trip, and system modelling equations

Figure 7.16 is the input data for the weather disturbance analysis [169]. The weather data consists of historical data for each of the terminal stations of the route (i.e. Toronto, ON). The data includes the solar irradiance, temperature, and wind speed.

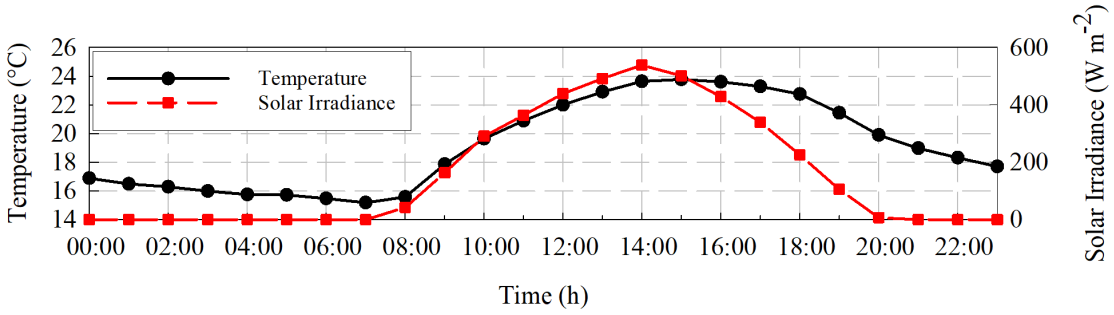

(a) Solar irradiance and ambient temperature

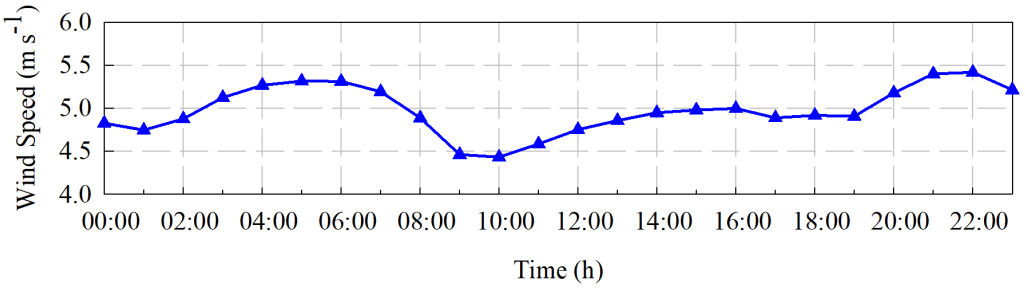

(b) Wind speed

Figure 7.16: Weather input data for Toronto, ON

Chapter 8

Results and Discussion

In earlier chapters, it was identified that railways are an important transit system for mass transportation of people and economic goods. However, an electric railway infrastructure is heavily dependent on a centralized electric grid, which is becoming more prone to outages due to various reasons. Resilient interconnected microgrids (RIMG) were proposed to allow for continuing operation of the railway network, to alleviate the dependence on the electric grid. Scenarios are developed to validate the proposed RIMG design and control system. For each case study, the following results are presented:

— The results of the proposed sizing analysis (Section 3.4) using the technical parameters of each energy system (Chapter 6)

— Using the Simulink model developed in Chapter 6, the three scenarios are simulated

— A summary of the resiliency key performance indicator (KPI) results

— A weather disturbance analysis is simulated for scenario 3, where the weather input data used is from historical weather data

The chapter concludes with a validation of the proposed models and techniques. An important note to consider is that each case study uses a different tack profiles, timetables, rolling stock, etc. Therefore, it is misleading to compare the results of all case studies presented. Each case study should be analyzed individually to understand the benefits of the proposed designs.

8.1 Simulation Scenarios

Four scenarios are used to demonstrate the effectiveness the proposed RIMG design and control system for railway infrastructures. The intended scenarios are outlined Figure 8.1, where each case study will be evaluated.

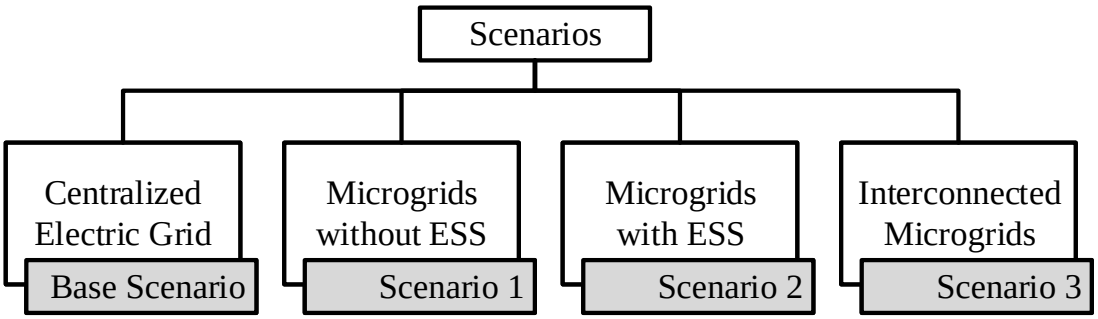

Figure 8.1: Proposed scenarios to evaluate the proposed RIMG design

Base Scenario (Centralized Electric Grid): This is a scenario mostly seen by railway operators across the world. The electricity demand of the railway infrastructure is supplied by the centralized electric grid [11–13].

Scenario 1 (Microgrid without Energy Storage System): This scenario considers the integration of the MG with only DERs (i.e. solar PV and WT) to the railway infrastructure. The MG can contribute to the supply of energy to meet the railway demand, using the MG regulation system. Any deficit between the MG generation and the demand of the railway infrastructure is met by the electric grid. Any recovered energy from braking operations of the rolling stock must be sold to the electric grid. No interconnection exists between any MG.

Scenario 2 (Microgrids with Energy Storage Systems): Building on scenario 1, this scenario features the addition of an ESS to each MG. The ESS can store energy recovered from the rolling stock during braking, and excess energy generated from any of the DERs. If a deficit exists between the MG generation and demand of the railway infrastructure, the ESS will be relied on first and then the electric grid. Any recovered energy from braking operations of the rolling stock or excess energy generated from the DERs that cannot be stored in the ESS must be sold to the electric grid. No interconnection exists between any MG.

Scenario 3 (Interconnected Microgrids): Building on scenario 2, this scenario features interconnected microgrids. This scenario evaluates the entire proposed design of IMGs, as well as the control system design with an IMGSC. Each IMG

can increase the amount of energy exported from the IMG to be imported by an IMG. The decision on whether to increase the export limit is decided using the IMG demand served KPI and game theory techniques within the IMGSC.

8.2 Case Study I Results and Discussion

Case study I consists of the High Speed 2 railway infrastructure between London Euston and Birmingham Curzon (see Section 7.2). In this case study there are two IMGs, which serve the demand of the High-Speed 2 railway infrastructure from London Euston to Birmingham Curzon, UK. One IMG is used to supply the traction and auxiliary demand of the rolling stock from London Euston to Birmingham Curzon, for a single ride. The other IMG supplies the demand of the rolling stock moving in the reverse direction, for a single ride.

8.2.1 Sizing Analysis Results

Figure 8.2 shows the sizing analysis for case study I, which uses the IMG diversity of supply, IMG electric grid dependence, and IMG reliance KPIs. The sizing analysis computes the KPIs by incrementing the solar PV nominal capacity, from 0 MW, and decrementing the WT nominal capacity, from the peak demand, in steps of 1.5 MW. The sum of the nominal capacities of the two DERs is equal to the sum of the peak demand at all times. The parameters selected, as a result of the sizing analysis, for the IMG DERs and the expected performance are listed in Table 8.1.

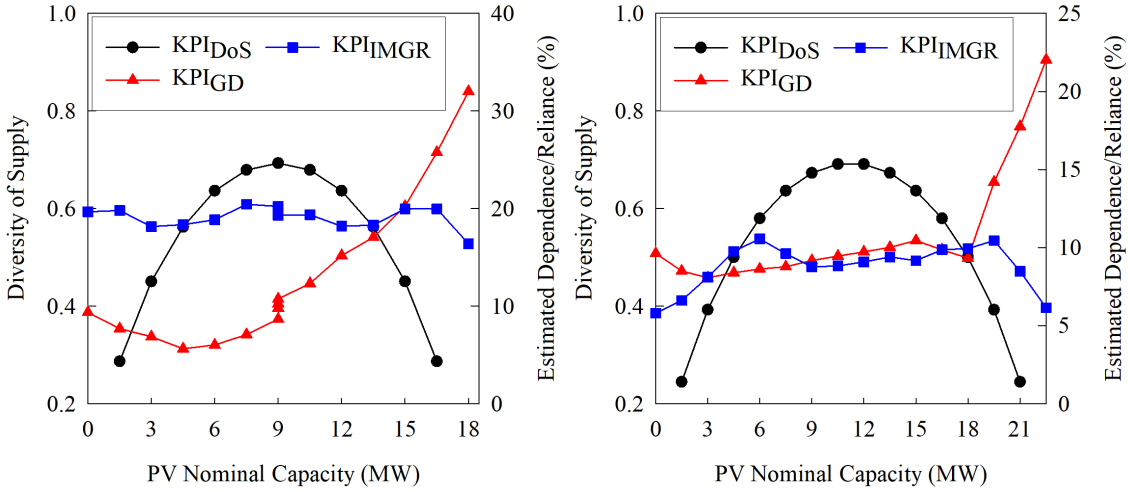

(a) Ldn Euston to Birm Curzon (IMG1) **(b)** Birm Curzon to Ldn Euston (IMG2)

Figure 8.2: Sizing analysis for case study I using resiliency KPIs

Table 8.1: Sizing parameters selected for simulation studies, and the expected KPIs for case study I

Parameter	**Ldn - Birm (IMG1)**	**Birm - Ldn (IMG2)**
Number of WTs, N_{WT}	9	13
Number of solar PV arrays, N_{PV}	45	30
Number of ESSs, N_{ESS}	18	12
IMG diversity of supply, KPI_{DoS}	0.5623	0.3927
Estimated IMG renewable generation, KPI_{RG} (%)	87.76	95.78
Estimated IMG electric grid dependence, KPI_{GD} (%)	5.63	12.18
Estimated IMG reliance, KPI_{IMGR} (%)	18.35	7.81

The rolling stock requires a high amount of energy to travel its route at a high speed, which results in a high dependence on the electric grid and reliance on the other IMG. As seen in the London-Birmingham route, the higher the solar PV nominal capacity, the higher the dependence on the electric grid. The solar irradiance is concentrated around a specific time of day. Therefore, a solar PV system is unable to supply a resilient stream of energy to the rolling stock. The IMG would not have been properly sized to meet the demand, which hinders the reliability of the railway infrastructure.

8.2.2 Simulation Results

Considering the baseline scenario, the demand of the railway infrastructure is supplied by the electric grid. The remaining scenarios are simulated using the system model presented in Figure 6.21. For each scenario, the IMG configuration and how the demand of the railway infrastructure is satisfied is described in Section 8.1. Refer to Appendix F for a notation on interpreting the simulation results.

8.2.2.1 Scenario 1

Figure 8.3 illustrates the RIMG model simulation results for scenario 1. In Figure 8.3a and Figure 8.3b, the active power profile of the rolling stock moving from London Euston to Birmingham Curzon and vice-versa, is shown, as well as how the demand is served by each bus within the MG and, if required, the electric grid.

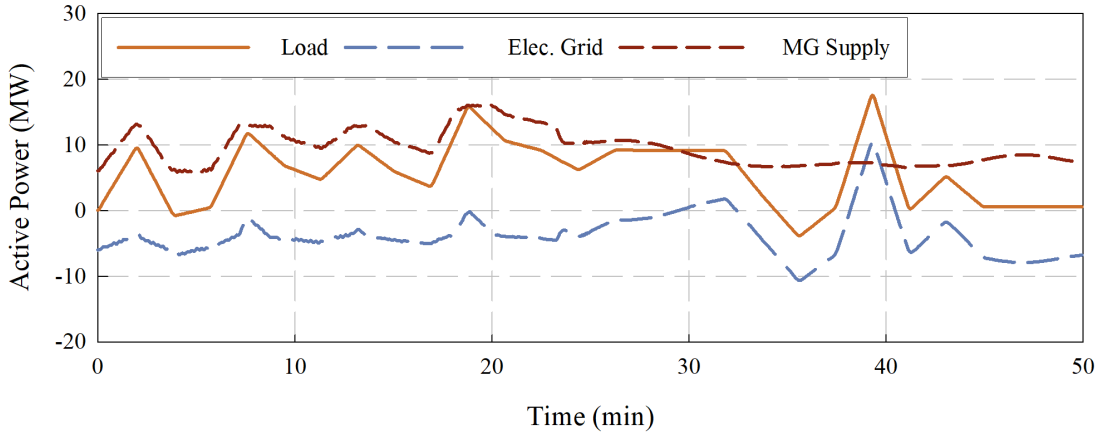

(a) London Euston to Birmingham Curzon (MG1)

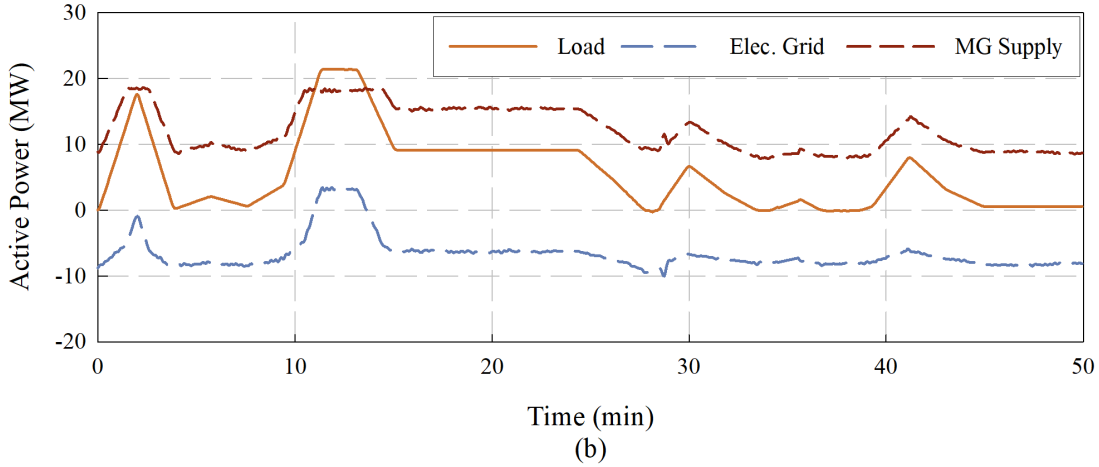

(b) Birmingham Curzon to London Euston (MG2)

Figure 8.3: Active power balance for scenario 1 for the MGs (case study I)

The results indicate that the sizing of each MG is suited to the active power profile, with the exception of few instances where each IMG must rely on the electric grid to satisfy the demand. These instances could be alleviated with the integration of an ESS or interconnection other MGs. Furthermore, instances where the MG must export the recovered energy from the rolling stock to the electric grid could be reduced with the integration of an ESS.

8.2.2.2 Scenario 2

Figure 8.4 illustrates the RIMG model simulation results for scenario 2. In Figure 8.4a and Figure 8.4b, the active power profile of the rolling stock moving from London Euston to Birmingham Curzon and vice-versa, is shown, as well as how the demand is served by each bus within the IMG and, if required, the electric grid. As

can be seen, the DC bus is able to capture some of the recovered braking energy and store the energy in the battery. This reduces the dependence on the electric grid and allows the MG to store energy for future use (i.e. emergency situations).

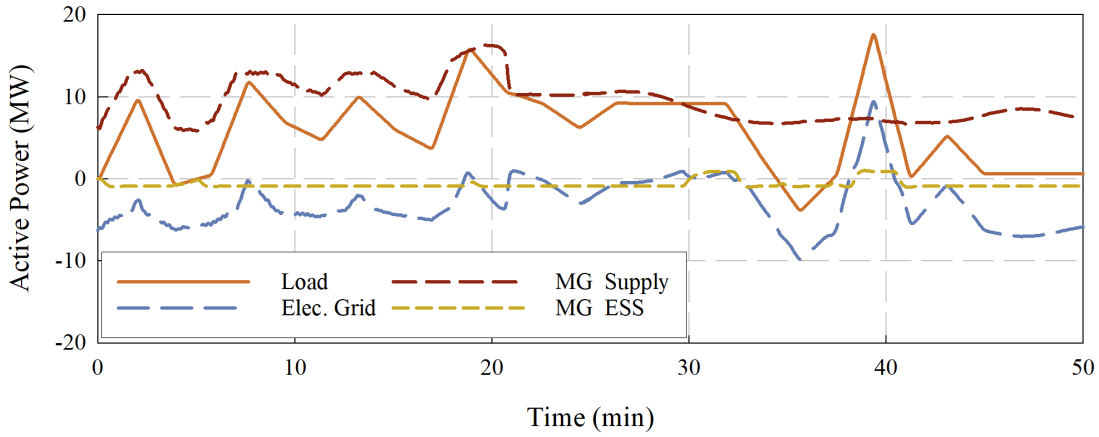

(a) London Euston to Birmingham Curzon (MG1)

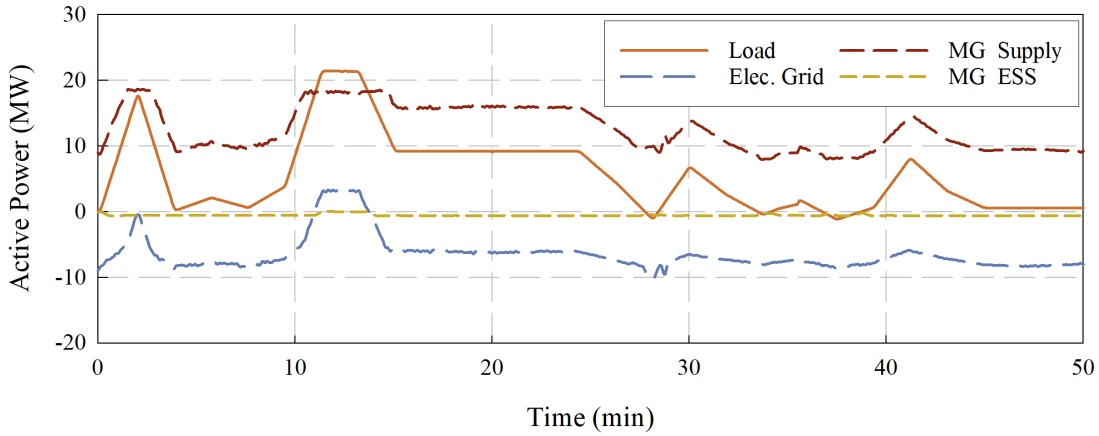

(b) Birmingham Curzon to London Euston (MG2)

Figure 8.4: Active power balance for scenario 2 for the MGs (case study I)

In comparison to the previous scenario, there is a slightly higher transfer of energy from the DC bus to the railway load, or vice-versa, either when the DERs cannot generate enough power for the load or in capturing energy recovered during braking. However, due to the magnitude of the deficit the electric grid must supply for both loads, the size of the ESS is unable to eliminate the dependence, especially for the route from London to Birmingham. The capital, operating and replacement costs around increasing the size of the ESS to cover the deficit may be outweighed by interconnecting MGs.

While the ESS does alleviate some dependence on the electric grid, it isn't a suf-

ficient solution due to the large energy requirements of the railway infrastructure under study. While increasing the size of the ESS could further alleviate the dependence on the electric grid, the costs of the technology could make this a prohibitive option. Interconnection of MGs will be able to alleviate the dependence on the electric grid better than the ESS technology.

8.2.2.3 Scenario 3

Figure 8.5 illustrates the RIMG model simulation results for scenario 3. In Figure 8.5a and Figure 8.5b, the active power profile of the rolling stock moving from London Euston to Birmingham Curzon and vice-versa is shown, as well as how the demand is served by each bus within the IMG and, if required, an IMG and the electric grid. Figure 8.5c shows the exchange of energy between the two IMGs under consideration, as determined by the IMGSC.

As can be seen in Figure 8.5a, there is a significant contribution from an IMG to serving the demand. For instance, in scenario 1 and 2, there was a large deficit between the demand and the IMG supply that was covered by the electric grid, approximately 38 minutes into the trip. In this scenario, the contribution from an IMG has reduced the deficit covered by the electric grid by approximately 5.25 MW, a 64% decrease in peak demand.

As can be seen in Figure 8.5b, there is a significant contribution from an IMG to serving the demand. For instance, in scenarios 1 and 2, there was a large deficit between the demand and the IMG supply that was covered by the electric grid, approximately 10 minutes into the trip. In this system, the proposed control strategy is able to satisfy the deficit between the IMG supply and demand. The elimination of the dependence on the electric grid to satisfy any deficit between IMG supply and the demand validates the proposed design.

8.2.3 Resiliency Key Performance Indicator Results

In Table 8.2, a comparison between the estimated and simulated **IMG renewable generation** KPI is made. The estimated KPI is the result of the sizing analysis, reported in Section 8.2.1. The simulated KPI is the result of the simulation performed for scenario 3.

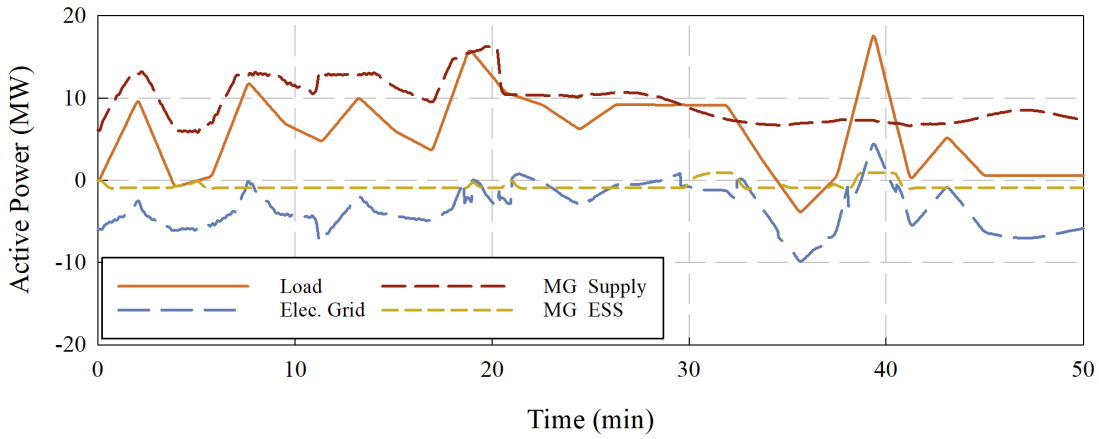

(a) London Euston to Birmingham Curzon (IMG1)

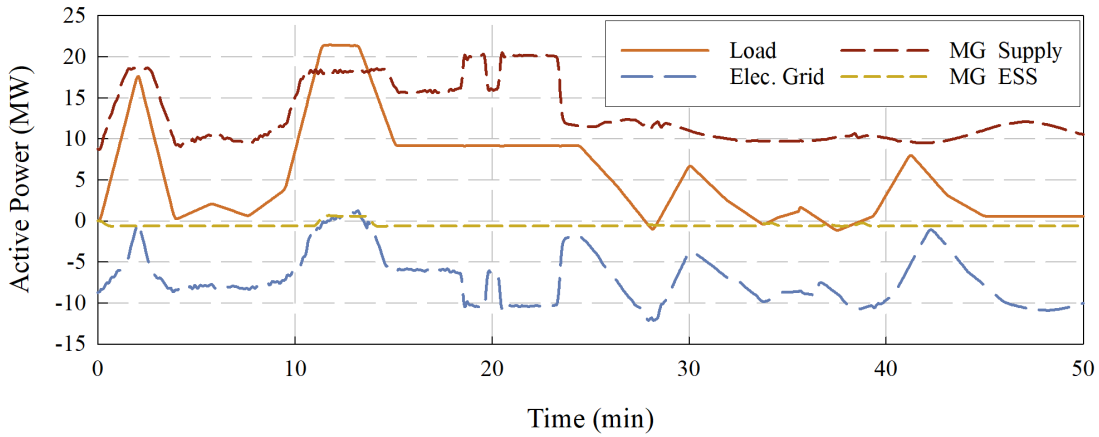

(b) Birmingham Curzon to London Euston (IMG2)

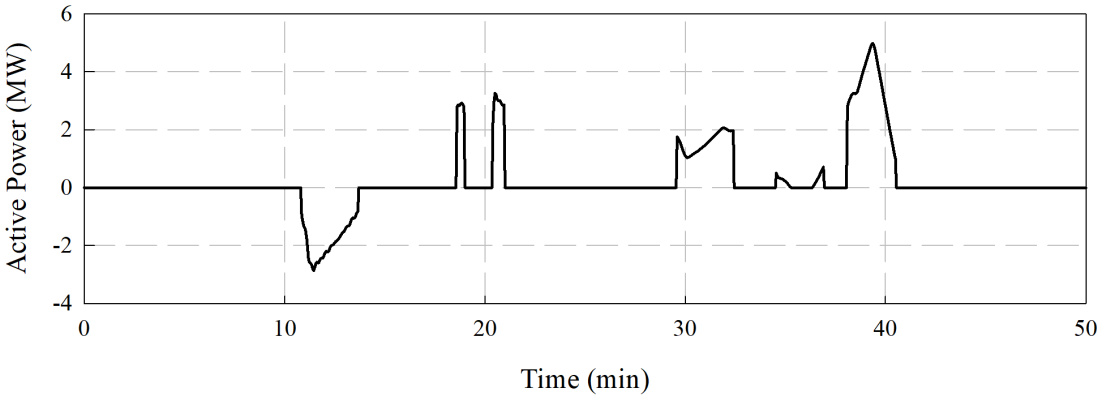

(c) Energy exchange between IMGs

Figure 8.5: Active power balance for scenario 3 for the IMGs (case study I)

Table 8.2: IMG renewable generation KPI results for case study I

IMG Renewable Generation, KPI_{RG}	**Ldn - Birm (IMG1)**	**Birm - Ldn (IMG2)**
Estimated KPI_{RG} (%)	87.76	95.78
Simulated KPI_{RG} (%)	96.05	99.00

The **IMG demand served** KPI is calculated overtime using the **IMG supply** and **IMG demand** KPIs. The KPI is used to determine the instances where an IMG cannot supply the entire demand. This is represented as the KPI evaluating to less than one. When the KPI evaluates to less than one, the control strategy (see Figure 5.4) dictates how the deficit will be covered. As seen in Figure 8.6, from scenario 1 to scenario 3 there is an incremental improvement to the performance of each IMG. The improvement demonstrates the benefits of the hierarchical control scheme, where the tertiary level of control can make quick, effective decisions to ensure the demand of the railway infrastructure is supplied without heavily relying on the electric grid.

Figure 8.7 offers a comparison of the **IMG electric grid dependence** KPI for each scenario for case study I. It also shows the reduction of the peak load and peak regenerative load, that the electric grid must supply and absorb, respectively. In Table 8.3, a comparison between the estimated and simulated **IMG reliance** KPI is made. It also lists the peak load supplied by the IMG.

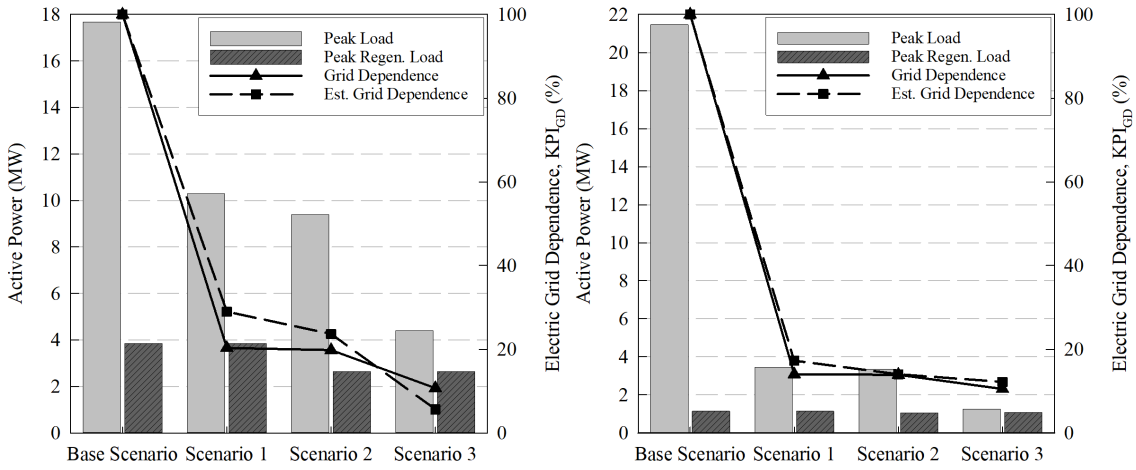

(a) Ldn Euston to Birm Curzon (IMG1) **(b)** Birm Curzon to Ldn Euston (IMG2)

Figure 8.7: IMG electric grid dependence KPI analysis for (case study I)

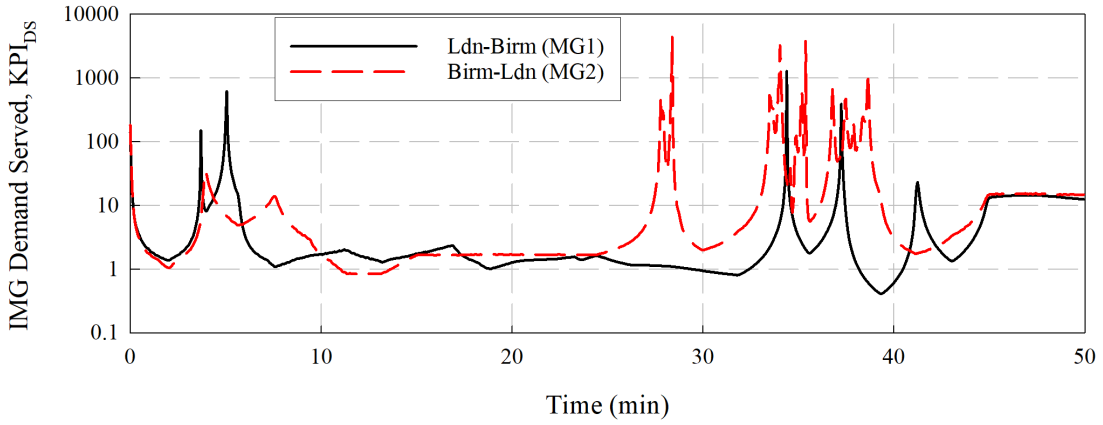

(a) Scenario 1

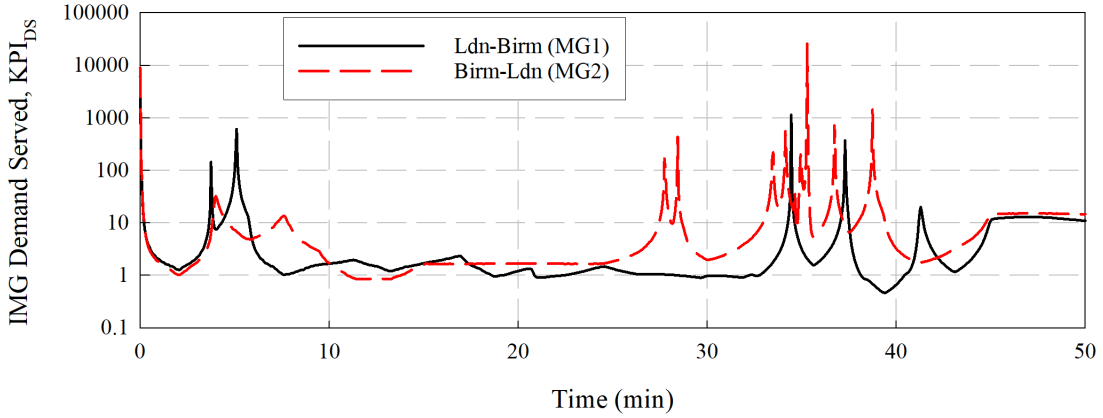

(b) Scenario 2

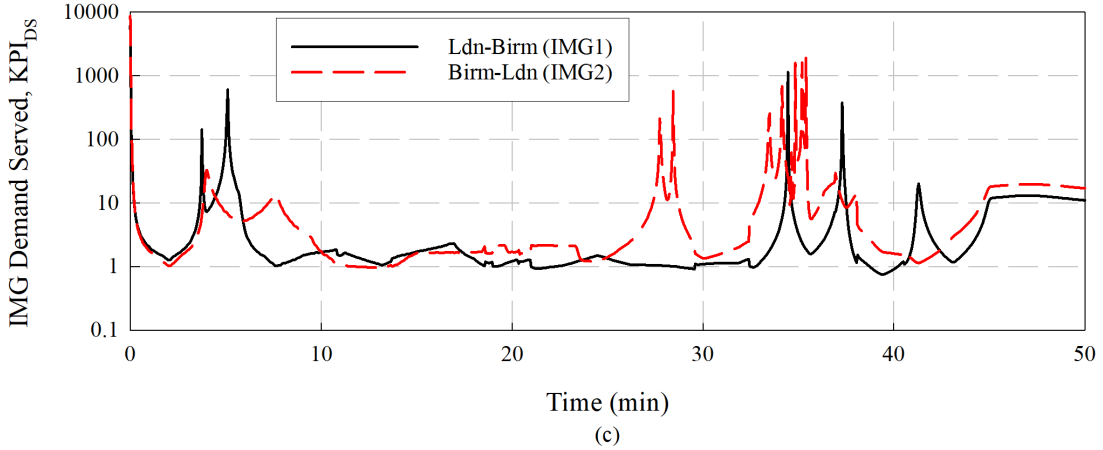

(c) Scenario 3

Figure 8.6: IMG demand served KPI comparison for case study I

Table 8.3: IMG reliance KPI results for case study I

Parameter	**Ldn - Birm (IMG1)**	**Birm - Ldn (IMG2)**
Estimated IMG reliance, KPI_{IMGR} (%)	18.35	7.81
Simulated IMG reliance, KPI_{IMGR} (%)	15.20	5.70
Peak Load (MW)	4.98	2.87

Interconnection of MGs for case I study shows a benefit in meeting the demand the railway infrastructure. The interconnection between MGs is able reduce the deficit between IMG supply and demand on the London-Birmingham route by 64%, which reduces the dependence on the electric grid by 12.5%. On the Birmingham-London route, the interconnection of IMGs eliminates the dependence of the IMG on the electric grid to satisfy the peak demand. This shows that IMGs are ideal for railway infrastructures with high energy requirements (i.e. high-speed, some intercity) as the interconnection of IMGs allows the operator to take advantage in the diversity of the loads, and not oversize the energy systems in any particular IMG.

As mentioned before, even with the lower diversity of supply for each IMG, the electric grid dependence is still reduced for both IMGs. The peak on the London-Birmingham route falls outside of the peak generation time for the PV system. Thus, by reducing the nominal capacity of the PV system, and increasing the WTs, the dependence on the electric can have a more impactful reduction compared to if the diversity of supply target was maintained.

8.2.4 Weather Disturbance Results

The simulation results presented in Section 8.2.2 use the weather data provided in Section 6.4. The proposed design is simulated with weather data for the terminal stations of the railway route. The weather data for each terminal station (London and Birmingham, UK) are provided in Section 7.2.

Figure 8.8 illustrates the RIMG model simulation results for the weather disturbance analysis. In Figure 8.8a and Figure 8.8b, the active power profile of the rolling stock moving from London Euston to Birmingham Curzon and vice-versa is shown, as well as how the demand is served by each bus within the IMG and, if required, an IMG and the electric grid. Figure 8.8c shows the exchange of energy between the two IMGs under consideration, as determined by the IMGSC. Table 8.4 provides the IMG renewable generation, IMG electric grid dependence, and IMG reliance KPI results for the weather disturbance analysis.

Table 8.4: Weather disturbance effects on KPIs for case study I

Key Performance Indicator	Ldn - Birm (IMG1)	Birm - Ldn (IMG2)
IMG renewable generation, KPI_{RG} (%)	82.94	97.61
IMG electric grid dependence, KPI_{GD} (%)	35.3	21.1
IMG reliance, KPI_{IMGR} (%)	43.4	9.7

8.3 Case Study II Results and Discussion

Case study II consists of the intercity railway infrastructure between Birmingham Moor Street and Stratford-upon-Avon (see Section 7.3). In this case study there are two IMGs, which serve the demand of the intercity railway infrastructure from Birmingham Moor Street to Stratford-upon-Avon, UK. One IMG is used to supply the traction and auxiliary demand of the rolling stock from Birmingham Moor Street to Stratford-upon-Avon, for a single ride. The other IMG supplies the demand of the rolling stock moving in the reverse direction, for a single ride.

8.3.1 Sizing Analysis Results

Figure 8.9 shows the sizing analysis for case study II, which uses the IMG diversity of supply, IMG electric grid dependence, and IMG reliance KPIs. For this case, the energy requirements for the rolling stock are low, such that in respect of design requirement 4-3, the nominal capacity of the wind turbine is held constant at 1.5 MW for each time step (except the first and last), and the nominal capacity of the solar PV is incremented in steps of 100 kW. The nominal capacity of the WT and solar PV is 3 MW and 0 MW, respectively for the initial time step. The final time step has no WT and the solar PV nominal capacity is equal to the peak demand. The parameters selected, as a result of the sizing analysis, for the IMG DERs and the expected performance are listed in Table 8.5.

In this case study, the nominal capacity of the solar PV system is not a major factor in reducing the dependence of each IMG on the electric grid. As a result, the nominal capacity of the solar PV is reduced, which slightly deviates from the design requirement 4-3, but does not affect the electric grid dependence KPI. However, due to the nature of this intercity railway infrastructure, the frequent braking operations of the rolling stock increases the dependence of each IMG on the electric grid. This occurs because the battery is not able to absorb power recovered from the rolling stock braking as quickly as other possible ESS technologies suitable for railway infrastructures.

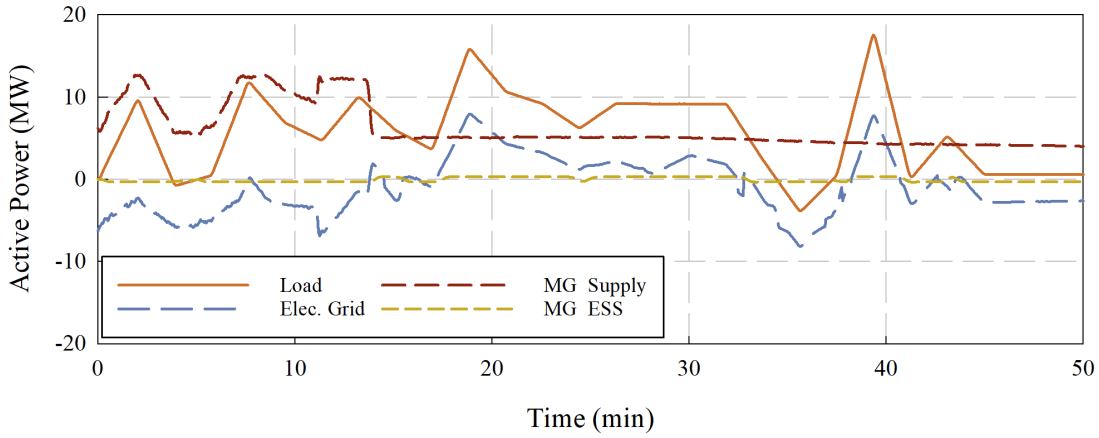

(a) London Euston to Birmingham Curzon (IMG1)

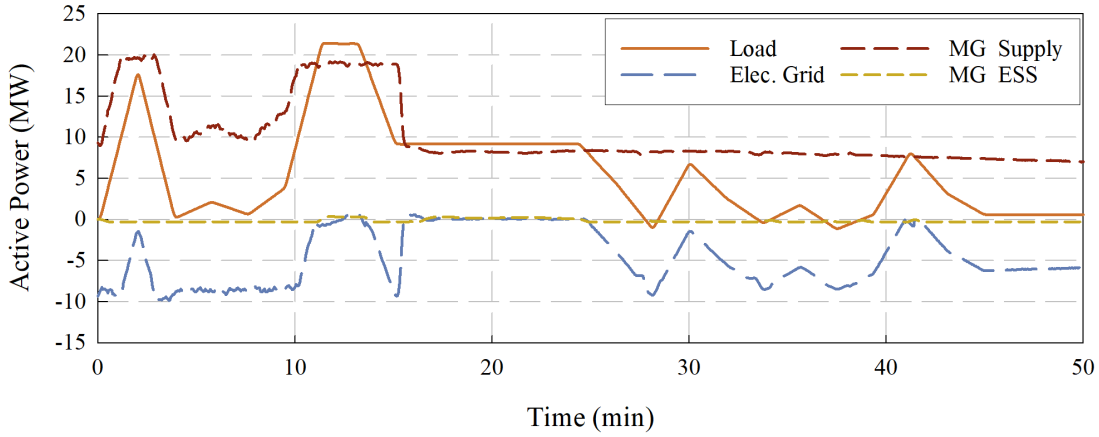

(b) Birmingham Curzon to London Euston (IMG2)

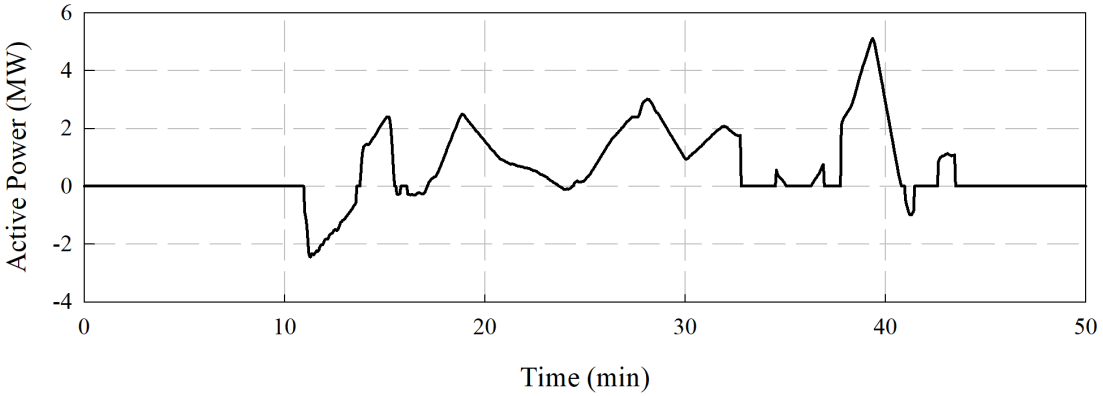

(c) Energy exchange between IMGs

Figure 8.8: Weather disturbance effects on active power balance (case study I)

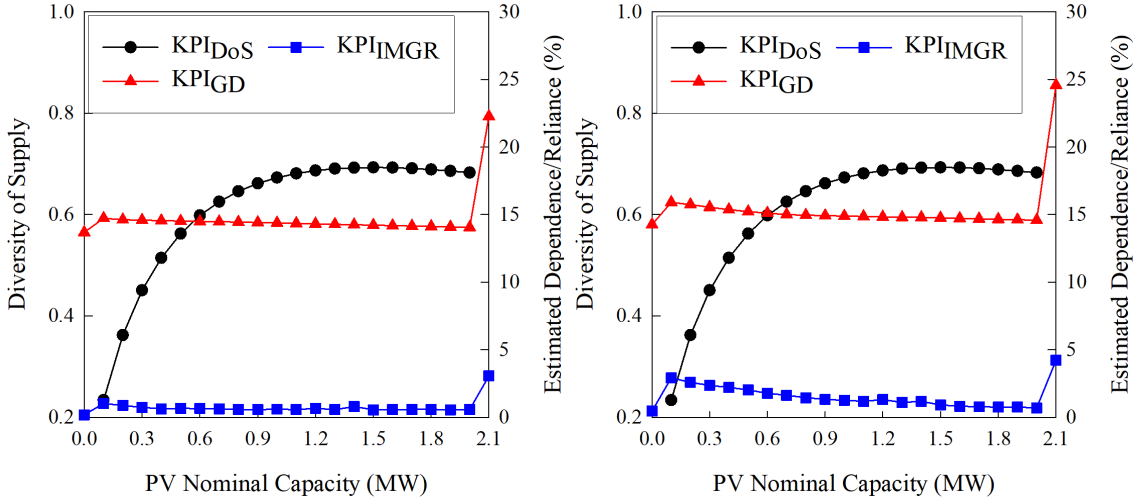

(a) Birm Moor St. to Strat (IMG1) **(b)** Strat to Birm Moor St. (IMG2)

Figure 8.9: Sizing analysis for case study II using resiliency KPIs

Table 8.5: Sizing parameters selected for simulation studies, and the expected KPIs for case study II

Parameter	**Birm - Strat (IMG1)**	**Strat - Birm (IMG2)**
Number of WTs, N_{WT}	1	1
Number of solar PV arrays, N_{PV}	11	13
Number of ESSs, N_{ESS}	6	6
IMG diversity of supply, KPI_{DoS}	0.6813	0.6906
Estimated IMG renewable generation, KPI_{RG} (%)	91.74	90.59
Estimated IMG electric grid dependence, KPI_{GD} (%)	14.52	14.80
Estimated IMG reliance, KPI_{IMGR} (%)	0.57	1.10

8.3.2 Simulation Results

Considering the baseline scenario, the demand of the railway infrastructure is supplied by the electric grid. The remaining scenarios are simulated using the RIMG model presented in Figure 6.21. For each scenario, the IMG configuration and how the demand of the railway infrastructure is satisfied is described in Section 8.1. Refer to Appendix F for a notation on interpreting the simulation results.

8.3.2.1 Scenario 1

Figure 8.10 illustrates the RIMG model simulation results for scenario 1. In Figure 8.10a and Figure 8.10b, the active power profile of the rolling stock moving from Birmingham Moor Street to Stratford-upon-Avon and vice-versa is shown, as well as how the demand is served by each bus within the MG and, if required, the electric

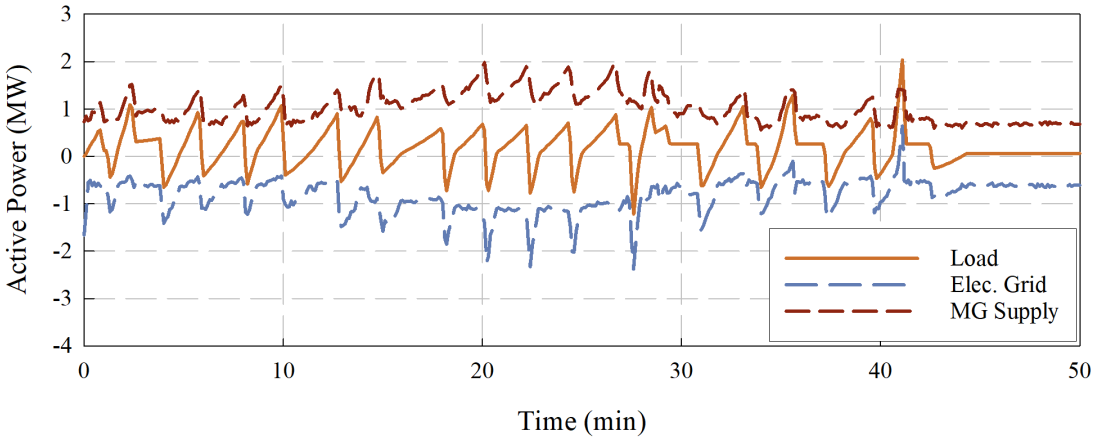

(a) Birmingham Moor Street to Stratford-upon-Avon (MG1)

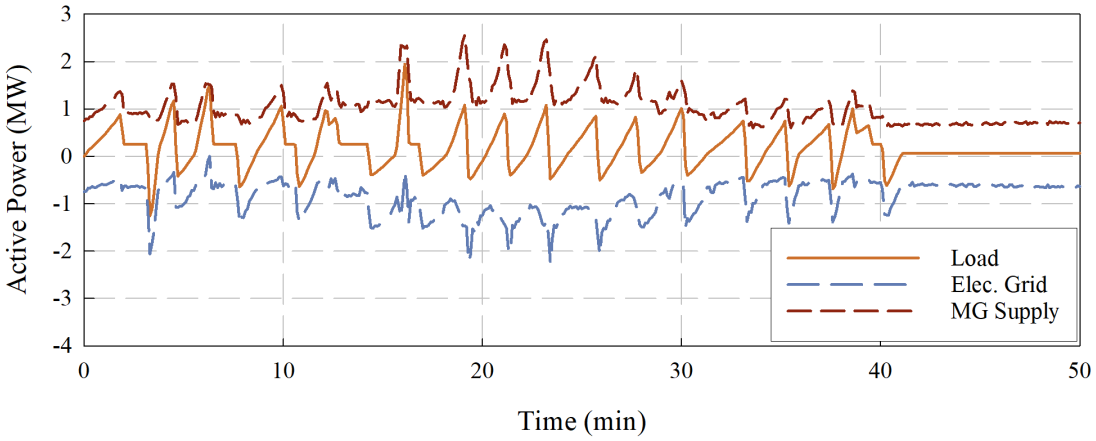

(b) Stratford-upon-Avon to Birmingham Moor Street (MG2)

Figure 8.10: Active power balance for scenario 1 for the MGs (case study II)

grid. In this profile, the MG is able to satisfy the demand of the rolling stock, but all energy recovered from the rolling stock during braking must be exported to the electric grid which creates a dependence. This dependence could be reduced with the integration of an ESS.

It is also important to note that since the railway infrastructure is considered an intercity rail line, there are more stops involved, which causes more peaks in the active power profile during both acceleration and deceleration. The frequent braking operations along both routes indicate that the energy being recovered is being exported to the electric grid, instead of conserved within the MG for emergency uses. This situation creates a dependence on the electric grid, since the MG is unable to store the recovered energy in an ESS.

8.3.2.2 Scenario 2

Figure 8.11 illustrates the RIMG model simulation results for scenario 2. In Figure 8.11a and Figure 8.11b, the active power profile of the rolling stock moving from Birmingham Moor Street to Stratford-upon-Avon and vice-versa is shown, as well as how the demand is served by each bus within the MG and, if required, the electric grid. As can be seen in the figure, the DC bus is able to capture some of the recovered braking energy and store the energy in the battery. This reduces the dependence on the electric grid and allows the MG to store energy for future use (i.e. emergency situations).

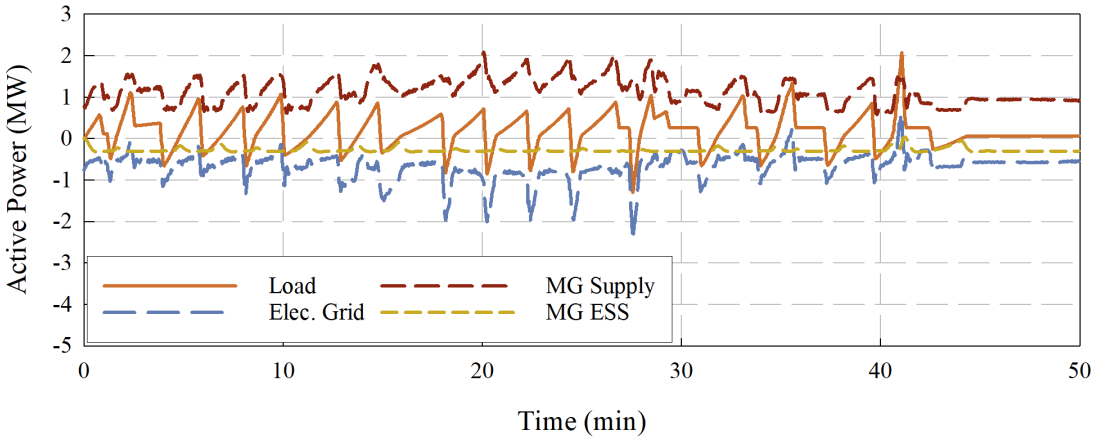

(a) Birmingham Moor Street to Stratford-upon-Avon (IMG1)

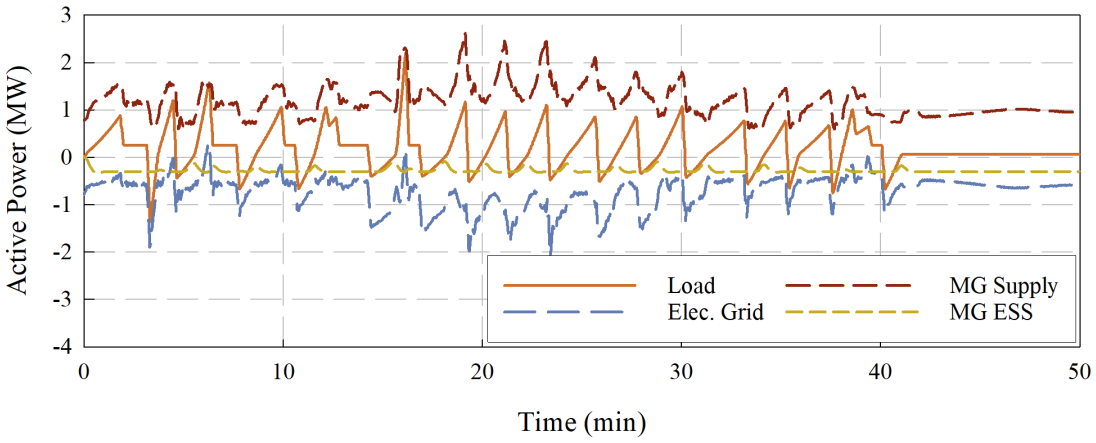

(b) Stratford-upon-Avon to Birmingham Moor Street (MG2)

Figure 8.11: Active power balance for scenario 2 for the MGs (case study II)

While having the battery installed in the MG would help store recovered energy from braking operations, there is still a noticeable dependence on the electric grid. This situation occurs due to the latency in the battery being able to respond to changes

in the demand of the rolling stock, and the poor specific power rating of battery technology. It is noticeable with this type of railway infrastructure (intercity) that there are more instances of acceleration and braking of the rolling stock that a supercapacitor or flywheel may be able to better handle than the battery.

8.3.2.3 Scenario 3

Figure 8.19 illustrates the RIMG model simulation results for scenario 3. In Figure 8.14a and Figure 8.14b, the active power profile of the rolling stock moving from Birmingham Moor Street to Stratford-upon-Avon and vice-versa is shown, as well as how the demand is served by each bus within the IMG and, if required, an IMG and the electric grid. Figure 8.14c shows the exchange of energy between the two IMGs under consideration, as determined by the IMGSC.

Due to the smaller energy requirements of the intercity railway infrastructure and proper sizing of the IMG components, there is a small dependence on an IMG to cover any deficit. Instances where the rolling stock is braking for long periods of time are minimal, indicating that the IMG has very few instances of just exporting to the electric grid, and thus unable to assist another IMG, if required.

8.3.3 Resiliency Key Performance Indicator Results

In Table 8.6, a comparison between the estimated and simulated **IMG renewable generation** KPI is made. The estimated KPI is the result of the sizing analysis, reported in Section 8.3.1. The simulated KPI is the result of the simulation performed for scenario 3.

Table 8.6: IMG renewable generation KPI results for case study II

IMG Renewable Generation, KPI_{RG}	**Birm - Strat (IMG1)**	**Strat - Birm (IMG2)**
Estimated KPI_{RG} (%)	91.74	90.59
Simulated KPI_{RG} (%)	99.87	99.77

The **IMG demand served** KPI is calculated overtime using the **IMG supply** and **IMG demand** KPIs. The KPI is used to determine the instances where an IMG cannot supply the entire demand. This is represented as the KPI evaluating to less than one. When the KPI evaluates to less than one, the control strategy (see Figure 5.4) dictates how the deficit will be covered. As seen in Figure 8.12, from scenario 1 to scenario 3 there is an incremental improvement to the performance of each IMG. The improvement demonstrates the benefits of the hierarchical control

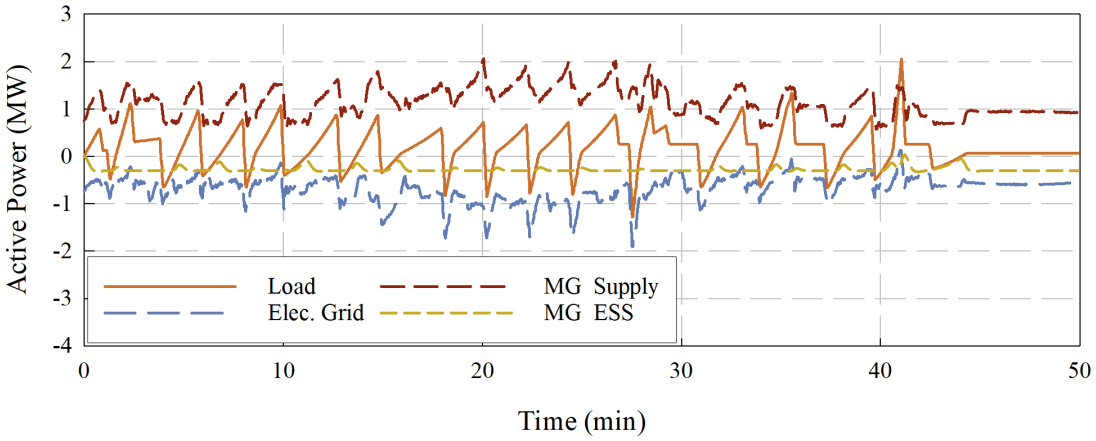

(a) Birmingham Moor Street to Stratford-upon-Avon (IMG1)

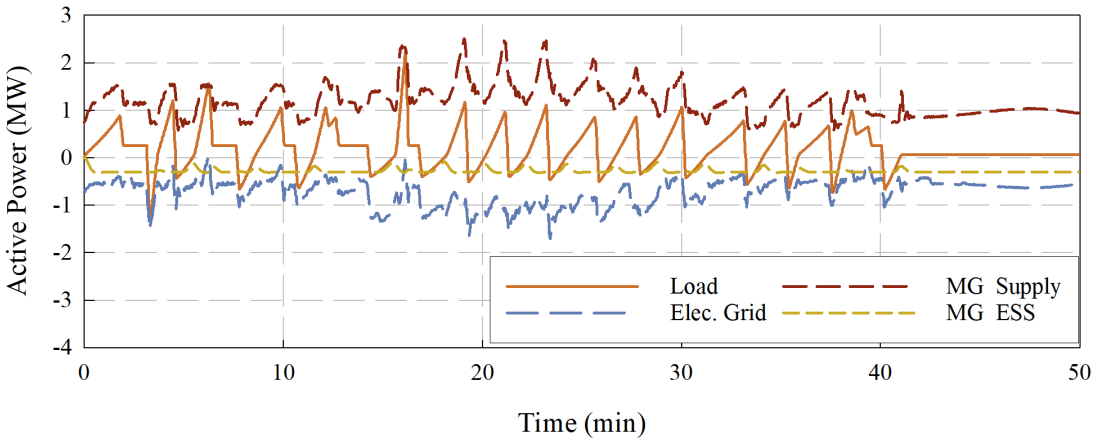

(b) Stratford-upon-Avon to Birmingham Moor Street (IMG2)

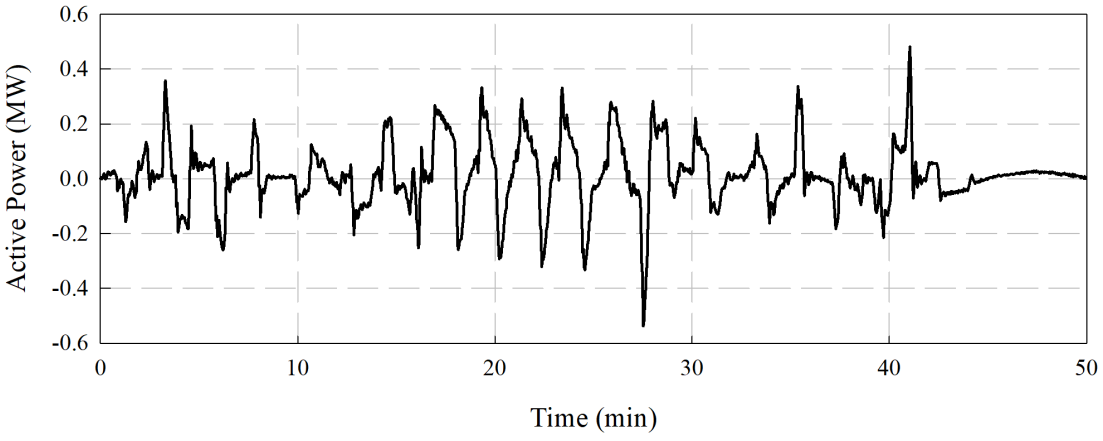

(c) Energy exchange between IMGs

Figure 8.14: Active power balance for scenario 3 for the IMGs (case study II)

scheme, where the tertiary level of control can make quick, effective decisions to

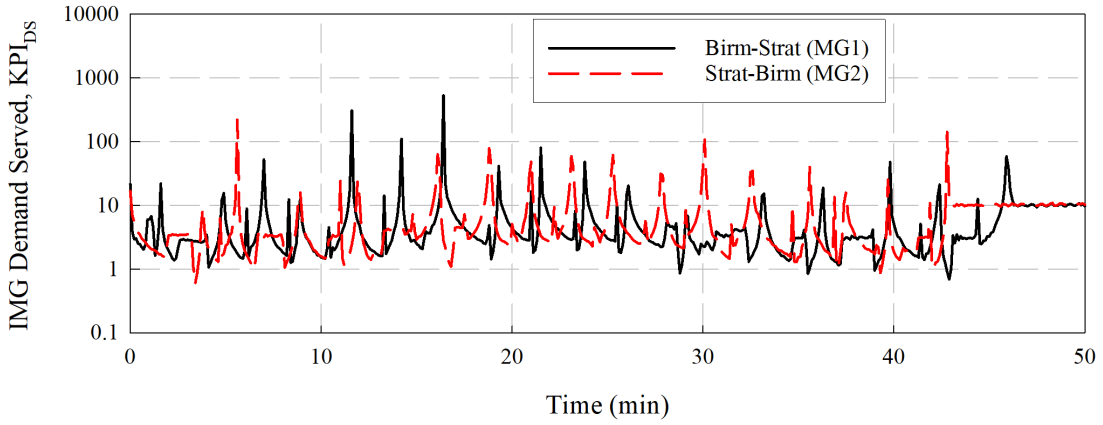

(a) Scenario 1

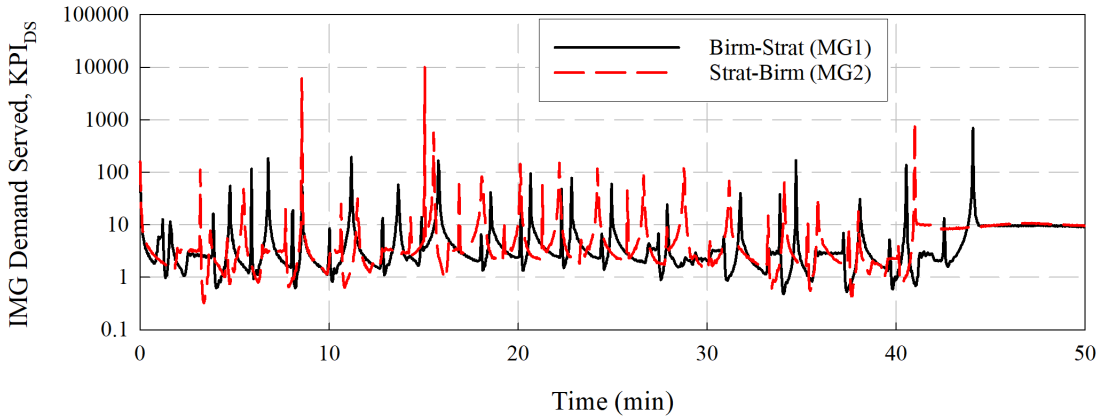

(b) Scenario 2

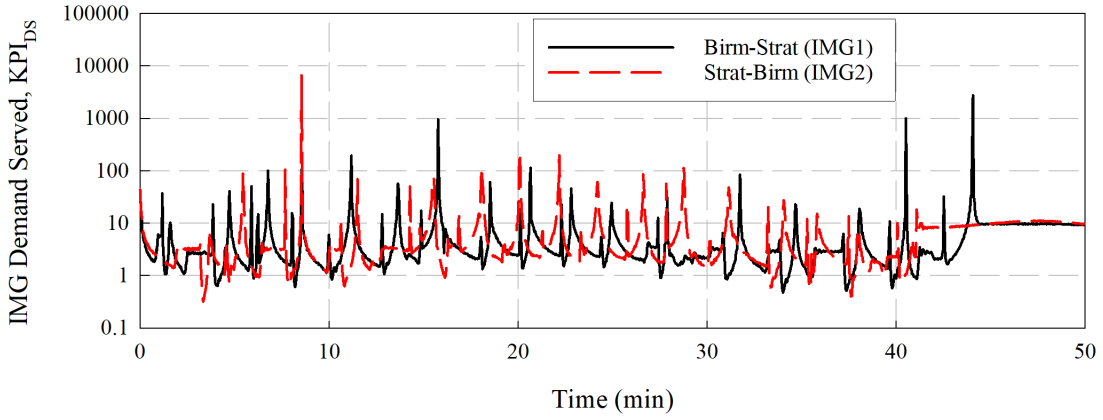

(c) Scenario 3

Figure 8.12: IMG demand served KPI comparison for case study II

ensure the demand of the railway infrastructure is supplied without heavily relying on the electric grid.

In Figure 8.13 a comparison of the **IMG electric grid dependence** KPI is shown for each scenario for case study II. It also shows the reduction of the peak load and peak regenerative load, that the electric grid must supply and absorb, receptively. In Table 8.7, a comparison between the estimated and simulated **IMG reliance** KPI is made. It also lists the peak load supplied by the IMG.

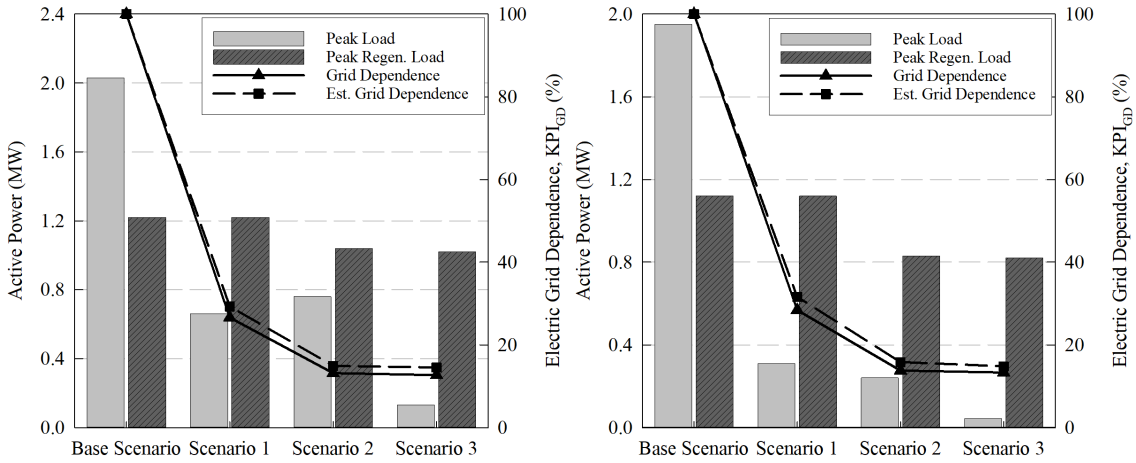

(a) Birm Moor St. to Strat (IMG1 **(b)** Start to Birm Moor St. (IMG2)

Figure 8.13: IMG electric grid dependence KPI analysis (case study II)

Table 8.7: IMG reliance KPI results for case study II

Parameter	**Birm - Strat (IMG1)**	**Strat - Birm (IMG2)**
Estimated IMG reliance, KPI_{IMGR} (%)	0.57	1.10
Simulated IMG reliance, KPI_{IMGR} (%)	1.79	1.44
Peak Load (MW)	0.48	0.26

For this case, the interconnection of IMGs plays an important role, but not as significantly as compared to a high-speed railway infrastructure. Due to the nature of the intercity railway infrastructure, this case study features a frequent stop-and-go driving pattern. This pattern creates a large power requirement during the acceleration and braking of the rolling stock. The sizing analysis of the IMGs for this case were well suited to supply the traction and auxiliary demand, even noting that the solar PV system could be reduced since the peak solar PV generation falls outside of the peak traction demand of the railway.

While the battery does recover some energy from the rolling stock during braking, it is not quick to respond to the braking operation of the rolling stock. This results in a dependence on the electric grid to absorb the remaining recovered energy. Other ESS technologies with better specific power ratings may be more suitable for intercity railway infrastructures, while the battery plays a role in providing a steady stream of energy to the rolling stock in the long-term.

8.3.4 Weather Disturbance Results

The simulation results presented in Section 8.3.2 use the weather data provided in Section 6.4. The proposed design is simulated with weather data for the terminal stations of the railway route. The weather data for each terminal station (Stratford-upon-Avon and Birmingham, UK) are provided in Section 7.3.

Figure 8.15 illustrates the RIMG model simulation results for the weather disturbance analysis. In Figure 8.15a and Figure 8.15b, the active power profile of the rolling stock moving from Birmingham Moor Street to Stratford-upon-Avon and vice-versa is shown, as well as how the demand is served by each bus within the IMG and, if required, an IMG and the electric grid. Figure 8.15c shows the exchange of energy between the two IMGs under consideration, as determined by the IMGSC. Table 8.8 provides the IMG renewable generation, IMG electric grid dependence, and IMG reliance KPI results for the weather disturbance analysis.

Table 8.8: Weather disturbance effects on KPIs for case study II

Key Performance Indicator	**Birm - Strat (IMG1)**	**Strat - Birm (IMG2)**
IMG renewable generation, KPI_{RG} (%)	98.31	98.79
IMG electric grid dependence, KPI_{GD} (%)	20.4	19.6
IMG reliance, KPI_{IMGR} (%)	7.7	6

8.4 Case Study III Results and Discussion

Case study III consists of the GO Transit Network railway infrastructure, focusing on the Lakeshore East and West corridors (see Section 7.4). In this scenario there are two IMGs, which serve the demand of the Lakeshore corridors. One IMG is used to supply the traction and auxiliary demand of the rolling stock for the Lakeshore West corridor, for a single ride, leaving from Union Station. The other IMG supplies the demand of the rolling stock of the Lakeshore East corridor, for a single ride, leaving from Union Station.

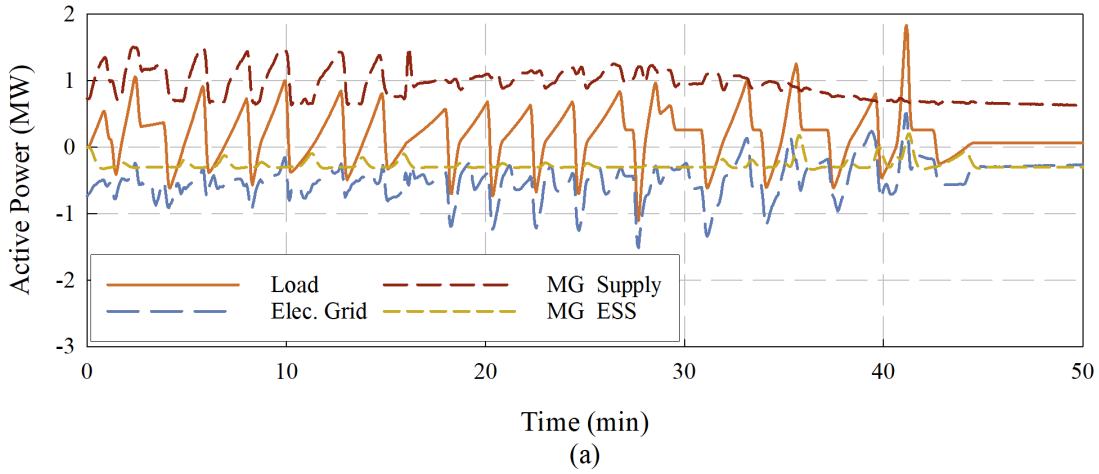

(a) Birmingham Moor St. to Stratford-upon-Avon (IMG1)

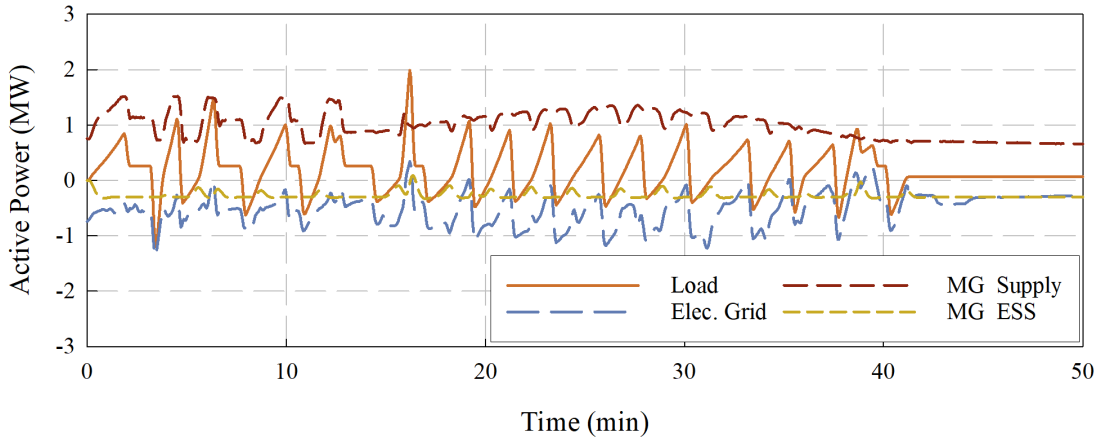

(b) Stratford-upon-Avon to Birmingham Moor St (IMG2)

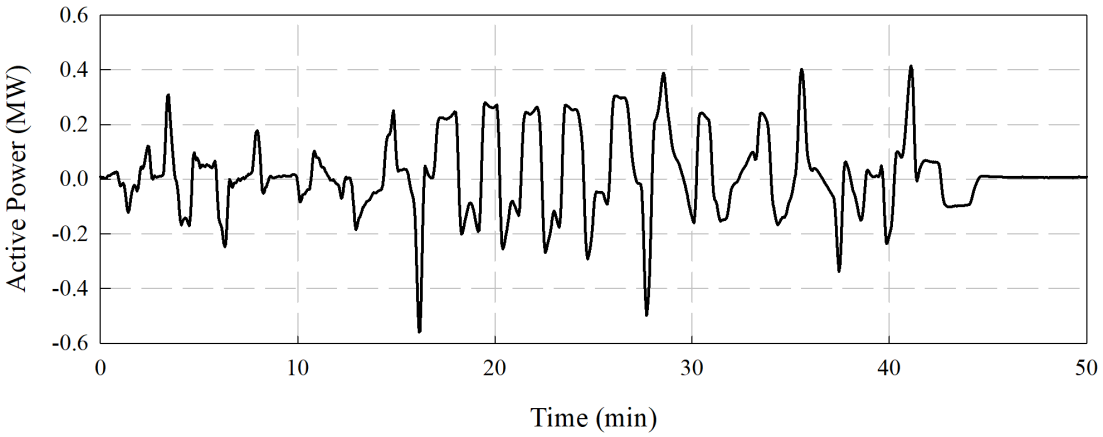

(c) Energy exchange between IMGs

Figure 8.15: Weather disturbance effects on active power balance for scenario 3 (case study II)

8.4.1 Sizing Analysis Results

Figure 8.16 shows the sizing analysis for case study III, which uses the IMG diversity of supply, IMG electric grid dependence, and IMG reliance KPIs. The sizing analysis computes the KPIs by incrementing the solar PV nominal capacity, from 0 MW, and decrementing the WT nominal capacity, from the peak demand, in steps of 1.5 MW. The sum of the nominal capacities of the two DERs is equal to the sum of the peak demand at all times. The parameters selected, as a result of the sizing analysis, for the IMG DERs and the expected performance are listed in Table 8.9.

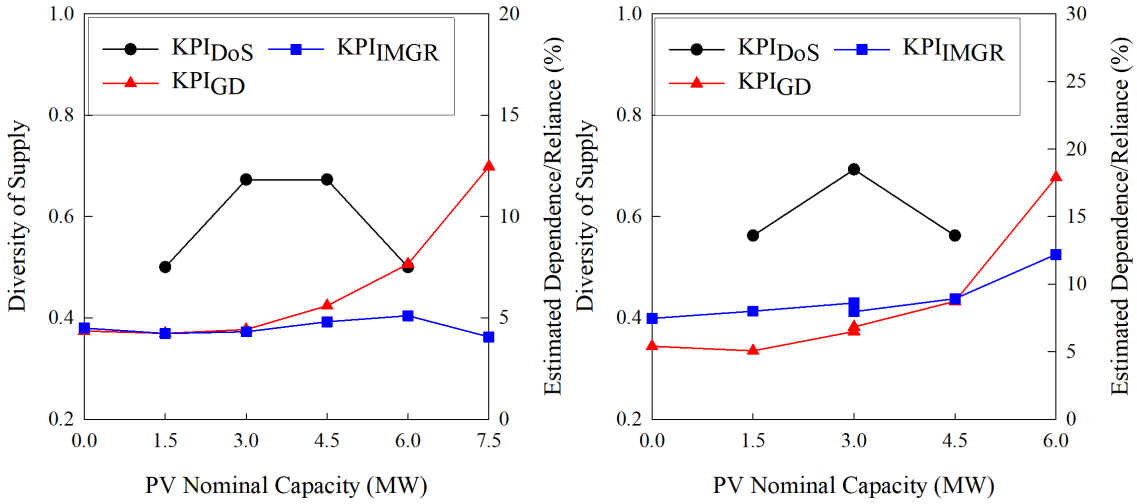

(a) Lakeshore East (IMG1) **(b)** Lakeshore West (IMG2)

Figure 8.16: Sizing analysis for case study III using resiliency KPIs

Table 8.9: Sizing parameters selected for simulation studies, and the expected KPIs for case study III

Parameter	**Lakeshore East (IMG1)**	**Lakeshore West (IMG2)**
Number of WTs, N_{WT}	4	3
Number of solar PV arrays, N_{PV}	15	15
Number of ESSs, N_{ESS}	6	6
IMG diversity of supply, KPI_{DoS}	0.5004	0.5623
Estimated IMG renewable generation, KPI_{RG} (%)	95.64	93.05
Estimated IMG electric grid dependence, KPI_{GD} (%)	6.98	5.07
Estimated IMG reliance, KPI_{IMGR} (%)	4.24	8.01

In this case, the sizing analysis shows that the lowest IMG electric grid dependence, which meets design requirement 4-5 is if the solar PV nominal capacity is 1.5 MW, which reduces the IMG diversity of supply from its target. The IMG reliance KPI

is still well below the design requirement, and similar to case study I, the interconnection of MGs plays an essential role in providing energy to supply any deficits between the IMG supply and demand.

8.4.2 Simulation Results

Considering the baseline scenario, the demand of the railway infrastructure is supplied by the electric grid. The remaining scenarios are simulated using the system model presented in Figure 6.21. For each scenario, the MG configuration and how the demand of the railway infrastructure is satisfied is described in Section 8.1. Refer to Appendix F for a notation on interpreting the simulation results.

8.4.2.1 Scenario 1

Figure 8.17 illustrates the RIMG model simulation results for scenario 1. In Figure 8.17a and Figure 8.17b, the active power profile of the rolling stock moving along the Lakeshore East and Lakeshore West corridors is shown, respectively, as well as how the demand is served by each bus within the MG and, if required, the electric grid.

As seen in the profiles above, there are instances where the electric grid must cover the deficit between the MG supply and demand. While the integration of an ESS or interconnection of MGs may alleviate the dependence, it should also be noted that the timing of the station stops for both routes are very identical. This may result in the ESS or interconnection of MGs not providing any further value to this case study, and result in increasing the nominal capacity of each MG.

8.4.2.2 Scenario 2

Figure 8.18 illustrates the RIMG model simulation results for scenario 2. In Figure 8.18a and Figure 8.18b, the active power profile of the rolling stock moving along the Lakeshore East and Lakeshore West corridors is shown, respectively, as well as how the demand is served by each bus within the MG and, if required, the electric grid. As can be seen in the figure, the DC bus is able to capture some of the recovered braking energy and store the energy in the battery. This reduces the dependence on the electric grid and allows the MG to store energy for future use (i.e. emergency situations).

In both routes, for each MG, there are multiple instances where each MG is not capable of serving the demand, and the railway infrastructure must rely on the

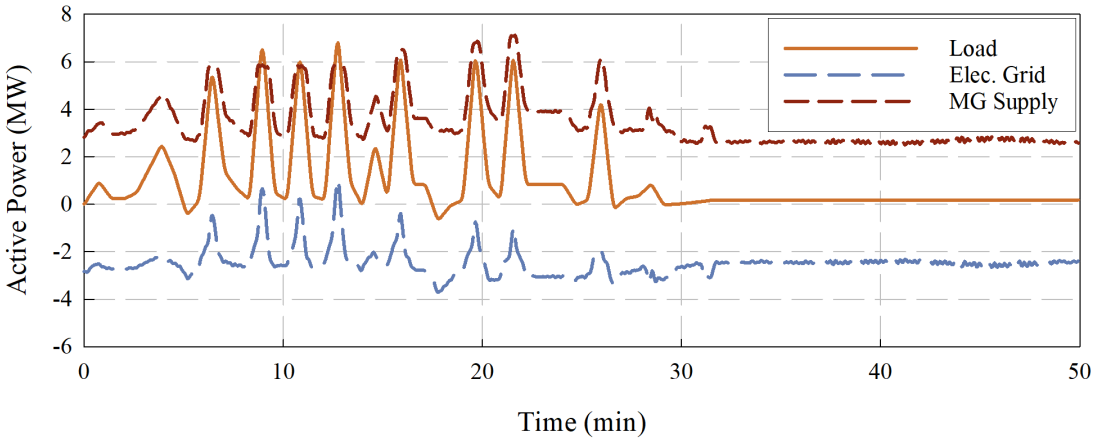

(a) Lakeshore East (MG1)

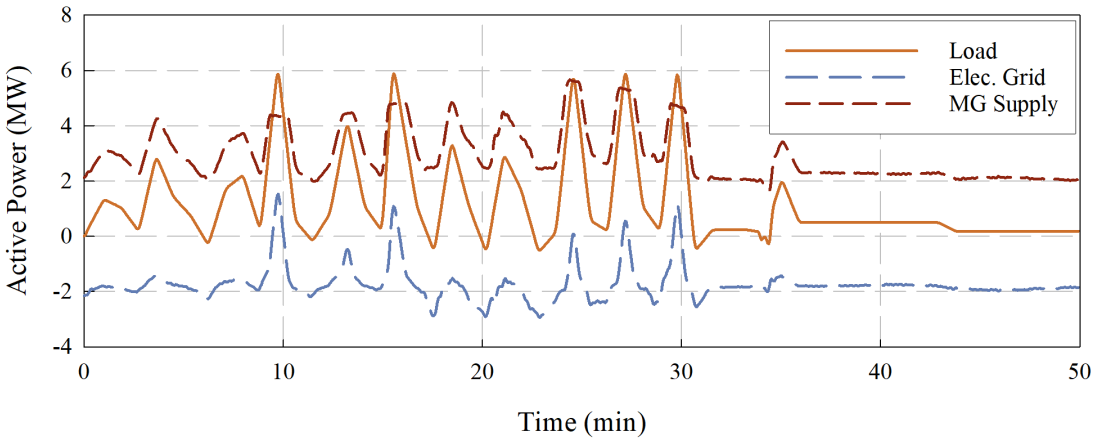

(b) Lakeshore West (MG2)

Figure 8.17: Active power balance for scenario 1 for the MGs (case study III)

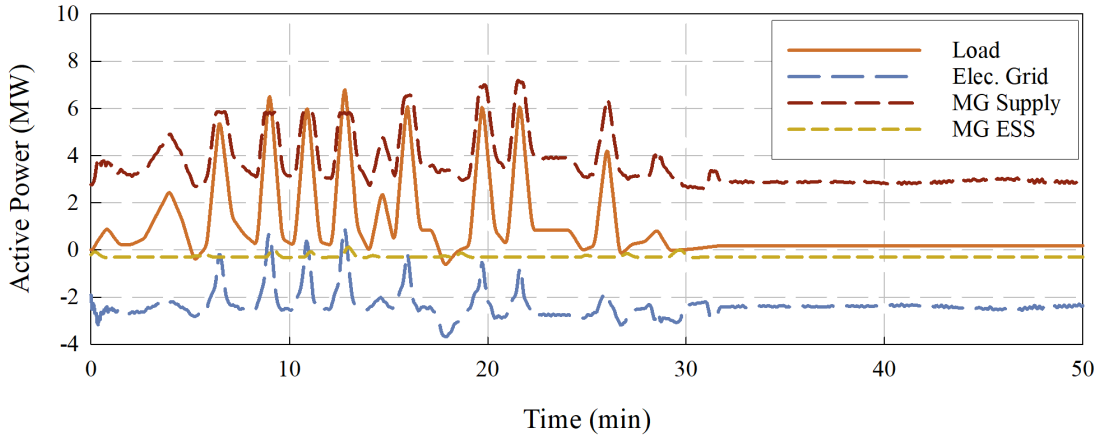

(a) Lakeshore East (IMG1)

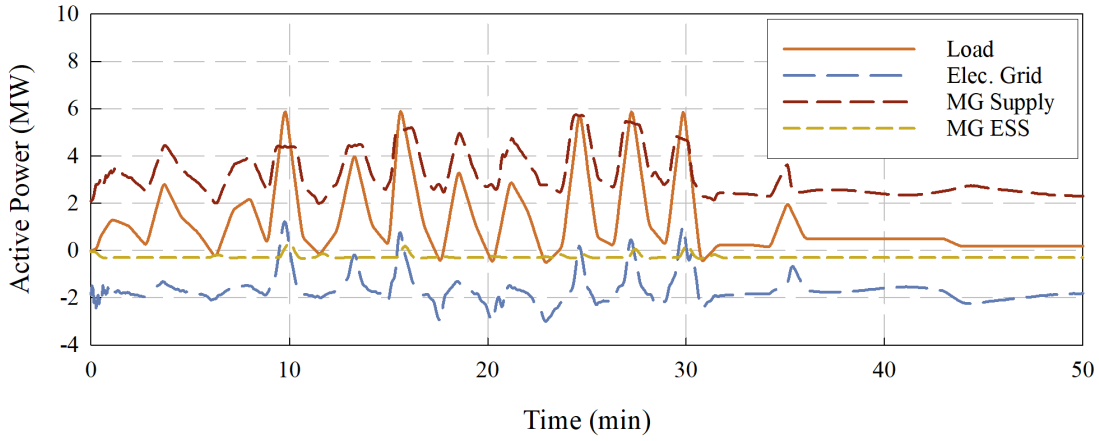

(b) Lakeshore West (MG2)

Figure 8.18: Active power balance for scenario 2 for the MGs (case study III)

electric grid for the deficit. While the ESS does alleviate some dependence on the electric grid, there are still some small peak requirements of the railway load. This could be alleviated either by increasing the size of the ESS technology or interconnecting MGs. It should be noted that increasing the size of the ESS technology could result in higher costs and poor utilization of the asset.

8.4.2.3 Scenario 3

Figure 8.19 illustrates the RIMG model simulation results for scenario 3. In Figure 8.19a and Figure 8.19b, the active power profile of the rolling stock moving along the Lakeshore East and Lakeshore West corridors is shown, respectively, as well as how the demand is served by each bus within the IMG and, if required, an IMG and the electric grid. Figure 8.19c shows the exchange of energy between the two IMGs under consideration, as determined by the IMGSC.

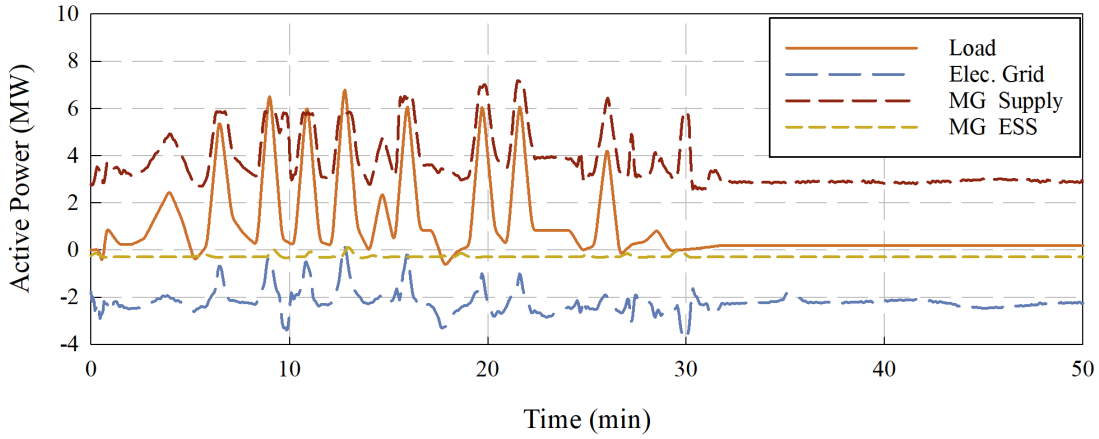

(a) Lakeshore East (IMG1)

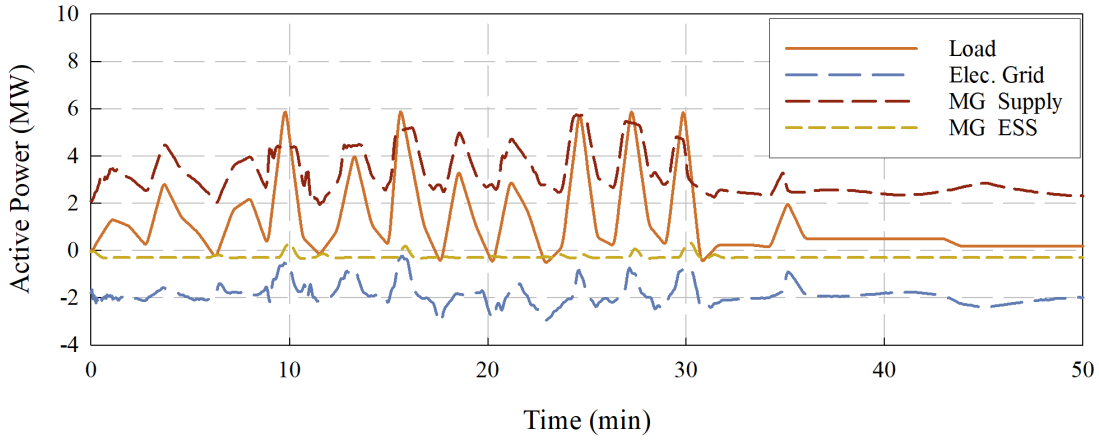

(b) Lakeshore West (IMG2)

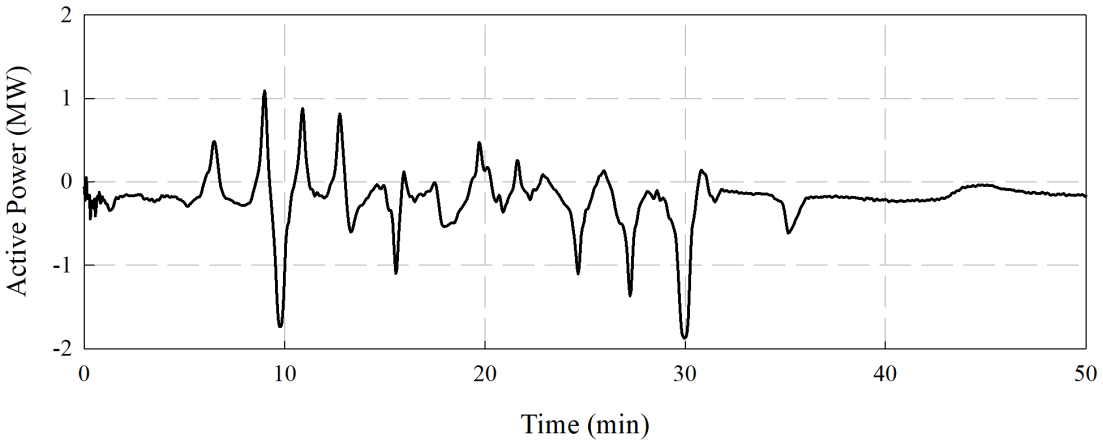

(c) Energy exchange between IMGs

Figure 8.19: Active power balance for scenario 3 for the IMGs (case study III)

Unlike in previous scenarios, where the deficit between the IMG demand and the IMG supply was covered by the electric grid, in this scenario it is instead mostly

covered by an IMG. The electric grid is mostly relied upon to export any energy that the ESS cannot absorb when the rolling stock is braking. The integration of the IMG shows an incremental benefit in reducing the dependence on the electric grid, the addition of additional rolling stock on each corridor (and thus added load) may prove the benefit of integrating IMGs to share energy within the railway infrastructure, however, may require optimization of the operational schedule.

8.4.3 Resiliency Key Performance Indicator Results

In Table 8.10, a comparison between the estimated and simulated **IMG renewable generation** KPI is made. The estimated KPI is the result of the sizing analysis, reported in Section 8.4.1. The simulated KPI is the result of the simulation performed for scenario 3.

Table 8.10: IMG renewable generation KPI results for case study III

IMG Renewable Generation, KPI_{RG}	**Lakeshore East (IMG1)**	**Lakeshore West (IMG2)**
Estimated KPI_{RG} (%)	95.64	93.05
Simulated KPI_{RG} (%)	99.78	98.82

The **IMG demand served** KPI is calculated overtime using the **IMG supply** and **IMG demand** KPIs. The KPI is used to determine the instances where an IMG cannot supply the entire demand. This is represented as the KPI evaluating to less than one. When the KPI evaluates to less than one, the control strategy (see Figure 5.4) dictates how the deficit will be covered. As seen in Figure 8.20, from scenario 1 to scenario 3 there is an incremental improvement to the performance of each IMG. The improvement demonstrates the benefits of the hierarchical control scheme, where the tertiary level of control can make quick, effective decisions to ensure the demand of the railway infrastructure is supplied without heavily relying on the electric grid.

In Figure 8.21 offers a comparison of the **IMG electric grid dependence** KPI for each scenario for case study III. It also shows the reduction of the peak load and peak regenerative load, that the electric grid must supply and absorb, receptively. In Table 8.11, a comparison between the estimated and simulated **IMG reliance** KPI is made. It also lists the peak load supplied by the IMG.

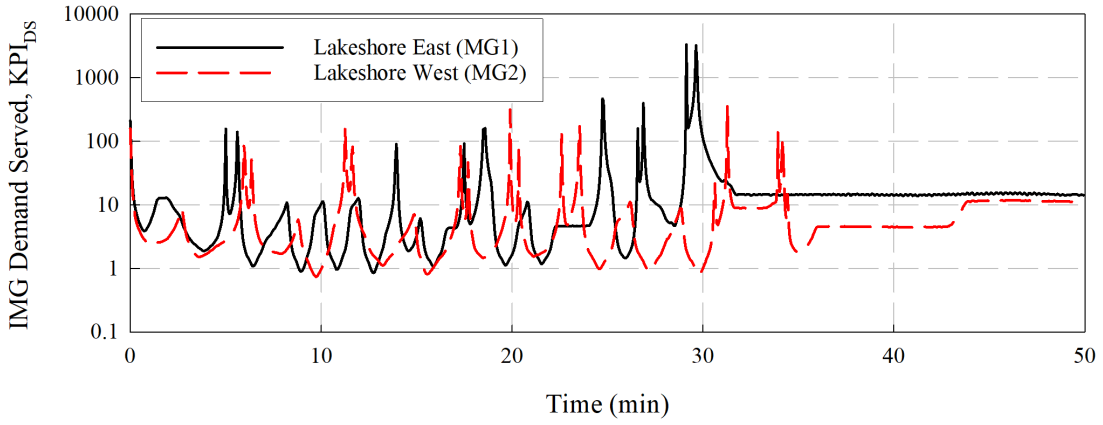

(a) Scenario 1

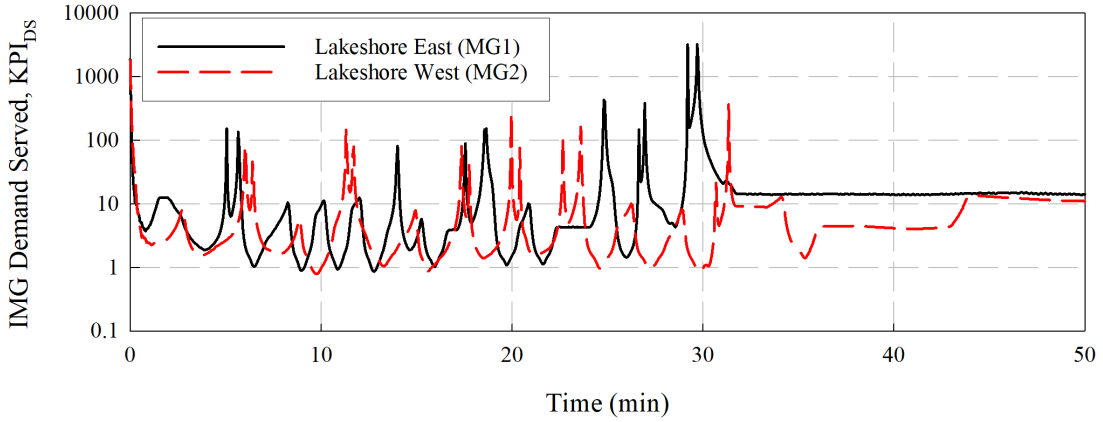

(b) Scenario 2

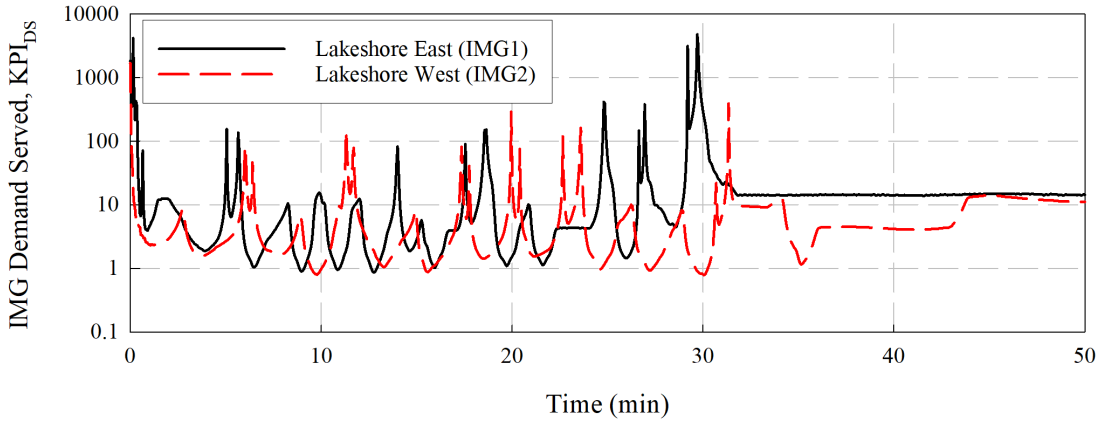

(c) Scenario 3

Figure 8.20: IMG demand served KPI comparison for case study III

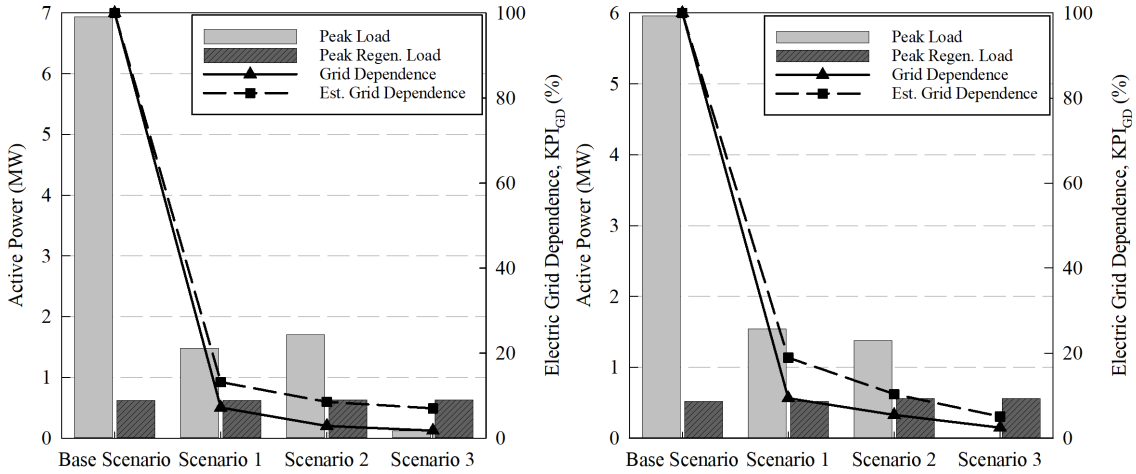

(a) Lakeshore East (IMG1) **(b)** Lakeshore West (IMG2)

Figure 8.21: IMG electric grid dependence KPI analysis (case study III)

Table 8.11: IMG reliance KPI results for case study III

Parameter	**Lakeshore East (IMG1)**	**Lakeshore West (IMG2)**
Estimated IMG reliance, KPI_{IMGR} (%)	4.24	8.01
IMG reliance, KPI_{IMGR} (%)	1.17	3.95
Peak load (MW)	1.23	1.93

In this case study, the sizing of the IMG resulted in a lower diversity of supply compared to case studies II or IV, however the interconnection of IMGs still proved effective in covering any deficit between the IMG supply and demand. The interconnection is able to reduce the peak demand covered by the electric grid for the Lakeshore West route, with a small peak remaining for Lakeshore East, which could be remedied with increasing the size of a DER or ESS.

8.4.4 Weather Disturbance Results

The simulation results presented in Section 8.4.2 use the weather data provided in Section 6.4. The proposed design is simulated with weather data for the terminal stations of the railway route. The weather data for each terminal station (Oshawa and Hamilton, ON) are provided in Section 7.4.

Figure 8.22 illustrates the RIMG model simulation results for the weather disturbance analysis. In Figure 8.22a and Figure 8.22b, the active power profile of the rolling stock moving for the Lakeshore East and Lakeshore West corridors, respectively, is shown, as well as how the demand is served by each bus within the IMG

and, if required, an IMG and the electric grid. Figure 8.22c shows the exchange of energy between the two IMGs under consideration, as determined by the IMGSC. Table 8.12 provides the IMG renewable generation, IMG electric grid dependence, and IMG reliance KPI results for the weather disturbance analysis.

Table 8.12: Weather disturbance effects on KPIs for case study III

Key Performance Indicator	**Lakeshore East (IMG1)**	**Lakeshore West (IMG2)**
IMG renewable generation, KPI_{RG} (%)	96.53	91.12
IMG electric grid dependence, KPI_{GD} (%)	7.6	12.4
IMG reliance, KPI_{IMGR} (%)	8.5	15.7

8.5 Case Study IV Results and Discussion

Case study IV consists of the UP Express railway infrastructure between Union Station and Pearson Airport (see Section 7.5). In this scenario there are two IMGs, which serve the demand of the Union Pearson Express Airport Rail Link. One IMG is used to supply the traction and auxiliary demand of the rolling stock from Union Station to Pearson Airport, for a single ride. The other IMG supplies the demand of the rolling stock moving in the reverse direction, for a single ride.

8.5.1 Sizing Analysis Results

Figure 8.23 shows the sizing analysis for case study IV, which uses the IMG diversity of supply, IMG electric grid dependence and IMG reliance KPIs. For this case the energy requirements for the rolling stock are low, such that in respect of design requirement 4-3, the nominal capacity of the WT is held constant at 1.5 MW for each time step (except the first and last), and the nominal capacity of the solar PV is incremented in steps of 100 kW. The nominal capacity of the WT and solar PV is 3 MW and 0 MW, respectively for the initial time step. The final time step has no WT and the solar PV nominal capacity is equal to the peak demand.

Similar to case study II, due to the smaller energy requirements of the rolling stock, the nominal capacity of the IMG is much smaller in comparison to case studies I and III. In addition, unlike case study II, this case study has fewer stops and longer periods of braking, which allows the battery to absorb all the energy recovered when the rolling stock is braking. This allow for a wide range in the possible nominal capacity of the PV system for both IMGs, which result in no dependence on the electric grid. However, it should also be noted that the sizing of both IMGs needs

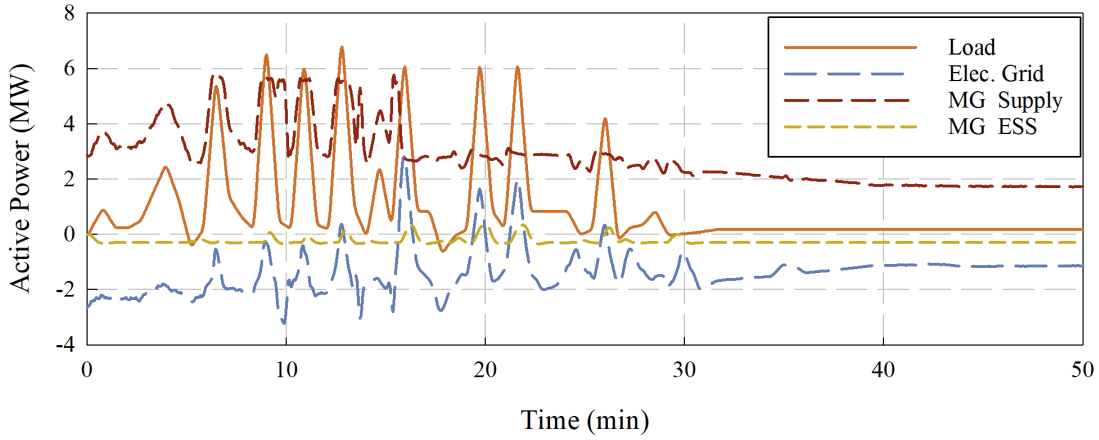

(a) Lakeshore East (IMG1)

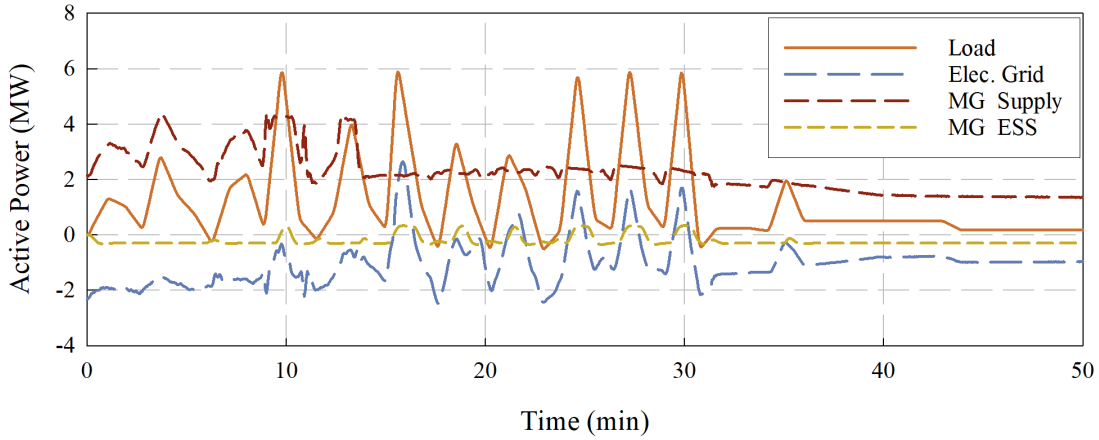

(b) Lakeshore West (IMG2)

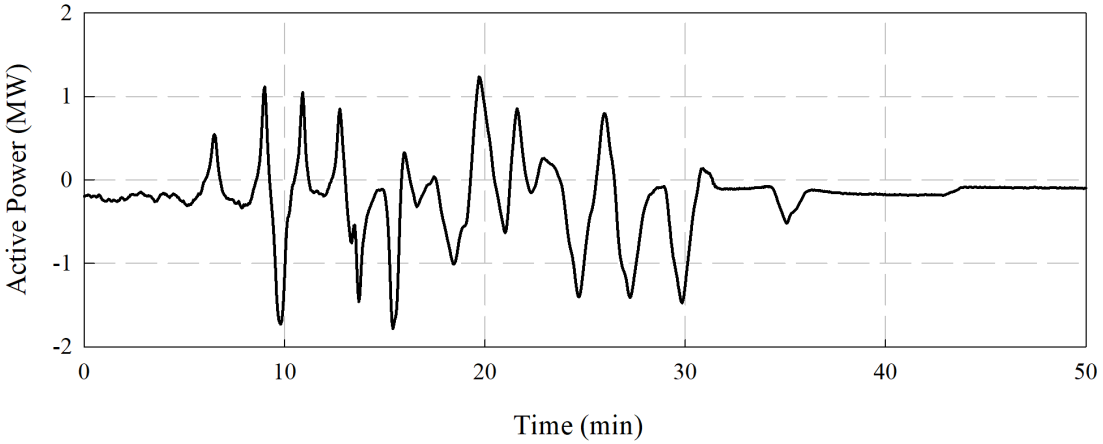

(c) Energy exchange between IMGs

Figure 8.22: Weather disturbance effects on active power balance for scenario 3 (case study III)

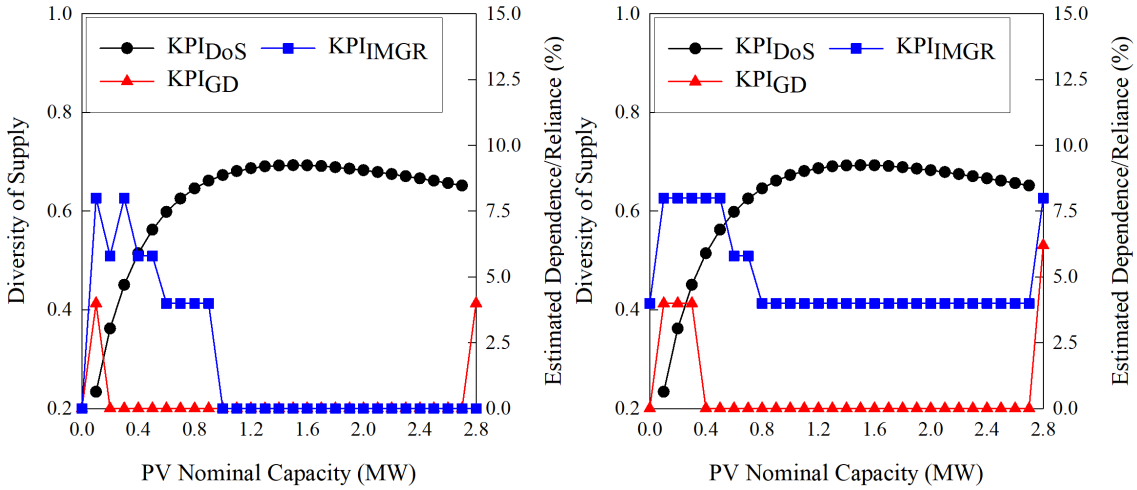

(a) Union Stn to Pearson Airport (IMG1) **(b)** Pearson Airport to Union Stn (IMG2)

Figure 8.23: Sizing analysis for case study IV using resiliency KPIs

Table 8.13: Sizing parameters selected for simulation studies, and the expected KPIs for case study IV

Parameter	**Union Station - Pearson Airport (IMG1)**	**Pearson Airport - Union Station (IMG2)**
Number of WTs, N_{WT}	1	1
Number of solar PV arrays, N_{PV}	11	12
Number of ESSs, N_{ESS}	6	6
IMG diversity of supply, KPI_{DoS}	0.6813	0.6869
Estimated IMG renewable generation, KPI_{RG} (%)	100	96.32
Estimated IMG electric grid dependence, KPI_{GD} (%)	0	4
Estimated IMG reliance, KPI_{IMGR} (%)	0	6.16

to be considered at the same time. This allows for the IMG, which may not have a dependence on either the electric grid or an IMG, to exchange energy with another IMG, which may experience a deficit between IMG supply and demand.

8.5.2 Simulation Results

Considering the baseline scenario, the demand of the railway infrastructure is supplied by the electric grid. The remaining scenarios are simulated using the system model presented in Figure 6.21. For each scenario, the MG configuration and how the demand of the railway infrastructure is satisfied is described in Section 8.1. Refer to Appendix F for a notation on interpreting the simulation results.

8.5.2.1 Scenario 1

Figure 8.24 illustrates the RIMG model simulation results for scenario 1. In Figure 8.24a and Figure 8.24b, the active power profile of the rolling stock moving from Union Station to Pearson Airport and vice-versa is shown, as well as how the demand is served by each bus within the MG and, if required, the electric grid. In this profile, the MG is able to satisfy the demand of the rolling stock, but all energy recovered from the rolling stock during braking must be exported to the electric grid which creates a dependence. This dependence could be reduced with the integration of an ESS.

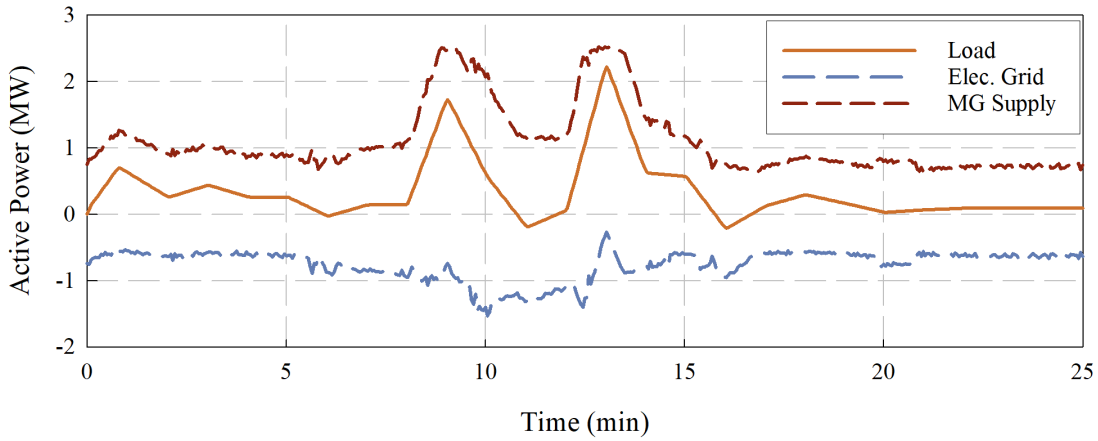

(a) Union Station to Pearson Airport (MG1)

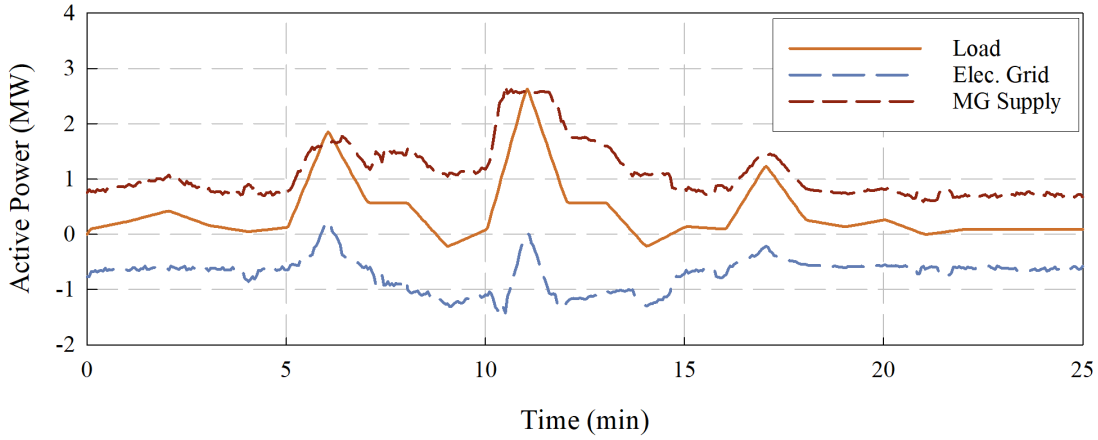

(b) Pearson Airport to Union Station (MG2)

Figure 8.24: Active power balance for scenario 1 for the MGs (case study IV)

8.5.2.2 Scenario 2

Figure 8.25 illustrates the RIMG model simulation results for scenario 2. In Figure 8.25a Figure 8.25b, the active power profile of the rolling stock moving from

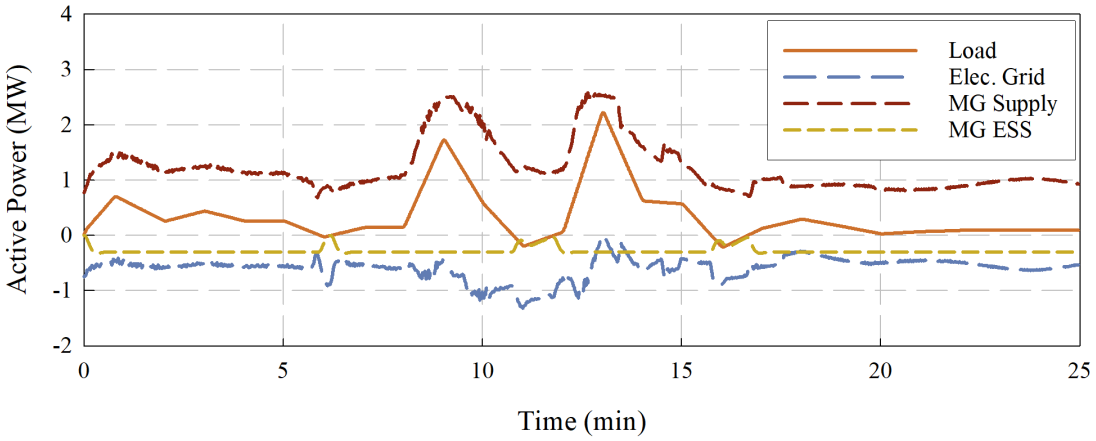

(a) Union Station to Pearson Airport (MG1)

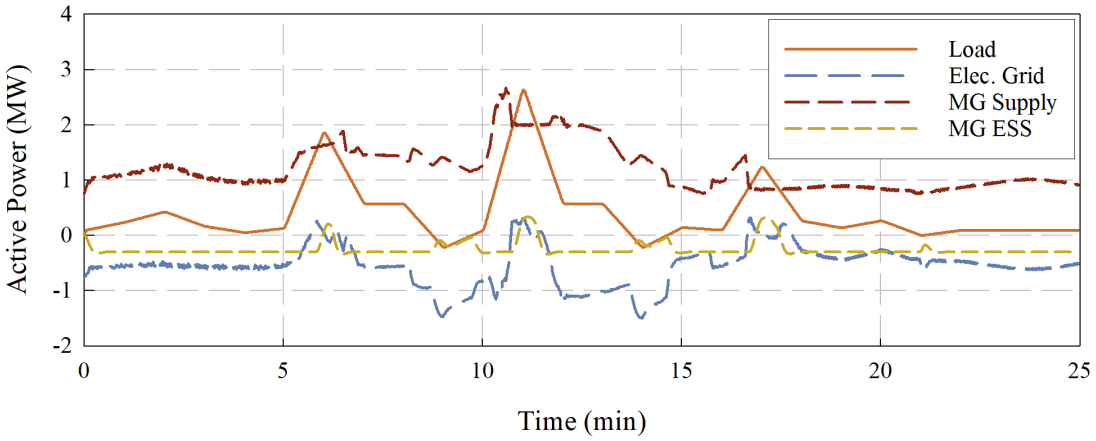

(b) Pearson Airport to Union Station (MG2)

Figure 8.25: Active power balance for scenario 2 for the MGs (case study IV)

Union Station to Pearson Airport and vice-versa is shown, as well as how the demand is served by each bus within the MG and, if required, the electric grid. As can be seen in the figure, the DC bus is able to capture some of the recovered braking energy and store the energy in the battery. This reduces the dependence on the electric grid and allows the MG to store energy for future use (i.e. emergency situations). For this profile, the battery eliminates the dependence of the MG on the electric grid.

As noted earlier, the battery can eliminate the dependence of the MG for a trip from Union Station to Pearson Airport from the electric grid. This shows the added benefit of the ESS to the MG to improve the resilience of the railway infrastructure. Should the electric grid be disconnected, the MG would have the potential to meet the demand of the rolling stock. For the route from Pearson Airport to Union Station, the latency in the battery being able to respond to changes in the demand of the rolling stock, causes a higher dependence on the electric grid. Interconnection

of MGs should further help alleviate this dependence.

8.5.2.3 Scenario 3

Figure 8.26 illustrates the RIMG model simulation results for scenario 3. In Figure 8.26a and Figure 8.26b, the active power profile of the rolling stock moving from Union Station to Pearson Airport and vice-versa is shown, as well as how the demand is served by each bus within the IMG and, if required, an IMG and the electric grid. Figure 8.26c shows the exchange of energy between the two IMGs under consideration, as determined by the IMGSC.

As in the previous scenario, the Union Station to Pearson Airport route does not dependon the electric grid to satisfy the demand of the rolling stock. The lower energy requirements of the rolling stock, proper sizing of all IMG sub-systems, and the integration of an ESS do not create a situation where the IMG cannot supply the demand. However, even though this particular IMG does not depend on another IMG to satisfy any deficit between the demand and supply, the IMG may be of use when another IMG cannot satisfy the demand.

While the IMG serving the Union Station to Pearson Airport does not have a dependence on either an IMG or the electric grid, this route does have a deficit that is covered by the IMG. This shows that even if a single IMG does not have a dependence on others, it can still be of use for those that may have a deficit from time to time.

As mentioned in the previous scenario, the integration of an ESS removed the dependence of the IMG serving the Union to Pearson route, but did not for the reverse direction. The integration of IMGs has allowed for the Pearson to Union route to further reduce its dependence on the electric grid by shifting the dependence to an IMG. This further exemplifies the statement that even if one IMG can supply its demand from its own DERs and ESS, that it can also be of use to another IMG which cannot.

8.5.3 Resiliency Key Performance Indicator Results

In Table 8.14, a comparison between the estimated and simulated **IMG renewable generation** KPI is made. The estimated KPI is the result of the sizing analysis, reported in Section 8.5.1. The simulated KPI is the result of the simulation performed for scenario 3.

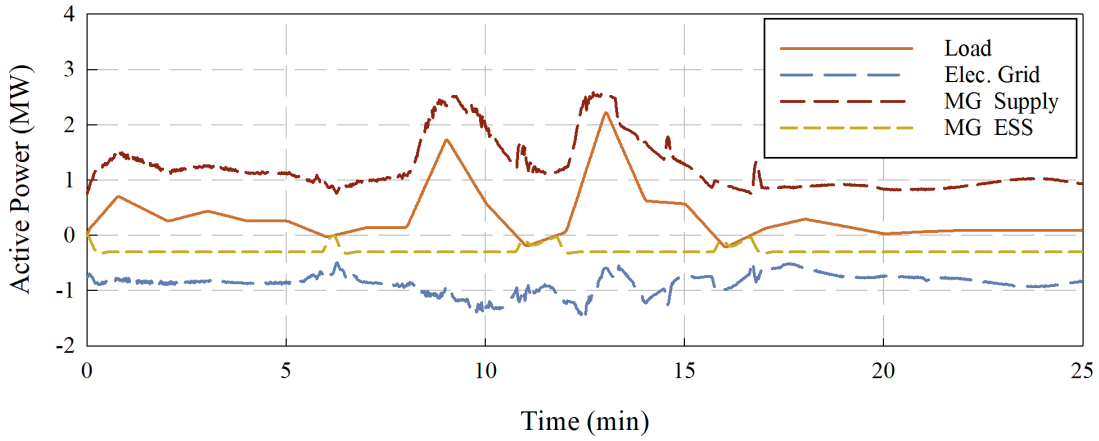

(a) Union Station to Pearson Airport (IMG1)

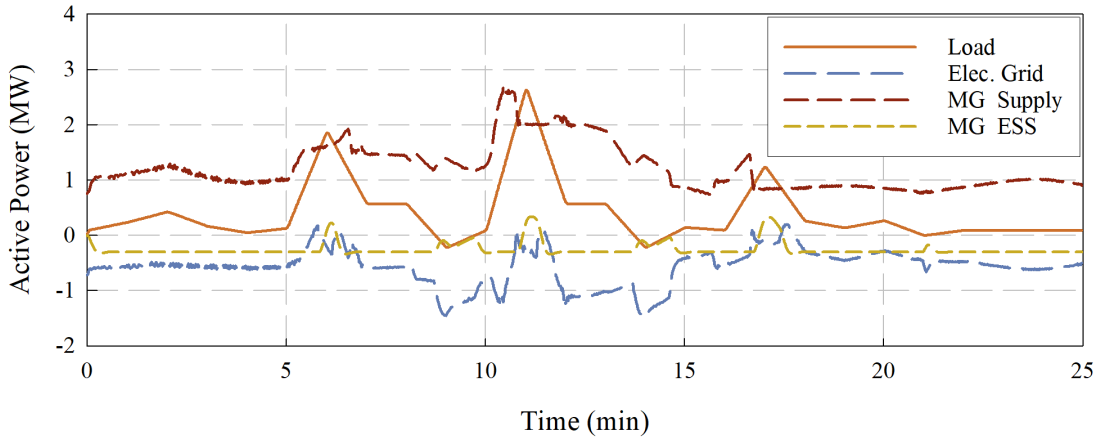

(b) Pearson Airport to Union Station (IMG2)

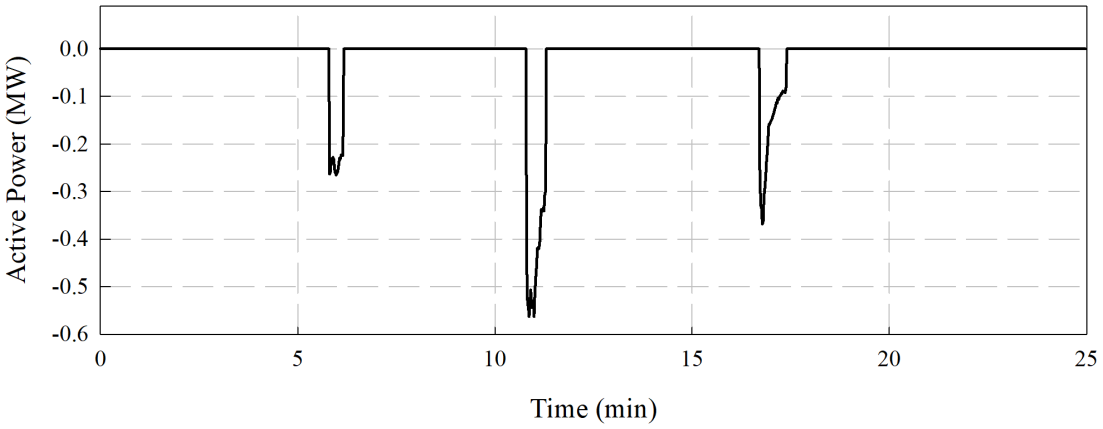

(c) Energy exchange between IMGs

Figure 8.26: Active power balance for scenario 3 for the IMGs (case study IV)

Table 8.14: IMG renewable generation KPI results for case study IV

IMG Renewable Generation, KPI_{RG}	**Union Station - Pearson Airport (IMG1)**	**Pearson Airport - Union Station (IMG2)**
Estimated KPI_{RG} (%)	100	96.32
Simulated KPI_{RG} (%)	100	98.59

The **IMG demand served** KPI is calculated overtime using the **IMG supply** and **IMG demand** KPIs. The KPI is used to determine the instances where an IMG cannot supply the entire demand. This is represented as the KPI evaluating to less than one. When the KPI evaluates to less than one, the control strategy (see Figure 5.4) dictates how the deficit will be covered. As seen in Figure 8.27, from scenario 1 to scenario 3 there is an incremental improvement to the performance of each IMG. The improvement demonstrates the benefits of the hierarchical control scheme, where the tertiary level of control can make quick, effective decisions to ensure the demand of the railway infrastructure is supplied without heavily relying on the electric grid. Unlike the other case studies, there are very few instances of the KPI evaluating to less than one for either IMG. This indicates proper sizing of the IMGs for the specified load, as well as the suitability of using IMGs for railway infrastructures with smaller demand.

In Figure 8.29 offers a comparison of the **IMG electric grid dependence** KPI for each scenario for case study IV. It also shows the reduction of the peak load and peak regenerative load, that the electric grid must supply and absorb, receptively. In Table 8.16, a comparison between the estimated and simulated **IMG reliance** KPI is made. It also lists the peak load supplied by the IMG.

In this case study, the sizing analysis determined ideal sub-system results. This showed through the scenarios that with the integration of IMGs and an ESS, the dependence on the electric grid could be eliminated, and that IMGs could be relied upon if the IMG wasn't able to meet its demand. This shows that for railway infrastructures will low energy requirements, the sizing analysis is ideal, and IMGs can be used to energize the railway infrastructure. The interconnection adds benefit for the situations where the IMG might have a malfunctioning DER or ESS, or in the worst-case scenario the electric grid is under threat, and the IMGs need to island themselves from the electric grid.

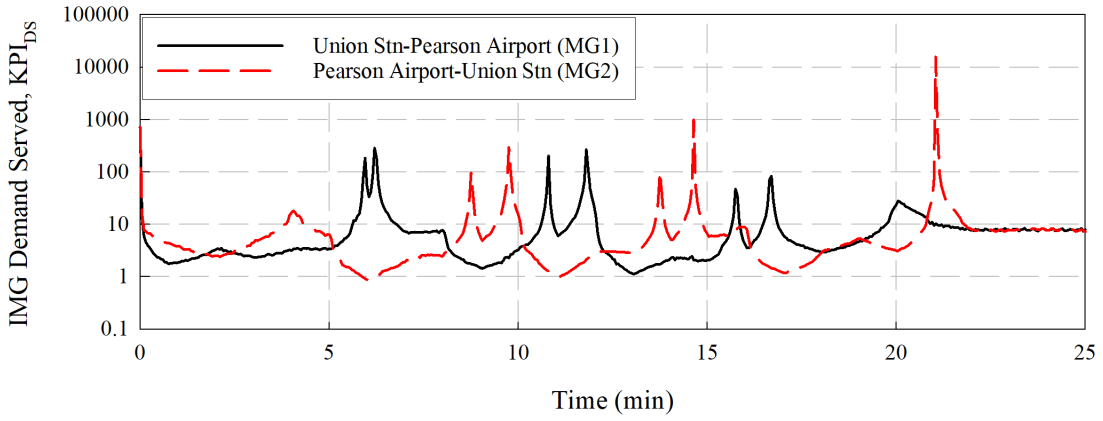

(a) Scenario 1

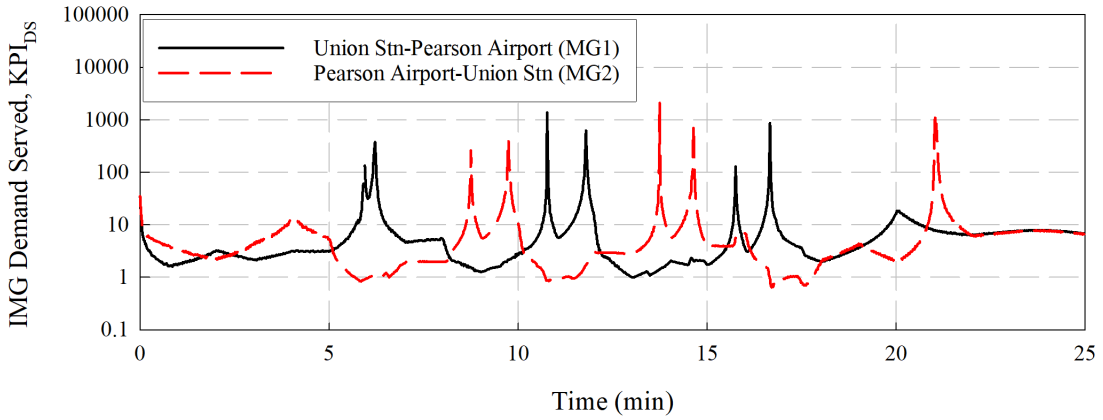

(b) Scenario 2

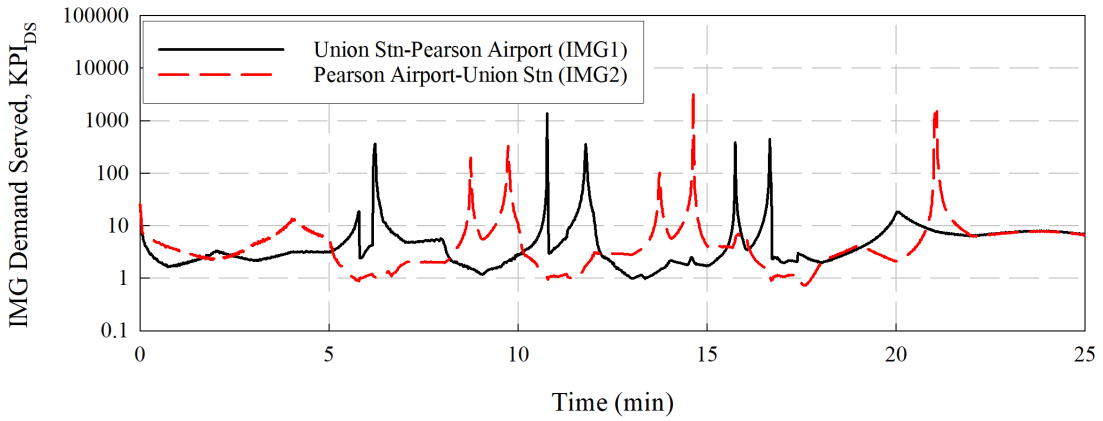

(c) Scenario 3

Figure 8.27: IMG demand served KPI comparison for case study IV

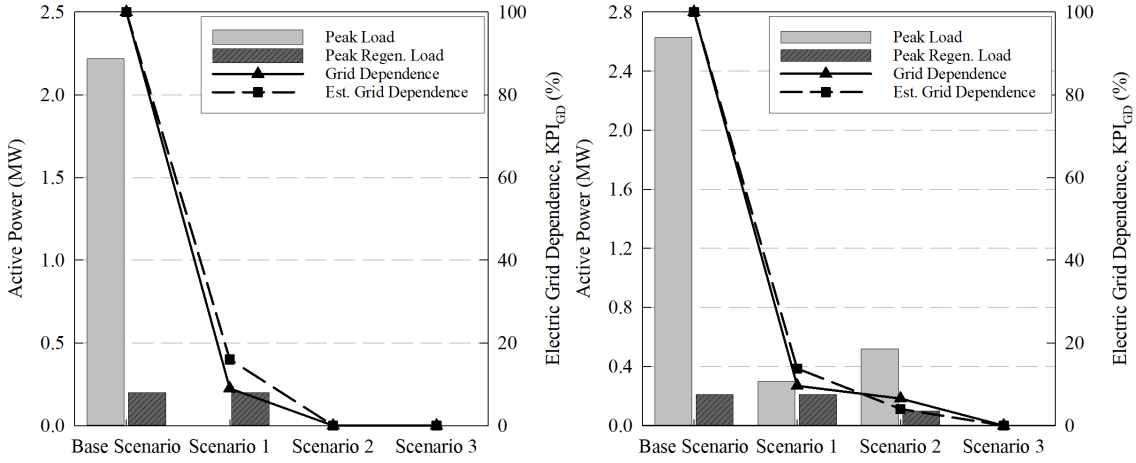

(a) Union Station to Pearson Airport (IMG1)

(b) Pearson Airport to Union Station (IMG2)

Figure 8.29: IMG electric grid dependence KPI analysis (case study IV)

Table 8.16: IMG reliance KPI results for case study IV

Parameter	**Union Station - Pearson Airport (IMG1)**	**Pearson Airport - Union Station (IMG2)**
Estimated IMG reliance, KPI_{IMGR} (%)	0	4
IMG reliance, KPI_{IMGR} (%)	0	6.16
Peak load (MW)	0	0.56

8.5.4 Weather Disturbance Results

The simulation results presented in Section 8.5.2 use the weather data provided in Section 6.4. The proposed design is simulated with weather data for the terminal stations of the railway route. The weather data for each terminal station (Toronto, ON) are provided in Section 7.5.

Figure 8.28 illustrates the RIMG model simulation results for the weather disturbance analysis. In Figure 8.28a and Figure 8.28b, the active power profile of the rolling stock moving from Union Station to Pearson Airport and vice-versa is shown, as well as how the demand is served by each bus within the IMG and, if required, an IMG and the electric grid. Figure 8.28c shows the exchange of energy between the two IMGs under consideration, as determined by the IMGSC. Table 8.15 provides the IMG renewable generation, IMG electric grid dependence, and IMG reliance KPI results for the weather disturbance analysis.

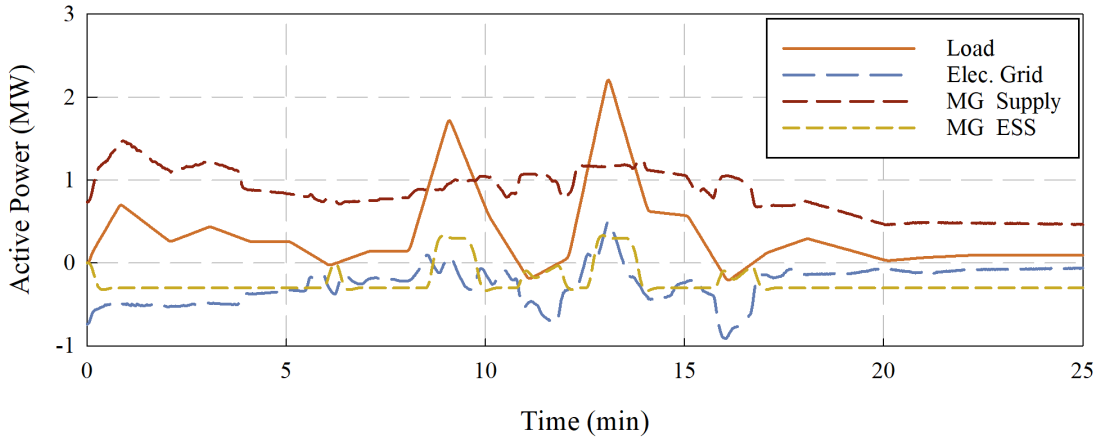

(a) Union Station to Pearson Airport (IMG1)

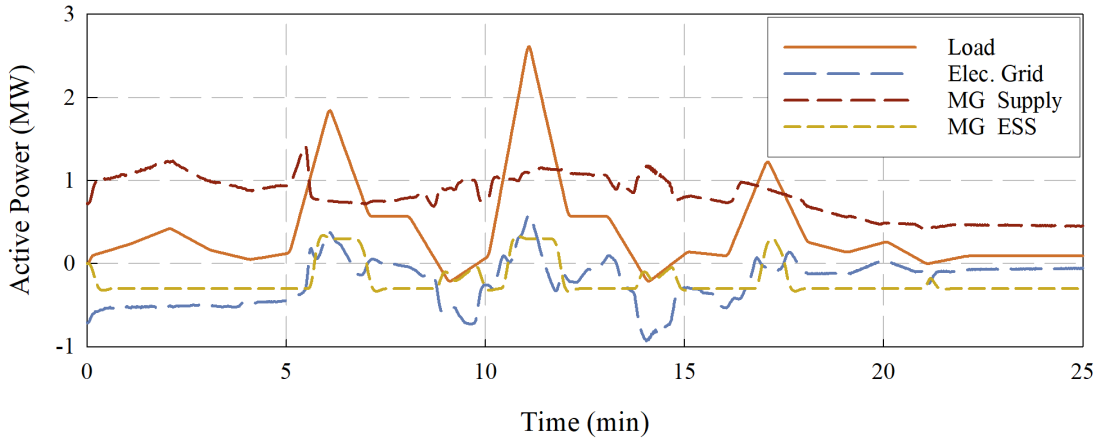

(b) Pearson Airport to Union Station (IMG2)

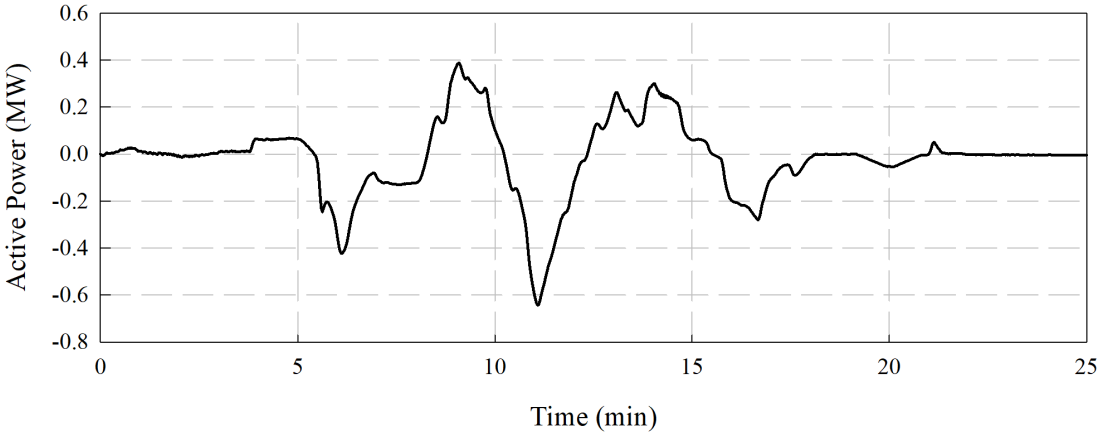

(c) Energy exchange between IMGs

Figure 8.28: Weather disturbance effects on active power balance for scenario 3 (case study IV)

Table 8.15: Weather disturbance effects on KPIs for case study IV

Key Performance Indicator	Union Station – Pearson Airport (IMG1)	Pearson Airport – Union Station (IMG2)
IMG renewable generation, KPI_{RG} (%)	96.52	93.42
IMG electric grid dependence, KPI_{GD} (%)	7.2	12
IMG reliance, KPI_{IMGR} (%)	10.1	14.7

8.6 Validation and Comparison of Results

The proposed designs and methods are demonstrated with four case studies. Each case study features a different type of railway infrastructure, which features differing speed-distance profile and rolling stock characteristics. The purpose of using four case studies is to demonstrate the benefit of using IMGs to provide a resilient supply of energy to the railway infrastructure. The results vary from case to case, but ultimately the proposed RIMG design is able to severely reduce the dependence of the railway infrastructure on the electric grid.

8.6.1 Validation of Methods

An engineering design framework was proposed in Chapter 3 to integrate RIMGs within an existing AC electrified, passenger railway infrastructure. The design framework proposed was carried out within this thesis, as described in Chapter 4 through Chapter 7. As part of the engineering design framework, the final process is to ensure the proposed design meets the requirements. The results of the design requirements associated with a resiliency KPI are compared for each case study.

In Chapter 3, a set of KPIs were introduced to evaluate the resiliency of the IMGs. A subset of the KPIs have been associated with the design requirements listed in Chapter 4. The expected performance of the KPI is provided as the output of the sizing analysis and compared to the KPI of the simulated performance. For each case study, the simulated performance shows an improvement to each of the KPIs, as seen in Table 8.17.

In addition, there were three scenarios used to demonstrate the effectiveness of the proposed RIMG design. These three scenarios were compared to the baseline scenario, where the demand of the railway infrastructure is supplied entirely by the electric grid. Figure 8.30 demonstrates a trend that IMGs (scenario 3) shows the lowest dependence on the electric grid in comparison to the other scenarios.

Table 8.17: Comparison of resiliency KPIs between design requirements, expected performance, and simulated performance

KPI	IMG Diversity of Supply	IMG Renewable Generation		IMG Reliance		IMG Electric Grid Dependence	
Design Requirement	0.693	>90%		<20%		<5%	
Case Study I		Expected	Simulated	Expected	Simulated	Expected	Simulated
IMG 1	0.5623	87.76	96.05	18.35	15.20	5.63	10.7
IMG 2	0.3927	95.78	99.0	7.81	5.70	12.18	10.5
Case Study II		Expected	Simulated	Expected	Simulated	Expected	Simulated
IMG 1	0.6813	91.74	99.87	0.57	1.79	14.52	12.7
IMG 2	0.6906	90.59	99.77	1.10	1.44	14.80	13.3
Case Study III		Expected	Simulated	Expected	Simulated	Expected	Simulated
IMG 1	0.5004	95.64	99.78	4.24	1.17	6.98	1.76
IMG 2	0.5623	93.05	98.82	8.01	3.95	5.07	2.46
Case Study IV		Expected	Simulated	Expected	Simulated	Expected	Simulated
IMG 1	0.6813	100	100	0	0	0	0
IMG 2	0.6869	96.32	98.59	6.416	4	4	0

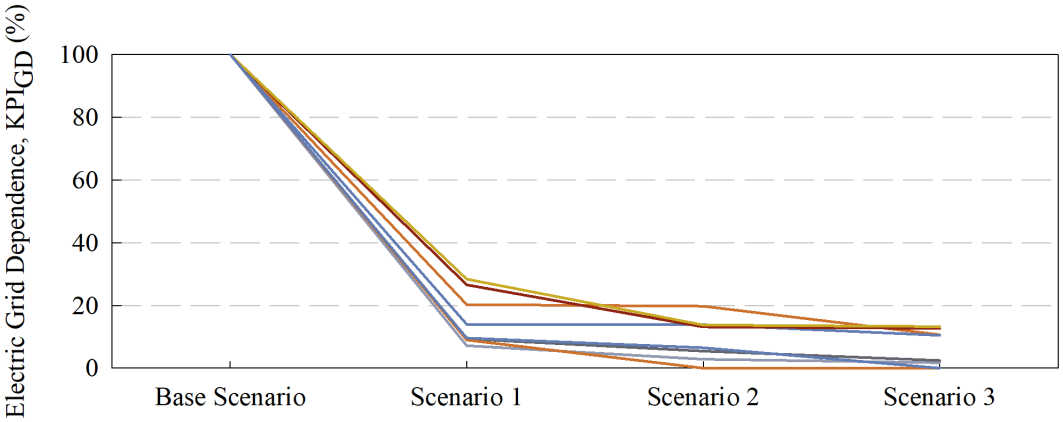

Figure 8.30: Trend in IMG electric grid dependence KPI as scenarios are evaluated for the proposed RIMG design

The remainder of the KPIs are introduced and modelled as dynamic KPIs. The IMG demand served KPI, which also requires the IMG supply and IMG demand KPIs, has been demonstrated in the results for each case study. The improvement of the KPI from scenario 1 to scenario 3, demonstrates the effectiveness of the proposed RIMG model and techniques proposed for the tertiary level of control.

The nominal capacities selected, as a result of the sizing analysis, are validated with the simulation results. The sizing analysis uses existing DER and ESS models that do not consider specific details of each MG sub-system (e.g. power conversion stages). The output for the sizing analysis is the expected performance of particular KPIs (i.e. IMG diversity of supply, IMG reliance, IMG electric grid dependence, and IMG renewable generation). The nominal capacities that meet the design requirements associated with KPI targets, or as close as possible understanding trade-offs

between them, are selected. The expected KPI results are compared to the simulated results for each case study. The simulated results show an improved KPI result over the expected (see Table 8.17). This is attributed to the finer detail included in the proposed RIMG model and the interconnection of IMGs, which has not been previously studied in research.

8.6.2 Validation of Model

Of the many simulation model validation techniques described by Sargent [172], comparison with an existing model is used for the RIMG model. The RIMG model, proposed in Chapter 5 and modelled in Chapter 6, is compared with existing literature. Basir-Khan et al. [173] propose a single MG with RESs (WT, solar PV, and hydro) and a diesel generator to satisfy the demand. Due to assumptions in each model and source of the data, there are some minor differences in the results.

Using certain information from Basir-Khan et al. [173], a simulation is executed using the proposed RIMG model. In lieu of a diesel generator and small-scale hydro plant, the electric grid is used to provide any deficit between the supply and demand. Figure 8.31a shows the simulation results for the proposed RIMG model, using the input data (i.e. load profile, wind speed, and solar irradiance) and parameters of the solar PV, WT, and ESS provided in the literature. Figure 8.31b illustrates the results reported in literature, for comparison purposes.

The RES generation from the solar PV and WT show a good match between the RIMG model and the data in the existing literature. The strategy of the battery ESS is different between the two models, as the battery in the RIMG model is relied on whenever there is a deficit between the IMG supply and demand. This strategy results in the battery ESS being discharged throughout the simulation to minimize the dependence of the IMG on the electric grid. Table 8.18 provides a comparison of KPIs between the simulation results using the proposed RIMG model and the results reported in the literature[3]. The simulation results are further validated by assuming the diesel generators and small-scale hydro in the model presented Basir-Khan et al. are replaced by the electric grid.

[3]Average energy utilization rate is a measure of the actual output of an RES to the maximum possible output of the RES over time. For this exercise, the energy utilization rate is averaged for all RESs within the studied MG.

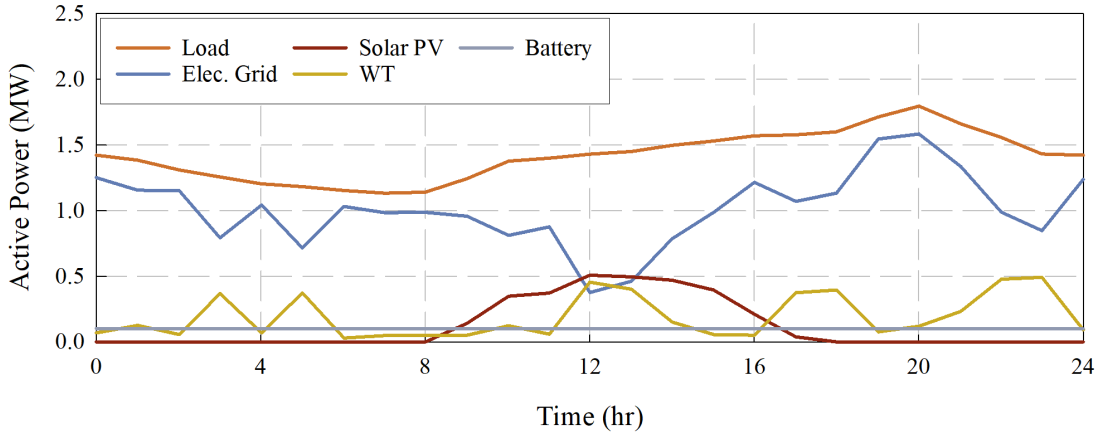

(a) Simulation results using the proposed RIMG model and the input data from Basir-Khan et al. [173]

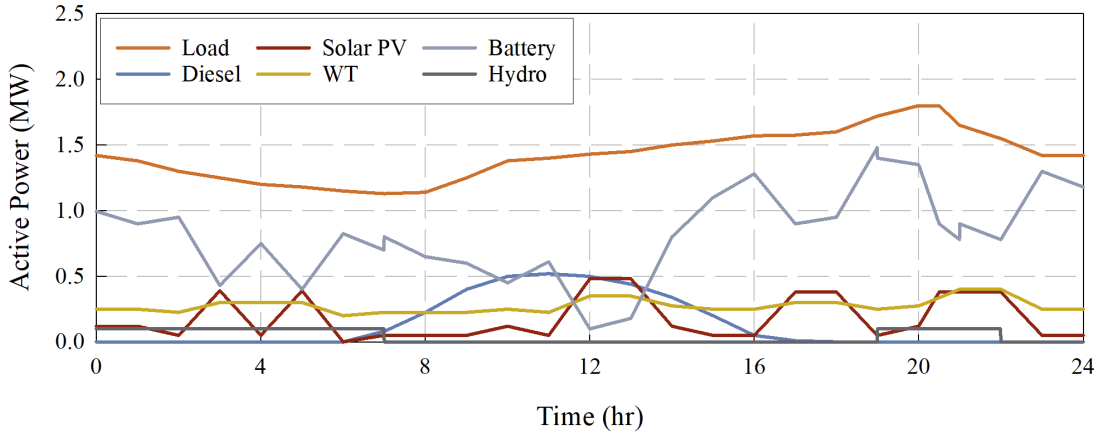

(b) Simulation results reported in Basir-Khan et al. [173]

Figure 8.31: Comparison of simulation results between the proposed RIMG model and existing literature

Table 8.18: Comparison of KPIs between the proposed RIMG model and with existing literature

Key Performance Indicator	**Thesis**	**Existing Literature [173]**	**Existing Literature without Hydro & Diesel [173]**
Diversity of supply, KPI_{DoS}	0.635 (0.693)	0.983 (1.386)	0.635 (0.693)
Renewable generation, KPI_{RG} (%)	22.94	40.8	21.8
Electric grid dependence, KPI_{GD} (%)	100	0	100
Avergage energy utilization rate	0.26	0.36	0.25

8.6.3 Validation of Techniques

Similar to the validation of the model, the validation of the proposed techniques and algorithm implemented in the tertiary level of control, validation by comparison is used [172]. The proposed RIMG design uses game theory techniques, as described in Chapter 5. The techniques have been previously validated in existing literature by Cohen et al. [142]. The control techniques in the RIMG model, proposed in Chapter 5 and modelled in Chapter 6, are compared with existing literature. Lv et al. [174] and Lu et al. [175] propose multi-MGs within a distribution system[4]. Due to assumptions in each model and source of the data, there are some minor differences in the results.

Using certain information from Lv et al. [174] and Lu et al. [175], a simulation is executed using the proposed techniques and RIMG model. Figure 8.32 illustrates a comparison between the energy exchanged with the electric grid. The simulation results for the techniques and RIMG model proposed in this thesis are compared to the results reported by Lv et al. [174] for a centralized EM strategy and their proposed bi-level multi-objective optimization EM strategy. Each set of results uses the same input data (i.e. load profile, wind speed, and solar irradiance) and parameters of the solar PV, WT, and ESS provided in Lv et al. [174] and Lu et al. [175]. Table 8.19 provides a comparison of certain KPIs between the three strategies. The RIMG model proposed in this thesis exports more energy to the electric grid than the proposed strategies in the existing literature, which indicates if the electric grid and MGs were to disconnect the MGs would be able to supply the demand without any load shedding.

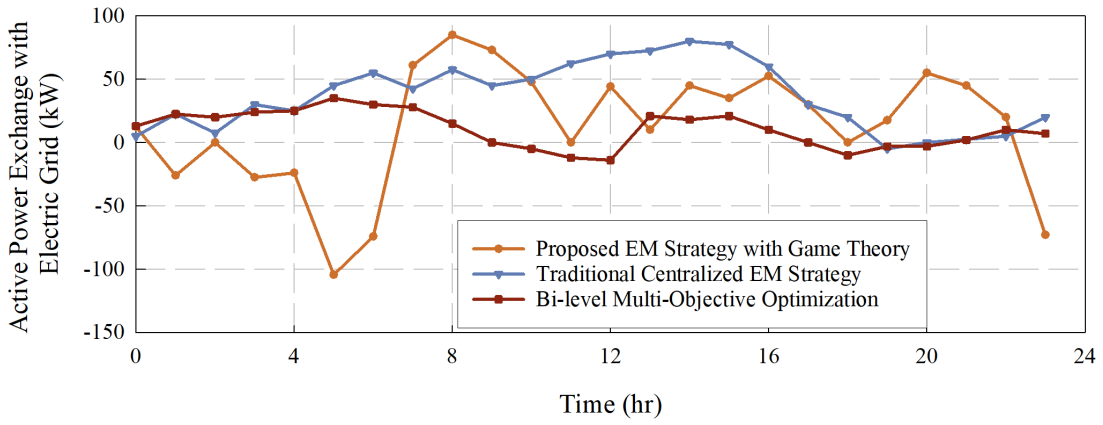

Figure 8.32: Comparison of simulation results between the proposed techniques and RIMG model and existing literature

[4]The work reported by each journal article is done by the same research group. The first author uses a different last name for each journal article.

Table 8.19: Comparison of KPIs between the proposed techniques and RIMG model with existing literature

Technique	**Average Energy Utilization Rate**	**Total Energy Exchange with Electric Grid (kWh)**
Proposed EM strategy with game theory	0.73	-85.5
Traditional centralized EM strategy	0.85	15
Bi-level multi-objective optimization	0.94	-6

Chapter 9

Conclusions and Recommendations

It was identified that railway infrastructures are an integral mass transit system in the movement of the world's population and economic goods. As such, the objective of this thesis was to design resilient interconnected microgrids to reduce the dependence of the railway infrastructure on the electric grid.

This chapter will explore the following topics to determine if the objectives were satisfied:

— A summary of the work carried out in this thesis as it relates to the objectives

— A list of the contributions made from this thesis and their impact

— Recommendations for future research work, which has been uncovered throughout the work of this thesis

9.1 Summary of Work

Mass transit systems were identified as a critical infrastructure and rely heavily on a centralized electric grid. Railway infrastructures, in particular, are responsible for moving millions of people and billions worth of economic goods every day. Approximately 30% of passenger railway infrastructures in the world are electrified, with more proposed or transitioning to electrification. However, due to the continuing rise of threats our infrastructures face, the resilience of the electric grid is weakening and hindering the reliability of electrified railway infrastructures around the world. The focus of this thesis was to design RIMGs in order to provide resilient energy for AC electrified passenger railway infrastructures.

A thorough technical literature review was first completed to understand the relationship between railway infrastructures and the electric grid. In order to reduce the dependence of the electrified railway infrastructures on the electric grid, the design of the MG was explored. The literature review is composed of six major topics:

— Microgrids

— Energy systems for microgrids

— Sizing of the microgrid energy systems

— Microgrid control architectures

— Game theory

— Resiliency analysis of microgrids

Using the proposed engineering design framework, KPI targets were defined to measure the resilience of the proposed RIMG design. The resiliency plan defined a target system which consisted of using IMGs, autonomous controlled systems that generate energy from local RESs and store excess energy in an ESS, which are interconnected with each other. The interconnection of the MGs augments the resilience of the energy supply for the railway infrastructure, as it allows one IMG to assist another IMG for various reasons.

Using the details of the proposed target system, a requirement analysis was carried out using the proposed requirement analysis methodology, quality function deployment. In this thesis, there are multiple stakeholders (i.e. passenger, railway operator, regulator, utility and technology providers) involved, each with their own requirements for the proposed target system. Quality function deployment is an ideal tool in allowing multiple stakeholders to voice their requirements, and then determine how they compare and contrast with each other. The requirements from each stakeholder were mapped to a house of quality. The house of quality allowed the customer requirements to be mapped to engineering design requirements, with specific targets. Some of the design requirements defined targets for the resiliency KPIs previously defined.

As a summary, the design requirements were:

— IMGs integrated at each traction power substation (25 kV, 60 Hz) to supply energy to the rolling stock (single-phase)

— Supervisory control scheme to monitor the IMGs, quickly respond to any disturbances, and facilitate the exchange of energy between any two IMGs

— Each IMG has a diverse supply of energy, where energy generation from RESs is at least 90% and emits minimal GHG emissions

— Rolling stock equipped with regenerative braking technology, to store recovered energy in a battery storage system

— Each IMG is dependent on the electric grid for less than 5% of the time, and reliant on any other IMG for less than 20% of the time

Using the design requirements, the target system was translated into a conceptual design, which envisioned MGs integrated at each traction power substation of the railway infrastructure. The MGs would be interconnected through the railway distribution system, so as to avoid implementing an additional bus for the interconnection. A preliminary design was derived for a single IMG, which is organized in a hybrid AC-DC configuration. A DC bus was used for the DC DERs and ESSs (i.e. solar PV and battery ESS), while the AC DERs and ESSs were segregated to an AC bus (i.e. wind turbine). Since an AC electrified railway infrastructure is studied, an inverter is integrated between the DC bus and AC bus, railway load, and electric grid. Using the preliminary design, a detailed design was proposed for each IMG.

Due to the complexity of the proposed design, and importance placed on coordination of the IMGs, a hierarchical control architecture with three layers of control was proposed. Each of the three layers served a specific purpose:

— The **primary** controllers are used to control the output of the DERs and ESS based on the set-point provided by the secondary control level.

— The **secondary** control level (MG regulation system) determines the exchange of energy within the IMG and computes the set-point for each primary controller.

— The **tertiary** control level (IMG supervisory control), supervises the interconnection of MGs and is implemented with game theory techniques, which makes effective decisions related to the resilience of the railway infrastructure.

The IMG supervisory control layer incorporates computational intelligence into the proposed control system. Game theory techniques were embedded in the control layer to make effective decisions using the IMG demand served KPI.

The proposed detailed design of RIMGs was mapped to Simulink, such that simu-

lations of the design could be validated using case studies of railway infrastructures around the world. The use of commonly available DER and ESS technology was used for the modelling of these components, as well as the sizing and simulation analysis.

There were four case studies selected to evaluate and validate the proposed design. The case studies selected consist of four railway infrastructures, either currently in operation or proposed, that are already electrified or are proposed to be, and that serve a large population. Using information provided by previous research studies or assessment reports, the technical parameters of the rolling stock and the speed-distance profiles for each route were used to derive the active power profile for each case study.

The following case studies were selected:

High Speed 2, a high-speed railway approved by the United Kingdom Government in 2017 to transport passengers between London Euston and Birmingham Curzon Street. High-speed railway infrastructures are becoming an important transportation mode in the UK to relieve capacity constraints on existing railway networks, reduce passenger travel time and push for an increase in electrified railways.

North Warwickshire Line, an intercity railway transporting passengers between Birmingham Moor St. and Stratford-upon-Avon. The Birmingham Moor St. terminus station is proposed to be adjacent to the Birmingham terminus of the High-Speed 2 project, which will result in a higher passenger demand in the future on the intercity railway.

GO Transit Network – Lakeshore Corridor consists of two intercity lines (east and west), each departing from Union Station in downtown Toronto, Ontario. Metrolinx (GO Transit operator) and the Ontario Government are currently targeting an increase in service from its current form to all-day, two-way, 15-minute electrified GO service by 2025.

Union Pearson Express Airport Rail Link, the first dedicated link in North America between two major transportation hubs in the Greater Toronto Area: Union Station and Pearson Airport. As part of the assessment of electrifying the GO transit infrastructure, plans to electrify the UP Express are included due to the importance of this transportation link and the expected growth in ridership.

Each case study is analyzed individually to understand the benefits of the proposed designs. For each case study, a sizing analysis, resiliency KPI analysis using the simulation results, and a weather disturbance analysis are performed.

The active power profiles for each case study, and the technical parameters of the DER and ESS technology, were used to perform the sizing analysis for each IMG. The results of the sizing analysis show the expected performance of the proposed design for each case study. Highlights of the sizing analysis indicate:

— That an IMG with a higher nominal capacity of PV will create a higher dependence on the electric grid, unlike wind turbines, which provide a more reliable stream of energy.

— Using a single KPI to determine the sizing of the DERs results in a poor performance of the IMG. It is ideal to incorporate multiple KPIs in the design process to understand the trade-offs between two KPIs based on a specific sizing selection.

— All IMGs needs to be considered in parallel when performing the sizing analysis. This allows for the IMG, which may not have a dependence on either the electric grid or an IMG, to exchange energy with another IMG, which may experience a deficit between IMG supply and demand.

— The requirement to have the electric grid dependence less than 5% and equal proportion of the supply mix of the IMG DERs were in conflict with each other. The solar PV energy system can only convert sunlight to electricity within a specified time period (i.e. during daylight), whereas the WT energy system is more likely to receive a steady stream of wind of varying speed.

— A greater importance was placed on the electric grid dependence KPI over the diversity of supply, as the electric grid dependence accounts for the variation in the weather. It also informs operators on how well the proposed design will perform if disconnected from the electric grid.

— In comparison to the IMG electric grid dependence KPI, the IMG reliance KPI is not greatly effected by varying the nominal capacities of the solar PV and WT. This indicates that there is a certain amount of diversity in the demand of the railway infrastructure that will allow for the possibility of energy sharing between IMGs, which will reduce the dependence on the electric grid.

Four scenarios were put forward to validate the proposed design. The scenarios were derived to show the value of augmenting the railway infrastructure resilience as specific components within the proposed design were introduced. Simulations for

the scenarios were executed for each of the four case studies using Simulink. The scenarios derived for this thesis were:

— **Baseline Scenario**: a baseline scenario where the railway infrastructure relies on a centralized electric grid

— **Scenario 1**: the integration of MGs with only DERs (no ESS or MG interconnection)

— **Scenario 2**: the integration of ESSs in each MG, where the ESS can absorb energy recovered by the rolling stock during braking, or excess energy generated by any DER

— **Scenario 3**: IMGs, as well as the full implementation of the proposed control system design; featuring the IMG supervisory controller, which uses the proposed game theory algorithm and IMG demand served KPI

For each case study there are two IMGs which serve the demand of the railway infrastructure. One IMG is used to supply the traction and auxiliary demand of the rolling stock from one terminal station to the other terminal station, for a single ride. The other IMG supplies the demand of the rolling stock moving in the reverse direction, for a single ride. For example, in case study I IMG1 is denoted for the IMG serving the London Euston to Birmingham Curzon route and IMG2 is denoted for the IMG serving the Birmingham Curzon to London Euston route (reverse direction).

The resiliency KPIs for each case study (considering the entire proposed designs, otherwise known as scenario 3), are as follows:

Case Study I

— IMG diversity of supply is 0.5623 (IMG1) and 0.3927 (IMG2)

— IMG renewable generation is 96.05% (IMG1) and 99.0% (IMG2)

— IMG reliance is 15.2% (IMG1) and 5.7% (IMG2)

— IMG electric grid dependence is 10.7% (IMG1) and 10.5% (IMG2)

Case Study II

— IMG diversity of supply is 0.6813 (IMG1) and 0.6906 (IMG2)

— IMG renewable generation is 99.87% (IMG1) and 99.77% (IMG2)

— IMG reliance is 1.79% (IMG1) and 1.44% (IMG2)

— IMG electric grid dependence is 12.7% (IMG1) and 13.3% (IMG2)

Case Study III

— IMG diversity of supply is 0.5004 (IMG1) and 0.5623 (IMG2)

— IMG renewable generation is 99.78% (IMG1) and 98.82% (IMG2)

— IMG reliance is 1.17% (IMG1) and 3.95% (IMG2)

— IMG electric grid dependence is 1.76% (IMG1) and 2.46% (IMG2)

Case Study IV

— IMG diversity of supply is 0.6813 (IMG1) and 0.6869 (IMG2)

— IMG renewable generation is 100% (IMG1) and 98.59% (IMG2)

— IMG reliance is 0% (IMG1) and 6.16% (IMG2)

— IMG electric grid dependence is 0% (IMG1) and 0% (IMG2)

The results from scenario 1 show that the integration of MGs reduces the dependence on the electric grid for each case study by at least 70%. In scenario 2, the battery as an ESS performed well for railway infrastructures which exhibit long acceleration, cruising and deceleration cycles (as seen in case studies I and IV), compared to railway infrastructures that experience short travel times between stations (as seen in case studies II and III). In scenario 3, IMGs showed the highest benefit for railway infrastructures with large energy requirements (as seen in case study I). For all other cases, IMGs were able to severely reduce, if not eliminate, the deficit between the IMG supply and demand, which was previously covered by the electric grid.

A weather disturbance analysis was performed for each case study. In lieu of the weather data assumed for the sizing analysis and simulations, the weather disturbance analysis uses historical weather data for the terminal stations of each case study. The highlights of the weather disturbance analysis results for each case study, with respect to the applicable resiliency KPIs, are as follows:

Case Study I

— IMG renewable generation is 82.94% (IMG1) and 97.61% (IMG2)

— IMG reliance is 43.4% (IMG1) and 9.7% (IMG2)

— IMG electric grid depdendence is 35.3% (IMG1) and 21.1% (IMG2)

Case Study II

— The IMG renewable generation is 98.31% (IMG1) and 98.79% (IMG2)

— The IMG reliance is 7.7% (IMG1) and 6% (IMG2)

— The electric grid depdendence is 20.4% (IMG1) and 19.6% (IMG2)

Case Study III

— The IMG renewable generation is 96.53% (IMG1) and 91.12% (IMG2)

— The IMG reliance is 8.5% (IMG1) and 15.7% (IMG2)

— The electric grid depdendence is 7.6% (IMG1) and 12.4% (IMG2)

Case Study IV

— The IMG renewable generation is 96.52% (IMG1) and 93.42% (IMG2)

— The IMG reliance is 7.2% (IMG1) and 12% (IMG2)

— The electric grid depdendence is 10.1% (IMG1) and 14.7% (IMG2)

Each of the contributions are validated and discussed. An overall trend is identified that RIMGs show the lowest dependence on the electric grid, in comparison to the scenarios evaluated. The RIMG model is compared against a model from existing literature of the MG. The results between the proposed RIMG model and existing literature show a good match. The techniques in the tertiary level of the control architecture are also compared to alternate techniques proposed in research of IMGs.

Overall, the objective of this thesis was to design RIMGs for railway infrastructures, as well as propose a suitable control system for the RIMG design. The results listed above show the effectiveness in the proposed design and control system in improving the resilience of the energy supply to support the railway infrastructure.

9.2 Contributions of this Thesis

The main contributions of this thesis are summarized as follows:

1. A novel engineering design framework to integrate resilient interconnected microgrids within an existing AC electrified passenger railway infrastructure.
2. Modelling and evaluating resiliency KPIs, consisting of commonly used KPIs from familiar domains (e.g. socio-cultural, economic, technical), that can be used to provide an understanding of the resiliency of IMGs.
3. An iterative sizing analysis method that uses multiple resiliency KPIs to size the IMG components.

4. A RIMG model to provide resilient energy to a railway infrastructure. The flexible model includes RESs and ESSs, the ability for integration of other energy systems, and can be applied to various railway infrastructures around the world. The model features an interconnection between MGs, which is demonstrated to increase the resilience of the energy supply for the railway infrastructure.

5. A hierarchical control scheme to handle coordination of IMGs. Within the control scheme, the implementation of an algorithm, using game theory techniques and the IMG demand served KPI, in the tertiary control layer to handle the energy exchange interaction between IMGs.

To take an existing railway infrastructure in its current form into one with RIMGs requires a framework for the engineering design. In this thesis, an engineering design framework was proposed to take an existing railway infrastructure, which is dependent on the electric grid, to one which is resilient with the incorporation of IMGs. This framework can be applied to any mass transit system that requires resilience improvements. The framework provides a roadmap to move forward, on the backbone of clean energy, and build resilience into our critical infrastructures.

The proposed sizing analysis method was performed for each case study using multiple resilience KPIs. The sizing method demonstrates its benefit for railway infrastructures with low energy requirements (1-4 MW range), and a low reliance on an IMG. However, for railway infrastructure with larger energy requirements the reliance on IMGs plays a crucial role in serving the demand of each IMG.

The proposed design of a RIMGs has been mapped to a model, that can be used to assess the resilience of the energy supply for a railway infrastructure. The application of RIMGs for railway infrastructure reduces the dependence of the railway infrastructure on the electric grid. The flexible RIMG model can incorporate other RES and ESS technologies for study.

A supervisory control scheme was proposed to manage the complexities of managing IMGs. The tertiary level has been proposed to manage the interactions between IMGs. The proposed control architecture and delegated tasks to each level allow for each IMG to react quickly to changes within the system, thus improving the resilience of the energy supply for the railway infrastructure. A tool was developed to solve the decision-making problem of the IMGSC (tertiary level of control). The tool proposed maps the multi-objective decision making between IMGs using game theory techniques. The results of the game are used to determine whether two IMGs

should proceed with an exchange of energy. Using game theory techniques removes fixing the decision ahead of time and allows the IMGSC to maintain the stability of the entire system, through the consideration of the IMG demand served KPI.

9.3 Recommendations for Future Work

The following multi-disciplinary topics are recommended for future research:

— Evaluate, model and implement developing ESS technologies for mass transit systems, and derive adequate sizing methods for ESSs in IMGs

— Develop models of threats to various energy system threats (e.g. natural disasters, terrorism, geo-political conflict) and model the resilience of IMGs and mass transit systems

— Enhancements to the resilient interconnected model sub-systems (e.g. rolling stock, DC bus inverter)

— Synthesize a strategy for the IMG control system to handle when one or more IMGs operates in islanding mode

— Develop stability analysis models for IMG and mass transit systems

— Develop computational intelligence for the primary level of control in the IMG

— Expand the scope of this thesis from electrified passenger railway infrastructures to other mass transit systems

In this thesis, the design of IMGs focusses on commonly available RESs (solar PV and wind turbines) and energy storage systems (battery). As technology continues to mature, future research should revolve around the integration of new systems in the design of IMGs for railway infrastructures. The proposed design is flexible, such that the future technologies can easily be implemented to satisfy the demand of the railway infrastructure. For example, as ESSs such as supercapacitors and flywheels continue to grow and become more economically viable, they should be considered for integration in the proposed design as they may be able to better handle the acceleration and braking of the railway infrastructure. In addition, sizing methods of ESSs should be improved to better accommodate resiliency objectives.

Various threats to energy and transportation infrastructures were presented earlier in this thesis, which led to the motivation of this research. With the proposed design of RIMGs, probabilistic models should be developed to evaluate the resilience of the IMG design and the mass transit system under study.

While this thesis took a 'systems thinking' approach, the RIMG model can be improved when looking at specific sub-systems. To demonstrate and prove the proposed solution, certain assumptions were made for modelling the sub-systems. In this thesis, the default parameters were used for the PLL in the DC bus inverter. Methods to tune the inverter should be researched and applied to this model to ensure system stability. A fixed drive-train and regenerative braking efficiency were used when determining the energy requirements of the rolling stock for each case study. A more detailed approach to the drive-train and regenerative braking efficiency, which will vary with the speed and loading conditions of the rolling stock should be considered. Also, the energy requirements for an entire railway infrastructure (multi-train) over a specified time period (e.g. day, week, year) should be studied to demonstrate the effectiveness of the proposed designs.

One of the KPIs evaluated in this thesis was the dependence of each IMG on the electric grid. This thesis assumed a constant connection to the electric grid; however, an IMG can also operate in islanding mode (disconnect from the electric grid for various reasons). Strategies must be synthesized and incorporated into the IMG control system to handle a disconnect from the electric grid, either planned or unplanned. A strategy on how to handle an islanding situation may also result further reduction in IMG reliance on the electric grid in normal situations.

The main concern when designing a control system is the stability of its system. Due to the complexities of an IMG design, with multiple IMGs operating in parallel and various levels of control, a proper stability analysis of the proposed IMG design is important. Stability analysis techniques need to be derived to validate the proposed IMG design and control system before implementation of the system can be realized. The stability analysis will also be used to evaluate the incremental benefit of implementing IMGs for mass transit systems.

This thesis involved the incorporation of computational intelligence in the tertiary level of the control system. The primary level used simple PID controllers to follow the set-points provided by the MG regulation system. Future work should be done to incorporate computational intelligence into the primary control level for each component of the IMG. This work would allow each DER and ESS to better handle the transients (i.e. acceleration and braking) associated with a mass transit system and be able to respond to energy exchange requests between IMGs.

The railway infrastructures studied in this thesis are not the only mass transit

systems that many people rely on every day. The scope of this thesis should be expanded to assess the resilience other mass transit systems, which include but are not limited to, freight railways, metro systems, busses, air and marine vehicles. Each of these mass transit systems depend heavily on our energy systems and move billions of people and economic goods every day. Improving resilience is a necessity, not an option, in the face of our changing world.

Bibliography

[1] "Railway Handbook 2017," International Energy Agency & International Union of Railways, Paris, Tech. Rep., 2017. [Online]. Available: https://uic.org/IMG/pdf/handbook_iea-uic_2017_web3.pdf

[2] "Rail Transportation - Transport Canada." [Online]. Available: https://www.tc.gc.ca/eng/policy/anre-menu-3020.htm

[3] R. A. of Canada, "Railways 101," 2016. [Online]. Available: https://www.railcan.ca/railways-101/

[4] I. Dincer and C. Zamfirescu, "A review of novel energy options for clean rail applications," *Journal of Natural Gas Science and Engineering*, vol. 28, pp. 461–478, Jan. 2016.

[5] H. Douglas, C. Roberts, S. Hillmansen, and F. Schmid, "An assessment of available measures to reduce traction energy use in railway networks," *Energy Conversion and Management*, vol. 106, pp. 1149–1165, Nov. 2015.

[6] Q. Chiotti, K. Chan, E. Gulecoglu, A. Belaieff, and G. Noxon, "Planning for resiliency: Toward a corporate climate adaptation plan," Metrolinx, Toronto, Tech. Rep. September, 2017. [Online]. Available: http://www.metrolinx.com/en/aboutus/sustainability/Planning_for_Resiliency_2017_EN_final.pdf

[7] G. Bang, "Energy security and climate change concerns: Triggers for energy policy change in the United States?" *Energy Policy*, vol. 38, no. 4, pp. 1645–1653, Apr. 2010.

[8] H. Engerer and M. Horn, "Natural gas vehicles: An option for Europe," *Energy Policy*, vol. 38, no. 2, pp. 1017–1029, Feb. 2010.

[9] A. Hoffrichter, C. Roberts, and S. Hillmansen, "Conceptual propulsion system design for a hydrogen-powered regional train," *IET Electrical Systems in Transportation*, vol. 6, no. 2, pp. 56–66, Jun. 2016.

[10] N. Afgan and A. Veziroglu, "Sustainable resilience of hydrogen energy system," *International Journal of Hydrogen Energy*, vol. 37, no. 7, pp. 5461–5467, Apr. 2012.

[11] A. González-Gil, R. Palacin, P. Batty, and J. P. Powell, "A systems approach to reduce urban rail energy consumption," *Energy Conversion and Management*, vol. 80, pp. 509–524, Apr. 2014.

[12] F. Schmid and C. Goodman, "Overview of Electric Railway Systems," in *IET Conference Proceedings*, vol. 44. The Institution of Engineering & Technology, 2014, pp. 1–15.

[13] Á. J. López-López, R. R. Pecharromán, A. Fernández-Cardador, and A. P. Cucala, "Assessment of energy-saving techniques in direct-current-electrified mass transit systems," *Transportation Research Part C: Emerging Technologies*, vol. 38, pp. 85–100, Oct. 2014.

[14] A. Sharifi and Y. Yamagata, "Principles and criteria for assessing urban energy resilience: A literature review," *Renewable and Sustainable Energy Reviews*, vol. 60, pp. 1654–1677, Jul. 2016.

[15] M. Schwartz, "Hurricane Maria's Aftermath in Puerto Rico," 2017. [Online]. Available: http://nymag.com/daily/intelligencer/2017/12/hurricane-maria-man-made-disaster.html

[16] A. Gholami, F. Aminifar, and M. Shahidehpour, "Front Lines Against the Darkness," *IEEE Electrification Magazine*, pp. 18–24, Mar. 2016.

[17] S. Kaufman, C. Qing, N. Levenson, and M. Hanson, "Transportation During and After Hurricane Sandy," Tech. Rep. November, 2012.

[18] C. W. Anderson, J. R. Santos, and Y. Y. Haimes, "A Risk-based Input-Output Methodology for Measuring the Effects of the August 2003 Northeast Blackout," *Economics Systems Research*, vol. 19, no. 2, pp. 183–204, Jun. 2007.

[19] L.-A. Dupigny-Giroux, "Impacts and consequences of the ice storm of 1998 for the North American north-east," *Weather*, vol. 55, no. 1, pp. 7–15, Jan. 2000.

[20] US Department of Energy, "Electric Disturbance Events (OE-417) Annual Summaries." [Online]. Available: http://www.oe.netl.doe.gov/OE417_annual_summary.aspx

[21] X. Lu, J. Wang, and L. Guo, "Using microgrids to enhance energy security and resilience," *Electricity Journal*, vol. 29, no. 10, pp. 8–15, Dec. 2016.

[22] M. Panteli and P. Mancarella, "Influence of extreme weather and climate change on the resilience of power systems: Impacts and possible mitigation strategies," *Electric Power Systems Research*, vol. 127, pp. 259–270, Jun. 2015.

[23] Y. Kwon, A. Kwasinski, and A. Kwasinski, "Coordinated Energy Management in Resilient Microgrids for Wireless Communication Networks," *IEEE Journal of Emerging and Selected Topics in Power Electronics*, vol. 4, no. 4, pp. 1158–1173, Dec. 2016.

[24] S. Li, X. Zheng, T. Zhang, and Y. Zhang, "Power Trading Mode in Multi-Microgrids with Controllable Distributed Generation: A Game-Theoretic Approach," *Proceedings - 1st IEEE International Conference on Energy Internet, ICEI 2017*, pp. 165–170, 2017.

[25] S. Ma, B. Chen, and Z. Wang, "Resilience Enhancement Strategy for Distribution Systems Under Extreme Weather Events," *IEEE Transactions on Smart Grid*, vol. 9, no. 2, pp. 1442–1451, Mar. 2018.

[26] Y. Xu, C.-C. Liu, K. P. Schneider, F. K. Tuffner, and D. T. Ton, "Microgrids for Service Restoration to Critical Load in a Resilient Distribution System," *IEEE Transactions on Smart Grid*, vol. 9, no. 1, pp. 426–437, Jan. 2018.

[27] T. Din and S. Hillmansen, "Energy consumption and carbon dioxide emissions analysis for a concept design of a hydrogen hybrid railway vehicle," *IET Electrical Systems in Transportation*, vol. 8, no. 2, pp. 112–121, Nov. 2017.

[28] S. Bird and C. Hotaling, "Multi-stakeholder microgrids for resilience and sustainability," *Environmental Hazards*, vol. 16, no. 2, pp. 116–132, Apr. 2017.

[29] A. Hoffrichter, S. Hillmansen, and C. Roberts, "Review and assessment of hydrogen propelled railway vehicles," in *IET Conference on Railway Traction Systems*. Birmingham, UK: IET, 2010, pp. 39–39.

[30] T. Ratniyomchai, P. Tricoli, and S. Hillmansen, "Recent developments and applications of energy storage devices in electrified railways," *IET Electrical Systems in Transportation*, vol. 4, no. 1, pp. 9–20, Mar. 2014.

[31] M. Dominguez, A. Fernandez-Cardador, A. P. Cucala, and R. R. Pecharroman, "Energy Savings in Metropolitan Railway Substations Through Regenerative Energy Recovery and Optimal Design of ATO Speed Profiles," *IEEE Transactions on Automation Science and Engineering*, vol. 9, no. 3, pp. 496–504, Jul. 2012.

[32] A. Clerici, E. Tironi, and F. Castelli-Dezza, "Multiport Converters and ESS on 3-kV DC Railway Lines: Case Study for Braking Energy Savings," *IEEE Transactions on Industry Applications*, vol. 54, no. 3, pp. 2740–2750, May 2018.

[33] F. Ciccarelli, A. Del Pizzo, and D. Iannuzzi, "Improvement of Energy Efficiency in Light Railway Vehicles Based on Power Management Control of Wayside Lithium-Ion Capacitor Storage," *IEEE Transactions on Power Electronics*, vol. 29, no. 1, pp. 275–286, Jan. 2014.

[34] V. Gelman, "Energy Storage That May Be Too Good to Be True: Comparison Between Wayside Storage and Reversible Thyristor Controlled Rectifiers for Heavy Rail," *IEEE Vehicular Technology Magazine*, vol. 8, no. 4, pp. 70–80, Dec. 2013.

[35] D. Ronanki, S. A. Singh, and S. S. Williamson, "Comprehensive Topological Overview of Rolling Stock Architectures and Recent Trends in Electric Railway Traction Systems," *IEEE Transactions on Transportation Electrification*, vol. 3, no. 3, pp. 724–738, Sep. 2017.

[36] S. Mohagheghi and S. Rebennack, "Optimal resilient power grid operation during the course of a progressing wildfire," *International Journal of Electrical Power & Energy Systems*, vol. 73, pp. 843–852, Dec. 2015.

[37] M. Stadler, G. Cardoso, S. Mashayekh, T. Forget, N. DeForest, A. Agarwal, and A. Schönbein, "Value streams in microgrids: A literature review," *Applied Energy*, vol. 162, pp. 980–989, Jan. 2016.

[38] K. Schneider, F. Tuffner, M. Elizondo, C.-C. Liu, Y. Xu, and D. Ton, "Evaluating the Feasibility to Use Microgrids as a Resiliency Resource," *IEEE Transactions on Smart Grid*, vol. 8, no. 2, pp. 687–696, Mar. 2017.

[39] K. Field, "Siemens Chicago Pilot Reimagines The Grid As Patchwork Of Microgrids," 2018. [Online]. Available: https://cleantechnica.com/2018/04/05/siemens-chicago-pilot-reimagines-the-grid-as-patchwork-of-microgrids/

[40] D. E. Olivares, A. Mehrizi-Sani, A. H. Etemadi, C. A. Cañizares, R. Iravani, M. Kazerani, A. H. Hajimiragha, O. Gomis-Bellmunt, M. Saeedifard, R. Palma-Behnke, G. A. Jiménez-Estévez, and N. D. Hatziargyriou, "Trends in microgrid control," *IEEE Transactions on Smart Grid*, vol. 5, no. 4, pp. 1905–1919, Jul. 2014.

[41] G. A. Bakke, *The grid : the fraying wires between Americans and our energy future*. New York: Bloomsbury USA, 2016.

[42] A. Hirsch, Y. Parag, and J. Guerrero, "Microgrids: A review of technologies, key drivers, and outstanding issues," *Renewable and Sustainable Energy Reviews*, vol. 90, pp. 402–411, Mar. 2018.

[43] N. Anglani, G. Oriti, and M. Colombini, "Optimized Energy Management System to Reduce Fuel Consumption in Remote Military Microgrids," *IEEE Transactions on Industry Applications*, vol. 53, no. 6, pp. 5777–5785, Nov. 2017.

[44] P. W. Mccahill, E. E. Noste, A. J. Rossman, and D. W. Callaway, "Integration of Energy Analytics and Smart Energy Microgrid into Mobile Medicine Operations for the 2012 Democratic National Convention," *Prehospital and Disaster Medicine*, vol. 29, no. 06, pp. 600–607, Nov. 2014.

[45] X. E. Yu, Y. Xue, S. Sirouspour, and A. Emadi, "Microgrid and transportation electrification: A review," in *2012 IEEE Transportation Electrification Conference and Expo, ITEC 2012*, Dearborn, MI, Jun. 2012, pp. 1–6.

[46] G. Comodi, A. Giantomassi, M. Severini, S. Squartini, F. Ferracuti, A. Fonti, D. Nardi Cesarini, M. Morodo, and F. Polonara, "Multi-apartment residential microgrid with electrical and thermal storage devices: Experimental analysis and simulation of energy management strategies," *Applied Energy*, vol. 137, pp. 854–866, Jul. 2015.

[47] L. G. Meegahapola, D. Robinson, A. P. Agalgaonkar, S. Perera, and P. Ciufo, "Microgrids of commercial buildings: Strategies to manage mode transfer from grid connected to islanded mode," *IEEE Transactions on Sustainable Energy*, vol. 5, no. 4, pp. 1337–1347, Oct. 2014.

[48] P. Sreedharan, J. Farbes, E. Cutter, C. K. Woo, and J. Wang, "Microgrid and renewable generation integration: University of California, San Diego," *Applied Energy*, vol. 169, pp. 709–720, Feb. 2016.

[49] R. Atia and N. Yamada, "Sizing and Analysis of Renewable Energy and Battery Systems in Residential Microgrids," *IEEE Transactions on Smart Grid*, vol. 7, no. 3, pp. 1204–1213, May 2016.

[50] C. Abbey, D. Cornforth, N. Hatziargyriou, K. Hirose, A. Kwasinski, E. Kyriakides, G. Platt, L. Reyes, and S. Suryanarayanan, "Powering Through the Storm: Microgrids Operation for More Efficient Disaster Recovery," *IEEE Power and Energy Magazine*, vol. 12, no. 3, pp. 67–76, May 2014.

[51] D. Wagman, "$17 Billion Modernization Plan for Puerto Rico's Grid Is Released," 2017. [Online]. Available: https://spectrum.ieee.org/energywise/energy/the-smarter-grid/17-billion-modernization-plan-for-puerto-rico-is-released

[52] F. T. Administration and N. J. T. Corporation, "NJ Transitgrid Traction Power System: Final scoping document," Tech. Rep. May, 2016.

[53] A. Khayatian, M. Barati, and G. J. Lim, "Integrated Microgrid Expansion Planning in Electricity Market With Uncertainty," *IEEE Transactions on Power Systems*, vol. 33, no. 4, pp. 3634–3643, Jul. 2018.

[54] E. Unamuno and J. A. Barrena, "Hybrid ac/dc microgrids - Part II: Review and classification of control strategies," *Renewable and Sustainable Energy Reviews*, vol. 52, pp. 1123–1134, Dec. 2015.

[55] Center for Sustainable Energy, "What is a microgrid?" [Online]. Available: https://energycenter.org/self-generation-incentive-program/business/technologies/microgrid

[56] S. Kumar Tiwari, B. Singh, and P. K. Goel, "Design and Control of Microgrid Fed by Renewable Energy Generating Sources," *IEEE Transactions on Industry Applications*, vol. 54, no. 3, pp. 2041–2050, May 2018.

[57] A. Parida, S. Choudhury, and D. Chatterjee, "Microgrid Based Hybrid Energy Co-Operative for Grid-Isolated Remote Rural Village Power Supply for East Coast Zone of India," *IEEE Transactions on Sustainable Energy*, vol. 9, no. 3, pp. 1375–1383, Jul. 2018.

[58] M. Nasir, H. A. Khan, A. Hussain, L. Mateen, and N. A. Zaffar, "Solar PV-Based Scalable DC Microgrid for Rural Electrification in Developing Regions," *IEEE Transactions on Sustainable Energy*, vol. 9, no. 1, pp. 390–399, Jan. 2018.

[59] K. Ubilla, G. A. Jimenez-Estevez, R. Hernadez, L. Reyes-Chamorro, C. Hernandez Irigoyen, B. Severino, and R. Palma-Behnke, "Smart Microgrids as a Solution for Rural Electrification: Ensuring Long-Term Sustainability Through Cadastre and Business Models," *IEEE Transactions on Sustainable Energy*, vol. 5, no. 4, pp. 1310–1318, Oct. 2014.

[60] A. Kumar, A. R. Singh, Y. Deng, X. He, P. Kumar, and R. C. Bansal, "A Novel Methodological Framework for the Design of Sustainable Rural Microgrid for Developing Nations," *IEEE Access*, vol. 6, pp. 24 925–24 951, 2018.

[61] I. Alsaidan, A. Khodaei, and W. Gao, "A Comprehensive Battery Energy Storage Optimal Sizing Model for Microgrid Applications," *IEEE Transactions on Power Systems*, vol. 33, no. 4, pp. 3968–3980, Jul. 2018.

[62] M. Ross, C. Abbey, F. Bouffard, and G. Joos, "Microgrid Economic Dispatch With Energy Storage Systems," *IEEE Transactions on Smart Grid*, vol. 9, no. 4, pp. 3039–3047, Jul. 2018.

[63] Y. Han, K. Zhang, H. Li, E. A. A. Coelho, and J. M. Guerrero, "MAS-Based Distributed Coordinated Control and Optimization in Microgrid and Microgrid Clusters: A Comprehensive Overview," *IEEE Transactions on Power Electronics*, vol. 33, no. 8, pp. 6488–6508, Aug. 2018.

[64] J. Chen and Q. Zhu, "A Game-Theoretic Framework for Resilient and Distributed Generation Control of Renewable Energies in Microgrids," *IEEE Transactions on Smart Grid*, vol. 8, no. 1, pp. 285–295, Jan. 2017.

[65] Y. Li, P. Zhang, and P. B. Luh, "Formal Analysis of Networked Microgrids Dynamics," *IEEE Transactions on Power Systems*, vol. 33, no. 3, pp. 3418–3427, May 2018.

[66] K. S. A. Sedzro, A. J. Lamadrid, and L. F. Zuluaga, "Allocation of Resources Using a Microgrid Formation Approach for Resilient Electric Grids," *IEEE Transactions on Power Systems*, vol. 33, no. 3, pp. 2633–2643, May 2018.

[67] X. Li, L. Guo, Y. Li, C. Hong, Y. Zhang, Z. Guo, D. Huang, and C. Wang, "Flexible Interlinking and Coordinated Power Control of Multiple DC Microgrids Clusters," *IEEE Transactions on Sustainable Energy*, vol. 9, no. 2, pp. 904–915, Apr. 2018.

[68] M. Fathi and H. Bevrani, "Statistical Cooperative Power Dispatching in Interconnected Microgrids," *IEEE Transactions on Sustainable Energy*, vol. 4, no. 3, pp. 586–593, Jul. 2013.

[69] M. J. Hossain, M. A. Mahmud, F. Milano, S. Bacha, and A. Hably, "Design of Robust Distributed Control for Interconnected Microgrids," *IEEE Transactions on Smart Grid*, vol. 7, no. 6, pp. 2724–2735, Nov. 2016.

[70] H. Wang and J. Huang, "Incentivizing Energy Trading for Interconnected Microgrids," *IEEE Transactions on Smart Grid*, vol. 9, no. 4, pp. 2647–2657, Jul. 2018.

[71] Z. Xu, P. Yang, Y. Zhang, Z. Zeng, C. Zheng, and J. Peng, "Control devices development of multi-microgrids based on hierarchical structure," *IET Generation, Transmission & Distribution*, vol. 10, no. 16, pp. 4249–4256, Dec. 2016.

[72] T. Egan, H. A. Gabbar, A. M. Othman, and R. Milman, "Design and control of resilient interconnected microgrid for sustained railway," in *2017 5th IEEE International Conference on Smart Energy Grid Engineering, SEGE 2017*, Oshawa, Aug. 2017, pp. 131–136.

[73] D. Seifried and W. Witzel, *Renewable Energy - The Facts*. London: Earthscan, 2010.

[74] "Global Statistics - Strong Outlook for Wind Power," 2017. [Online]. Available: http://gwec.net/global-figures/graphs/

[75] "Our Portfolio of Wind Turbines." [Online]. Available: https://www.gerenewableenergy.com/wind-energy/turbines

[76] "City commits $250M to switch operations to wind power," 2009. [Online]. Available: http://www.cbc.ca/news/canada/calgary/city-commits-250m-to-switch-operations-to-wind-power-1.800930

[77] D. Jegede, "Top 10 largest solar photovoltaic plants in the world," 2016. [Online]. Available: http://www.imeche.org/news/news-article/top-10-solar-photovoltaic-plants-in-the-world

[78] E. Wesoff, "IEA: Global Installed PV Capacity Leaps to 303 Gigawatts," 2017. [Online]. Available: https://www.greentechmedia.com/articles/read/iea-global-installed-pv-capacity-leaps-to-303-gw#gs.ok3pEH8

[79] X. Tan, Q. Li, and H. Wang, "Advances and trends of energy storage technology in Microgrid," *International Journal of Electrical Power and Energy Systems*, vol. 44, no. 1, pp. 179–191, Aug. 2013.

[80] A. H. Fathima and K. Palanisamy, "Optimization in microgrids with hybrid energy systems - A review," *Renewable and Sustainable Energy Reviews*, vol. 45, pp. 431–446, Feb. 2015.

[81] N. W. Lidula and A. D. Rajapakse, "Microgrids research: A review of experimental microgrids and test systems," *Renewable and Sustainable Energy Reviews*, vol. 15, no. 1, pp. 186–202, Sep. 2011.

[82] J. A. Aguado, A. J. Sanchez Racero, and S. de la Torre, "Optimal Operation of Electric Railways With Renewable Energy and Electric Storage Systems," *IEEE Transactions on Smart Grid*, vol. 9, no. 2, pp. 993–1001, Mar. 2018.

[83] S. De La Torre, A. J. Sánchez-Racero, J. A. Aguado, M. Reyes, and O. Martínez, "Optimal Sizing of Energy Storage for Regenerative Braking in Electric Railway Systems," *IEEE Transactions on Power Systems*, vol. 30, no. 3, pp. 1492–1500, May 2015.

[84] A. González-Gil, R. Palacin, and P. Batty, "Sustainable urban rail systems: Strategies and technologies for optimal management of regenerative braking energy," *Energy Conversion and Management*, vol. 75, pp. 374–388, Nov. 2013.

[85] S. Ahmad Hamidi, D. M. Ionel, and A. Nasiri, "Modeling and Management of Batteries and Ultracapacitors for Renewable Energy Support in Electric Power Systems-An Overview," *Electric Power Components and Systems*, vol. 43, no. 12, pp. 1434–1452, Jul. 2015.

[86] F. Díaz-González, A. Sumper, O. Gomis-Bellmunt, and R. Villafáfila-Robles, "A review of energy storage technologies for wind power applications," *Renewable and Sustainable Energy Reviews*, vol. 16, no. 4, pp. 2154–2171, May 2012.

[87] Z. Zhang, J. Wang, and X. Wang, "An improved charging/discharging strategy of lithium batteries considering depreciation cost in day-ahead microgrid scheduling," *Energy Conversion and Management*, vol. 105, pp. 675–684, Nov. 2015.

[88] E. Banguero, A. Correcher, Á. Pérez-Navarro, F. Morant, and A. Aristizabal, "A Review on Battery Charging and Discharging Control Strategies: Application to Renewable Energy Systems," *Energies*, vol. 11, no. 4, pp. 1–15, Apr. 2018.

[89] S. Teleke, M. Baran, A. Huang, S. Bhattacharya, and L. Anderson, "Control Strategies for Battery Energy Storage for Wind Farm Dispatching," *IEEE Transactions on Energy Conversion*, vol. 24, no. 3, pp. 725–732, Sep. 2009.

[90] R. Salas-Puente, S. Marzal, R. Gonzalez-Medina, E. Figueres, and G. Garcera, "Practical Analysis and Design of a Battery Management System for a Grid-Connected DC Microgrid for the Reduction of the Tariff Cost and Battery Life Maximization," *Energies*, vol. 11, no. 7, pp. 1889–1920, Jul. 2018.

[91] W. Liu, S. Wang, Y. Chen, X. Chen, S. Niu, and Z. Liu, "Coordinate Optimization of the Distribution Network Electricity Price, Energy Storage Operation Strategy, and Capacity under a Shared Mechanism," *Sustainability*, vol. 9, no. 6, Jun. 2017.

[92] A. Hussain, V.-H. Bui, H.-M. Kim, A. Hussain, V.-H. Bui, and H.-M. Kim, "Fuzzy Logic-Based Operation of Battery Energy Storage Systems (BESSs) for Enhancing the Resiliency of Hybrid Microgrids," *Energies*, vol. 10, no. 3, p. 271, Feb. 2017.

[93] A. Farraj, E. Hammad, and D. Kundur, "A Storage-Based Multiagent Regulation Framework for Smart Grid Resilience," *IEEE Transactions on Industrial Informatics*, vol. 14, no. 9, pp. 3859–3869, Sep. 2018.

[94] A. Chauhan and R. P. Saini, "A review on Integrated Renewable Energy System based power generation for stand-alone applications: Configurations, storage options, sizing methodologies and control," *Renewable and Sustainable Energy Reviews*, vol. 38, pp. 99–120, Oct. 2014.

[95] C. Gamarra and J. M. Guerrero, "Computational optimization techniques applied to microgrids planning: A review," *Renewable and Sustainable Energy Reviews*, vol. 48, pp. 413–424, Aug. 2015.

[96] I. Ismail and A. H. Halim, "Comparative Study of Meta-heuristics Optimization Algorithm using Benchmark Function," *International Journal of Electrical and Computer Engineering (IJECE)*, vol. 7, no. 3, pp. 1643–1650, Jun. 2017.

[97] L. Cavanini, L. Ciabattoni, F. Ferracuti, G. Ippoliti, S. Longhi, and U. Politecnica, "Microgrid sizing via profit maximization : a population based optimization approach," in *2016 IEEE 14th International Conference on Industrial Informatics (INDIN)*. IEEE, 2016, pp. 663–668.

[98] N. D. Laws, K. Anderson, N. A. DiOrio, X. Li, and J. McLaren, "Impacts of valuing resilience on cost-optimal PV and storage systems for commercial buildings," *Renewable Energy*, vol. 127, pp. 896–909, Nov. 2018.

[99] J. Li, W. Wei, and J. Xiang, "A simple sizing algorithm for stand-alone PV/Wind/Battery hybrid microgrids," *Energies*, vol. 5, no. 12, pp. 5307–5323, Dec. 2012.

[100] L. Bartolucci, S. Cordiner, V. Mulone, V. Rocco, and J. L. Rossi, "Hybrid renewable energy systems for renewable integration in microgrids: Influence of sizing on performance," *Energy*, vol. 152, pp. 744–758, Mar. 2018.

[101] M. A. Ramli, H. R. Bouchekara, and A. S. Alghamdi, "Optimal sizing of PV/wind/diesel hybrid microgrid system using multi-objective self-adaptive differential evolution algorithm," *Renewable Energy*, vol. 121, pp. 400–411, Jan. 2018.

[102] U. Akram, M. Khalid, and S. Shafiq, "Optimal sizing of a wind/solar/battery hybrid grid-connected microgrid system," *IET Renewable Power Generation*, vol. 12, no. 1, pp. 72–80, Jan. 2018.

[103] T. S. Ustun, C. Ozansoy, and A. Zayegh, "Recent developments in microgrids and example cases around the world - A review," *Renewable and Sustainable Energy Reviews*, vol. 15, no. 8, pp. 4030–4041, Aug. 2011.

[104] F. Martin-Martínez, A. Sánchez-Miralles, and M. Rivier, "A literature review of Microgrids: A functional layer based classification," *Renewable and Sustainable Energy Reviews*, vol. 62, pp. 1133–1153, Sep. 2016.

[105] X. Feng, A. Shekhar, F. Yang, R. E. Hebner, and P. Bauer, "Comparison of Hierarchical Control and Distributed Control for Microgrid," *Electric Power Components and Systems*, vol. 45, no. 10, pp. 1043–1056, Jun. 2017.

[106] A. Bidram and A. Davoudi, "Hierarchical structure of microgrids control system," *IEEE Transactions on Smart Grid*, vol. 3, no. 4, pp. 1963–1976, Dec. 2012.

[107] C.-X. Dou and B. Liu, "Multi-Agent Based Hierarchical Hybrid Control for Smart Microgrid," *IEEE Transactions on Smart Grid*, vol. 4, no. 2, pp. 771–778, Jun. 2013.

[108] M. H. Cintuglu, T. Youssef, and O. A. Mohammed, "Development and Application of a Real-Time Testbed for Multiagent System Interoperability: A Case Study on Hierarchical Microgrid Control," *IEEE Transactions on Smart Grid*, vol. 9, no. 3, pp. 1759–1768, May 2018.

[109] S. K. Sahoo, A. K. Sinha, and N. K. Kishore, "Control Techniques in AC, DC, and Hybrid AC-DC Microgrid: A Review," *IEEE Journal of Emerging and Selected Topics in Power Electronics*, vol. 6, no. 2, pp. 738–759, Jun. 2018.

[110] M. S. Mahmoud, F. M. A.L.-Sunni, and M. Saif Ur Rahman, "Review of microgrid architectures – a system of systems perspective," *IET Renewable Power Generation*, vol. 9, no. 8, pp. 1064–1078, Nov. 2015.

[111] Q. Zhang and G. Li, "A Game Theory Energy Management Strategy for a Fuel Cell/Battery Hybrid Energy Storage System," *Mathematical Problems in Engineering*, vol. 2019, pp. 1–13, Jan. 2019.

[112] J. Zeng, Q. Wang, J. Liu, J. Chen, and H. Chen, "A Potential Game Approach to Distributed Operational Optimization for Microgrid Energy Management with Renewable Energy and Demand Response," *IEEE Transactions on Industrial Electronics*, vol. 66, no. 6, pp. 4479–4489, Jun. 2018.

[113] L. Ma, N. Liu, J. Zhang, W. Tushar, and C. Yuen, "Energy Management for Joint Operation of CHP and PV Prosumers Inside a Grid-Connected Microgrid: A Game Theoretic Approach," *IEEE Transactions on Industrial Informatics*, vol. 12, no. 5, pp. 1930–1942, Oct. 2016.

[114] M. Pilz and L. Al-Fagih, "Recent Advances in Local Energy Trading in the Smart Grid Based on Game–Theoretic Approaches," *IEEE Transactions on Smart Grid*, vol. 10, no. 2, pp. 1363–1371, Mar. 2019.

[115] C. S. Karavas, K. Arvanitis, and G. Papadakis, "A game theory approach to multi-agent decentralized energy management of autonomous polygeneration microgrids," *Energies*, vol. 10, no. 11, Nov. 2017.

[116] S. Mei, W. Wei, and F. Liu, "On engineering game theory with its application in power systems," *Control Theory and Technology*, vol. 15, no. 1, pp. 1–12, Feb. 2017.

[117] W. Saad, Z. Han, H. V. Poor, and T. Başar, "Game-Theoretic Methods for the Smart Grid: An Overview of Microgrid Systems, Demand-Side Management, and Smart Grid Communications," *IEEE Signal Processing Magazine*, vol. 29, no. 5, pp. 86–105, Sep. 2012.

[118] J. Lee, J. Guo, J. K. Choi, and M. Zukerman, "Distributed Energy Trading in Microgrids: A Game Theoretic Model and Its Equilibrium Analysis," *IEEE Transactions on Industrial Electronics*, vol. 62, no. 6, pp. 3524 – 3533, Jun. 2015.

[119] S. Park, J. Lee, S. Bae, G. Hwang, and J. K. Choi, "Contribution-Based Energy-Trading Mechanism in Microgrids for Future Smart Grid: A Game Theoretic Approach," *IEEE Transactions on Industrial Electronics*, vol. 63, no. 7, pp. 4255–4265, Jul. 2016.

[120] N. Yaagoubi and H. T. Mouftah, "Energy trading in the smart grid: A distributed game-theoretic approach," *Canadian Journal of Electrical and Computer Engineering*, vol. 40, no. 2, pp. 57–65, 2017.

[121] H. Xiao, Y. Du, W. Pei, and L. Kong, "Coordinated economic dispatch and cost allocation of cooperative multi-microgrids," *The Journal of Engineering*, vol. 2017, no. 13, pp. 2363–2367, Jan. 2017.

[122] J. Ni and Q. Ai, "Economic power transaction using coalitional game strategy in micro-grids," *IET Generation, Transmission & Distribution*, vol. 10, no. 1, pp. 10–18, Jan. 2016.

[123] Y. Lin, P. Dong, X. Sun, and M. Liu, "Two-level game algorithm for multi-microgrid in electricity market," *IET Renewable Power Generation*, vol. 11, no. 14, pp. 1733–1740, Dec. 2017.

[124] L. Hou and C. Wang, "Market-based mechanisms for smart grid management: Necessity, applications and opportunities," in *2017 IEEE International Conference on Systems, Man, and Cybernetics (SMC)*. IEEE, Oct. 2017, pp. 2613–2618.

[125] R. Francis and B. Bekera, "A metric and frameworks for resilience analysis of engineered and infrastructure systems," *Reliability Engineering and System Safety*, vol. 121, pp. 90–103, Jan. 2014.

[126] S. Tyler and M. Moench, "A framework for urban climate resilience," *Climate and Development*, vol. 4, no. 4, pp. 311–326, Oct. 2012.

[127] L. Strigini, "Fault Tolerance and Resilience: Meanings, Measures and Assessment," in *Resilience Assessment and Evaluation of Computing Systems*. Springer, 2012, ch. 1, pp. 3–25.

[128] H. Farzin, M. Fotuhi-Firuzabad, and M. Moeini-Aghtaie, "Enhancing Power System Resilience Through Hierarchical Outage Management in Multi-Microgrids," *IEEE Transactions on Smart Grid*, vol. 7, no. 6, pp. 2869–2879, Nov. 2016.

[129] J. Matzenberger, N. Hargreaves, D. Raha, and P. Dias, "A novel approach to assess resilience of energy systems," *International Journal of Disaster Resilience in the Built Environment*, vol. 6, no. 2, pp. 168–181, Jun. 2015.

[130] P. E. Roege, Z. A. Collier, J. Mancillas, J. A. McDonagh, and I. Linkov, "Metrics for energy resilience," *Energy Policy*, vol. 72, pp. 249–256, Sep. 2014.

[131] C. Yuan, "Resilient distribution systems with commuity microgrids," Ph.D. dissertation, The Ohio State University, 2016.

[132] A. Kwasinski, "Quantitative model and metrics of electrical grids' resilience evaluated at a power distribution level," *Energies*, vol. 9, no. 2, pp. 1–27, Feb. 2016.

[133] X. Xu, J. Mitra, N. Cai, and L. Mou, "Planning of reliable microgrids in the presence of random and catastrophic events," *International Transactions on Electrical Energy Systems*, vol. 24, no. 8, pp. 1151–1167, Aug. 2014.

[134] S. Cano-Andrade, M. V. Spakovsky, and A. Fuentes, "Multi-objective optimization for the sustainable-resilient synthesis/design/operation of a power network coupled to distributed power producers via microgrids," in *ASME 2012 International Mechanical Engineering Congress & Exposition*, Houston, 2017, pp. 1–16.

[135] A. González-Gil, R. Palacin, and P. Batty, "Optimal energy management of urban rail systems: Key performance indicators," *Energy Conversion and Management*, vol. 90, pp. 282–291, Jan. 2015.

[136] F. E. Pacheco and J. C. Foreman, "Microgrid Reference Methodology for Understanding Utility and Customer Interactions in Microgrid Projects," *The Electricity Journal*, vol. 30, no. 3, pp. 44–50, Apr. 2017.

[137] *Simscape Electrical Reference (Specialized Power Systems)*, R2017a ed. Natick: Hydro-Quebec and The Mathworks, Inc., 2017. [Online]. Available: www.mathworks.com

[138] J. Martchamadol and S. Kumar, "Thailand's energy security indicators," *Renewable and Sustainable Energy Reviews*, vol. 16, no. 8, pp. 6103–6122, Oct. 2012.

[139] N. Honarmand, "Key performance indicators modeling for optimized microgrid configuration," Master's thesis, University of Ontario Institute of Technology, Nov. 2015.

[140] "Quality Function Deployment," Creative Industries Research Institute, Auckland, Tech. Rep. [Online]. Available: http://www.fme.aegean.gr/sites/default/files/cn/quality_function_deployment.pdf

[141] A. Chaouachi, R. M. Kamel, R. Andoulsi, and K. Nagasaka, "Multiobjective Intelligent Energy Management for a Microgrid," *IEEE Transactions on Industrial Electronics*, vol. 60, no. 4, pp. 1688–1699, Apr. 2013.

[142] J. E. Cohen, E. Marchi, and J. A. Oviedo, "Perturbation theory of completely mixed bimatrix games," *Linear Algebra and its Applications*, vol. 114-115, pp. 169–180, Mar. 1989.

[143] W. Doorsamy, W. A. Cronje, L. Lakay-doorsamy, and A. W. E. Trilemma, "A systems engineering framework : Requirements analysis for the development of rural microgrids," in *2015 IEEE International Conference on Industrial Technology (ICIT)*. Seville: IEEE, 2015, pp. 1251–1256.

[144] "Metro LRT Design Criteria Manual," METRO, Phoenix, Tech. Rep., 2007.

[145] IESO, "FIT/microFIT Price Schedule Available – August 31, 2016," 2016. [Online]. Available: http://www.ieso.ca/sector-participants/feed-in-tariff-program/news-and-updates/price-schedule-available

[146] "Appendix 7 Conceptual Design of Electrification System," Delcan Corporation & Arup Canada Inc., Toronto, Tech. Rep. December, 2010.

[147] "GO Electrification Study Final Report," Delcan Arup, Toronto, Tech. Rep., 2010. [Online]. Available: http://www.gotransit.com/electrification/en/project_history/docs/ElectricificationStudy_FinalReport.pdf

[148] Y. Han, P. Shen, X. Zhao, and J. M. Guerrero, "Control Strategies for Islanded Microgrid using Enhanced Hierarchical Control Structure with Multiple Current - Loop Damping Schemes," *IEEE Transactions on Smart Grid*, vol. 8, no. 3, pp. 1–15, May 2015.

[149] D. Polhill, "Key Train Requirements," Association of Train Operating Conditions, London, Tech. Rep. 4, 2016.

[150] Z. Shuai, Y. Sun, Z. J. Shen, W. Tian, C. Tu, Y. Li, and X. Yin, "Microgrid stability: Classification and a review," *Renewable and Sustainable Energy Reviews*, vol. 58, pp. 167–179, Jan. 2016.

[151] D. Hasegawa, G. L. Nicholson, C. Roberts, and F. Schmid, "Standardised approach to energy consumption calculations for high-speed rail," *IET Electrical Systems in Transportation*, vol. 6, no. 3, pp. 179–189, Sep. 2016.

[152] S. S. Thale, R. G. Wandhare, and V. Agarwal, "A Novel Reconfigurable Microgrid Architecture With Renewable Energy Sources and Storage," *IEEE Transactions on Industry Applications*, vol. 51, no. 2, pp. 1805–1816, Mar. 2015.

[153] T. Morstyn, B. Hredzak, and V. G. Agelidis, "Control Strategies for Microgrids with Distributed Energy Storage Systems: An Overview," *IEEE Transactions on Smart Grid*, vol. 9, no. 4, pp. 3652–3666, Jul. 2016.

[154] S. Sen and V. Kumar, "Microgrid modelling: A comprehensive survey," *Annual Reviews in Control*, vol. 46, pp. 216–250, Oct. 2018.

[155] H. Gaber, A. M. Othman, and K. Singh, "Heuristics-based Central Controller in Resilient Microgrids (RMGs) for Transportation Systems," vol. 100, 2016, pp. 352–359.

[156] R. Teymourfar, B. Asaei, H. Iman-Eini, and R. Nejati Fard, "Stationary supercapacitor energy storage system to save regenerative braking energy in a metro line," *Energy Conversion and Management*, vol. 56, pp. 206–214, Jan. 2012.

[157] G. Petrone, C. A. Ramos-Paja, and G. Spagnuolo, *Photovoltaic Sources Modeling*. John Wiley & Sons, Ltd, 2017.

[158] F. Blaabjerg and D. M. Ionel, *Renewable Energy Devices and Systems with Simulations in MATLAB and ANSYS*. Boca Raton: CRC Press, 2017.

[159] V. Vittal and R. Ayyanar, *Grid Integration and Dynamic Impact of Wind Energy*. New York, NY: Springer New York, 2013.

[160] Y. Xia, K. H. Ahmed, and B. W. Williams, "Wind Turbine Power Coefficient Analysis of a New Maximum Power Point Tracking Technique," *IEEE Transactions on Industrial Electronics*, vol. 60, no. 3, pp. 1122–1132, Mar. 2013.

[161] "Sunpower SPR-305-WHT-U (305W) Solar Panel." [Online]. Available: http://www.solardesigntool.com/components/module-panel-solar/Sunpower/514/SPR-305-WHT-U/specification-data-sheet.html

[162] A. S. M. K. Hasan, D. Chowdhury, and M. Z. R. Khan, "Performance Analysis of a Scalable DC Microgrid Offering Solar Power Based Energy Access and Efficient Control for Domestic Loads," in *International Conference on Developments in Renewable Energy Technology (ICDRET)*, 2018, pp. 1–5.

[163] J. Jiang and C. Zhang, *Fundamentals and applications of lithium-ion batteries in electric drive vehicles*. Singapore: Wiley, 2015.

[164] "Tesla." [Online]. Available: https://www.tesla.com/en_CA/

[165] N. Kondrath, "Bidirectional DC-DC converter topologies and control strategies for interfacing energy storage systems in microgrids: An overview," in *2017 IEEE International Conference on Smart Energy Grid Engineering (SEGE)*. IEEE, Aug. 2017, pp. 341–345.

[166] F. Blaabjerg, R. Teodorescu, M. Liserre, and A. Timbus, "Overview of Control and Grid Synchronization for Distributed Power Generation Systems," *IEEE Transactions on Industrial Electronics*, vol. 53, no. 5, pp. 1398–1409, Oct. 2006.

[167] H. Douglas, P. Weston, D. Kirkwood, S. Hillmansen, and C. Roberts, "Method for validating the train motion equations used for passenger rail vehicle simula-

tion," *Proceedings of the Institution of Mechanical Engineers, Part F: Journal of Rail and Rapid Transit*, vol. 231, no. 4, pp. 455–469, Apr. 2017.

[168] Z. Tian, P. Weston, N. Zhao, S. Hillmansen, C. Roberts, and L. Chen, "System energy optimisation strategies for metros with regeneration," *Transportation Research Part C: Emerging Technologies*, vol. 75, pp. 120–135, Dec. 2017.

[169] "Weather - meteoblue." [Online]. Available: https://www.meteoblue.com/

[170] Ministry of Transportation, "All-Day, Two-Way GO Train Service Coming to Communities Across GTHA," 2018. [Online]. Available: https://news.ontario.ca/mto/en/2018/03/all-day-two-way-go-train-service-coming-to-communities-across-gtha.html

[171] "Traction Power System Modeling and Simulations of the Metrolinx Airport Rail Link, Lakeshore Lines and Kitchener Line Electrification Systems," LTK Engineering Services, Ambler, Tech. Rep., 2012. [Online]. Available: http://www.gotransit.com/electrification/en/docs/TractionPowerSimulationsReport-Final-12-28-12.pdf

[172] R. G. Sargent, "Verification and validation of simulation models," *Journal of Simulation*, vol. 7, no. 1, pp. 12–24, Dec. 2013.

[173] M. R. Basir Khan, R. Jidin, and J. Pasupuleti, "Multi-agent based distributed control architecture for microgrid energy management and optimization," *Energy Conversion and Management*, vol. 112, pp. 288–307, Mar. 2016.

[174] T. Lv and Q. Ai, "Interactive energy management of networked microgrids-based active distribution system considering large-scale integration of renewable energy resources," *Applied Energy*, vol. 163, pp. 408–422, Dec. 2016.

[175] T. Lu, Z. Wang, Q. Ai, and W. J. Lee, "Interactive Model for Energy Management of Clustered Microgrids," *IEEE Transactions on Industry Applications*, vol. 53, no. 3, pp. 1739–1750, May 2017.

[176] NeTIRail, "Power supply technologies and practices of low and high-density railways, identifying learning points and future opportunities," NeTIRail-INFRA, Tech. Rep., 2015. [Online]. Available: http://netirail.eu/IMG/pdf/netirail-wp3-d3_1-pu-v1_0-final_public.pdf

[177] "Toronto Transit Subway System - Railway Technology." [Online]. Available: http://www.railway-technology.com/projects/toronto-transit/

[178] S. Davis, "Waterloo region light rail transit – Overview and design challenge," in *Resilient Infrastructure*, London, 2016. [Online]. Available: http://ir.lib.uwo.ca/cgi/viewcontent.cgi?article=1266&context=csce2016

[179] "Vancouver SkyTrain—A Proven Success Story Segregated Elevated Guideway," Tech. Rep., 1998. [Online]. Available: http://www.ejrcf.or.jp/jrtr/jrtr16/pdf/f44_vancouver.pdf

[180] "La distribution électrique." [Online]. Available: http://www.logiquefloue.ca/metro/articles/distribution-electrique/

[181] "Confederation Line Background," Rideau Transit Group, Ottawa, Tech. Rep., 2013. [Online]. Available: http://www.ligneconfederationline.ca/wp-content/uploads/2013/12/confederation-line-background_eng.pdf

[182] T. Pedwell, "Via Rail's $4B plan for Quebec-Ontario route opts for 'frequency' over speed," 2016. [Online]. Available: http://www.cbc.ca/news/canada/montreal/via-rail-quebec-ontario-1.3537019

[183] M. Iordache, "Optimal Strategy to Innovate and Reduce Energy Consumption in Urban Rail Systems," Seven Framework Programme, Tech. Rep., 2013.

[184] S. Nasr, M. Iordache, and M. Petit, "Smart micro-grid integration in DC railway systems," in *IEEE PES Innovative Smart Grid Technologies Conference Europe*, Istanbul, 2015, pp. 1–6.

Appendix A

Further Reading on Railway Infrastructures

Railway infrastructures are classified under two types of transport: passenger and freight [4]. Figure A.1 depicts the classification of the numerous modes employed by railway infrastructures [4]. Passenger railway infrastructures consist of smaller sets of rolling stock, compared to freight systems, and are used to transport people for work and/or leisure purposes.

In railway electrification, electric power is supplied to the railway without the need for a local fuel supply. An electrified railway network does not emit any GHG emissions or pollutants from the rolling stock. It is important to realize that GHG emissions may be present at the source of electric generation, however the source is typically far away from the railway infrastructure and population.

An electrified railway infrastructure is either a DC or AC electric system. DC systems are typically used in urban areas, where the railway network may be completely or partially underground. DC voltages will typically be 600, 750, 1,500 or 3,000 V DC. AC systems are typically used for railway networks that travel larger distances and do not pass through tunnels. Today, a 25 kV, 50/60 Hz AC system is commonly used (frequency depends on local electric power system). The contact system used for DC power systems is typically a power rail (i.e. 3rd rail, 4th rail). AC systems use overhead wires, otherwise known as catenary overhead system, and can be used for some DC systems operating at higher voltages (i.e. 1500 – 3000 V DC) [12].

Within Canada, numerous electrified railway infrastructures exist using different railway electrification systems. Table A.2 provides a list of cities with electrified

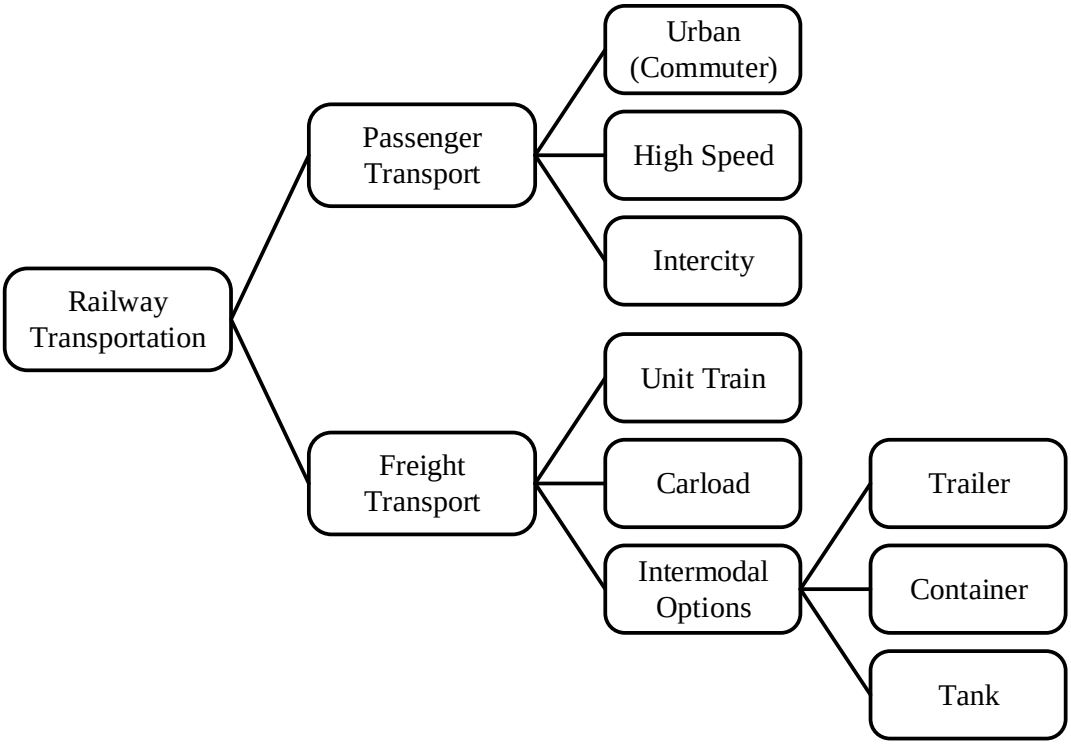

Figure A.1: Classification of railway transportation modes

Table A.1: Characteristics of passenger railway infrastructures

Type	Key Characteristics
Urban	— Transport high volume of passengers quickly around a city
	— Large number of stations with short interstation distance
	— Low rolling stock speed (10-45 km h^{-1})
	— Rolling stock required to stop at all stations
	— Passengers typically stand during peak times
	— Dedicated railway track for frequent service
	— Typically, 600-1,500 V DC electric systems
High Speed	— Transport a large number of people between major transit hubs
	— Special infrastructure for high speed travel (>200 km h^{-1})
	— Few stations along the specified route
	— Considerable interstation distance
	— Larger passenger capacity (comfort is prioritized)
	— Typically, 25 kV AC, 50/60 Hz electric systems
Intercity	— Classified as a network or line type
	— Mixed traffic lines, running passenger and freight services
	— Rolling stock speed lower than high speed rail
	— Considerable interstation distance
	— Many stations but not all served regularly (customized schedule)
	— Typically, 1,500-3,000 V DC or 25 kV, 50/60 Hz electric systems

Table A.2: Electrified railway infrastructures in Canada

City	System Name	Voltage	Contact
Toronto	Toronto Transit Commission Streetcars	600 V DC	Overhead
	Toronto Transit Commission Subway	600V DC	3^{rd} rail
Calgary	Calgary Transit C-Train	600 V DC	Overhead
Edmonton	Edmonton Transit Light Rail Train	600 V DC	Overhead
Vancouver	Expo & Millenium lines	650 V DC	Power Rail
	Canada line	750 V DC	3^{rd} rail
Waterloo	Ion Rapid Transit (in progress)	750 V DC	Overhead
Montreal	Metro de Montreal	750 V DC	4^{th} rail
	Deux-Montagnes Lines	25 kV, 60 Hz	Overhead
Ottawa	Confederation Line (in progress)	1,500 V DC	Overhead

railway infrastructures, either already existing or in the process of being implemented [176–181]. Most of the railway infrastructures in Canada operate on DC systems, except the Deux-Montagnes lines in Montreal, which use an AC power system. While originally built with a DC system, the lines were refurbished in the early 1990's to the 25 kV, 60 Hz AC system primarily used for commuter rolling stock.

Other existing railway infrastructures have also considered adopting electrification due to concerns over GHGs and waning availability of fossil fuels. Studies have been performed to consider electrification of the GO Train network in the Greater Toronto Area [6, 147, 170] and a portion of the Windsor-Quebec City corridor operated by VIA Rail [182].

The rolling stock requires energy to meet six basic operations [11]:

— Acceleration

— Traction

— Overcoming longitudinal gradients (i.e. climbing a hill)

— Lighting

— Control and communication systems

— Heating, ventilation and air conditioning (HVAC)

The traction energy (energy required to move the rolling stock) accounts for 60-80% of a rolling stock's energy consumption [5]. The remainder of the consumption is primarily used by the auxiliary services of the rolling stock (e.g. communication and signalling systems, lighting, and HVAC). The auxiliary consumption will vary

based on the rolling stock features, the local climate, and time of year. Figure A.2 provides an illustrative description of the flow of energy in a railway infrastructure and potential losses in energy [11].

Figure A.3 depicts a simplified profile of the velocity, acceleration and traction power of a single rolling stock moving between two stations [183]. In any given day, multiple rolling stock will be moving based on passenger demand, headway, and route topology.

Figure A.4 presents a simplified schedule of rolling stock participating in short drive cycles [183]. When multiple rolling stock are scheduled to operate in a day, the demand on the traction power substation (TPS) fluctuates frequently.

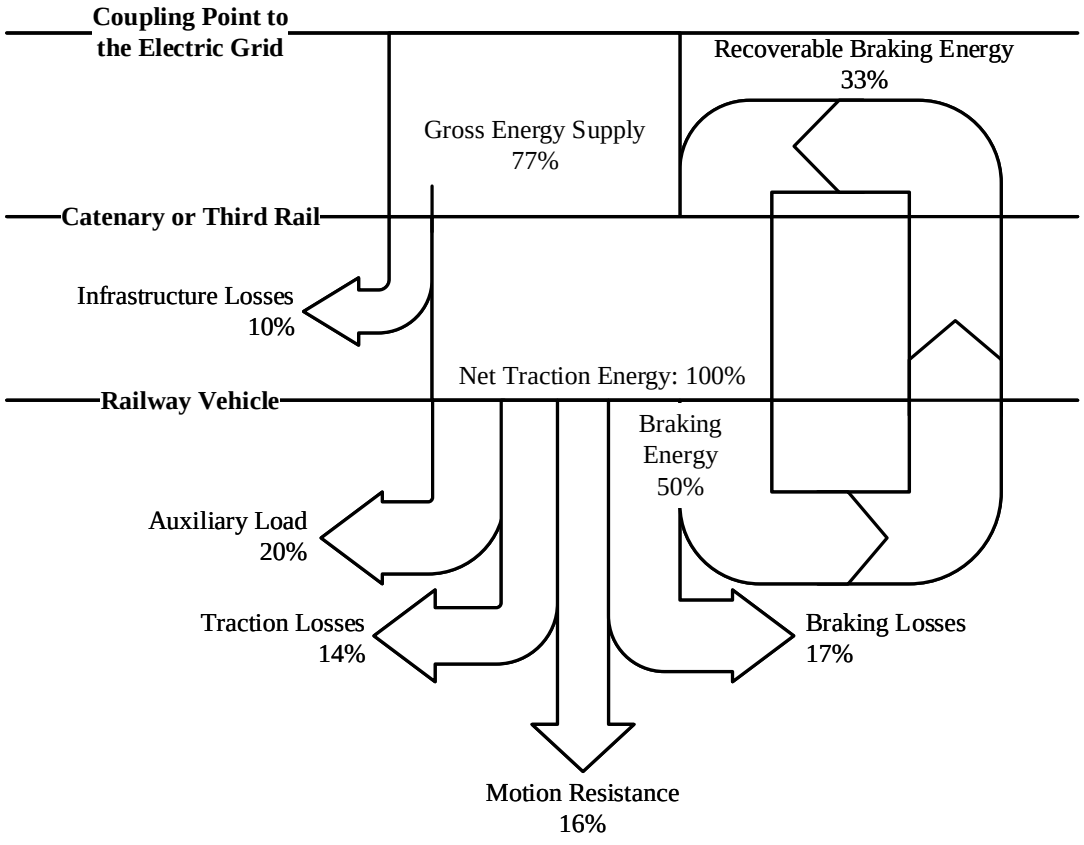

Figure A.2: Typical flow of energy within a passenger railway infrastructure

Figure A.5a shows a simplified TPS power profile considering the previous two figures [183]. The majority of railway electrification systems today feature unidirectional TPS. As such, energy recovered from regenerative braking cannot be exported to the electric grid. With the advent of new technologies and methods to reduce energy consumption of the rolling stock, regenerative braking is becoming an at-

tractive feature. The negative aspect of the power profile in Figure A.5b depicts a rolling stock recovering energy to be used for various purposes, which was typically dissipated in the past on resistor banks. Advances in bidirectional functionality in a TPS make this a possibility in the near future [13, 156].

One of the main energy concerns with an electrified railway infrastructure is the amount of energy lost due to braking. Unlike an AC electrification system, the TPS for a DC electrification system consists of a diode rectifier, which does not permit the energy recovered from braking to be exported to the electric grid [11, 184]. However, combining advances in regenerative braking technologies, the advent of the "smart grid" and advances in bidirectional TPSs, the railway operator has many options for reuse of the recovered energy, instead of just dissipating the energy on resistor banks.

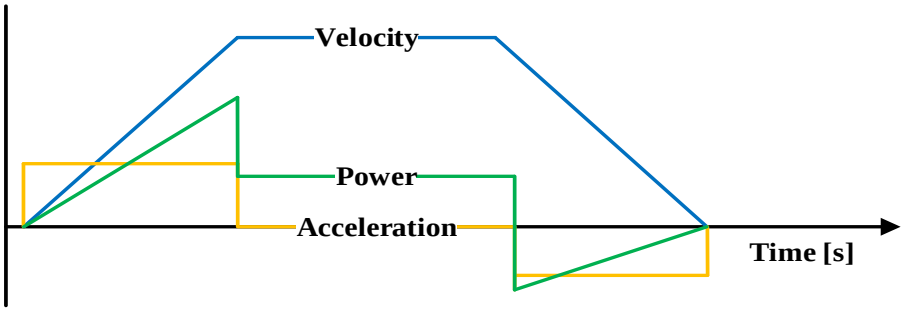

Figure A.3: Velocity, acceleration and power profile of single rolling stock

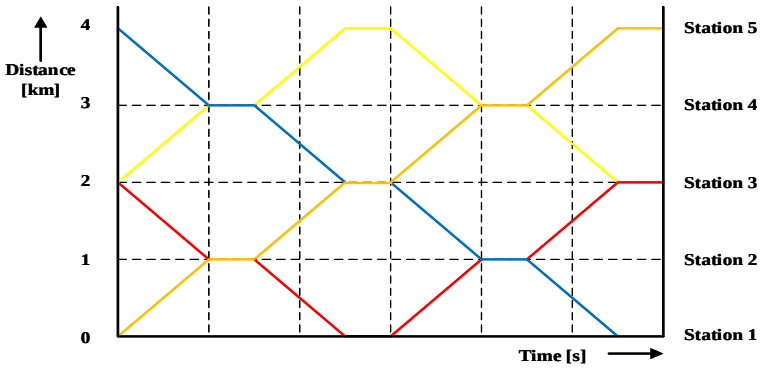

Figure A.4: Simplified schedule of multiple rolling stock

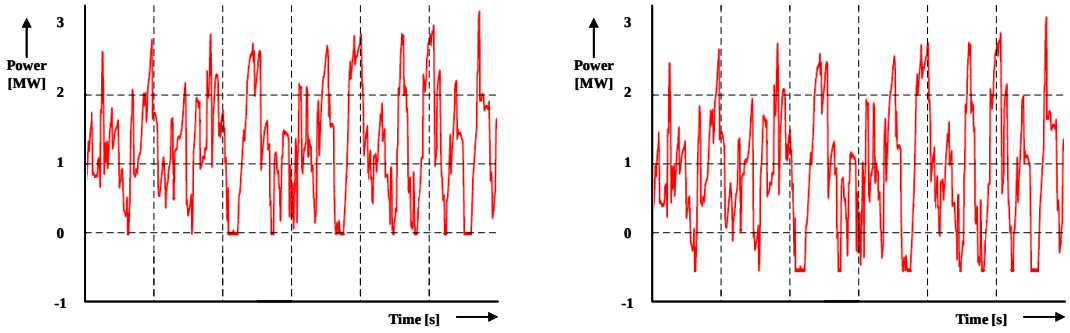

(a) Unidirectional power flow **(b)** Bidirectional power flow

Figure A.5: Sample traction substation power profile of an electrified railway system (a) today, which can only handle unidirectional power flow from the electric grid to the railway infrastructure and (b) in the future, where bidirectional power capabilities are deployed [183]

It is estimated that 1/3 of energy lost during braking can be recovered [5, 11]. The kinetic energy of the rolling stock is converted into electrical energy, which can be used for various purposes. If no regenerative options are available the energy would need to be dissipated, but this is wasteful and does not increase the energy efficiency of the railway infrastructure [5,184]. Employing regenerative braking techniques has numerous advantages for the rail and electric grid operators. By taking advantage of regenerative braking, the dependence on the electric grid is reduced, and a higher energy consumption efficiency for the rail operator, which leads to reduced operating costs [83]. Recuperating the maximum amount of energy typically lost by braking is ideal in high volume networks with frequent stops, such as an urban railway infrastructure [83]. The recovered energy of the deaccelerating rolling stock can be [5, 83, 184]:

1. Used to supply a rolling stock accelerating nearby
   - — Reduce cost of buying electrificty from electric grid (e.g. energy and demand charges)
   - — Difficulty with schedule optimization
2. Stored in on-board energy storage system (ESS) (depends on the configuration of the rolling stock)
   - — Energy available immediately
   - — Increased weight of rolling stock
   - — Reduced energy losses

- — Increased cost of rolling stock
- — Decrease in passenger capacity

3. Stored in wayside ESS
   - — ESS can be sized larger compared to on-board ESS
   - — Transmission losses between rolling stock and ESS
   - — Flexibility during emergency events
   - — Requires central controller
   - — ESS can be located throughout railway infrastructure
   - — Requires bidirectional equipment on rolling stock
4. Used to serve the auxiliary demand of the rolling stock
5. Sold to the electric grid via the closest TPS
   - — Sell electricity to electric grid to recover costs of buying electricity from the electric grid
   - — Transmission losses
   - — Higher capital investment in bidirectional technology
   - — TPS needs to be outfitted with bidirectional technology
   - — Over-sizing of equipment to handle sudden peaks of energy

Appendix B

Matlab Code - Sizing Analysis

The following code is used for the IMG sizing, as described in Section 3.4. It is implemented as an m.file in MATLAB.

```
function [] = SizingSweep()
%% PV Parameters
eta_PV = 0.187; %From data sheet
A_PV = 538;     %Dimensions from data sheet
PV_unit = 0.1;

%% WT Parameters
WT_unit = 1.5;
WindSpeed_CutIn = 3.5;  %From data sheet
WindSpeed_Rated = 11;   %From data sheet
WindSpeed_CutOut = 25;  %From data sheet
A_WT = 4657;            %From data sheet
rho_Air = 1.2;          %Constant

c1 = 0.5176; c2 = 116; c3 = 0.4; c4 = 5; c5 = 21; c6 =
    0.0068;  %From literature
lambda = 8.1; beta = 0; %From literature
lambda_i = ((1/(lambda + 0.08*beta)) - (0.035 / (beta^3 + 1)
    ))^-1;
Cp = c1 * (c2/lambda_i - c3*beta - c4) * exp(-1*c5/lambda_i)
     + c6*lambda;

P_Rated = (0.5 * rho_Air * Cp * A_WT * WindSpeed_Rated^3) /
    1e6;

%% ESS Parameters
P_chg_limit = -0.1;
P_dsch_limit = 0.1;
Batt_SOC_Max = 0.9; %From literature
Batt_SOC_Min = 0.2; %From literature
ESSCap = 200;       %From data sheet
```

```
ESSVolt = 480;          %From data sheet

%% Main Program
while 1
    %Select input data
    num = -1;
    while (num < 0 || num > 4)
        disp('Determine case study (1 = London/Birmingham; 2
            = Birmingham/Stratford; 3 = Lakeshore; 4 = UP
            Express; 0 = End Program');
        num = input('Select a case study: ');
    end

    %Select case used for quick execution of thesis case
       studies
    switch num
        case 0
            break;
        case 1
            load LondonBirminghamData.txt
            Time = LondonBirminghamData(:,1);
            Irradiance = LondonBirminghamData(:,2);
            WindSpeed = LondonBirminghamData(:,3);
            P_Load_IMG1 = LondonBirminghamData(:,4);
            P_Load_IMG2 = LondonBirminghamData(:,5);
            TimeScale = 50;
            ESSflag = true;
            PVSize_IMG1 = linspace (0,22.5,16)';
            WTSize_IMG1 = [22.5; 21; 19.5; 18; 16.5; 15;
               13.5; 12; 10.5; 9; 7.5; 6; 4.5; 3; 1.5; 0];
            PVSize_IMG2 = linspace (0,18,13)';
            WTSize_IMG2 = [18; 16.5; 15; 13.5; 12; 10.5;
               9;9;9;9; 7.5; 6; 4.5; 3; 1.5; 0];
        case 2
            load BirminghamStratfordData.txt
            Time = BirminghamStratfordData(:,1);
            Irradiance = BirminghamStratfordData(:,2);
            WindSpeed = BirminghamStratfordData(:,3);
            P_Load_IMG1 = BirminghamStratfordData(:,4);
            P_Load_IMG2 = BirminghamStratfordData(:,5);
            TimeScale = 50;
            ESSflag = false;
            PVSize_IMG1 = linspace (0,2.1,22)';
            WTSize_IMG1 = 1.5*ones(size(PVSize_IMG1));
            WTSize_IMG1(1) = 3; WTSize_IMG1(22) = 0;
            PVSize_IMG2 = linspace (0,2.1,22)';
            WTSize_IMG2 = 1.5*ones(size(PVSize_IMG2));
            WTSize_IMG2(1) = 3; WTSize_IMG2(22) = 0;
```

```
    case 3
        load LakeshoreData.txt
        Time = LakeshoreData(:,1);
        Irradiance = LakeshoreData(:,2);
        WindSpeed = LakeshoreData(:,3);
        P_Load_IMG1 = LakeshoreData(:,4);
        P_Load_IMG2 = LakeshoreData(:,5);
        TimeScale = 50;
        ESSflag = true;
        PVSize_IMG1 = [6; 4.5; 3; 3; 1.5; 0];
        WTSize_IMG1 = [0; 1.5; 3; 3; 4.5; 6];
        PVSize_IMG2 = linspace (7.5,0, 6)';
        WTSize_IMG2 = linspace (0,7.5, 6)';
    case 4
        load UPExpressData.txt
        Time = UPExpressData(:,1);
        Irradiance = UPExpressData(:,2);
        WindSpeed = UPExpressData(:,3);
        P_Load_IMG1 = UPExpressData(:,4);
        P_Load_IMG2 = UPExpressData(:,5);
        TimeScale = 25;
        ESSflag = false;
        PVSize_IMG1 = linspace (0,2.8,29)';
        WTSize_IMG1 = 1.5*ones(size(PVSize_IMG1));
        WTSize_IMG1(1) = 3; WTSize_IMG1(29) = 0;
        PVSize_IMG2 = linspace (0,2.8,29)';
        WTSize_IMG2 = 1.5*ones(size(PVSize_IMG2));
        WTSize_IMG2(1) = 3; WTSize_IMG2(29) = 0;
End

% Initialize number of ESS variables based on number of
    iterations
NumESS_IMG1 = zeros(size(PVSize_IMG1));
NumESS_IMG2 = zeros(size(PVSize_IMG2));

% Initialize KPIs for each sizing iteration
GridDependenceKPI_IMG1 = zeros(size(PVSize_IMG1));
    GridDependenceKPI_IMG2 = zeros(size(PVSize_IMG2));
DiversityOfSupplyKPI_IMG1 = zeros(size(PVSize_IMG1));
    DiversityOfSupplyKPI_IMG2 = zeros(size(PVSize_IMG2));
IMGRelianceKPI_IMG1 = zeros(size(PVSize_IMG1));
    IMGRelianceKPI_IMG2 = zeros(size(PVSize_IMG2));
RenewableGenKPI_IMG1 = zeros(size(PVSize_IMG1));
    RenewableGenKPI_IMG2 = zeros(size(PVSize_IMG2));

for k = 1:length(PVSize_IMG1)
    %Calculate diversity of supply IMG1
    IMGCap = PVSize_IMG1(k) + WTSize_IMG1(k);
```

```
PV_pu = PVSize_IMG1(k) / IMGCap; WT_pu = WTSize_IMG1
    (k) / IMGCap;
DiversityOfSupplyKPI_IMG1(k) = -1 * (PV_pu*log(PV_pu
    ) + WT_pu*log(WT_pu));

%Calculate diversity of supply IMG2
IMGCap = PVSize_IMG2(k) + WTSize_IMG2(k);
PV_pu = PVSize_IMG2(k) / IMGCap; WT_pu = WTSize_IMG2
    (k) / IMGCap;
DiversityOfSupplyKPI_IMG2(k) = -1 * (PV_pu*log(PV_pu
    ) + WT_pu*log(WT_pu));

%Initialize unit size based on nominal capacity
NumPV_IMG1 = PVSize_IMG1(k)/PV_unit;
NumWT_IMG1 = WTSize_IMG1(k)/WT_unit;
NumPV_IMG2 = PVSize_IMG2(k)/PV_unit;
NumWT_IMG2 = WTSize_IMG2(k)/WT_unit;

%Determine number of ESS in each IMG (case study
    dependent)
if(ESSflag == true)
     NumESS_IMG1(k) = PVSize_IMG1(k)/1.5 * 3;
     NumESS_IMG2(k) = PVSize_IMG2(k)/1.5 * 3;
elseif(ESSflag == false)
     if(PVSize_IMG1(k) == 0)
          NumESS_IMG1(k) = 0 ; NumESS_IMG1 =
              NumESS_IMG1(k);
     elseif(PVSize_IMG1(k) > 0 && PVSize_IMG1(k) <=
         1.5)
          NumESS_IMG1(k) = 3; NumESS_IMG1 =
              NumESS_IMG1(k);
     else
          NumESS_IMG1(k) = 6; NumESS_IMG1 =
              NumESS_IMG1(k);
     end

     if(PVSize_IMG2(k) == 0)
          NumESS_IMG2(k) = 0 ; NumESS_IMG2 =
              NumESS_IMG2(k);
     elseif(PVSize_IMG2(k) > 0 && PVSize_IMG2(k) <=
         1.5)
          NumESS_IMG2(k) = 3; NumESS_IMG2 =
              NumESS_IMG2(k);
     else
          NumESS_IMG2(k) = 6; NumESS_IMG2 =
              NumESS_IMG2(k);
     end
end
```

```
%Initialize ESS SOC to 70% for number of ESS in each
    IMG
SOC_MG1 = 0.7*ones(NumESS_IMG1(k),1); SOC_MG2 = 0.7*
    ones(NumESS_IMG2(k),1);

%Reset dependence to 0
Delta_MG1 = 0; Delta_MG2 = 0;
Delta_IMG_MG1 = 0; Delta_IMG_MG2 = 0;
SumRenEnergy_IMG1 = 0; SumRenEnergy_IMG2 = 0;
SumSysEnergy_IMG1 = 0; SumSysEnergy_IMG2 = 0;
P_Grid_MG1 = 0; P_Grid_MG2 = 0; P_IMG_MG1 = 0;
   P_IMG_MG2 = 0;

for j = 1:length(Time)
    P_Batt_MG1 = 0;
    P_Batt_MG2 = 0;

    %Calculate power generated by PV (MW)
    %Simplified equation used in literature for PV
       sizing problems
    %Limitation: does not account for varying
       temperature
    P_PV_MG1 = NumPV_IMG1 * ((eta_PV * A_PV *
       Irradiance(j)) / 1e6);
    P_PV_MG2 = NumPV_IMG2 * ((eta_PV * A_PV *
       Irradiance(j)) / 1e6);

    %Calculate power generated by WT (MW)
    %Simplified equation used in literature for WT
       sizing problems
    %Limitation: does not account for conversion
       losses, or
    %features of generator
    if (WindSpeed(j) < WindSpeed_CutIn || WindSpeed(
       j) > WindSpeed_CutOut)
        P_WT_MG1 = 0;
        P_WT_MG2 = 0;
    elseif(WindSpeed(j) >= WindSpeed_CutIn &&
       WindSpeed(j) < WindSpeed_Rated)
        P_WT_MG1 = NumWT_IMG1 * P_Rated * (WindSpeed
           (j)^3 - WindSpeed_CutIn^3)/(
           WindSpeed_Rated^3 - WindSpeed_CutIn^3);
        P_WT_MG2 = NumWT_IMG2 * P_Rated * (WindSpeed
           (j)^3 - WindSpeed_CutIn^3)/(
           WindSpeed_Rated^3 - WindSpeed_CutIn^3);
    else
        P_WT_MG1 = NumWT_IMG1 * P_Rated;
```

```
    P_WT_MG2 = NumWT_IMG2 * P_Rated;
end

%Determine battery power requirements for IMG1
%If load is greater than 0, and cannot be
   satisfied by DERS,
%discharge battery
%Simplified equations used in literature for ESS
    sizing
%problems
%Limitation: does not account for intricacies of
    ESS technology
if(P_Load_IMG1(j) > 0 && P_Load_IMG1(j) > (
   P_WT_MG1 + P_PV_MG1))
    for i = 1:NumESS_IMG1
        Batt_SOC = SOC_MG1(i);
        if(Batt_SOC > Batt_SOC_Min)
            P_Batt = (P_Load_IMG1(j) - P_PV_MG1
               - P_WT_MG1)/NumESS_IMG1;

            if(P_Batt > P_dsch_limit)
                P_Batt = P_dsch_limit;
            end

            if(j > 1)
                SOC_MG1(i) = Batt_SOC + ((P_Batt
                    * (Time(j) - Time(j-1)))/(
                   ESSCap * ESSVolt));
            else
                SOC_MG1(i) = Batt_SOC + ((P_Batt
                    * (Time(j) - 0))/(ESSCap *
                   ESSVolt));
            end
        else
            P_Batt = 0;
        end
        P_Batt_MG1 = P_Batt_MG1 + P_Batt;
    end

    %Else if load is less than 0 charge the
       battery
elseif(P_Load_IMG1(j) < 0)
    for i = 1:NumESS_IMG1
        Batt_SOC = SOC_MG1(i);
        if(Batt_SOC < Batt_SOC_Max)
            P_Batt = P_Load_IMG1(j)/NumESS_IMG1;

            if(P_Batt < P_chg_limit)
```

```
                P_Batt = P_chg_limit;
            end

            if(j > 1)
                SOC_MG1(i) = Batt_SOC + ((P_Batt
                    * (Time(j) - Time(j-1)))/(
                    ESSCap * ESSVolt));
            else
                SOC_MG1(i) = Batt_SOC + ((P_Batt
                    * (Time(j) - 0))/(ESSCap *
                    ESSVolt));
            end
        else
            P_Batt = 0;
        end
        P_Batt_MG1 = P_Batt_MG1 + P_Batt;
    end
end

%Determine battery power requirements for IMG2
%If load is greater than 0, and cannot be
    satisfied by DERS,
%discharge battery
if(P_Load_IMG2(j) > 0 && P_Load_IMG2(j) > (
   P_WT_MG2 + P_PV_MG2))
    for i = 1:NumESS_IMG2
        Batt_SOC = SOC_MG2(i);
        if(Batt_SOC > Batt_SOC_Min)
            P_Batt = (P_Load_IMG2(j) - P_PV_MG2
               - P_WT_MG2)/NumESS_IMG2;
            if(P_Batt > P_dsch_limit)
                P_Batt = P_dsch_limit;
            end

            if(j > 1)
                SOC_MG2(i) = Batt_SOC + ((P_Batt
                    * (Time(j) - Time(j-1)))/(
                    ESSCap * ESSVolt));
            else
                SOC_MG2(i) = Batt_SOC + ((P_Batt
                    * (Time(j) - 0))/(ESSCap *
                    ESSVolt));
            end
        else
            P_Batt = 0;
        end
        P_Batt_MG2 = P_Batt_MG2 + P_Batt;
    end
```

```
elseif(P_Load_IMG2(j) < 0)
    for i = 1:NumESS_IMG2
        Batt_SOC = SOC_MG2(i);
        if(Batt_SOC < Batt_SOC_Max)
            P_Batt = P_Load_IMG2(j)/NumESS_IMG2;

            if(P_Batt < P_chg_limit)
                P_Batt = P_chg_limit;
            end

            if(j > 1)
                SOC_MG2(i) = Batt_SOC + ((P_Batt
                    * (Time(j) - Time(j-1)))/(
                    ESSCap * ESSVolt));
            else
                SOC_MG2(i) = Batt_SOC + ((P_Batt
                    * (Time(j) - 0))/(ESSCap *
                    ESSVolt));
            end
        else
            P_Batt = 0;
        end
        P_Batt_MG2 = P_Batt_MG2 + P_Batt;
    end
end

%Determine if IMG requires support
%Calculate if energy transferred from MG2 to MG1
    required
if(P_Load_IMG1(j) > (P_PV_MG1 + P_WT_MG1 +
   P_Batt_MG1) && P_Load_IMG2(j) < (P_PV_MG2 +
   P_WT_MG2))
    P_IMG_MG1 = (P_PV_MG2 + P_WT_MG2 -
        P_Load_IMG2(j));
    Delta_IMG_MG1 = Delta_IMG_MG1 + (Time(j) -
        Time(j-1));
    %Calculate if energy transferred from MG1 to
        MG2 required
elseif(P_Load_IMG2(j) > (P_PV_MG2 + P_WT_MG2 +
   P_Batt_MG2) && P_Load_IMG1(j) < (P_PV_MG1 +
   P_WT_MG1))
    P_IMG_MG2 = (P_PV_MG1 + P_WT_MG1 -
        P_Load_IMG1);
    Delta_IMG_MG2 = Delta_IMG_MG2 + (Time(j) -
        Time(j-1));
else
    P_IMG_MG1 = 0;
    P_IMG_MG2 = 0;
```

```
end

%Calculate if the electric grid is required for
    IMG1 for the timestep
if(j > 1)
    if((P_Load_IMG1(j) - P_PV_MG1 - P_WT_MG1 -
        P_Batt_MG1 - P_IMG_MG1)> 0)
        P_Grid_MG1 = P_Load_IMG1(j) - P_PV_MG1 -
            P_WT_MG1 - P_Batt_MG1 - P_IMG_MG1;
        Delta_MG1 = Delta_MG1 + (Time(j) - Time(
            j-1));
    elseif(P_Load_IMG1(j) < 0 && (P_Load_IMG1(j)
        < P_Batt_MG1))% && (abs(P_Load_MG1(j) -
        P_Batt_MG1 > 0.00001)))
        Delta_MG1 = Delta_MG1 + (Time(j) - Time(
            j-1));
    end
end

%Calculate if the electric grid is required for
    IMG2 for the timestep
if(j > 1)
    if((P_Load_IMG2(j) - P_PV_MG2 - P_WT_MG2 -
        P_Batt_MG2 - P_IMG_MG2)> 0)
        P_Grid_MG2 = P_Load_IMG2(j) - P_PV_MG2 -
            P_WT_MG2 - P_Batt_MG2 - P_IMG_MG2;
        Delta_MG2 = Delta_MG2 + (Time(j) - Time(
            j-1));
    elseif(P_Load_IMG2(j) < 0 && (P_Load_IMG2(j)
        < P_Batt_MG2))% && (abs(P_Load_MG2(j) -
        P_Batt_MG2 > 0.00001)))
        Delta_MG2 = Delta_MG2 + (Time(j) - Time(
            j-1));
    end
end

%Compute the renewable energy generation and
    total system generation
%for IMG1 for the timestep
if(P_Load_IMG1(j) > 0 && j > 1)
    SumRenEnergy_IMG1 = SumRenEnergy_IMG1 + (
        P_PV_MG1 + P_WT_MG1) * (Time(j) - Time(j
        -1));
    SumSysEnergy_IMG1 = SumSysEnergy_IMG1 + (
        P_PV_MG1 + P_WT_MG1 + P_Batt_MG1 +
        P_IMG_MG1 + P_Grid_MG1) * (Time(j) - Time
        (j-1));
end
```

```
            %Compute the renewable energy generation and
                total system generation
            %for IMG2 for the timestep
            if(P_Load_IMG2(j) > 0 && j > 1)
                SumRenEnergy_IMG2 = SumRenEnergy_IMG2 + (
                    P_PV_MG2 + P_WT_MG2) * (Time(j) - Time(j
                    -1));
                SumSysEnergy_IMG2 = SumSysEnergy_IMG2 + (
                    P_PV_MG2 + P_WT_MG2 + P_Batt_MG2 +
                    P_IMG_MG2 + P_Grid_MG2) * (Time(j) - Time
                    (j-1));
            end

        end

        %Calculate Electric Grid Dependence KPI for each IMG
        GridDependenceKPI_IMG1(k) = Delta_MG1/TimeScale*100;
        GridDependenceKPI_IMG2(k) = Delta_MG2/TimeScale*100;

        %Calculate IMG Reliance KPI for each IMG
        IMGRelianceKPI_IMG1(k) = Delta_IMG_MG1/TimeScale
            *100;
        IMGRelianceKPI_IMG2(k) = Delta_IMG_MG2/TimeScale
            *100;

        %Calculate IMG Renewable Generation KPI for each IMG
        RenewableGenKPI_IMG1(k) = (SumRenEnergy_IMG1 /
            SumSysEnergy_IMG1) * 100;
        RenewableGenKPI_IMG2(k) = (SumRenEnergy_IMG2 /
            SumSysEnergy_IMG2(1)) * 100;
    end

    %Output results for each IMG to Excel file
    writetable(table(PVSize_IMG1, WTSize_IMG1, NumESS_IMG1,
        DiversityOfSupplyKPI_IMG1, GridDependenceKPI_IMG1,
        IMGRelianceKPI_IMG1, RenewableGenKPI_IMG1),'MG1.xlsx'
        );
    writetable(table(PVSize_IMG2, WTSize_IMG2, NumESS_IMG2,
        DiversityOfSupplyKPI_IMG2, GridDependenceKPI_IMG2,
        IMGRelianceKPI_IMG2, RenewableGenKPI_IMG2),'MG2.xlsx'
        );
end
end
```

Appendix C

Simulink Code for Resilient Interconnected Microgrid Model

The following codes are implemented in the IMG model, presented in Chapter 6.

C.1 Solar PV MPPT Algorithm

The following code is used for the solar photovoltaic MPPT, as described in Section 6.2.2.

```
function D = PandO(Param, Enabled, V, I)
% MPPT controller based on the Perturb & Observe algorithm

% D output = Duty cycle of the boost converter
% (value between 0 & 1)
% Enabled input = 1 to enable the MPPT controller
% V input = PV array terminal voltage (V)
% I input = PV array current (A)

% Param input:
Dinit = Param(1);  %Initial value for D output (0.5)
Dmax = Param(2);   %Maximum value for D (0.52)
Dmin = Param(3);   %Minimum value for D (0.42)
deltaD = Param(4); %Increment value used to increase/
    decrease
% the duty cycle D (increasing D = decreasing Vref)  (3e-4)

persistent Vold Pold Dold;

dataType = 'double';

if isempty(Vold)
    Vold=0;
    Pold=0;
```

```
    Dold=Dinit;
end
P= V*I;
dV= V - Vold;
dP= P - Pold;

if dP ~= 0 & Enabled ~=0
    if dP < 0
        if dV < 0
            D = Dold - deltaD;
        else
            D = Dold + deltaD;
        end
    else
        if dV < 0
            D = Dold + deltaD;
        else
            D = Dold - deltaD;
        end
    end
else D=Dold;
end

if D >= Dmax | D<= Dmin
    D=Dold;
end

Dold=D;
Vold=V;
Pold=P;
```

C.2 Microgrid Regulation System

The following code is used for the microgrid regulation system for each interconnected microgrid, as described in Section 5.2.4 and Section 6.2.6.

```
function [WT_Ref_MG2,PV_Ref_MG2,Batt_Ref_MG2,
    switch_DC2Train_MG2,switch_AC2Grid_MG2,
    switch_Grid2Train_MG2,switch_AC2Train_MG2,
    switch_DC2Grid_MG2] = MGCC(P_AC2Grid_MG2,~,P_DC2Grid_MG2,
     ~,P_ACBus_MG2,P_DCBus_MG2,PV_Gen_MG2,WT_Gen_MG2,
    TrainDemand_MG2, Batt_SOC_MG2, WT_Export_MG2,
    PV_Export_MG2)

% System constraints of DERs and ESS
NumArray = 15;
PV_BaseExport = 20;
```

```
PV_Nameplate = 100*NumArray;
PV_Limit = (PV_Export_MG2 + PV_BaseExport)*NumArray;

NumWT = 11;
WT_BaseExport = 500;
WT_Nameplate = 1.5e3*NumWT;
WT_Limit = (WT_Export_MG2 + WT_BaseExport)*NumWT;

Batt_SOC_Min = 20;
Batt_SOC_Max = 90;
ESSNum = 3;

% Initialization of reference variables
WT_Ref_MG2 = 0;
PV_Ref_MG2 = 0;
Batt_Ref_MG2 = zeros(ESSNum, 1);
P_dis_limit = 100;
P_chg_limit = -100;
Batt_SOC = 0;
Batt_Ref = 0;

% Initialize switch variables
switch_DC2Train_MG2 = 0;
switch_AC2Grid_MG2 = 1;
switch_Grid2Train_MG2 = 0;
switch_AC2Train_MG2 = 0;
switch_DC2Grid_MG2 = 1;

if(TrainDemand_MG2 > 0)
    if((PV_Gen_MG2)<0&&(WT_Gen_MG2)<0)
        switch_DC2Train_MG2=0;
        switch_AC2Grid_MG2=1;
        switch_Grid2Train_MG2=1;
        switch_AC2Train_MG2=0;
        switch_DC2Grid_MG2=1;
    elseif((PV_Gen_MG2)>=TrainDemand_MG2 && (WT_Gen_MG2)>=0)
        switch_DC2Train_MG2=1;
        switch_AC2Grid_MG2=1;
        switch_Grid2Train_MG2=0;
        switch_AC2Train_MG2=0;
        switch_DC2Grid_MG2=1;
    elseif((PV_Gen_MG2)>=TrainDemand_MG2&&(WT_Gen_MG2)<0)
        switch_DC2Train_MG2=1;
        switch_DC2Grid_MG2=1;
        switch_AC2Grid_MG2=1;
        switch_Grid2Train_MG2=0;
        switch_AC2Train_MG2=0;
```

```
elseif((PV_Gen_MG2)>=0&&(PV_Gen_MG2)<TrainDemand_MG2&&(
    WT_Gen_MG2)>=0 && ((PV_Gen_MG2)+(WT_Gen_MG2) >
    TrainDemand_MG2))
        switch_DC2Train_MG2=1;
        switch_AC2Grid_MG2=1;
        switch_Grid2Train_MG2=0;
        switch_AC2Train_MG2=1;
        switch_DC2Grid_MG2=0;
elseif((PV_Gen_MG2)>=0&&(PV_Gen_MG2)<TrainDemand_MG2&&(
    WT_Gen_MG2>=0 && ((PV_Gen_MG2)+(WT_Gen_MG2) <
    TrainDemand_MG2)))
        switch_DC2Train_MG2=1;
        switch_AC2Grid_MG2=0;
        switch_Grid2Train_MG2=1;
        switch_AC2Train_MG2=1;
        switch_DC2Grid_MG2=0;
     elseif((PV_Gen_MG2)<0&&(WT_Gen_MG2)>=0 && (WT_Gen_MG2) <
         TrainDemand_MG2)
        switch_DC2Train_MG2=0;
        switch_AC2Grid_MG2=0;
        switch_Grid2Train_MG2=1;
        switch_AC2Train_MG2=1;
        switch_DC2Grid_MG2=1;
elseif((PV_Gen_MG2)>=0&&(PV_Gen_MG2)<TrainDemand_MG2&&(
    WT_Gen_MG2)<0)
        switch_DC2Train_MG2=1;
        switch_AC2Grid_MG2=1;
        switch_Grid2Train_MG2=1;
        switch_AC2Train_MG2=0;
        switch_DC2Grid_MG2=0;
     end

     %% Calculate ESS Setpoint
         for k = 1:ESSNum
             Batt_SOC = Batt_SOC_MG2(k);
             if(Batt_SOC > Batt_SOC_Min && (TrainDemand_MG2-
                 PV_Gen_MG2-WT_Gen_MG2 > 0))
                 Batt_Ref = (TrainDemand_MG2 - PV_Gen_MG2 -
                     WT_Gen_MG2)/ESSNum;
                 if(Batt_Ref > P_dis_limit)
                     Batt_Ref = P_dis_limit;
                 end
             elseif(Batt_Ref < Batt_SOC_Max)
                 Batt_Ref = P_chg_limit;
             else
                 Batt_Ref = 0;
             end
             Batt_Ref_MG2(k) = Batt_Ref;
```

```
        end

%% Calculate PV Setpoint
    if(PV_Gen_MG2 < PV_Nameplate && TrainDemand_MG2 >
       PV_Gen_MG2)
        PV_Ref_MG2 = 1;
    elseif(TrainDemand_MG2 < PV_Gen_MG2)
        PV_Ref_MG2 = (P_DCBus_MG2 - P_DC2Grid_MG2 + PV_Limit
           )/PV_Nameplate;
    end

%% Calculate WT Setpoint
    if(WT_Gen_MG2 < WT_Nameplate && TrainDemand_MG2 >
       WT_Gen_MG2)
        WT_Ref_MG2 = 1;
    else
        WT_Ref_MG2 = (P_ACBus_MG2 - P_AC2Grid_MG2 + WT_Limit
           )/WT_Nameplate;
    end

elseif(TrainDemand_MG2 <= 0)
    switch_AC2Grid_MG2 = 1;
    switch_AC2Train_MG2 = 0;
    switch_DC2Train_MG2 = 0;
    switch_DC2Grid_MG2 =1;

    for k = 1:ESSNum
            Batt_SOC = Batt_SOC_MG2(k);
            if(Batt_SOC < Batt_SOC_Max)
                Batt_Ref = TrainDemand_MG2/ESSNum;
                switch_DC2Train_MG2 = 1;

                if(Batt_Ref< P_chg_limit)
                    Batt_Ref = P_chg_limit;
                end

                if(TrainDemand_MG2 < P_chg_limit*ESSNum)
                    switch_Grid2Train_MG2 = 1;
                else
                    switch_Grid2Train_MG2 = 0;
                end
            else
                Batt_Ref = 0;
                switch_Grid2Train_MG2 = 1;
            end
            Batt_Ref_MG2(k) = Batt_Ref;
        end
```

```
        if(PV_Gen_MG2 < ((abs(sum(Batt_Ref_MG2)) + PV_Limit)))
            PV_Ref_MG2 = 1;
        else
            PV_Ref_MG2 = (P_DCBus_MG2 - P_DC2Grid_MG2 + PV_Limit
                )/PV_Nameplate;
        end

        if(WT_Gen_MG2 < WT_Limit)
            WT_Ref_MG2 = 1;
        else
            WT_Ref_MG2 = (P_ACBus_MG2 - P_AC2Grid_MG2 + WT_Limit
                )/WT_Nameplate;
        end

    end
end
```

C.3 Interconnected Microgrid Supervisory Controller

The following code is used for the microgrid regulation system for each interconnected microgrid, as described in Section 5.2.5 and Section 6.2.7.

```
function [SetpointMG1, SetpointMG2] = MGCC(P_DC_MG1,
    P_AC_MG1, P_Load_MG1, P_DC_MG2, P_AC_MG2, P_Load_MG2)

% Initial setpoint is base limit
SetpointMG1 = 0;
SetpointMG2 = 0;
Base = 0;

% Calculate each MG resiliency KPI
KPI_MG1 = (abs((P_DC_MG1 + P_AC_MG1) / P_Load_MG1));
KPI_MG2 = (abs((P_DC_MG2 + P_AC_MG2) / P_Load_MG2));

% Determine how to handle scenarios
% Case 1: Both have a surplus of energy. No need to support
    each other.
% Case 2: Both have a deficit of energy. Neither can support
    each other.
% Case 3: MG1 has a deficit and MG2 has a surplus.
% Case 4: MG2 has a deficit and MG1 has a surplus.

if ((KPI_MG1 >= 1) && (KPI_MG2 >= 1))
    % Both have a surplus of energy available. Allow each MG
        to export the
    % maximum limit imposed by the electric grid regulator.
```

```
    SetpointMG1 = Base;
    SetpointMG2 = Base;

elseif (KPI_MG1 < 1 && KPI_MG2 < 1)
    %Neither MG can support itself. Each MG should not
       generate any power
    %to export but retain as much as possible. Dependency on
        electric grid
    %required.
    SetpointMG1 = 0;
    SetpointMG2 = 0;

elseif (KPI_MG1 < 1)
    % MG1 needs support, and MG2 has a surplus of energy
       which can be
    % transferred to MG1. Need to determine whether it is
       ideal to handle
    % the transfer of energy or rely on the electric grid.

    P_IMG = (P_Load_MG1 - (P_DC_MG1 + P_AC_MG1))*1.1;

    % Adjust P_IMG to account for available supply from MG2
    if (P_IMG < (P_Load_MG2 - (P_DC_MG2 + P_AC_MG2)))
        P_IMG = (P_DC_MG2 + P_AC_MG2) - P_Load_MG2;
    end

    KPI_MG1_U = log(abs((P_DC_MG1 + P_AC_MG1 + P_IMG) /
       P_Load_MG1));
    KPI_MG2_U = log(abs((P_DC_MG2 + P_AC_MG2) / (P_Load_MG2
       + P_IMG)));

    mat = {[log(KPI_MG1) log(KPI_MG2)] [0 0]
        [0 0]    [KPI_MG1_U KPI_MG2_U]};

    [~, ~, A_s, B_s]=GTbimatrixgames(mat, 0,0);

    if (A_s(2) > A_s(1) && B_s(2) > B_s(1))
        SetpointMG1 = 0;
        SetpointMG2 = Base + P_IMG;
    else
        SetpointMG1 = Base;
        SetpointMG2 = Base;

    end
elseif (KPI_MG2 < 1)
    % MG1 needs support, and MG2 has a surplus of energy
       which can be
```

```
    % transferred to MG1. Need to determine whether it is
        ideal to handle
    % the transfer of energy or rely on the electric grid.

    P_IMG = (P_Load_MG2 - (P_DC_MG2 + P_AC_MG2))*1.1;

    % Adjust P_IMG to account for available supply from MG1
    if (P_IMG < (P_Load_MG1 - (P_DC_MG1 + P_AC_MG1)))
        P_IMG = (P_DC_MG1 + P_AC_MG1) - P_Load_MG1;
    end

    KPI_MG1_U = log(abs((P_DC_MG1 + P_AC_MG1) / (P_Load_MG1
        + P_IMG)));
    KPI_MG2_U = log(abs((P_DC_MG2 + P_AC_MG2 + P_IMG) /
        P_Load_MG2));

    mat = {[log(KPI_MG1) log(KPI_MG2)] [0 0]
        [0 0] [KPI_MG1_U KPI_MG2_U]};

    [~, ~, A_s, B_s]=GTbimatrixgames(mat, 0,0);

    if (A_s(2) > A_s(1) && B_s(2) > B_s(1))
        SetpointMG1 = Base + P_IMG;
        SetpointMG2 = 0;
    else
        SetpointMG1 = Base;
        SetpointMG2 = Base;
     end
end
end

function [v1,v2,A_s,B_s]= GTbimatrixgames(in_mat, ~,
    lin_flag)
% Solve nonantagonistic games (bimatrix game).
% [solve,A,B,]= GTbimatrixgames(in_mat, ~, solve_type)
% Input:
% M - a matrix of game
% solve_type - 1 linprog or 0 matrix solve
% Output:
% v - value of the game
% A - strategy of the gamer A.
% B - strategy of the gamer B.
%**********************************
[m,n]=size(in_mat);
A=[0 0;0 0];B=[0 0;0 0];
for i=1:m
    for j=1:n
        A(i,j)=in_mat{i,j}(1);
```

```
            B(i,j)=in_mat{i,j}(2);
        end
    end

    if ~lin_flag
        u=[1  1];
        v1=1/(sum(u*A^(-1)*u'));
        v2=1/(sum(u*B^(-1)*u'));
        A_s = v2*u*B^(-1);
        B_s = (v1*A^(-1)*u')';

    end
    end
```

Appendix D

Further Reading on Phase Lock Loop

This information provides further background on the phase lock loop, used in the DC bus inverter (see Section 6.2.4). The following information is extracted from MathWorks documentation [137].

Description

The PLL (3ph) block models a Phase Lock Loop (PLL) closed-loop control system, which tracks the frequency and phase of a sinusoidal three-phase signal by using an internal frequency oscillator. The control system adjusts the internal oscillator frequency to keep the phases difference to 0. Figure D.1 shows the internal diagram of the PLL.

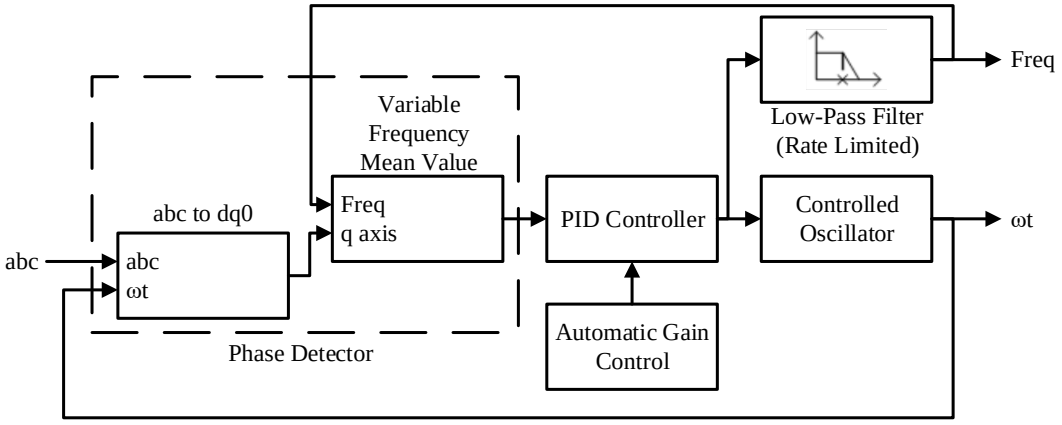

Figure D.1: Internal diagram of phase lock loop modelled in Simulink

The three-phase input signal is converted to a dq0 rotating frame (Park transform) using the angular speed of an internal oscillator. The quadrature axis of the signal, proportional to the phase difference between the abc signal and the internal oscillator rotating frame, is filtered with a Mean (Variable Frequency) block. A Proportional-Integral-Derivative (PID) controller, with an optional automatic gain control, keeps the phase difference to 0 by acting on a controlled oscillator. The PID output, corresponding to the angular velocity, is filtered and converted to the frequency, in hertz, which is used by the mean value.

Parameters

Minimum frequency (Hz)

— Specify the minimum expected frequency of the input signal. This parameter sets the buffer size of the Mean (Variable Frequency) block used inside the block to compute the mean value. Default is 45.

Initial inputs [Phase (degrees), Frequency (Hz)]

— Specify the initial phase and frequency of the input signal. Default is [0, 60].

Regulator gains [Kp, Ki, Kd]

— Specify the proportional, integral, and derivative gains of the internal PID controller. Use the gains to tune the PLL response time, overshoot, and steady-state error performances. Default is [180, 3200, 1].

Time constant for derivative action (s)

— Specify the time constant for the first-order filter of the PID derivative block. Default is 1e-4.

Maximum rate of change of frequency (Hz/s)

— Specify the maximum positive and negative slope of the signal frequency. Default is 12.

Filter cut-off frequency for frequency measurement (Hz)

— Specify the second-order lowpass filter cut-off frequency. Default is 25.

Sample time

— Specify the sample time of the block, in seconds. Set to 0 to implement a continuous block. Default is 0.

Enable automatic gain control

— When this check box is selected, the PLL block optimizes its performances by scaling the PID regulator signal according to the input signal magnitude. Select this option when the input signal is not normalized. Default is selected.

Appendix E

Drive-Train Efficiency Parametric Analysis

The drive-train efficiency of a rolling stock, η_{trac}, will vary during operation, as the load conditions, passenger weight, geographical location and climate vary. A parametric analysis is performed on the drive-train efficiency, which can vary depending on many factors. In the results below, the case study information for Case I: High Speed 2 is being applied for scenario 3 (interconnected microgrids). The technical parameters of the rolling stock are listed in Table 7.1, and the speed-distance profile of the rolling stock, include a return trip, is provided in Figure 7.1 [151]. Figure E.1 illustrates the active power profile for the rolling stock with a drive-train efficiency varying from 60% to 90%.

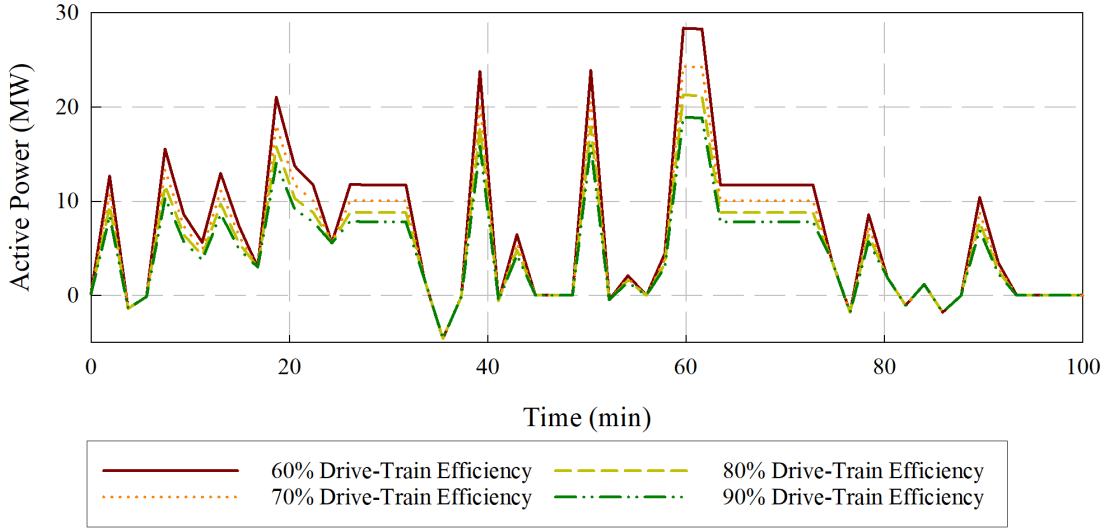

Figure E.1: Active power profile of the rolling stock moving from London Euston to Birmingham Curzon, including return trip, using a parameterized drive-train efficiency (60-90%)

Each load profile depicted in Figure E.1 is simulated in Simulink using the proposed RIMG model, similar to the results presented in Chapter 8. The results of the sizing analysis in Section 8.2.1 are used in the simulations. Figure E.2a shows a comparison of the IMG electric grid dependence KPI for each of the drive-train efficiencies considered in the parametric analysis. Figure E.2b shows a comparison of the IMG reliance KPI for each of the drive-train efficiencies considered in the parametric analysis.

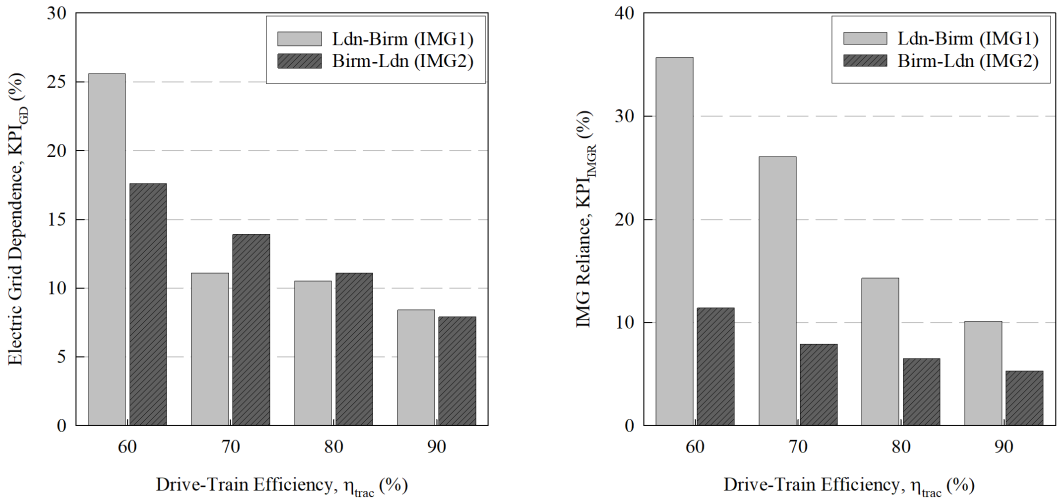

(a) IMG electric grid dependence KPI **(b)** IMG reliance KPI

Figure E.2: Comparison of the IMG KPIs in the parametric analysis

Appendix F

Interpreting Simulation Results

Below is a description on interpreting the simulation results in Chapter 8. Scenarios 1, 2, and 3 for each case study show how the demand of each IMG is met by the IMG DERs, ESSs, and electric grid. For scenario 3, the figure will also include the exchange of energy between two interconnected microgrids.

The notation for the simulation results are as follows:

— If the electric grid is negative, this indicates a surplus in IMG supply and is being exported to the electric grid.

— If the electric grid is positive, this indicates a deficit between IMG supply and IMG demand. The deficit is being imported from the electric grid.

— If the IMG ESS is negative, this indicates the ESS is being charged due to a surplus of IMG supply.

— If the IMG ESS is positive, this indicates the ESS is being discharged to satisfy a deficit between the IMG supply and IMG demand.

— If the load is positive, this indicates the power required by the rolling stock to move along the railway track.

— If the load is negative, this indicates the rolling stock is recovering energy typically lost during the braking operation.

— If the IMG supply (total generation from the wind turbine(s) and solar PV arrays) is positive, this indicates the DERs are generating power to supply the IMG demand. IMG supply is not negative in this thesis.

— If the power exchange between the two IMGs is negative, this indicates a transfer from IMG1 to IMG2 along the microgrid interconnection, as determined

by the IMGSC

— If the power exchange between the two IMGs is positive, this indicates a transfer from IMG2 to IMG1 along the microgrid interconnection, as determined by the IMGSC.